IV.E. Process Development and Manufacturing R&D at the National Laboratories

IV.E.1. Process Development and Scale Up of Advanced Active Battery Materials (ANL)

Gregory K Krumdick, ANL Program Manager
Argonne National Laboratory
9700 South Cass Avenue
Argonne, IL, 60439-4837
Phone: 630-252-3952; Fax: 630-252-1342
E-mail: gkrumdick@anl.gov

Peter Faguy, DOE Program Manager
U.S. Department of Energy
Vehicle Technologies Office
1000 Independence Avenue, SW
Washington, DC 20585
Phone: 202-586-1022
E-mail: Peter.Faguy@ee.doe.gov

Start Date: October 2010
End Date: September 2017

Abstract

Objectives

The program is a key link between the discovery of advanced active battery materials, market evaluation of these materials, and high-volume manufacturing to reduce the risk associated with their commercialization. We provide systematic process and material engineering researches to develop cost-effective customized processes and to produce sufficient quantities of these materials with high quality by optimizing synthesis processes, evaluating material purity profiles and applying emerging manufacturing technologies.

Accomplishments

- Core-Gradient structured material was selected and designed to stabilize high-capacity Ni-rich cathode material.

- To produce dense and high-performance Core-Gradient material, the synthesis condition of 5 μm Core NCM811 material was optimized by Design of Experiment and the optimized 5 μm Core NCM811 shows improved cycle life compared to a commercial NCM811 material.

- Two Core-Gradient materials were prepared using 20 L batch reactor and their particle structures were verified by cross-sectional SEM images and elemental mapping of individual particles.

- Synthesized Core-Gradient material shows improved electrochemical performance compared to two commercial NCM622 materials which have a same overall composition as the Core-Gradient material.

- To evaluate emerging manufacturing technologies, 10 L Taylor Vortex Reactor (TVR) was installed.

- To evaluate TVR process scalability, 40 L TVR installation is ongoing via international collaboration (CRADA) with equipment manufacturer (Laminar Co., Ltd.)

- To evaluate next generation technologies, the flame spray pyrolysis (FSP) system is being installed.

- Kilogram production of layered-layered-spinel material accomplished using 10 L TVR.

- NCM523, NCM622 and NCM811 were prepared using 1 L TVR and delivered to collaborators.

- Micronization of nano-size LFP slurry was completed by spray drying process.

Future Achievements

- Scale up of advanced active material: MERF is continually receiving requests across the DOE complex, in academia and industry for developing and/or scaling up customized active materials and chemistries that are not available commercially. The candidate materials will be prioritized for scale-up R&D based on a ranking criterion based on level of commercial interest, needs of the research community, benefits over commercial materials and consultations with DOE program managers. Currently, we focus on gradient material to improve poor thermal stability of Ni-rich cathode material and also layered-layered-spinel material to stabilize the layered-layered structure by the spinel phase.

- Process R&D of advanced active material: Alternative material synthesis processes will be developed and initially screened to select preferred synthesis pathways, including investigation of emerging manufacturing technologies to improve performance and reduce costs. In parallel, conceptual process designs will be developed and incorporated into process models for the synthesis of the materials to enable cost estimation and also to enable process simulation to identify key process variables.

- Evaluation of material purity profiles: Analytical methods will be developed to identify and prioritize candidate materials, to verify process operating conditions and key parameters and to establish quality control procedures to ensure consistency in product and process development at each stage of process scale-up. The evaluation of materials will be conducted both internally by the project team and also independently verified to ensure that the scaled materials achieve their expected performance targets.

- Evaluation of Taylor Vortex Reactor Synthesis as an emerging manufacturing technology: In collaboration with the Laminar Company, we will be evaluating the scalability of a Taylor Vortex Reactor (TVR) for the production of cathode precursors. TVR's have several advantages over conventional CSTR's including homogeneous micro-mixing, high mass and heat transfer and faster reaction kinetics resulting in reduced reaction time, denser particles and more uniform particle size and distribution. We currently have a 1 L and 10 L TVR and through collaboration with the equipment manufacturer Laminar, we plan to evaluate process scalability with 40 L unit.

- Evaluation of Flame Spray Pyrolysis Synthesis as a next generation manufacturing technology: In collaboration with Miki Oljaca at the Cabot Corporation and Sotiris Pratsinis at the Swiss Federal Institute of Technology, we are establishing a flame spray pyrolysis (FSP) reactor for the synthesis of cathode precursors as well as energy-related nano-particles. FSP is a thermochemical conversion process that can produce a broad range of high purity materials at potentially lower cost, smaller environmental footprint. Cabot has been a leading manufacturer of fine particles for more than 130 years and has experience in FSP synthesis and reactor design and Dr. Pratsinis is a recognized world expert in this field.

- Evaluation of Hydrothermal Synthesis of silicon and silicon-containing nanoparticles: We are proceeding with the design and construction of a turnkey hydrothermal synthesis (HyTS) reactor system, capable of batch production of 20 to 50 g of nanoparticles per run. This advanced bench scale HyTS process will be used for the production and evaluation of high-capacity engineered silicon nanoparticles and composites used as the active anode material in advanced lithium-ion batteries. The HyTS reactor could also be implemented in the production of other active electrode materials such a mixed transition metal oxide nanoparticles as advanced cathode materials.

- Workforce development and education: We will train, inspire and prepare the next generation of scientists and engineers on process R&D and scale up and emerging manufacturing technologies. Process R&D and scale-up is typically learned on the job, typically not at a university. When staffing the process R&D and scale-up programs at the MERF, skilled employees were recruited from industry, bringing this expertise to MERF. We will embed a university graduate student who has been working on bench scale research of energy storage materials developed at their university in the MERF. They will work hands-on alongside highly experienced process engineers and learn how to do the process R&D, scale and synthesize material which is of interest to DOE. This would enhance their professional profile and skill for future employment, further benefiting the battery industry.

Technical Discussion

Background

Newly invented advanced active materials have been synthesized in gram quantity at bench-scale without quality control and reproducibility which are not yet available commercially. The development of a tailored synthesis process and its optimization is the key issue in producing sufficient quantities of these materials with high quality. Barriers addressed are synthesis route selection, process optimization for maximum performance, quality control with process reproducibility and manufacturing cost reduction. The technical targets of this program are developing customized synthesis processes for newly invented advanced active battery materials, scaling up multi-kilogram material under rigorous quality control, providing a systematic material engineering research with reproducibility and evaluating emerging manufacturing technologies and their application.

Introduction

Newly invented advanced active battery materials are generally synthesized on the gram scale without quality control and reproducibility, which lack commercial availability. These chemistries need to be tested and validated in large format prototype cells before going to high-volume manufacturing which needs a fair amount of material. Moreover, for in-depth material characterizations and further applications such as surface coating, kilogram scale stocks of these materials are necessary as baseline materials. Therefore, the supplement of newly invented materials with high quality and large quantity is critical for both fundamental research and industrial validation.

However, from an engineering perspective, newly invented material needs to be synthesized and scaled via its own tailored synthesis process and optimization to maximize its performance and therefore it is challenging. The systematic material engineering and customized scaled process that we develop, will resolve the scale-up constraints of these materials and bridge the gap between basic material research and commercialization.

Approach

Innovative Approach: Kilogram material production with high quality will be accomplished by developing a customized synthesis process and systematic material engineering. We will use a systematic process to achieve the maximum quality of target material (See Figure IV-250).
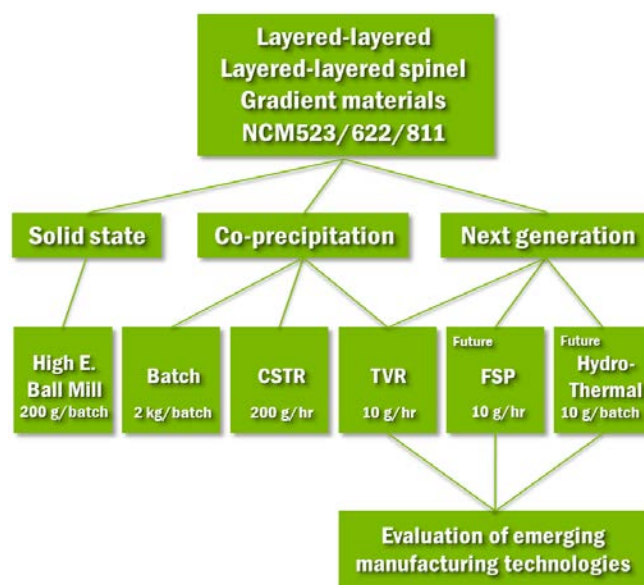

Figure IV-250: Flow chart of material scale-up

1. Define target material to be scaled by evaluating bench-scale samples from R&D groups.
2. Preliminary material synthesis and evaluation via conventional synthesis processes (High E. ball Mill, Batch and CSTR) together with emerging technologies (TVR, FSP and Hydrothermal).
3. Select a customized synthesis process.
4. Evaluate and select synthesis route.
5. Optimize synthesis process by Design of Experiments (ANOVA).
6. Produce 100g intermediate product for material evaluation and reproducibility check.
7. Kilogram production, characterization, delivery and feedback from collaborators.

Results

1. Particle structural design of Gradient materials (completed)

Nickel-rich cathode material has high reversible capacity of around 200 mAh/g but shows poor thermal stability and cycle life, especially at elevated temperature, that should be improved. As an alternative, Core-Shell and Full Concentration-Gradient materials were chosen and are being studied to enable long cycle life and excellent abuse tolerance. These gradient materials are composed of Ni-rich central bulk together with Mn-rich outer layer so that Ni concentration decreases gradually or stepwise while Mn and Co concentrations increase as the surface is approached. Ni-rich central bulk has high capacity but low thermal stability and Mn-rich outer layer has low capacity but high thermal stability as shown in Figure IV-251. These central bulk and outer layer compositions have different volume expansion during charge and discharge and thereby gradient material will experience mechanical stress caused by insertion and extraction of lithium ions which lead to the formation of micro-cracks and segregation between the central bulk and outer. Therefore, the particle structure design and the composition combination of gradient material are important to maximize both capacity and stability and minimize particle crack.

Typical particle structures of gradient material are shown in Figure IV-251. We need to get the optimal thickness ratio of core, gradient and shell layers. There are several structural options for gradient material such as Core-Shell, Core-Gradient, Core-Gradient-Shell and Full Concentration-Gradient. For FY16, Core-Gradient structured material was selected for synthesis and characterization before going to Full Concentration-Gradient and/or other particle structures in order to understand the trade-off between normal NCM811 and gradient materials. We used NCM811 as core and NCM424 as surface composition to produce Core-Gradient material.
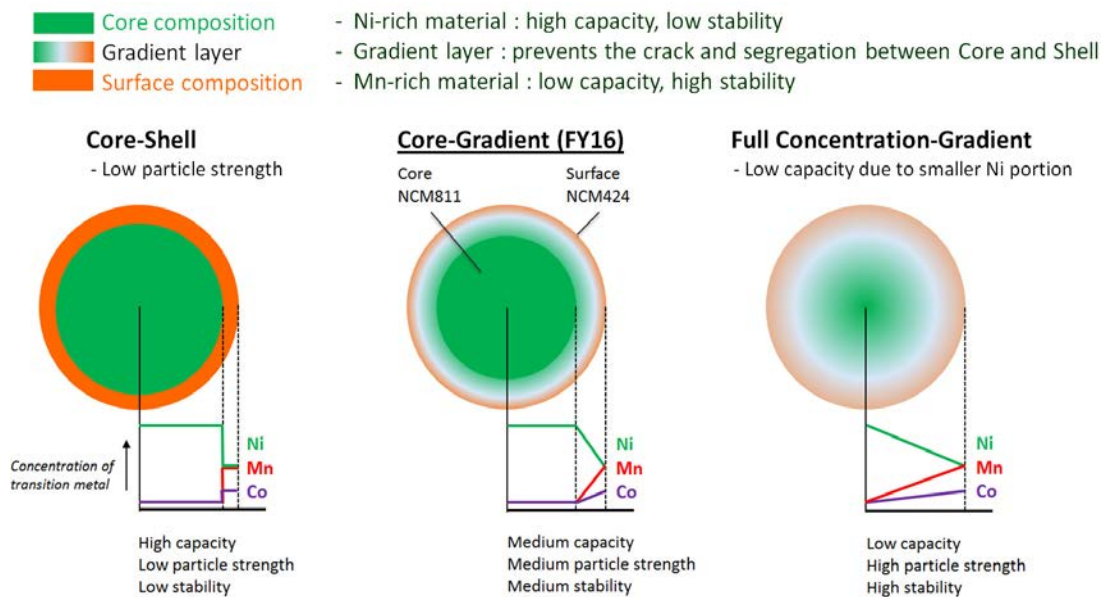

Figure IV-251: Typical particle structure of gradient materials

2. Synthesis optimization of core NCM811 to get dense Core-Gradient material (completed)

To get dense Core-Gradient material with higher mechanical strength, the porosity of particles need to be reduced. Spherical particle morphology and uniform particle size are critical to maximize the structural effect of Core-Gradient over normal NCM material. Therefore, we carried out the precursor optimization for core NCM811 by multilevel factorial design. 12-time 20 hr co-precipitations using 20 L batch reactor were carried out by the change of pH and ammonium hydroxide ratio to transition metal. The target of core NCM811 was 5 µm, dense, spherical morphology with narrow particle size distribution which is not commercially available.

Figure IV-252 shows the microscope images of precursors obtained from each 20 hr co-precipitation. The particle size of precursor increases when the pH decreases from 12 to 10.5 and the particle size distribution is narrowed when ammonium hydroxide ratio to transition metal decreases from 3 to 1. We measured the tap density and carried out particle size analysis of each precursor. Figure IV-253 shows 3D mesh plots of precursor particle size (D50) and tap density according to pH and ammonium hydroxide ratio to transition metal to evaluate the effect of process variables. This 3D mesh plot of precursor particle size (D50) clearly indicates that pH of co-precipitation is a major variable to determine the particle size but the effect of ammonium hydroxide ratio to transition metal on particle size is less significant to NCM811 precursor formation. Low pH condition of co-precipitation will increase the size of secondary precursor particle but it doesn't always increase of tap density according to the size of secondary precursor particle. To increase the tap density of precursor, dense packing of primary particles in secondary precursor particle is critical. The 3D mesh plot of tap density shows that the precursor tap density increases when pH decreases from 12 to 11.5 because of the secondary particle growth. When pH decreases further from 11.5 to 10.5, the precursor tap density decreases because of loose packing of primary particles even though secondary particle grows. Based on these precursor images and 3D mesh plots, pH 11.5 and ammonium hydroxide ratio to transition metal of 2 was selected to obtain core NCM811.
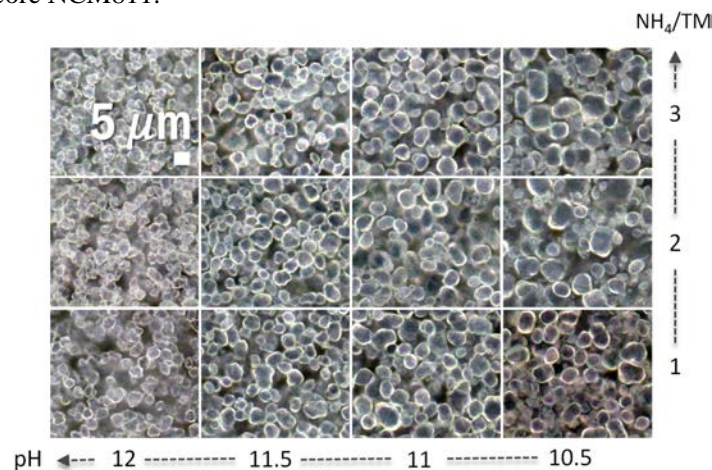

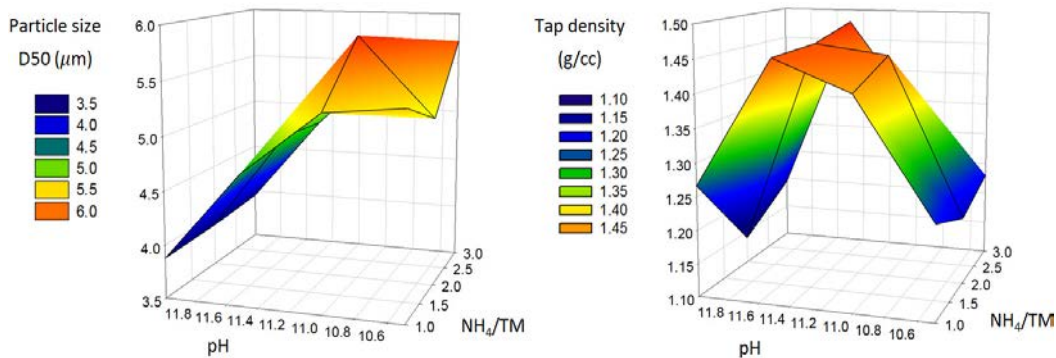Figure IV-252: Microscope images of precursors obtained from 12-time 20 hr co-precipitations

Figure IV-253: 3D mesh plots of precursor particle size and tap density according to pH and ammonium hydroxide ratio to transition metal

We prepared core NCM811 using 20 L batch reactor via hydroxide co-precipitation which has 5 µm size (D50) and narrow particle size distribution compared to a commercial NCM811 product as shown in Figure IV-254. The prepared 5 µm core NCM811 has uniform spherical morphology which is critical to generate a high-quality Core-Gradient material. To check the electrochemical performance of this prepared material, we carried out coin cell test. Figure IV-255 shows the electrochemical performance comparison of 5 µm core NCM811 and commercial NCM811 at C/10 cycling at 30°C between 3 and 4.4 voltages. The commercial NCM811 seems to have slightly better initial discharge capacity but its capacity retention after 40 cycles is lower than the optimized core NCM811. This capacity retention gap between the commercial NCM811 and optimized core NCM811 is serious at higher C-rate. As shown in Figure IV-256, when cycled at 1C, 30°C between 3 and 4.4 voltages, optimized core NCM811 has improved capacity retention of 75% at 100 cycles but the commercial NCM811 shows only 50% capacity retention. Therefore, the quality of 5 μm core NCM811 was verified.
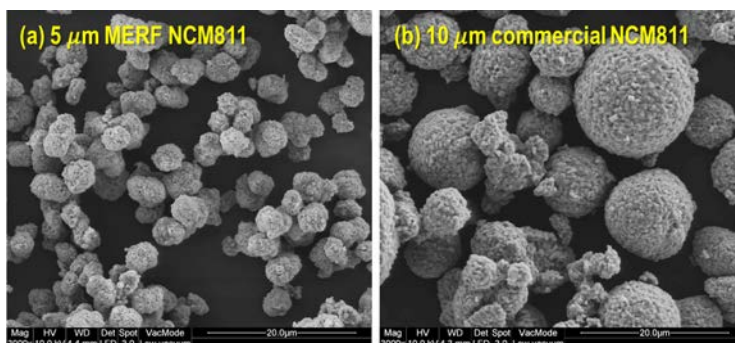

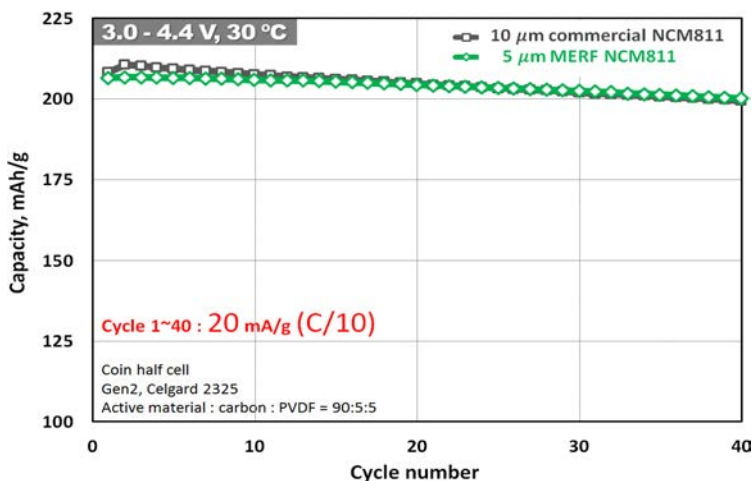**Figure IV-254: (a) Optimized core NCM811 and (b) commercial NCM811 product**

Figure IV-255: Coin cell result of 5 µm core NCM811 and commercial NCM811 at C/10
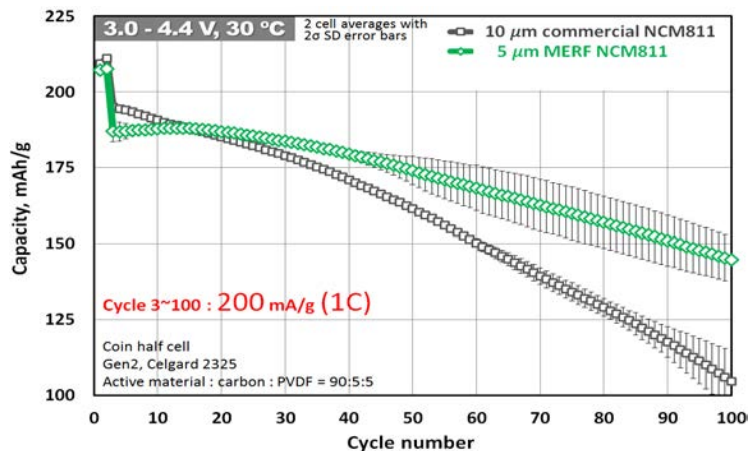
Figure IV-256: Coin cell result of 5 µm core NCM811 and commercial NCM811 at 1 C

3. Core-Gradient material preparation and evaluation (completed)

Based on the synthesis optimization of core NCM811, we started the preparation of Core-Gradient material. Figure IV-257 shows the set-up of 20 L batch reactor used and the particle structure design for Core-Gradient material composed of NCM811 as core and NCM424 as surface composition.
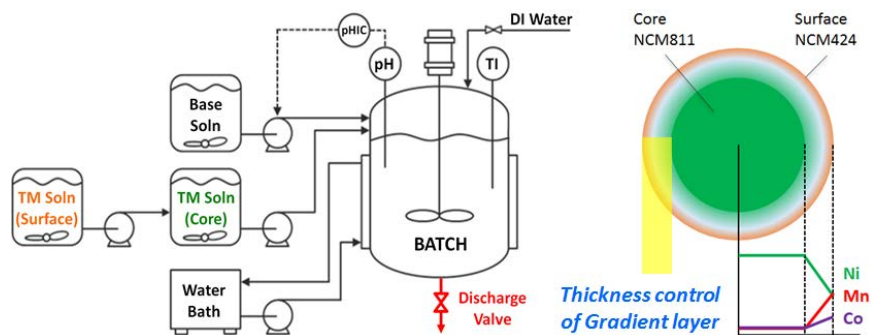

Figure IV-257: 20 L batch reactor and particle structure design for Core-Gradient material
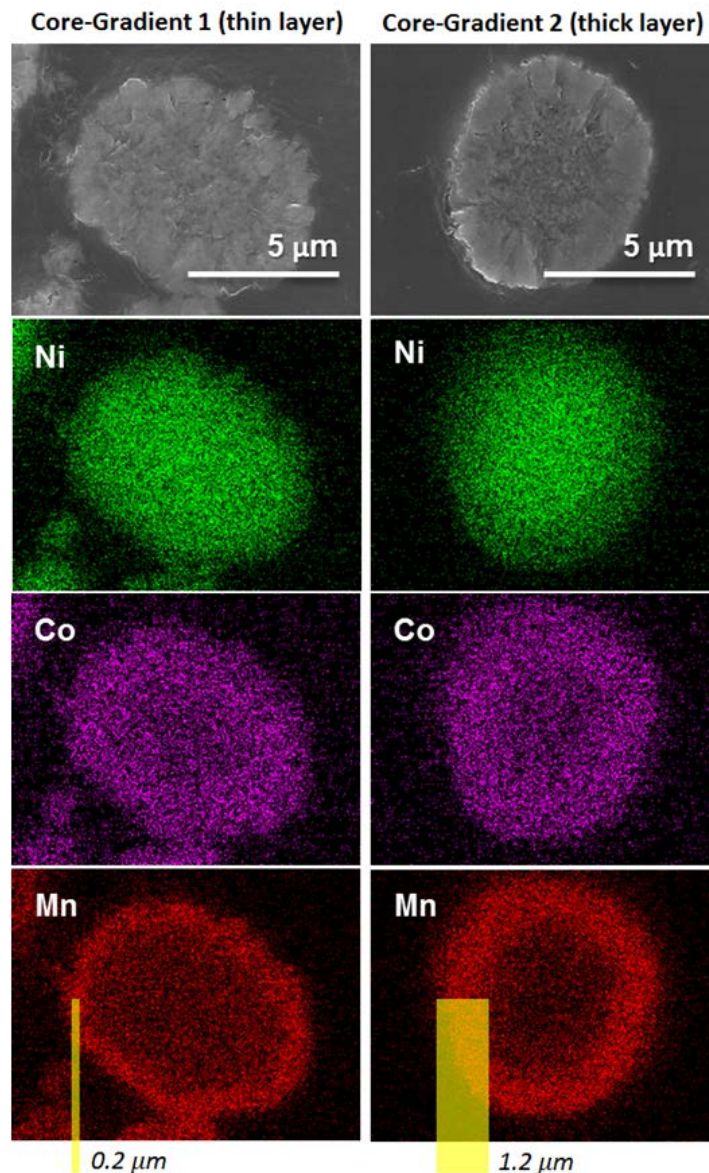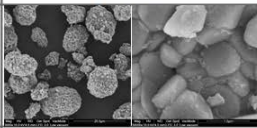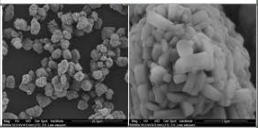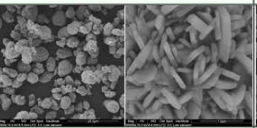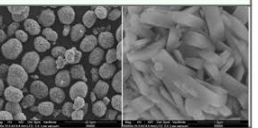
Figure IV-258: Cross-sectional SEM images and elemental mapping of two Core-Gradient materials

To synthesize Core-Gradient material, core transition metal solution was injected to batch reactor for a certain period of time. Then, surface TM solution was injected to core TM solution feed tank which results in the gradual change of core TM to surface TM solution. As can be seen at the schematic particle structure drawing in Figure IV-257, core composition is NCM811, surface composition is NCM424 and we controlled the thickness of gradient layer. We prepared two Core-Gradient materials with thin gradient layer or thick gradient layer. After the preparation, we have applied cross-sectional elemental mapping to verify the Core-Gradient structure. Figure IV-258 shows the cross-sectional SEM images and elemental mapping of individual particles. This elemental mapping of nickel, cobalt and manganese clearly shows the Core-Gradient structure and the thickness of gradient layer. One is 0.2 μm and the other is 1.2 μm as average thickness designed from the beginning. Taking a closer look at the images, Ni concentration decreases from the core to the surface. On the other hand, Co and Mn concentrations show the opposite that matches of the schematic particle drawing as shown in Figure IV-257. We successfully prepared two Core-Gradient materials and controlled the thickness of their gradient layers. Figure IV-259 is a comparison of all the prepared materials (optimized core NCM811, Core-Gradient 1 thin layer and Core-Gradient 2 thick layer). A commercial NCM622 product was selected for comparison because it is similar to the overall composition of Core-Gradient 1. Looking at all the materials prepared, the primary and secondary particle sizes are small and this makes their surface areas bigger than the commercial NCM622. Core-Gradient 1 shows similar discharge capacity compared to the commercial

NCM622 but has better first cycle efficiency. Core-Gradient 2 shows lower capacity because its overall Ni content is lower than the commercial NCM622.

Material	NCM622	NCM811 (no layer)	Core-Gradient 1 (thin layer)	Core-Gradient 2 (thick layer)
Scale / status	Commercial product	MERF pre-pilot Optimized	MERF pre-pilot Preliminary	MERF pre-pilot Preliminary
SEM 3,000x 50,000x				
Composition	NCM622	NCM811	~ NCM622	~ NCM523
ICP-MS analysis	$Li_{1.04}Ni_{0.60}Co_{0.20}Mn_{0.20}O_y$	$Li_{1.00}Ni_{0.77}Co_{0.12}Mn_{0.12}O_y$	$Li_{1.07}Ni_{0.57}Co_{0.17}Mn_{0.26}O_y$	$Li_{1.1}Ni_{0.46}Co_{0.19}Mn_{0.35}O_y$
Particle size D_{50} [µm]	11.3	4.7	5.1	7.0
Tap density [g/cc]	2.3	1.7	1.8	2.5
* FCE [%]	90.5	92.1	93.1	93.2
* Initial discharge capacity [mAh/g]	188	207	185	178

* At C/10, 3.0 – 4.4 V and 30°C

Figure IV-259: Process comparison between batch, CSTR and TVR

Figure IV-260 shows the voltage profiles of 1st cycle (C/10) and 3rd cycle (1C) of synthesized Core-Gradient 1 and commercial NCM622 product. This graph shows that Core-Gradient 1 has a similar capacity compared to the commercial NCM622 at C/10 but a lower capacity at 1C which means Gradient layer needs to be optimized for better lithium-ion conductivity. However, looking at those 1C cycling and capacity retention as shown in Figure IV-261, Core-Gradient 1 has the better stability than the commercial NCM622 products. Therefore, Core-Gradient structure has the best of Core and Surface compositions which means it has a longer cycle life and better thermal stability than normal NCM material with same overall composition. It is challenging to make this gradient material better and economical. We will keep developing its customized synthesis process, inventing novel particle structure, optimizing the thickness of gradient layer and researching other combinations of core and surface compositions to achieve better capacity and thermal stability.
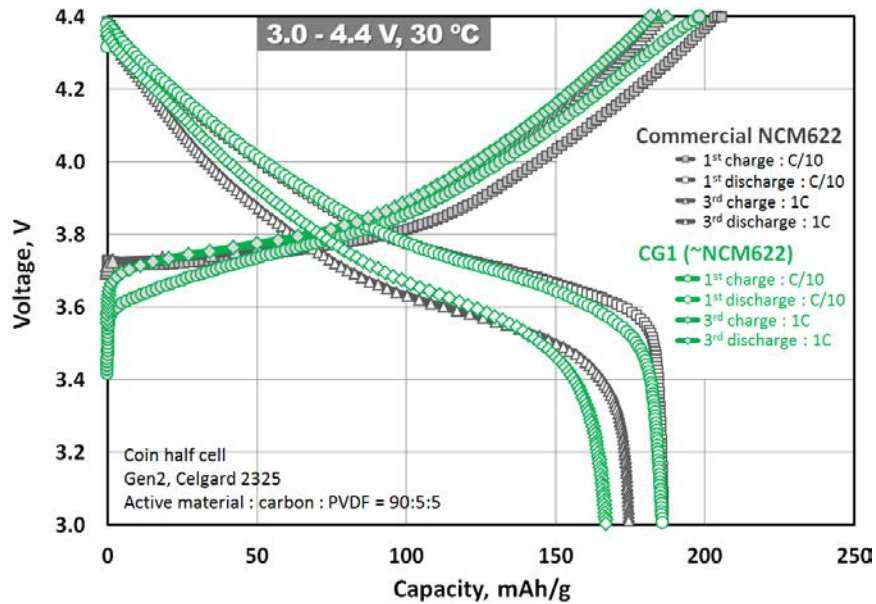
Figure IV-260: Voltage profiles of Core-Gradient 1 and commercial NCM622
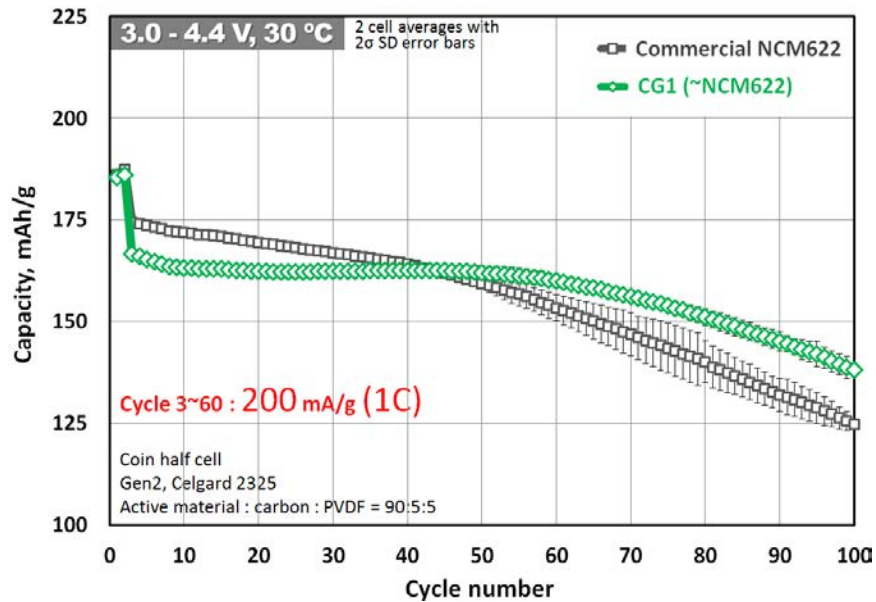
Figure IV-261: 1 C cycling comparison of Core-Gradient 1 and commercial NCM622

4. Evaluation of emerging manufacturing technology: 10 L & 40 L Taylor Vortex Reactor (ongoing)

Active battery material needs to be synthesized and scaled via its own tailored synthesis process and optimization to maximize its performance because the physical and electrochemical properties of the synthesized material strongly depend on its synthesis process. As a new synthesis process, TVR technology shows better material properties such as spherical morphology, narrow particle size, and high tap density compared to conventional synthesis processes. This TVR provides a homogeneous intense micro-mixing zone inside reactor and enables simplified operation, product uniformity and shorter residence time which increase economic feasibility. We try to enhance the cathode precursor particle features using this emerging manufacturing technology which also provides various applications in the field of precipitation, crystallization, polymerization, sol-gel process and coatings.

Figure IV-262: Installed 10 L Taylor Vortex Reactor
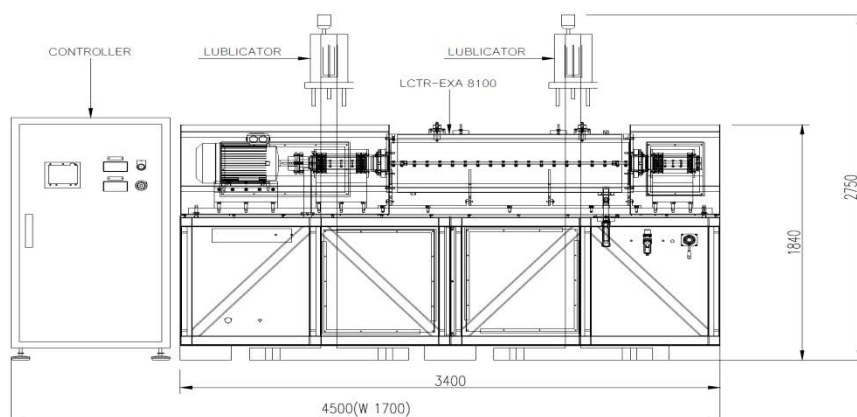
Figure IV-263: Overall dimension of designed 40 L Taylor Vortex Reactor

Figure IV-264: System drawing of 40 L Taylor Vortex Reactor

Last year, we installed a 1 L TVR in order to start evaluating emerging manufacturing technology. We synthesized size-controlled NCM materials using the 1L TVR and those products were delivered to our collaborators to support their research. To accelerate material synthesis and process scalability research, a new 10 L TVR (Figure IV-262) was installed with DOE support and a 40 L TVR (Figure IV-263 and Figure IV-

264) is being set up in collaboration with the equipment manufacturer Laminar. Based on the data from the 1L, 10L and 40L TVRs, we will evaluate its process performance and resolve its process scale-up constraints to facilitate the development and scale-up of TVR process.

5. Evaluation of next generation technology: Flame Spray Pyrolysis for nano-material synthesis (ongoing)

As another advanced manufacturing technology, we are setting up a Flame Spray Pyrolysis system with DOE support for nano-material synthesis. We intend to establish an aerosol based particle synthesis capability focusing on flame assisted spray pyrolysis concept for the production of nano-particles related to energy storage materials. In this flame assisted spray pyrolysis, the heat source is provided by the burning fuel gases such as methane, butane, propane, acetylene and etc. The precursor solution is injected with or without organic content. The aerosol is sprayed in-line with the flame and the reactions happen in milliseconds to few seconds depending on operation conditions such as the flow rate of carrier gas stream, ratio of carrier gas to burner gas, concentration/viscosity of precursor solution, feed flow rate and etc. An additional heating chamber can be placed in where flame assisted spray is introduced in order to allow agglomeration/densification of the particles by increasing their residence time at high temperature. The system is planned to be designed with flexible components such as different types of atomization units, nozzles and heating sources in order to get better configuration and obtain desired particle features. Our major concern will be to achieve uniform, spherical particles with low porosity, sharp particle size distribution and acceptable usage for energy storage materials.
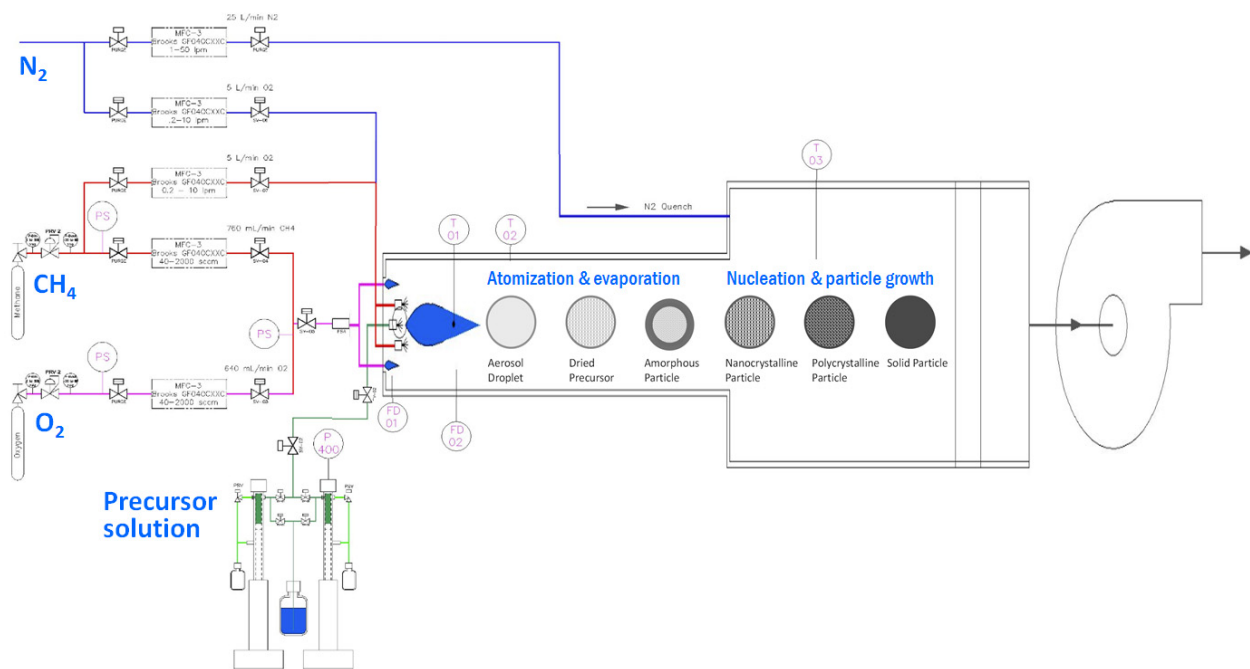

Figure IV-265: P&ID of Flame Spray Pyrolysis

As seen at the P&ID in Figure IV-265, methane will be used as a fuel gas which will generate flame inside reaction zone with oxygen and precursor solution is sprayed into the flame. So, the precursor solution will experience atomization, evaporation, nucleation, particle growth and then calcination. We are collaborating with Cabot and Swiss Federal Institute of Technology to design this system. The basic design and system drawing were prepared and installation will be completed by Jan. 2017. The target production rate is one hundred gram per day. Figure IV-266 shows the system drawing of Flame Spray Pyrolysis which is composed of gas cabinet, spray feed hood, syringe pumps, spray burner hood, burner control panel, tube furnace, blower, filter box for particle collection, fume hood, gas quench pipe and ventilation duct. The detailed configuration of spray burner system is shown in Figure IV-267. NFPA 86 guidelines were followed to provide flame supervision and emergency shutoff. A commercial company was commissioned to design and fabricate a burner controls panel and a commercial industrial burner expert was commissioned to provide burner design and controls review as well as on-site presence during initial burner commissioning.
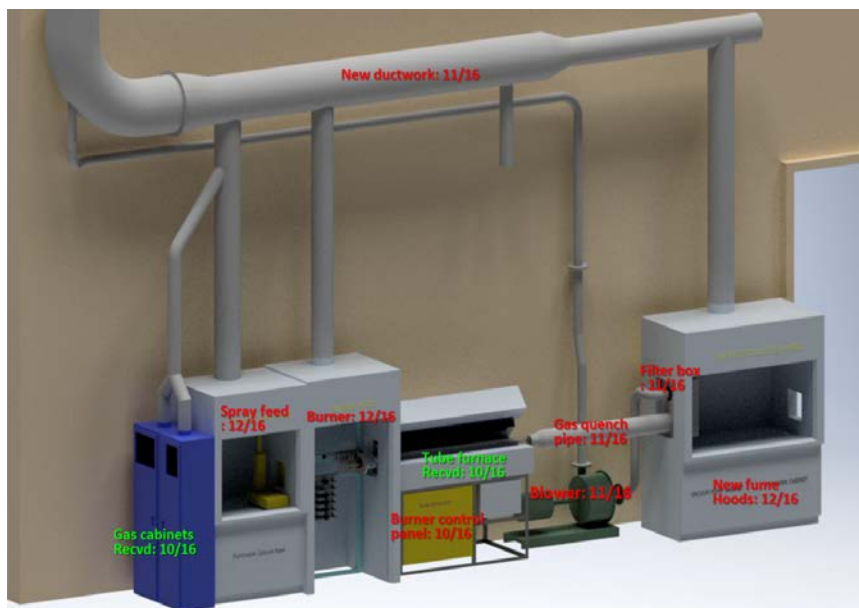
Figure IV-266: System drawing of Frame Spray Pyrolysis
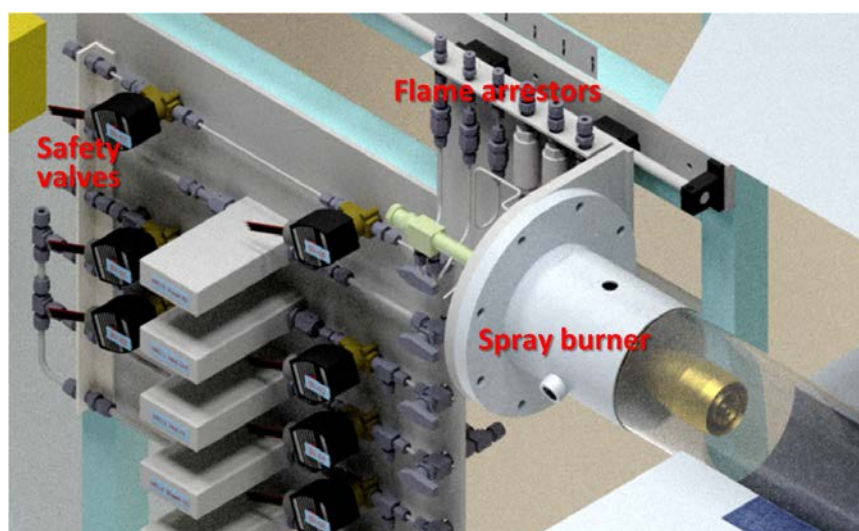
Figure IV-267: Detailed configuration of spray burner system

6. Material production: Layered-layered-spinel (Li$_{1.195}$Ni$_{0.27}$Mn$_{0.54}$Co$_{0.19}$O$_Y$) material (completed)

As a previous material scale-up task, layered-layered-spinel material was selected and prepared to support basic R&D of Michael M. Thackeray's research group at Argonne National Laboratory. As reported at FY15, we prepared layered-layered-spinel materials with 2, 5, 10 and 15% spinel content using hydroxide synthesis route. These materials were used to evaluate the spinel effect and to optimize spinel content. In addition, these systematic material engineering efforts have made a considerable improvement to the basic understanding of layered-layered-spinel structure and to the performance enhancement in the cyclability and rate performance.

To deepen the fundamental research and industrial validation in large format cells of layered-layered-spinel material, kilogram production of this material was requested via carbonate synthesis route. Especially, spherical particle morphology and narrow size distribution were desired for further surface modification of this material.

Figure IV-268 shows the scaled layered-layered-spinel material which has 9.6 μm as particle size (D50), 2.0 g/cc as tap density and $Li_{1.195}Ni_{0.27}Mn_{0.54}Co_{0.19}O_y$ as composition. As shown at SEM images, the scaled material has spherical morphology and meets the target specification. To check the electrochemical performance of the scaled material, coin half cell was used and cycled between 2.0 and 4.6 V for the 1st cycle and between 2.5 and 4.45 V for the rest cycles at C/13 and 30°C. The scaled carbonate LLS material (FY16-YS160830) shows improved initial capacity than the previous preliminary scaled carbonate LLS material (FY15-YS140402) and the bench-scale oxalate sample as shown in Figure IV-269. The scaled product was delivered to basic R&D group and CAMP facility for further fundamental research and industrial validation in large format cells.

Analysis		Target	Results	Judgement	Note	Method
Particle Size Distribution	D10 (μm)	—	5.7			Particle Size Analyzer
	D50 (μm)	—	9.6			
	D90 (μm)	—	16.2			
Specific Surface Area (m²/g)		—	Ongoing			BET
Tap Density (g/cc)		2 or more	2.0			Tap Density Meter
Element mol %	Li / (Ni+Mn+Co)	1.19	1.195			ICP-MASS
	Ni / (Ni+Mn+Co)	0.28	0.27			
	Mn / (Ni+Mn+Co)	0.53	0.54			
	Co / (Ni+Mn+Co)	0.19	0.19			
For Use		Lithium Ion Secondary Battery				
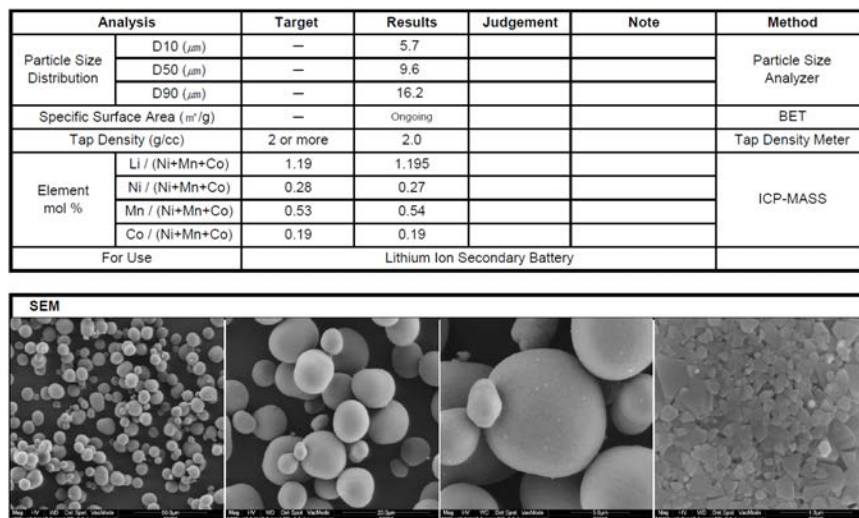
Figure IV-268: Analysis data sheet of 1 kg layered-layered-spinel material
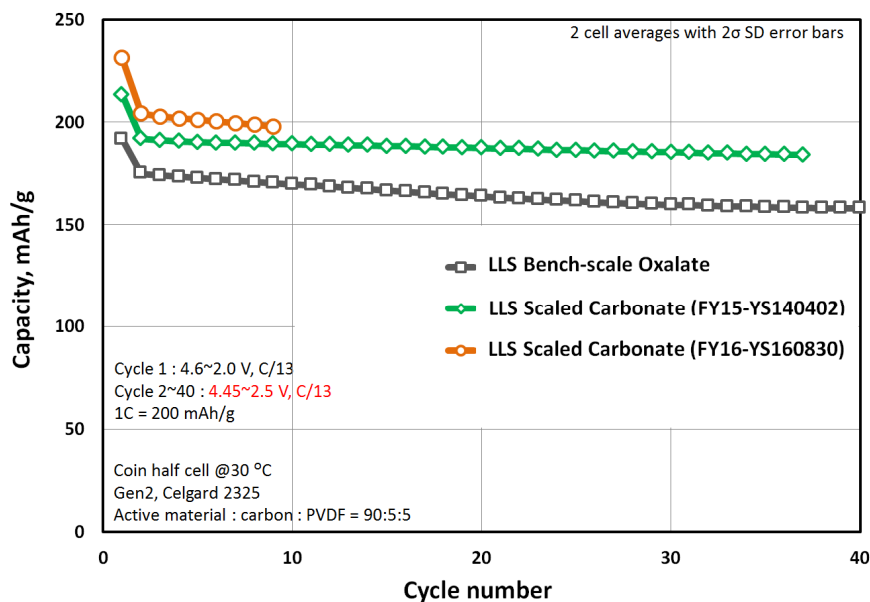
Figure IV-269: Comparison of scaled layered-layered-spinel materials

7. Material production: NCM materials (completed)

To evaluate the performance of TVR as an emerging synthesis technology and support our collaborators, we have employed the TVR (1 L and 10 L) for producing different NCM chemistries by applying hydroxide co-precipitation route. The prepared precursors were calcined using lithium carbonate at high temperature around 850°C. Figure IV-270 shows the SEM images, tap densities, particle sizes and surface areas of prepared NCM materials which have uniform spherical morphology. The NCM products yielded high tap densities with narrow particle size distribution and showed comparable electrochemical properties with the commercial NCM

powders. By exploiting advantages of TVR as an emerging synthesis technology, we synthesized various batches of size-controlled NCM523, NCM622 and NCM811 using 1 L and 10 L TVR. Those NCM products were delivered to our collaborators to support their research (see Figure IV-271). Technische Universität Braunschweig (Dr. Wolfgang Haselrieder) is a collaborator to carry out fracture analysis, hardness and Young´s modulus determination of these prepared NCM materials. We will carry out systematic process scale-up research and continue to provide high-quality active battery materials for basic R&D support and industrial evaluation based on 1 L, 10 L and 40 L TVRs.
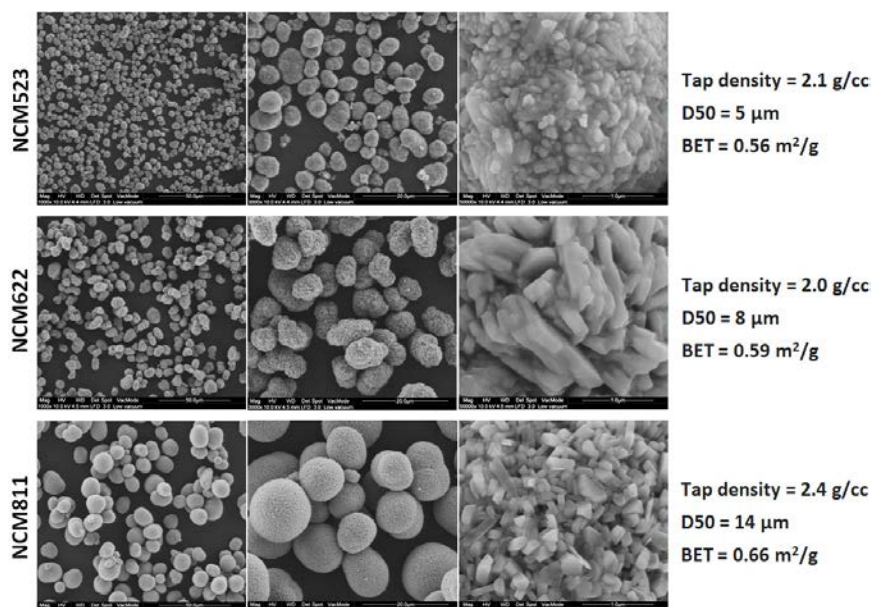

Figure IV-270: NCM materials prepared using 1 L TVR

FY	Date	Material	Lot #	Process	To
16	03/04/2016	$Li_{1.02}Ni_{0.48}Mn_{0.31}Co_{0.21}O_y$	OKF160216_P	1 L TVR	Technische Universität Braunschweig / CAMP
	03/07/2016	$Li_{1.01}Ni_{0.48}Mn_{0.31}Co_{0.21}O_y$	OKF160216_WS	1 L TVR + Water treatment	ANL - CAMP
	05/13/2016	$LiNi_{0.47}Mn_{0.32}Co_{0.21}O_y$	OKF160509_P	1 L TVR	ANL - CAMP
	05/20/2016	$LiNi_{0.47}Mn_{0.32}Co_{0.21}O_y$	OKF160509_WS	1 L TVR + Water treatment	ANL - CAMP
	06/28/2016	$Li_{1.02}Ni_{0.60}Mn_{0.20}Co_{0.20}O_y$	OKF151209	1 L TVR	Technische Universität Braunschweig / CAMP
	06/28/2016	$Li_{1.02}Ni_{0.80}Mn_{0.10}Co_{0.10}O_y$	OKF160222	1 L TVR	Technische Universität Braunschweig / CAMP
	09/20/2016	$Ni_{0.27}Mn_{0.54}Co_{0.19}CO_3$	YS160830_P	10 L TVR	ANL - M. Thackeray's group
	10/17/2016	$Li_{1.195}Ni_{0.27}Mn_{0.54}Co_{0.19}O_y$	YS160830_C	10 L TVR	ANL - M. Thackeray's group

Figure IV-271: Material prepared using 1 L & 10 L TVRs

8. Material production: Micronization of nano-size lithium ion phosphate slurry (completed)

To assist a commercial process development and scale-up of active material, lithium ion phosphate, we cooperated with a battery company in the United States. That company is producing 500 nm LFP precursor slurry by high energy mill and tried to increase its particle size from sub-micron to 5 ~ 10 microns. This sub-micron slurry product needs to be micronized for battery material application. Using the spray dryer installed at MERF (see Figure IV-272), we carried out the micronization of this nano-size material and produced 4 kg 6 μm spherical powder as you can see in SEM images of Figure IV-273. We will keep providing systematic process and material engineering support to our industrial collaborators for their material scale-up and commercialization.
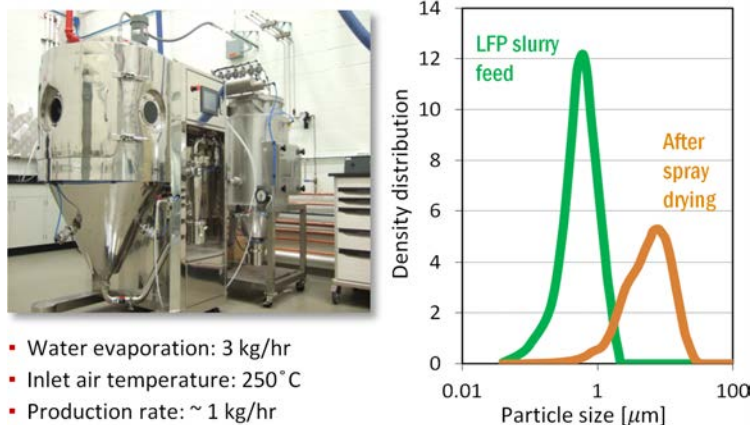
- Water evaporation: 3 kg/hr
- Inlet air temperature: 250°C
- Production rate: ~ 1 kg/hr

Figure IV-272: Spray dryer and particle size distribution of nano-sized feed and micronized product
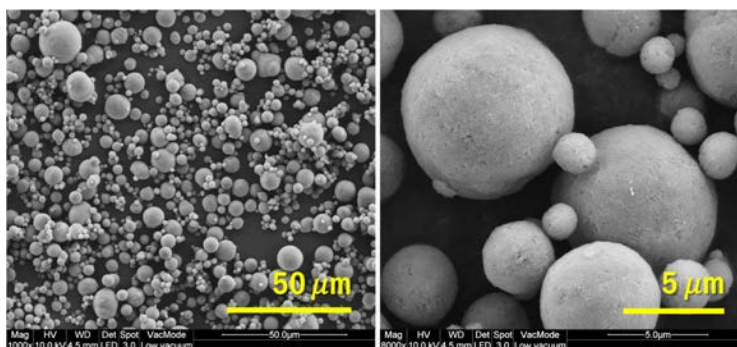

Figure IV-273: SEM images of micronized product

Conclusions

For material scale-up R&D, we have showed that Core-Gradient structured material has the best of core and surface compositions delivering better stability than normal NCM material. We will keep developing its customized synthesis process, optimized particle structure and improved combination of core and surface compositions to achieve both high capacity and thermal stability.

To assist the fundamental research of basic R&D groups, we produced a kilogram of layered-layered-spinel material with spherical particle morphology and narrow size distribution. The scaled product was delivered to basic R&D group and CAMP facility for further fundamental research and industrial validation in large format cells. Also, various batches of size-controlled NCM523, NCM622 and NCM811 were delivered to our collaborators to support their fundamental research.

Evaluation of emerging synthesis technologies is ongoing. A new 10 L TVR was installed with DOE support and 40 L TVR is being set up in collaboration with the equipment manufacturer Laminar. Based on 1 L, 10 L and 40 L TVRs, we will evaluate its process performance and resolve its process scale-up constraints to facilitate the development and scale-up of this process. As another advanced manufacturing technology, we are setting up a flame spray pyrolysis system with DOE support for nano-material synthesis. We intend to establish an aerosol based particle synthesis capability focusing on flame assisted spray pyrolysis concept for the production of nano-particles related to energy storage materials.

To assist a commercial process development and scale-up of active material, the micronization of the nano-size LFP slurry was carried out and we delivered 4 kg of 6 μm spherical powder for industrial collaboration. We will keep providing material engineering support to our industrial collaborators for their material scale-up and commercialization.

We will continually provide systematic process and material engineering researches to develop cost-effective customized processes and to produce sufficient quantities of these materials across the DOE complex, in academia and industry for developing and/or scaling up customized active materials and chemistries.

Products

Presentations/Publications/Patents

1. Y. Shin*, O. K. Feridun, and G. Krumdick, (2015). Synthesis and AlF3 Surface Coating of High Capacity Cathode to Improve Energy Density and Cycle Life, 11th Lithium Battery Power Conference, November 17-19, 2015, Baltimore, MD, USA, Oral Presentation.
2. G. Krumdick*, (2015). Process R&D and Scale-up at Argonne's Materials Engineering Research Facility, 11th Lithium Battery Power Conference, November 17-19, 2015, Baltimore, MD, USA, Oral Presentation.
3. Y. Shin*, O. K. Feridun, and G. Krumdick, (2016). Novel Synthesis Approach toward Long-Life Cathode Material, 6th Next Generation Energy Storage, April 18-20, 2016, San Diego, CA, USA, Oral presentation.
4. Y. Shin*, O. K. Feridun, and G. Krumdick, (2016). Tailoring Nickel-Rich LiNi0.8Co0.1Mn0.1O2 Cathode Material with LiNi0.4Co0.2Mn0.4O2 Surface Composition, 18th IMLB, June 19-24, 2016, Chicago, IL, USA, Poster presentation.
5. O. K. Feridun*, Y. Shin, and G. Krumdick, (2016). Nickel-Rich Cathode Precursor Synthesis By Taylor Vortex Reactor, 18th IMLB, June 19-24, 2016, Chicago, IL, USA, Poster presentation.
6. G. Krumdick*, Y. Shin, O. K. Feridun, K. Z. Pupek, and T. L. Dzwiniel, (2016). Process R&D and Scale-up of Advanced Battery Materials at Argonne's Materials Engineering Research Facility, 18th IMLB, June 19-24, 2016, Chicago, IL, USA, Poster presentation.
7. B. T. Yonemoto*, Y. Shin, J. R. Croy, and M. M. Thackeray, (2016). Design and Processing of Advanced Lithium-Ion Electrode Materials, 18th IMLB, June 19-24, 2016, Chicago, IL, USA, Poster presentation.
8. ANL-IN-14-086, "Surface-Modified Cathode active Materials for Lithium-ion Batteries", Christopher S. Johnson, John David Carter, Xiaoping Wang, Ana Kiricova, YoungHo Shin, filed May, 2016.
9. US 9,446,967, "Method for Producing Size Selected Particles", K. Krumdick, YoungHo Shin, Kaname Takeya, September 20, 2016.

IV.E.2. Process R&D and Scale Up of Critical Battery Materials (ANL)

Gregory K Krumdick, ANL Program Manager
Argonne National Laboratory
9700 South Cass Avenue
Argonne, IL, 60439-4837
Phone: 630-252-3952; Fax: 630-252-1342
E-mail: gkrumdick@anl.gov

Peter Faguy, DOE Program Manager
U.S. Department of Energy
Vehicle Technologies Office
1000 Independence Avenue, SW
Washington, DC 20585
Phone: 202-586-1022
E-mail: Peter.Faguy@ee.doe.gov

Start Date: October 2010
End Date: September 2017

Abstract

Objectives

The objective of this task is to conduct process research and development, then scale-up of advanced materials for lithium-ion batteries. New, innovative materials are being constantly invented to improve the safety, energy density, cycle, and calendar life of lithium-ion batteries for HEV and PHEV applications. Up to this point, these materials have only been synthesized in small batches providing amounts sufficient for basic research but not enough for full scale validation and prototyping. Scaling up the original route used by discovery scientists requires sometimes extensive modification of the bench-scale chemistry and process R&D to allow for safe and cost effective production, development of an engineering flow diagram, design of a mini-scale system layout, construction of the experimental system, and validation of the optimized process. The experimental system will be assembled and the materials will be manufactured in quantities sufficient for full scale industrial evaluation. The materials produced by the program will be fully characterized to confirm chemical identity and purity. Analytical methods will be developed for quality control. The electrochemical performance of the materials will be validated to confirm that the properties match the original sample generated by the discovery scientist.

Accomplishments

- Scale-up work has been completed on the following materials:
    - ORNL- Li-BMFMB (Li salt alternative to LiPF6).
    - TFPC (fluorinated electrolyte solvent).
    - GCMC (electrolyte additive).
    - LBNL-PPy (binder for Si-graphite anode).

- Several materials scaled up and processes developed at MERF have been licensed to two commercial manufacturers, Strem Chemicals and Sigma Aldrich for production and distribution for R&D use.

- Investigated physicochemical properties and electrochemical performance of scaled-up materials to support basic research.

- We are in the process of establishing capabilities and protocols for electrochemical study to develop material specifications (minimum required purity and impurity profile).

- Work on the following materials is ongoing:
    - Binder for advanced anode for lithium-ion cell.
    - LFO (Li-rich cathode additive).

- We have established a new capability to investigate advanced manufacturing techniques of next generation electrolyte materials utilizing a customized continuous flow reactor, Syrris ASIA320. This system will be used to develop more cost effective, safer, and environmentally benign processes.

Future Achievements

- MERF is actively seeking new materials with proven performance for scale up to kilogram quantity. Our goal is to develop processes and scale-up 3-5 new materials invented by discovery scientists across the DOE complex, in academia and industry. The objective is to develop a prioritized listing of advanced experimental battery materials that are under development in the Vehicle Technologies Office program or by a university or industrial battery material research program. Process R&D will be run to identify and develop preferred pathways for synthesis of the new materials. The selected pathway is characterized by straightforward adaptation into industrial scale process. The selected synthesis scheme will be validated to assure process reproducibility and finally applied to scaled-up synthesis of 1-10 kg material in a single batch. Sample of the materials will be distributed both to interested companies for evaluation and to researchers for continued R&D. Feedback will be solicited and data collected to build a database of the material performance in various applications. Technology Transfer Package containing detailed description of the process and engineering data will be provided to interested companies for cost modeling of full scale production. The materials under consideration for scale up are listed on Figure IV-274.
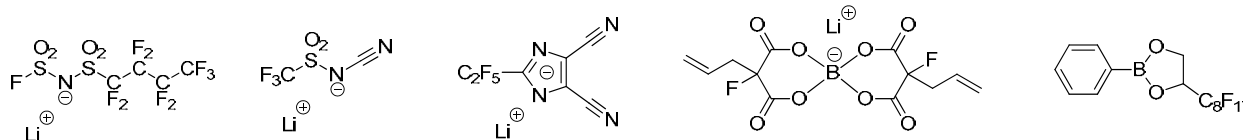

Figure IV-274: Materials under consideration for future scale up

- Argonne staff will evaluate emerging manufacturing technologies for the production and processing of advanced critical materials. Materials manufacturers typically use traditional batch synthesis techniques, such as stirred tank reactors which have changed little over the past 100 years, inhibiting the development of continuous production processes. New systems for continuous material manufacturing and other green processing techniques are being developed that promise higher levels of safety, improved material performance and/or lower production costs. This task includes an evaluation of the emerging manufacturing technology and determination of potential performance and cost benefits. Scalability will also be assessed. Flow reactors are also central to the 12 principles of green chemistry and engineering, enabling sustainable chemical reactions and production by minimizing waste and hazardous substances, reducing the risk to human health and the environment, enabling lower production costs and constant product quality.

- Workforce Development and Education. MERF will initiate collaboration with academia to help train, inspire and prepare the next generation of scientists and engineers on process R&D and scale up and emerging manufacturing technologies. Process R&D and scale-up is typically learned on the job, not at a university. We will select and host a university graduate student who has been working on bench scale research of energy storage materials at their university. They will work hands-on alongside MERF's highly experienced process engineers and learn how to do the process R&D, scale and synthesize material which is of interest to DOE. Materials produced would then be made available to the DOE research community, as well as the student's home university.

Technical Discussion

Background

Advanced battery materials are primarily synthesized in small batches by discovery scientists who produce gram quantities of substances. High quality, uniform materials in quantity sufficient for thorough investigation cannot be generated using bench-scale procedures as the procedures are labor intense, time-consuming, and unsuited for larger scale. In addition, bench-scale processes are often un-optimized, not validated, and generate materials with inconsistent purity and yield. A suitable process R&D and scale-up facility is required to

consistently manufacture quantities of new materials that allow for prototyping and thorough evaluation, all of which is required prior to commercialization.

Introduction

Researchers in the battery materials programs across the DOE complex commonly depict scale up as the synthesis of gram quantities of battery materials, and often combine multiple time consuming, small-scale runs. Purity and impurity profiles typically vary from batch-to-batch, making the materials and the process unsuitable for independent validation. There is a need for scalable synthetic processes of battery materials (primarily lithium-ion based batteries) to supply kilogram and tens-of-kilogram quantities at DOE labs. This allows for full scale evaluation, supports further research, and assists the transition of these technologies to industry. Prior to MERF, there was no such capability or program across the DOE complex that would accelerate the transition of new materials and technologies from discovery stage to high-volume manufacturing.

Argonne's Material Engineering Research Facility is equipped and staffed to take on a task of process R&D and scale-up of new advanced battery materials.

Approach

A formal approach to process R&D and scale-up of advanced battery materials has been defined. This approach starts with the initial discovery of a new material and an initial electrochemical evaluation. This determines if the material is to be added to the inventory database, ranked and prioritized. At this point, the scale-up process begins with a feasibility study, followed by proof of concept testing, 1st stage scale-up and final 2nd scale scale-up. Go/No Go decisions are located after feasibility determination and electrochemical validation testing.

For each material, we will develop a scalable manufacturing process, analytical methods and quality control procedures. We will also prepare a "technology transfer package" which will include:

- Summary of the original process used by discovery researchers to synthesize the material.
- Summary of the scalable (revised) process suitable for large scale manufacturing.
- Detailed procedure of the revised process for material synthesis.
- Analytical data/Certificate of Analysis for the material (chemical identity and purity).
- The material impurity profile.
- Electrochemical performance test data.
- Preliminary estimates of production cost.
- SDS for the material.
- Material specifications.

We will apply the newly developed process to make kilogram quantities of the material. We will fully characterize chemically each material and make samples available for industrial evaluation and to the research community. We will also provide feedback to discovery chemist helping guide future research.

Results

1. Process R&D and Scale-Up of ORNL- Li-BMFMB (completed)

ORNL- Li-BMFMB (lithium bis(2-fluoro-2-methylmalonoborate) or lithium 3,9-difluoro-3,9-dimethyl-2,4,8,10-tetraoxo-1,5,7,11-tetraoxa-6-boraspiro[5.5]undecan-6-uide) is a lithium salt invented at ORNL (Chem. Commun., 2015, 51, 9817). The material, due to its high thermal stability is considered an attractive alternative to commonly use but less stable lithium hexafluorophosphate.

The original synthesis procedure used by the inventors comprises several steps and required hazardous materials and conditions. The process required alkali metal (sodium) reacts with ethanol that liberates hydrogen gas. Also, large amount of concentrated hydrochloric acid was used as well as water-reactive chloroorganic auxiliary reagent (chlorotrimethylsilane).

The long, complex synthesis pathway and associated high hazard made the original procedure impractical. MERF undertook process R&D and developed a modified procedure for the synthesis of ORNL - Li-BMFMB. The new scheme (Figure IV-275) mitigates or completely eliminates the problematic steps from the original process, reducing the number of synthetic steps by 33%.
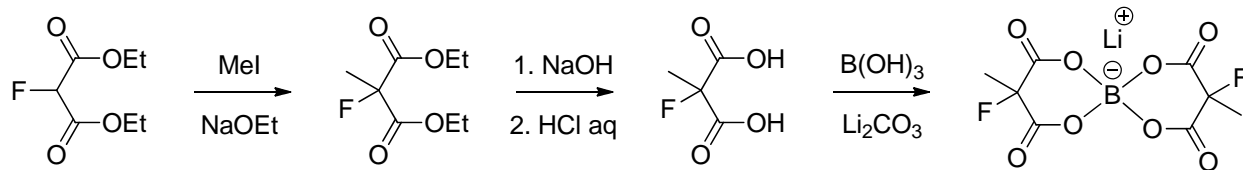

Figure IV-275: Improved synthesis scheme for ORNL - Li-BMFMB

No alkali metal, concentrated acid or water-reactive reagent were used in the modified procedure. MERF's procedure was piloted in 100 g scale. The material was fully characterized and samples are available by request.

2. Process R&D and Scale-Up of TFPC (completed)

TFPC (3,3,3-trifluoropropylene carbonate or 4-(trifluoromethyl)-1,3-dioxolan-2-one) is a partially fluorinated cyclic carbonate that imparts higher temperature and voltage stability. The float test at 4.9 V to 5.2 V (room temperature and 55°C) of 0.5 M LiPF6 in a mixture of TFPC and methyl 2,2,2-trifluoroethyl carbonate revealed decrease in current leakage compared to ethylene carbonate/2,2,2-trifluoroethyl carbonate solvents blend (Meinan He et. al. J. Electrochem. Soc. 2015; 162: A1725-A1729).

The material is currently available only by custom synthesis request in small batches of uncertain purity. Several researches in the battery community expressed an interest in battery grade material. MERF undertook the task to develop the process and produce sufficient amount of a uniform high purity materials.

Literature procedures to synthesize the material in a small scale frequently call for highly toxic phosgene as a source of carbonyl moiety and cyclization reagent. MERF developed an alternative route to synthesize TFPC in order to avoid the hazards associated with phosgene in a large scale (Figure IV-276). An additional benefit of the new scheme is the elimination of organic chlorinated reagents that makes the process environmental friendly. Imidazole, the only by-product of the reaction can be almost quantitatively recovered and recycled.
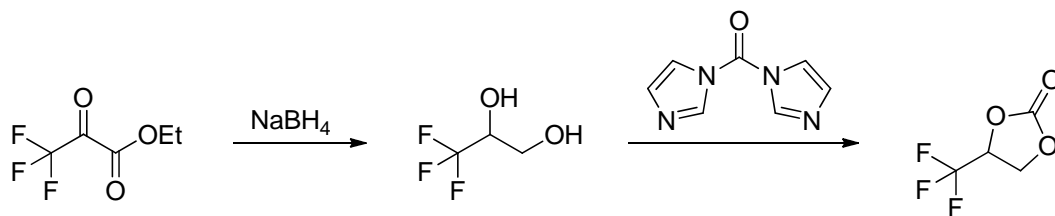

Figure IV-276: MERF's modified process for synthesis of TFPC

A pilot run of the new process produced over 100 g of the material with purity greater than 99.5%. Samples of the material (total 50 g) were provided to researchers.

3. Process R&D and Scale-Up of GCMC (completed)

GCMC (glycerol carbonate methyl carbonate or methyl ((2-oxo-1,3-dioxolan-4-yl)methyl) carbonate) is a derivative of glycerol bearing both cyclic and linear carbonate in the molecule. The parent triol (glycerol) can be obtained from renewable sources that makes GCMC an attractive alternative to fully synthetic compounds derived from petroleum.

It has been demonstrated that GCMC addition to certain electrolyte formulation improves capacity retention of the cell (Figure IV-277, a). More recently, the additive revealed promising results in 4.9 to 5.2 V current leakage test at 0.5% w/w level (Figure IV-277, b).
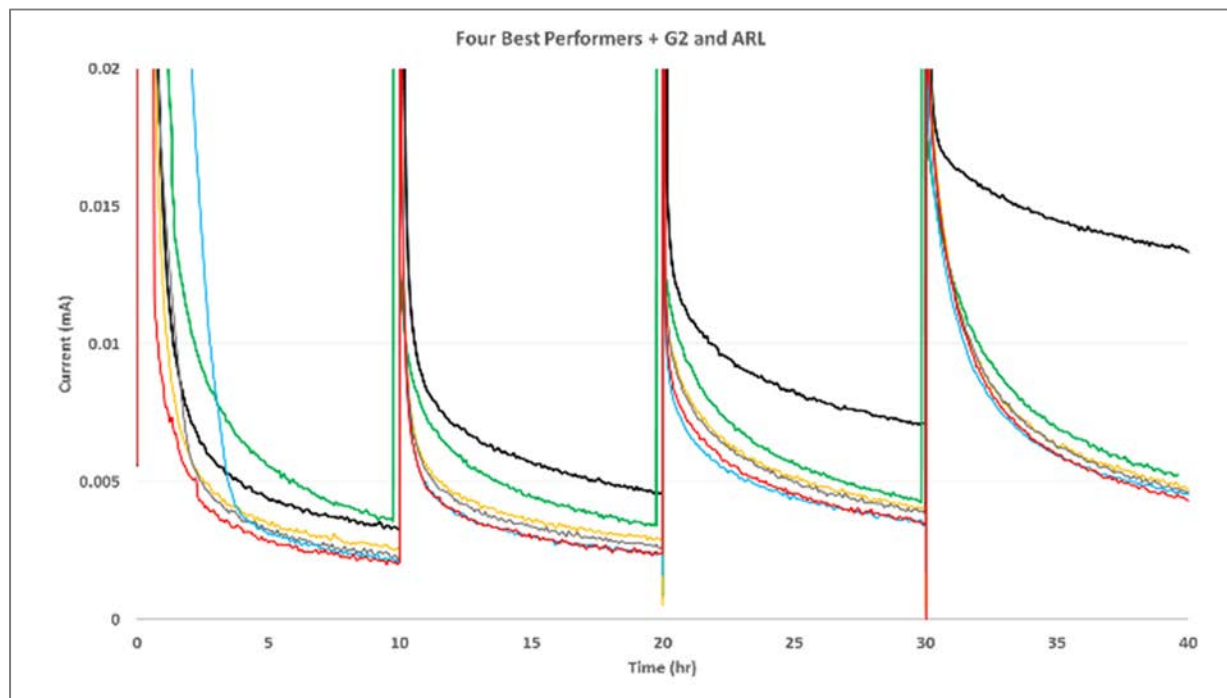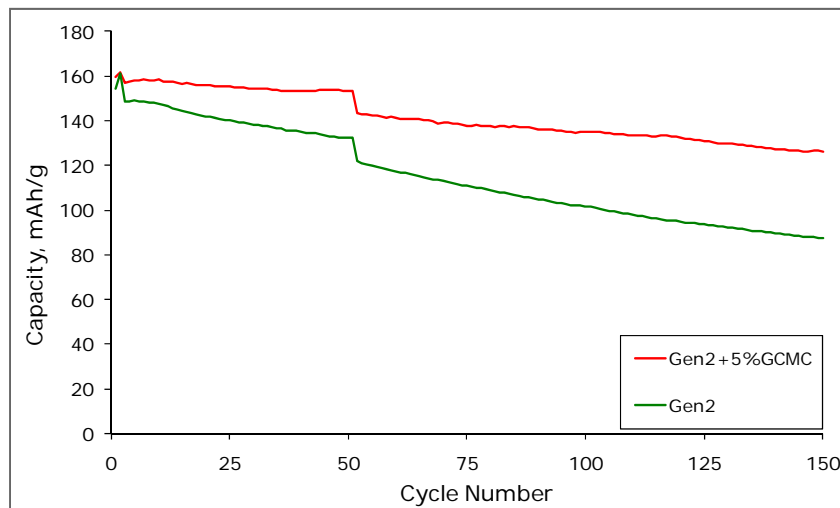
Figure IV-277: Effect of GCMC additive (upper) improved capacity retention and (lower) mitigate current leakage (red line on the plot)
Caption Credits/Source: (a) D. Abraham et al. (ANL), unpublished, 2010, (b) K. Xu et al. (ARL), 2016

The material is typically synthesized by reaction of glycerol carbonate (the compound bearing cyclic carbonate moiety and primary hydroxyl group) with methyl chloroformate in the presence of hydrogen chloride scavengers, typically tertiary amines like triethylamine or pyridine. This route requires an aqueous work-up of the post-reaction mixture to remove byproducts and the excess tertiary amine. The process generates

substantial amount of toxic waste. The reaction is frequently carried out in chlorinated solvent that contributes to an overall negative impact on the environment.

The key raw material for the reaction, glycerol carbonate, is available only as a low purity technical grade. The impurities are carried over in the process and therefore the material requires elaborate purification before it can be used as an electrolyte additive.

MERF developed a proprietary process for manufacturing high purity material (>99.9%) without the need for the non-scalable sublimation step typically used in a small-scale purification of GCMC (Figure IV-278). The new process eliminates aqueous wash-up step and minimize toxic waste. The test run of the process yielded 300 g of the material in a single batch. Samples were distributed to support further research.
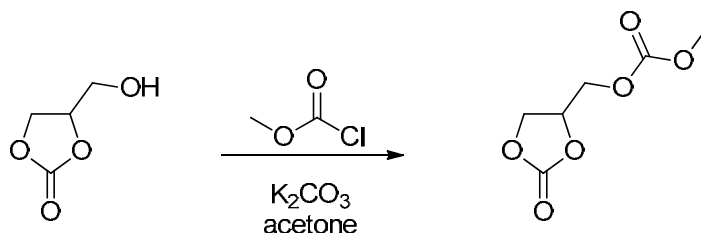
Figure IV-278: Synthesis scheme for GCMC

4. Scale-Up of LBNL-PPy (completed)

LBNL-PPyE is a copolymer of methacrylic acid 1-pyrenemethanol ester and methacrylic acid trietyleneglycol monomethyl ether. LBNL-PPy is a homopolymer of methacrylic acid 1-pyrenemethanol ester. Both materials were invented in LBNL and investigated as a conductive binder for silicone-graphite composite anode (Figure IV-279).
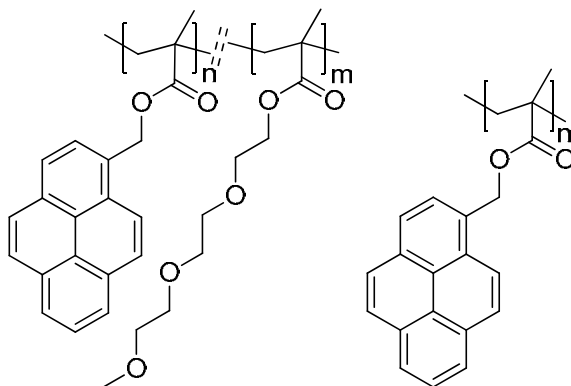
Figure IV-279: Structure of LBNL-PPyE and LBNL-PPy, respectively

We described the scale-up synthesis of LBNL-PPyE and silicon nanoparticle coating with the material for manufacturing of anode laminates (the laminates were made by Argonne's CAMP facility) in the previous reporting period. The investigation of the two materials, LBNL-PPyE and LBNL-PPy, is ongoing and there was a request for an additional amount of LBNL-PPy.

The material is made in two-step process starting with the synthesis of the monomer following free-radical polymerization (Figure IV-280).

Figure IV-280: Synthesis route to LBNL-PPy

MERF successfully synthesized LBNL-PPy and samples were provided to Argonne's CAMP facility (17g) and to LBNL (5g).

5. Materials licensed to Strem Chemicals and Sigma Aldrich

Nine materials scaled up by MERF were licensed to Strem Chemicals and three materials to Sigma-Aldrich for manufacturing and distribution for R&D use.

MERF provided the manufacturers with comprehensive Technology Transfer Packages for each material. The packages contain detailed synthesis procedures, process schematics, material mass balances, product physicochemical characterization, analytical and quality control methods and data. The detailed documentations enabled rapid deployment of the new materials to manufacturers' production pipeline. Figure IV-281 lists materials licensed to Stream Chemicals (RS21, RS5, 1S1M3, 1NM2, RS51, RS6, 1NM3, 2SM3, RS2) and to Sigma-Aldrich (1NM3, 2SM3, RS2).
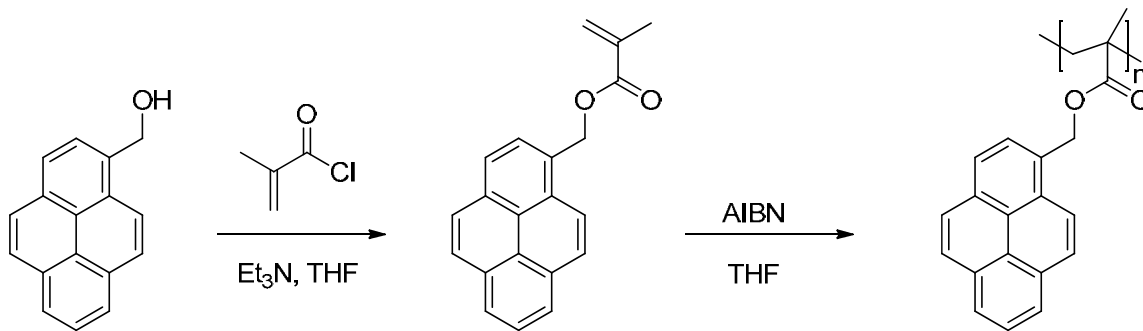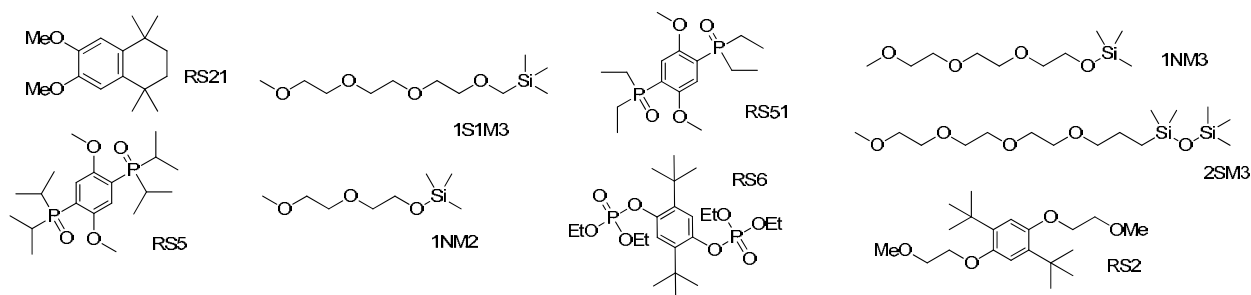

Figure IV-281: Materials licensed to Strem Chemicals and Sigma-Aldrich

6. Investigation of physicochemical properties and electrochemical performance of scaled-up materials to support basic research

We investigate basic physicochemical properties (density, viscosity, flash point, ability to dissolve salts) and electrochemical performance of selected materials scaled up at MERF ant their blends with other electrolyte materials.

In the last reporting period, we presented our research on LiFSI synthesis, specification development and impurity profile vs. electrochemical performance investigation. In this reporting period, we extended the research to comparative study of electrochemical performance of LiFSI based vs. LiPF$_6$ based electrolytes. The study was conducted in collaboration with Argonne's CSE Division. We compared cycling behavior of NCM523//silicon-graphite 20 mAh pouch cells (fabricated at Argonne's CAMP facility) with baseline (Gen2+ 10% w/w FEC) and the alternative electrolyte formulations.
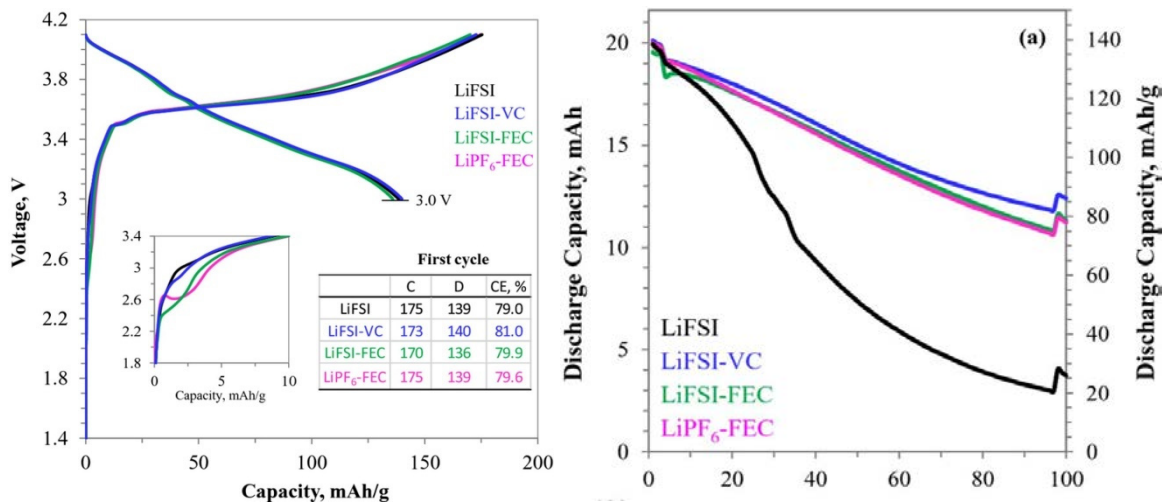
Figure IV-282: Capacity vs. voltage and capacity vs. cycle number for NCM523//Si-graphite pouch cells

In our study, the performance of LiFSI-FEC and LiPF$_6$-FEC cells are very similar indicating that the electrolyte salts play a much smaller role in performance degradation than the electrolyte solvent (Figure IV-282).

In a follow up investigation, we used electrolytes formulated from LiPF$_6$ and blends of non-fluorinated and fluorinated carbonate solvents scaled up at MERF. The objective of this study was to assess effect of solvent(s) on performance of NCM523//silicon-graphite electrodes pair. The study was conducted using coin cell format. Over 20 different electrolyte formulation, all based on LiPF$_6$ were produced and investigated to compare C-rate, capacity fade rate and cell impedance against baseline electrolyte (Gen2 + 10%w/w FEC).

We found out that the 2/8 w/w FEC/FEMC (fluoroethylene carbonate/methyl 2,2,2-trifluoroethyl carbonate) formulation provides slightly better capacity as well as lower initial (after forming cycles) and final (after 100 cycles) cell impedance compared to baseline electrolyte (Figure IV-283)

Figure IV-283: Capacity retention vs. cycle number and discharge impedance vs. voltage for NCM523//Si-graphite coin cells

In yet another study we evaluated effect of mixed-salts electrolytes in fluorinated carbonate solvents scaled up at MERF. Electrolytes based on LiPF$_6$, LiFSI, LiTFSI and combination thereof were evaluated in NCM523//silicone-graphite coin cells. Our study revealed that LiFSI in FEC/FEMC formulation provides slightly better capacity as well as lower initial (after forming cycles) and final (after 100 cycles) cell impedance compared to LiPF$_6$ based electrolyte (Figure IV-284).
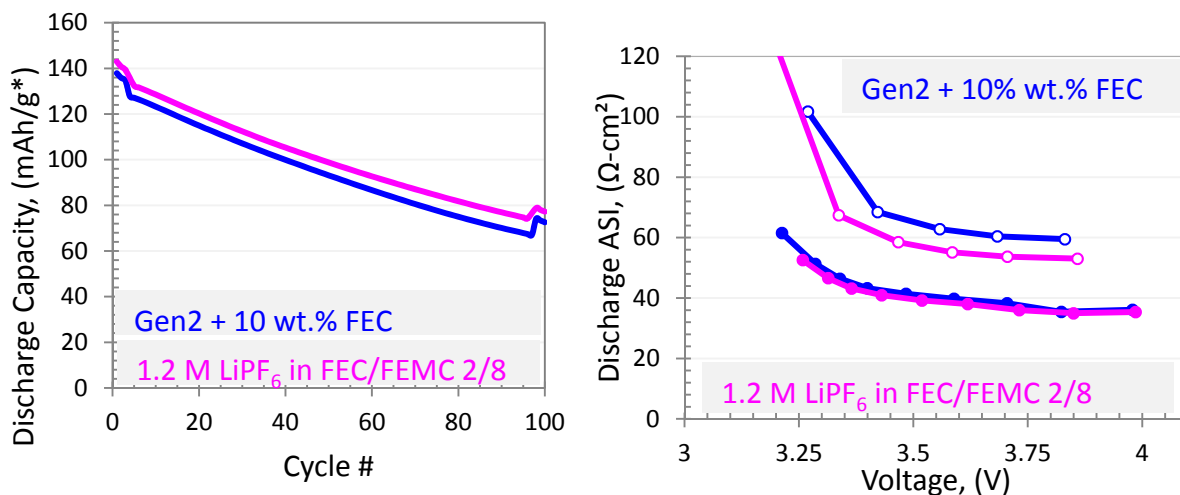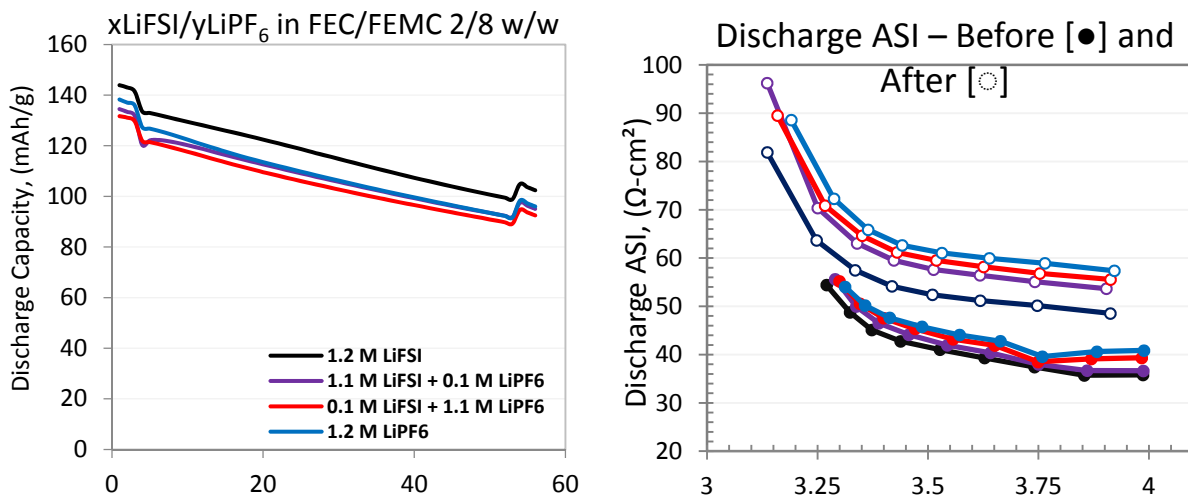
Figure IV-284: Capacity retention vs. cycle number and discharge impedance vs. voltage for NCM523//Si-graphite coin cells

7. Binder for advanced anode for Lithium-ion cell (project in progress)

Polymers with dynamic hydrogen bonds are known to exhibit "self-healing" properties, and have previously been reported as superior binders for Si microparticle anodes. We are investigating a series of copolymers with varying molar ratios of acrylamide, N-substituted acrylamides, and acrylic acids incorporated into the polymer chain (Figure IV-285). It is hypothesized that these copolymers will exhibit the self-healing capability of dynamic intra- and intermolecular hydrogen bonds expanding and contracting supramolecular structures thereby maintaining mechanical and electrical connections between the silicon particles of the anode during lithiation/delithiation cycles.

$R^1, R^2 =$ H, Alk, Ar, N-het, O-het, $CONR_2$, NR^3R^4

$R^3, R^4 =$ H, Alk, COAlk, COAr, $CONR_2$

hydrogen bond donors and acceptors sites
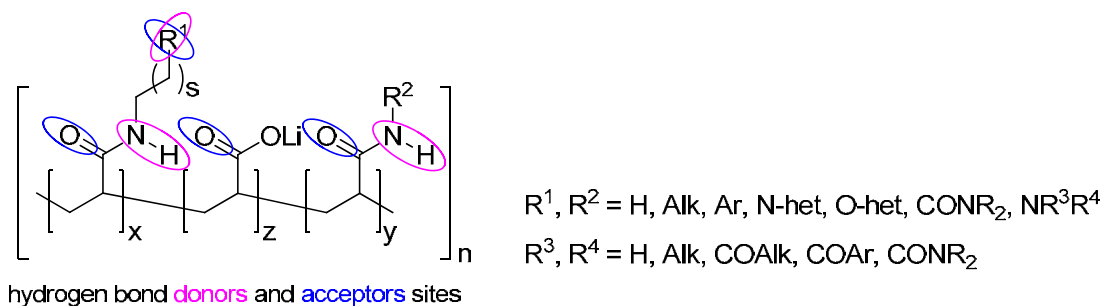
Figure IV-285: A schematic representation of a copolymer made up of three different monomers, showing potential incorporation of hydrogen bond donor/acceptor functional groups

A number of copolymer binders have been investigated in this first year of this project. Through a systematic variation of the monomer ratios and molecular weights, we are building a library of polymer binders which will then be tested in a number of ways to determine their effectiveness as binders for producing silicon anode laminates that are stable and maintain high capacity during extended cycling (Figure IV-286and Table IV-40).

m:n is the molar ratio of acrylamide (AAM) to N-[3-(Dimethylamino)propyl] acrylamide (DMAPA)
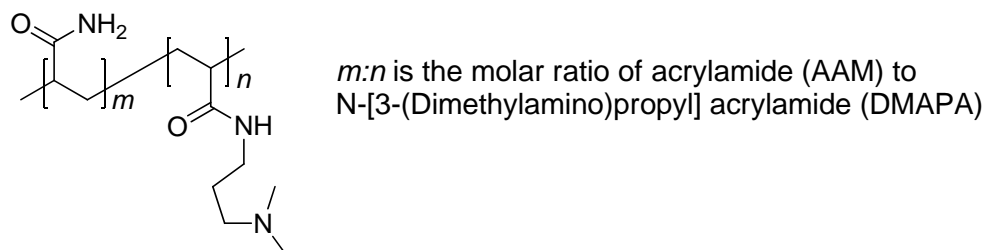
Figure IV-286: Poly(acrylamide-co-N-[3-(dimethylamino)propyl]acrylamide)

Table IV-40: Poly(acrylamide-co-N-[3-(dimethylamino)propyl]acrylamide) Synthesized

Entry	AAM, m (feed/product)	DMAPA, n (feed/product)	Target Mw (kDa)	Yield, %	Water or NMP Soluble?
1	0.943/-	0.057/-	25	98.9	No
2	0.975/-	0.025/-	23	122	No
3	0.985/-	0.015/-	22	84.0	No
4	0.995/-	0.005/-	22	101	No
5	0.997/-	0.003/-	22	124	No
6	0.999/-	0.001/-	22	127	No
7	0.696/0.706	0.304/0.294	8.1	87.1	
8	0.685/0.695	0.315/0.305	19	To be determined	Yes
9	0.506/0.494	0.494/0.502	20	To be determined	Yes
10	0.907/0.906	0.093/0.094	8.8	69.6	Yes
11	0.949/0.948	0.051/0.052	11	81.7	Yes
12	0.988/0.980	0.012/0.020	9.9	91.5	Yes
13	0.994/0.996	0.006/0.004	9.7	82.8	Yes
14	0.998/0.997	0.002/0.003	15	86.8	Yes

The use of poly(acrylamide-co-N-[3-(dimethylamino)propyl]acrylamide) as binder in anode laminates comprising 15% Si, 73% graphite, 10% binder, and 2% carbon black results in anodes that can be cycled repeatedly, but with lower initial capacities and faster capacity fade than the baseline CAMP silicon-graphite composite anode (partially lithiated poly(acrylic acid) is used as a binder in baseline anode). Polymer binders with lower percentages of acrylamide are currently being synthesized, and will be used to prepare anode laminates for evaluation in half-cell format. Capacity retention and coulombic efficiency vs. cycle number for electrodes with selected copolymer binders are shown on Figure IV-287.
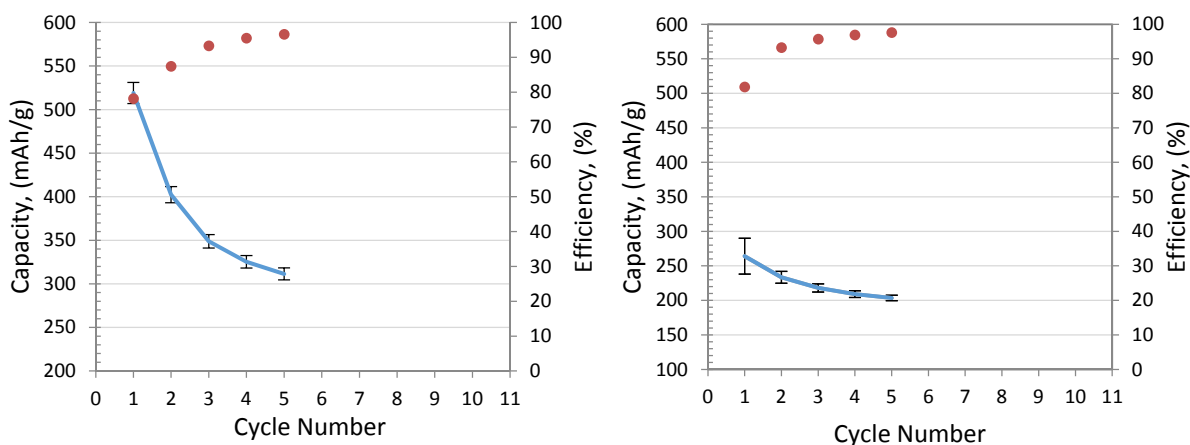
Figure IV-287: Capacity retention and efficiency vs. cycle number for cell with binder from (a) entry 10 and (b) entry 13

We are currently looking at expanding set of co-monomers to produce co-polymers with desirable properties.

8. Scale-up of LFO, lithium iron oxide (project in progress)

The material, Li_5FeO_4, is a sacrificial lithium source additive that was invented, investigated and subsequently requested to scale up by Argonne's CSE Division (Journal of Power Sources, 324 (2016), 150-157).

The material is made via solid state synthesis by step-wise heating in temperature range from room to 450°C following by heating to 600°C and rest for prolonged time at 800°C. The material was originally (CSE) made in a small scale using horizontal tube furnace from lithium hydroxide and iron(III) oxide (Figure IV-288). The question that needs to be addressed before large scale synthesis is a need for mixing during the process to achieve mass transfer required for uniformity of the material.

$$10 \; LiOH \cdot H_2O \; + \; Fe_2O_3 \longrightarrow 2 \; Li_5FeO_4 \; + \; 15 \; H_2O$$
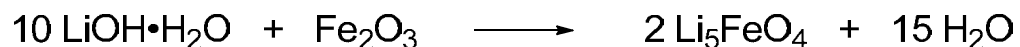
Figure IV-288: Chemical equation for the synthesis of LFO

Several reactions have been run at MERF using large bore vertical tube furnace to optimize condition and validate reproducibility (Figure IV-289, a).

Samples of the material made at MERF was provided to CSE for evaluation. XRD analysis revealed that he material is phase pure (Figure IV-289, b) but still not electrochemically optimized.
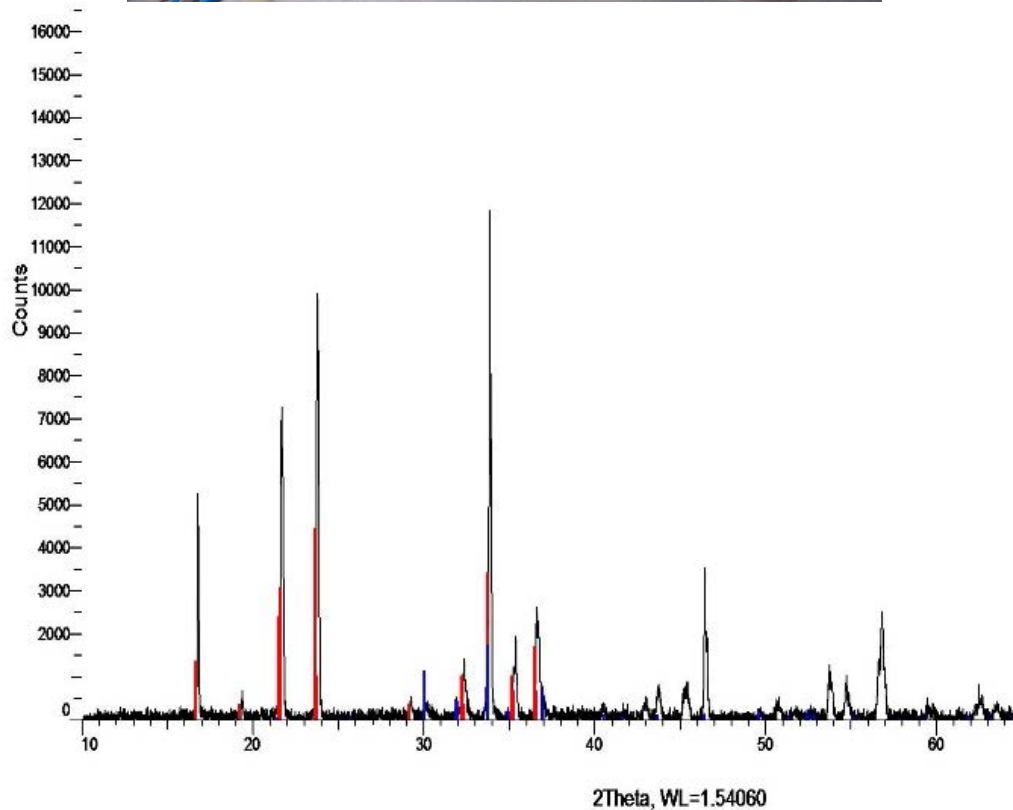
Figure IV-289: (above) Large bore vertical tube furnace for the synthesis of LFO at MERF and (below) overlapped XRD of the original LFO sample and material produced at MERF

MERF continues work on developing process for large scale synthesis of uniform, high quality LFO.

Conclusions

MERF's materials process R&D and scale-up program assists the battery research community and allows for a comprehensive evaluation of new materials by several independent laboratories.

In FY16, process R&D and the scale-up work were completed and technology transfer packages for three materials were created. Samples of the materials were distributed for further evaluation and to support basic research. Additional amount of LBNL 3rd generation conductive binder for advanced anode (LBNL-PPy) was synthesized and provided to researches (Argonne's CAMP and LBNL) for electrode manufacturing optimization. Over 120 samples of uniform, high quality experimental battery materials have been provided to researches since the program inception.

MERF targets 3-5 electrolyte materials for scale-up in FY17. Materials from DOE National Laboratories, Army Lab Research, universities and other organizations are all under evaluation.

MERF contributes to Advanced Anode Program by designing, synthesizing, electrode manufacturing and evaluating new class of binder for composite anode materials. MERF's ability for rapid synthesis and evaluation of large number of materials permits for developing structure - properties database. Such a database will allow for better understanding of performance binder requirements and assists in rationale design of a new material. MERF synthetized and evaluate 14 new materials for the program in FY16.

Evaluate emerging manufacturing technologies such as flow reactors, sonochemistry, microwave assisted reactions or reactive distillations to improve product quality while lowering manufacturing costs are all under consideration. MERF recently acquired customized Syrris ASIA320 flow reactor to develop expedient manufacturing processes by improving safety, minimize waste stream and lower material cost.

Products

Presentations/Publications/Patents

1. Restricting the Solubility of Polysulfides in Li-S Batteries Via Electrolyte Salt Selection. Chen, Junzheng; Han, Kee Sung; Henderson, Wesley A.; Lau, Kah Chun; Vijayakumar, Murugesan; Dzwiniel, Trevor; Pan, Huilin; Curtiss, Larry A.; Xiao, Jie; Mueller, Karl T.; et al. Advanced Energy Materials (2016), 6(11), 1600160.

2. Allotropic Control: How Certain Fluorinated Carbonate Electrolytes Protect Aluminum Current Collectors by Promoting the Formation of Insoluble Coordination Polymers. Shkrob, Ilya A.; Pupek, Krzysztof Z.; Abraham, Daniel P. Journal of Physical Chemistry C (2016), 120(33), 18435-18444.

3. Spontaneous Aggregation Of Lithium Ion Coordination Polymers In Fluorinated Electrolytes For High-Voltage Batteries. Malliakas, Christos D.; Leung, Kevin; Pupek, Krzysztof Z.; Shkrob, Ilya A.; Abraham, Daniel P. Physical Chemistry Chemical Physics (2016), 18(16), 10846-10849.

4. Performance of Full Cells Containing Carbonate-Based LiFSI Electrolytes And Silicon-Graphite Negative Electrodes. Trask, Stephen E.; Pupek, Krzysztof Z.; Gilbert, James A.; Klett, Matilda; Polzin, Bryant J.; Jansen, Andrew N. Abraham, Daniel P. Journal of the Electrochemical Society (2016), 163(3), A345-A350.

5. "Exploring Cycling Behavior of NMC532//Gr-Si Cell in Fluorinated Carbonates Electrolytes" Krzysztof Pupek, T.L. Dzwiniel, G.K. Krumdick, 229th ECS Meeting (May 29 - June 3, 2016), oral presentation.

6. "Graphite-Si Based Cell Performance in Alternative Electrolytes" Trevor Dzwiniel, Krzysztof Pupek, Gregory Krumdick, Daniel Abraham. International Meeting on Lithium Ion Batteries. Chicago, IL, June 19-22, 2016, poster presentation.

7. Process For The Production Of Low Flammability Electrolyte Solvents, Krumdick; Gregory K., Pupek; Krzysztof, Dzwiniel; Trevor L. US 9,263,769 February 16, 2016.

8. Manufacture of High Voltage Redox Shuttles For Lithium-Ion Secondary Batteries To Prevent Malfunction. Krumdick, Gregory K.; Dzwiniel, Trevor L.; Pupek, Krzysztof. U.S. Pat. Appl. Publ. (2015), US 20150221982 A1 20150806.

9. Process for Catalytically Silylating A Glycol With A Disilazane To Produce Low Flammability Electrolyte Solvents For Lithium Ion Secondary Batteries. Krumdick, Gregory K.; Pupek, Krzysztof; Dzwiniel, Trevor L. U.S. Pat. Appl. Publ. (2015), US 20150318574 A1 20151105.

10. ANL-IN-15-015 "Process for The Production of High Voltage Electrolyte Solvents For Lithium-ion Batteries" Trevor Dzwiniel, Krzysztof Pupek, and Gregory Krumdick, filed 9-12-2016.

11. ANL-IN-15-018 "Fluorinated Electrolyte Solvent" Trevor Dzwiniel, Krzysztof Pupek, and Gregory Krumdick, filed 9-20-2016.
12. ANL-IN-16-047 "Improved And Practical Process For The Synthesis Of Lithium Bis (2-Methyl-2 Fluoromalonato)Borate (LiBMFMB)" Trevor Dzwiniel, Krzysztof Pupek, and Gregory Krumdick, filed 9-22-2016.

IV.E.3. Electrode Coating Defect Analysis and Processing NDE for High-Energy Lithium-Ion Batteries (ORNL)

David L. Wood III, Principal Investigator
Oak Ridge National Laboratory
One Bethel Valley Road
P.O. Box 2008, MS 6065
Oak Ridge, TN 37831-6065
Phone: 865-574-1157
E-mail: wooddl@onrl.gov

Peter Faguy, DOE Program Manager
U.S. Department of Energy
Vehicle Technologies Office
1000 Independence Avenue, SW
Washington, DC 20585
Phone: 202-586-1022
E-mail: Peter.Faguy@ee.doe.gov

Start Date: October 1, 2014
End Date: September 30, 2019

Abstract

Objectives

- Reduce lithium-ion battery system cost by implementing in-line non-destructive evaluation (NDE) and electrode quality control (QC).

- Quantify the impact of different types of defects on rate performance and cycle life of full NMC-graphite cells.

- Develop a mechanistic understanding of cell failure by combining materials characterization with multi-physics models.

- Leverage NREL FCTO funds on fuel cell component in-line NDE with ORNL VTO funds on battery electrode in-line NDE.

- Measure electrode porosity in-line using thermal excitation and associated IR emissivity (ORNL/NREL).

- Determine electrode thickness or areal weight uniformity across and down the web using active IR thermography (ORNL/NREL).

Accomplishments

- Developed methods to introduce intentionally different electrode coating defects such as pinholes, blisters, large agglomerates, divots, and metal particle contaminants.

- Evaluated the impact of different coating defects on long-term capacity fade for full NMC-graphite cells in both coin cell and pouch cell formats.

- Re-installed in-line optical laser thickness measurement (at oven inlet) and IR thermography (at oven outlet) on ORNL slot-die coating line for routine electrode QC.

- Collaborated with NREL on establishing a method for measuring electrode porosity in-line based on thermal and structural properties.
  - Investigated the impact of electrode loading, thickness, and particle size systematically using 11 different coatings.

- Evaluated the impact of different line speeds between 2 and 10 ft/min.
- Compared active heating (using an IR heater) and passive heating (using the residual heat from the drying oven or calendering machine).

Future Achievements

- Relate various electrode manufacturing defects to the mechanism(s) of cell failure.
  - Characterize the impact of defects using electrochemical methods including evaluation of cycle life, rate capability, leakage current, and EIS.
  - Analyze cycled cells using microstructural characterization tools such as SEM and X-ray tomography.
- Develop multi-physics models to clarify the impact of defects on cell performance and compare with experimental results.
- Collaborate with battery makers for QC technology and feedback loop development.
- Refine model used to measure electrode porosity from thermal response.
  - Generate calibration curves.
  - Incorporate the impact of line speed, active material particle size, and electrode calendering.

Technical Discussion

Background

Quality control during the production of lithium-ion secondary cells is critical to maximize performance, reduce scrap rates, and improve safety.[1-4] Often flaws in the electrodes are not detected until formation cycling when the entire series of value-added manufacturing steps have been completed. The scrap rate of defective cells drive the costs of lithium secondary cells to an unacceptable level.[5] If electrode flaws and contaminants could be detected in-line near the particular processing steps that generate them, then the electrode material could be marked as unusable and the processing equipment could be adjusted to eliminate the defects more quickly. These in-line methods have been used effectively in other industries such as photovoltaic, flexible electronics, and semiconductor manufacturing. However, the equipment and measurement methods must be tailored for lithium secondary cell production.

Introduction

Capacity and cycle life of lithium-ion batteries (LIBs) depends strongly on the quality of the electrode coating. Reducing variability and flaws in electrode coatings will lead directly to improved battery durability and lower overall cost.[6] The electrode parameters that must be monitored and controlled are areal loading, thickness (or porosity), and uniformity. Currently, most electrode QC relies on beta transmission gauges to measure the electrode loading. While beta transmission gauges can measure loading accurately, they have high capital cost and pose ionizing radiation hazards. The goals of this program, therefore, are to develop a set of safe, inexpensive, in-line methods to monitor critical electrode properties and detect flaws.

Approach

ORNL has investigated several in-line analysis methods (FY12-15) such as:

1) Optical laser thickness sensing for improved homogeneity across and down the web.
2) Thermal IR imaging for detection of electrode inhomogeneity and coating defects.
3) Active IR thermography with incident IR heating to measure porosity in-line through thermal diffusivity modeling (collaboration with NREL).
4) Optical reflectance for identifying surface coating defects (collaboration with NREL).
5) X-ray fluorescence spectroscopy (XRF) for electrode transition-metal composition and areal weight uniformity (collaboration with NREL).

In order to develop effective methods for detecting electrode flaws, it is important to understand which types of defects have the most negative impact on cell performance. Our approach is to create different types of defects in NMC 532 cathode coatings intentionally. Defects include pinholes, blisters, large agglomerates, divots, and metal particle contaminants. In FY15 we completed our investigation of defective electrodes in full NMC-graphite coin cells. In FY16, we extended this work to study the same types of defects in full 1.5 Ah pouch cells. We analyzed the effect of the different defects on cell rate performance and capacity fade.

Porosity plays a major role in determining the electronic and ionic conductivity of electrodes, and must be optimized for the desired cell performance characteristics. In collaboration with NREL, a low-cost method for in-line porosity measurement based on IR emissivity is being developed. In FY15, proof-of-concept experiments were completed on four different electrodes under stationary conditions or with very low line speed (0.5 ft/min). In FY16, we successfully demonstrated the technique in-line at the oven outlet of the slot die coater at ORNL at line speeds ranging from 2 to 10 ft/min. The impact of electrode loading and particle size were studied systematically using a total of 11 different electrode coatings.

Results

Four different types of electrode defects were introduced intentionally into NMC 532 cathodes: (a) 1 line defect with 3 mm width, (b) 3 line defects with 1 mm width each, (c) pinholes, and (d) agglomerates (Figure IV-290). Line defects represent an extreme example of a non-uniform coating. Pinholes are typically caused by gas bubbles in the slurry, and agglomerates result from inadequate mixing. Agglomerates are clearly visible in the SEM and EDS images of a defective coating (Figure IV-291). Instead of a homogeneous coating, some regions are rich in the NMC active material, while other regions are rich in the carbon black conductive additive. The four types of defective cathodes were assembled into full 1.5 Ah pouch cells with graphite anodes (Figure IV-290).
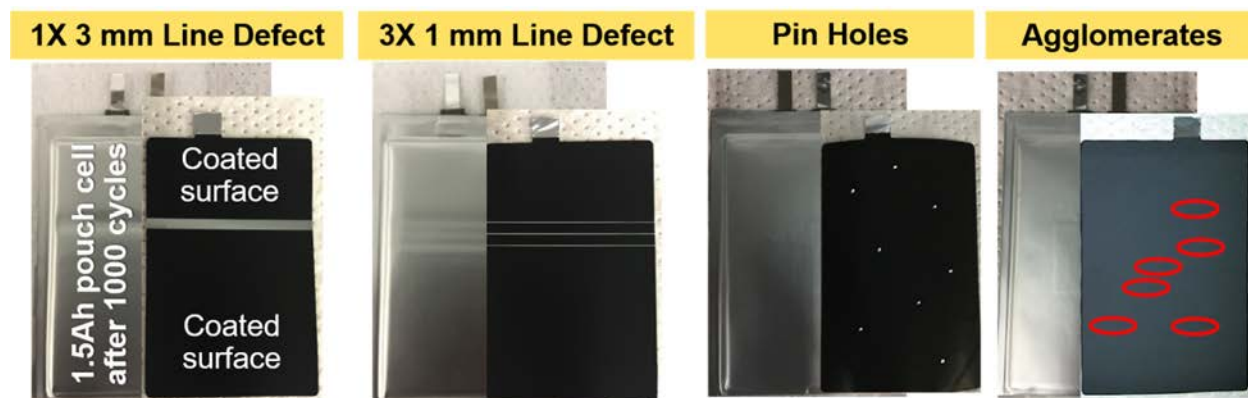
Figure IV-290: NMC 532 cathodes with four different types of defects. Cathodes with each of the different defects were assembled into 1.5 Ah NMC-graphite pouch cells for cycle life testing

1.5 Ah cells with the different defects were cycled at two different C-rates, C/3 and 1C, after formation cycling (Figure IV-292). At both C/3 and 1C rate, the cells with the pinhole defects have the highest initial capacity and best capacity retention. This suggests that small numbers of pinholes may not be detrimental to cell performance. If electrodes with this type of coating defect could still be used, scrap rates could be reduced. In contrast, line defects appear to be the most detrimental to long-term cycling stability. It is important to detect such flaws early in the coating process so that processing conditions can be adjusted.
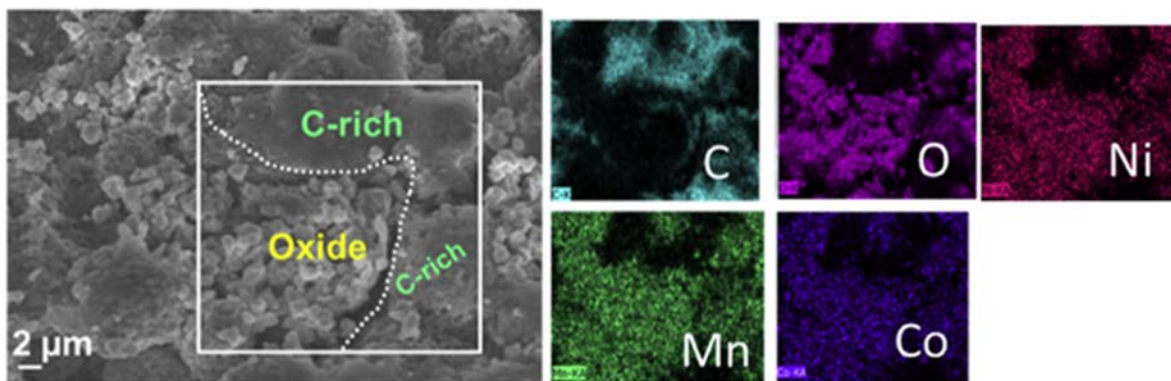
Figure IV-291: SEM micrograph and EDS analysis of the cathode made with agglomerates. Carbon-rich and carbon-poor regions are highlighted
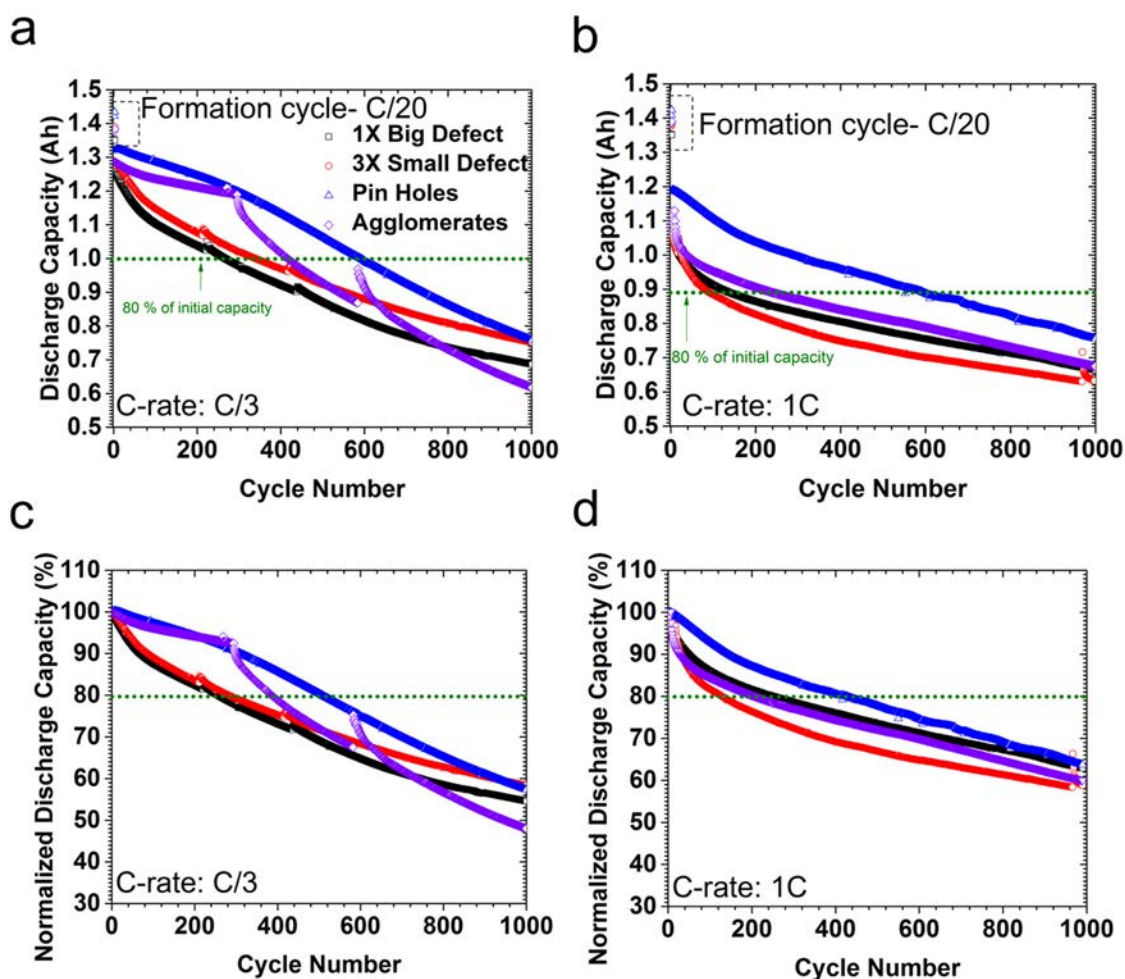
Figure IV-292: Long-term capacity fade for NMC-graphite cells with the four different types of defective cathodes. The discharge capacity in Ah is shown for charge-discharge cycling at (a) C/3 rate and (b) 1C rate. The discharge capacity normalized to the initial capacity is shown for (c) C/3 rate and (d) 1 C rate. The dotted green line shows where 80% of the initial capacity is reached

It is interesting to compare the results from 1.5 Ah pouch cells with earlier results for the same types of defects in coin cells (Figure IV-293). Clearly, dramatic differences between the different types of coating defects were observed in coin cells. Capacity retention varies from 12 to 65% for different defects in coin cells cycled at 2C. In contrast, much less variation for the different defects was measured in the pouch cell experiments. At 1C, all of the cells have around 60% capacity retention. Some of the difference between the two formats can be

explained by the different rates that were used. Coin cells were cycled at very high rate (2C and 5C discharge) whereas pouch cells were cycled at more moderate rates (C/3 and 1C discharge). However, much of the difference in capacity retention between the pouch cell and coin cells is likely due to the large differences in electrode area between the two formats. In pouch cells the defects account for a much smaller fraction of the total electrode area than in coin cells.

Figure IV-293: Comparison of capacity retention (%) for the different types of defects in pouch cells (left) and coin cells (right)

The results presented here clearly show that some types of coating defects are more detrimental to long-term cycling stability than others. To develop insights into the underlying mechanisms that drive cell failure, we plan to characterize the microstructure of cycled, defective cell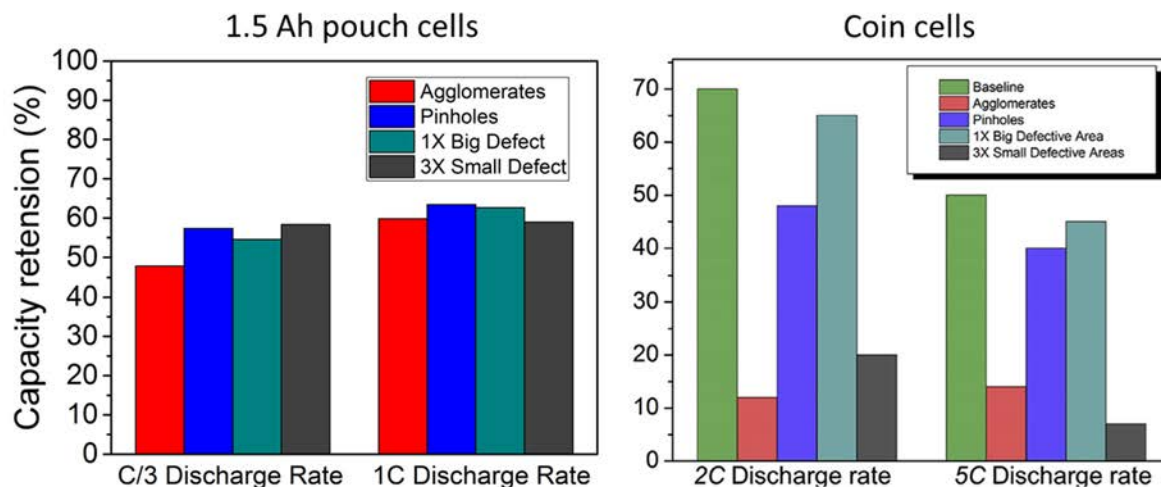s using SEM and X-ray tomography. Further, we plan to correlate these results with multi-physics models that couple the impact of defects on the electrochemical, thermal, and transport properties. We also plan to verify the cycling results presented here with some improvements in the experimental design. The results presented in Figure IV-292 and Figure IV-293 used defective electrodes that were not calendered. Therefore, the capacity fade is expected to be worse than our standard baseline using calendered electrodes. Previously, we experienced difficulties calendering the single-sided electrodes with coating defects, but we have since improved our calendering procedure. We plan to measure leakage current and impedance of defective cells, in addition to cycle life and rate capability.

One very promising approach for monitoring coating properties and detecting defects is IR thermography. Many defects, which are not obvious by visual inspection, are easily detected by IR imaging.[2] In previous annual reports (FY14 and FY15) we showed that IR thermography can be used to monitor electrode loading or porosity. Porosity has been measured in-line at the oven outlet of the slot die coater at ORNL. The Mori-Tanaka model is used to calculate the thermal conductivity of the porous, composite electrodes. In order to develop an accurate model, the impact of several variables must be understood. These include (i) coating thickness, (ii) coating porosity, (iii) active material particle size, (iv) coating line speed, (v) calendered vs. uncalendered electrodes, and (vi) active vs. passive heating. We made significant progress towards understanding how different electrode parameters impact thermal response by measuring 11 different coatings with different loadings, thicknesses, particle sizes, and particle size distributions. Table IV-41 lists the different cathode coatings that have been evaluated to date. In collaboration with NREL, we also made significant progress on understanding the impact of processing variables by measuring several different coatings at line speeds ranging from 2 to 10 ft/min at the slot die coater installed at ORNL. Most of these experiments were performed with active heating, where an IR source is used to increase the temperature of the electrode. Experiments were also undertaken to characterize passive heating, where only the residual heat from the drying oven or calender mill is used.
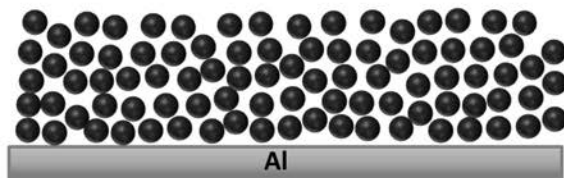
In our earlier models (FY14 and FY15) we assumed that the thermal response was primarily a function of porosity and thickness. To test this hypothesis, we leveraged several electrode coatings generated for AMO (Table IV-41 electrodes 616AMO1-6). These samples were unique in that they all have very similar thicknesses and porosities, but incorporate cathode particles with different sizes of 6 and 12 μm (Figure IV-294). Multi-layer structures were also tested (Table IV-41 electrodes 616AMO3-6). Electrodes with two layers were generated using two different methods, double pass and dual slot die coating (Figure IV-294).

Table IV-41: NMC 532 Coatings Evaluated for in-Line Porosity Measurement

Sample	Loading (mg/cm2)	Thickness (μm)	Notes
5161	6.4	34	
5162	12.3	60	
5163	15.2	78	
616AMO1	25.0	125	All small particles
616AMO2	24.7	119	Mixed particle sizes
616AMO3	26.6	129	Small particles on top, large particles on bottom, 2-pass
616AMO4	24.3	115	Small particles on bottom, large particles on top, 2-pass
616AMO5	25.8	128	Small particles on top, large particles on bottom, dual slot die
616AMO6	25.8	128	Small particles on bottom, large particles on top, dual slot die
NMCNMP2764	27.6	131	
NMCNMP98	9.8	60	

The thermal response of the AMO samples strongly depended on the coating type, despite all samples having similar thickness, loading, and porosity. Consequently, particle size must have a strong impact on the measured signal, most likely due to differences in emissivity and/or thermal conductivity. To describe the AMO coatings, the ability to define multilayer electrodes was added to the model, along with the ability to incorporate variable emissivity and reflectance to match the trends observed in the experiment. Future achievements focus on generating calibration curves, analyzing thermal stability in-line, and quantifying the impact of different line speeds. In addition to active heating, we will continue to works towards using passive heating either after electrode drying or after calendering.

Figure IV-294: Six of the different electrode coatings that are being used to develop the in-line porosity model

Conclusions

Cathodes with four different types of defects (1x 3 mm line defect, 3x 1 mm line defect, pinholes, and agglomerates) were incorporated into 1.5 Ah pouch cells with graphite anodes. Pinholes were found to have the least impact on long-term capacity fade, whereas line defects were found to be the most detrimental. Significant differences in capacity retention were found between defective coatings cycled in pouch cells compared to earlier work 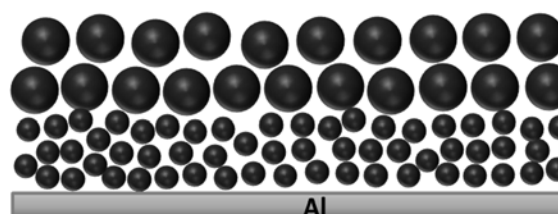in coin cells. Most of the difference is attributed to the large difference in electrode area between the two formats. In coin cells, the defective area makes up a much large fraction of the total electrode area. These results are important to develop appropriate in-line QC and reduce electrode scrap rates.

Significant progress was made in developing IR thermography to monitor electrode porosity. Variables that impact the thermal response of the coatings were studied systematically using 11 different coatings with different thickness, loading, and active material particle size. Particle size was found to have a significant impact on thermal properties, and efforts are currently underway to incorporate these effects into the porous electrode model of thermal conductivity. The impact of line-speed was evaluated by installing the IR heater and camera at the oven outlet of the slot die coater at ORNL. Porosity was measured at line speeds ranging from 2-10 ft/min. This work is highly complementary to our earlier work on in-line measurements of electrode thickness (using laser calipers) and uniformity (using IR imaging). By combining all three non-destructive techniques developed at ORNL, all of the relevant electrode properties can be monitored in-line. Improving coating uniformity will lead directly to improved battery safety, longer cycle life, and lower system-level cost.

Products

Presentations/Publications/Patents

1. Debasish Mohanty, Edward Hockaday, Jianlin Li, Dale Hensley, Claus Daniel, and David Wood, "Effect of electrode manufacturing defects on electrochemical performance in lithium-ion batteries; cognizance of the battery failure sources", Journal of Power Sources, 312 (2016) 70-79.
2. David Wood, Lamuel David, Debasish Mohanty, Jianlin Li, and Claus Daniel, "Performance effects of electrode coating defects and IR thermography NDE for high-energy lithium-ion batteries", The 2016 U.S. Department of Energy (DOE) Fuel Cell Technologies Office (FCTO) and Vehicle

Technologies Office (VTO) Annual Merit Review and Peer Evaluation Meeting (AMR), Washington, DC, June 6-10, 2016.

3. L. David, S. Kalnaus, D. Mohanty, Y. Sheng, J. Li, C. Daniel, and D. L. Wood, "Quantifying the Effect of Lithium-Ion Electrode Manufacturing Defects on Electrochemical Performance," Meet. Abstr. ECS PRiME2016, vol. MA2016–02, no. 6, p. 890, Sep. 2016.

4. B. Sopori, M. Ulsh, P. Rupnowski, G. Bender, M. Penev, J. Li, C. Daniel, and D.L. Wood, III, "Batch and Continuous Methods for Evaluating the Physical and Thermal Properties of Films," Filed March 8th, 2016, U.S. Patent Application No. 16/051,314 (Alliance for Sustainable Energy, LLC).

References

1. Mohanty, D.; Hockaday, E.; Li, J.; Hensley, D. K.; Daniel, C.; Wood, D. L., Effect of electrode manufacturing defects on electrochemical performance of lithium-ion batteries: Cognizance of the battery failure sources. J. Power Sources 2016, 312, 70-79.

2. Mohanty, D.; Li, J. L.; Born, R.; Maxey, L. C.; Dinwiddie, R. B.; Daniel, C.; Wood, D. L., Non-destructive evaluation of slot-die-coated lithium secondary battery electrodes by in-line laser caliper and IR thermography methods. Anal. Methods 2014, 6 (3), 674-683.

3. Etiemble, A.; Besnard, N.; Adrien, J.; Tran-Van, P.; Gautier, L.; Lestriez, B.; Maire, E., Quality control tool of electrode coating for lithium-ion batteries based on X-ray radiography. J. Power Sources 2015, 298, 285-291.

4. Just, P.; Rost, J.; Echelmeyer, T.; Ebert, L.; Roscher, M. A., A method to quantify coating thickness and porosity of electrodes for lithium-ion-batteries. Measurement 2016, 89, 312-315.

5. Batteries for Electric Cars: Challenges, Opportunities, and the Outlook to 2020. Boston Consutling Group, 2010.

6. Harris, S. J.; Lu, P., Effects of Inhomogeneities-Nanoscale to Mesoscale-on the Durability of Lithium-ion Batteries. J. Phys. Chem. C 2013, 117 (13), 6481-6492.

IV.E.4. Towards Solventless Processing of Thick Electron-Beam (EB) Cured LIB Cathodes (ORNL)

David Wood
Oak Ridge National Laboratory
One Bethel Valley Road
Oak Ridge, TN 37831
Phone: 865-574-1157; Fax: 865-241-4034
E-mail: wooddl@ornl.gov

Peter Faguy, DOE Program Manager
U.S. Department of Energy
Vehicle Technologies Office
1000 Independence Avenue, SW
Washington, DC 20585
Phone: 202-586-1022
E-mail: Peter.Faguy@ee.doe.gov
Start Date: October 1, 2014
End Date: September 30, 2019

Abstract

Objectives

- Significant process energy savings.

- Ultra-high electrode processing speed.

- Utilize much more compact equipment than conventional drying ovens.

Accomplishments

- EB curable resins screening on formability and electrochemical stability.

- Composite electrode formulation and curing.

- Full coin cell demonstration of electrode performance.

- Cost reduction estimation on high speed EB processing.

Future Achievements

- High curing speed at pilot-scale.

- 1.5 Ah pouch cells with thick electrode cured at high speed.

Technical Discussion

Background

Lithium-ion batteries have been extensively studied for the last two decades for application in portable electronics, energy storage and electric vehicles. However, the latter two applications need a further increase in battery performance and reduction in packaging cost. It has been reported that electrode processing, especially the positive electrode with conventional manufacturing methods accounts for one of the reasons for high costs of lithium-ion batteries, due to the use of polyvinylidene fluoride (PVDF)/N-methylpyrrolidone (NMP) (the state-of-the-art binder/solvent system for electrode processing). NMP is expensive (bulk-quantity price of $1.25 L−1 or higher) and toxic, and requires a costly solvent recovery process. On the other hand, the NMP evaporation in the electrode requires high energy input in thermal drying which limits the production speed.

Introduction

There are a variety of technical attributes to electron beam (EB) curing of LIB binders. EB curing uses solvent-free compositions that have low emissions (VOCs, etc.) and are recognized by federal, state and local governments as a more desirable technology. Solvent or water-based processing requires high drying energy and results in significant CO_2 emissions. EB curing offers significant process energy savings, is ultra-high speed, and utilizes much more compact equipment than conventional drying ovens (much less plant floor space required). Furthermore, it is a relatively cool process compatible with heat-sensitive substrates. Conventional thermal drying of LIB electrodes is typically conducted using multiple temperature stages; however, EB can be conducted in a single step. Solvent-free electrode compositions are rated as non-flammable, which translates into lower insurance costs, less stringent storage requirements and, a reduction in handling hazards.

EB treatment is a fast, robust materials processing technology that commonly delivers low cost and excellent performance for high-volume materials production. Based on decades of development and commercial deployment, self-shielded machines routinely operate with high reliability and low maintenance in industrial roll-to-roll production environments. ORNL is developing, demonstrating, and transitioning technology for high-speed roll-to-roll EB processing of LIB electrodes (i.e. coating formation and binder curing). Further specific advantages of this processing route for LIBs are:

Unmatched throughput – We estimate ≥ 600 m^2/min throughput can be achieved based on ≥ 300 m/min line speed for roll widths up to 2 m ($1.5-2.0M installed with machine footprint ~10 m^2).

Thicker electrodes (synergy with Task 1) – Up to 150 microns can be achieved at the throughput rate mentioned above. Coatings of several hundred microns could be processed at higher capital cost per unit throughput, modest reduction in energy efficiency, and larger equipment footprint.

Excellent energy efficiency – Electrical efficiencies $\geq 60\%$ are possible, including voltage transformer losses (i.e., $\geq 60\%$ of electrical line energy is converted to productive EB energy).

Environmentally friendly – EB processing requires no solvent and no initiator and has low emissions.

Approach

ORNL is working on a multiphase approach to develop, demonstrate, and transition EB processing of roll-to-roll battery materials.

Phase 1 – Demonstrate the technology's key differentiating attributes of high throughput and thick layer processing (FY15-16).

Phase 2 – Address the key challenges of binder material selection, heating effects, lithium loss, porosity control, and resulting material performance (FY17-18).

Phase 3 – Demonstrate an optimized curing system in conjunction with a high-speed coating line together with a key equipment partner and battery manufacturer (FY19).

Results

Figure IV-295 illustrates the EB curing process of lithium-ion battery electrodes. NMC and carbon black are first uniformly dispersed using low MW oligomers. Then the electrodes are placed under the electron beam for cross-linking of the acrylated polyurethane resin. The high MW cross-linked polymer functions effectively as a binder to adhere the active materials to the Al foil.

In order to confirm the cross-linking of the oligomers under electron beam, Figure IV-296a shows the FTIR spectroscopy of acrylated polyurethane before curing and after curing at a dose of 30 kGy. The characteristic absorption peak for the C=C bond in the acrylate group of the polyurethane dispersion is around 810 cm^{-1} and its intensity corresponds to the concentration of unreacted acrylate groups. The decrease in absorption intensity after 30 kGy curing in Figure IV-296a indicates that most of the acrylated groups have been cross-linked and thus the three-dimensional solid network structure of acrylated PU polymers is formed as the binder in the

electrode. Another indication of high cross-linking is that the liquid resin changed into a solid state after EB curing. Cyclic voltammetry (CV) is conducted to test the stability of EB cured polymers in Li half cells as shown in Figure IV-296b. The acrylated PU was coated onto Al foil and cured under EB. The consecutive nature of the CV curve is quite stable within the scanning voltage window and the faradaic current response is rather low compared to a previous report, implying that EB cured polymers are electrochemically inert at the potentials for cathode materials intercalation/de-intercalation.
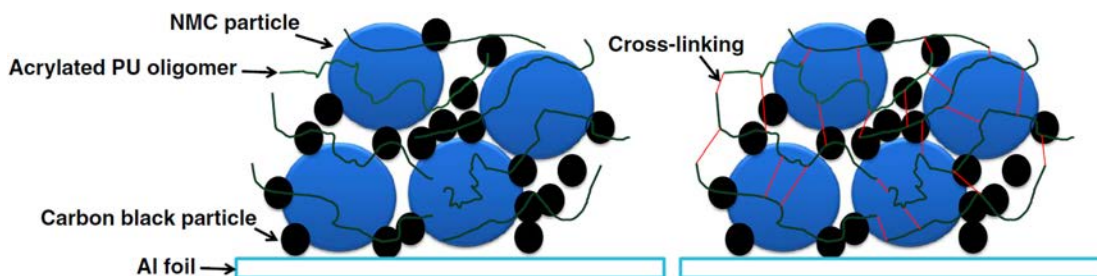
Figure IV-295: Concept of using acrylated PU oligomers as binders in Lithium-ion battery electrodes
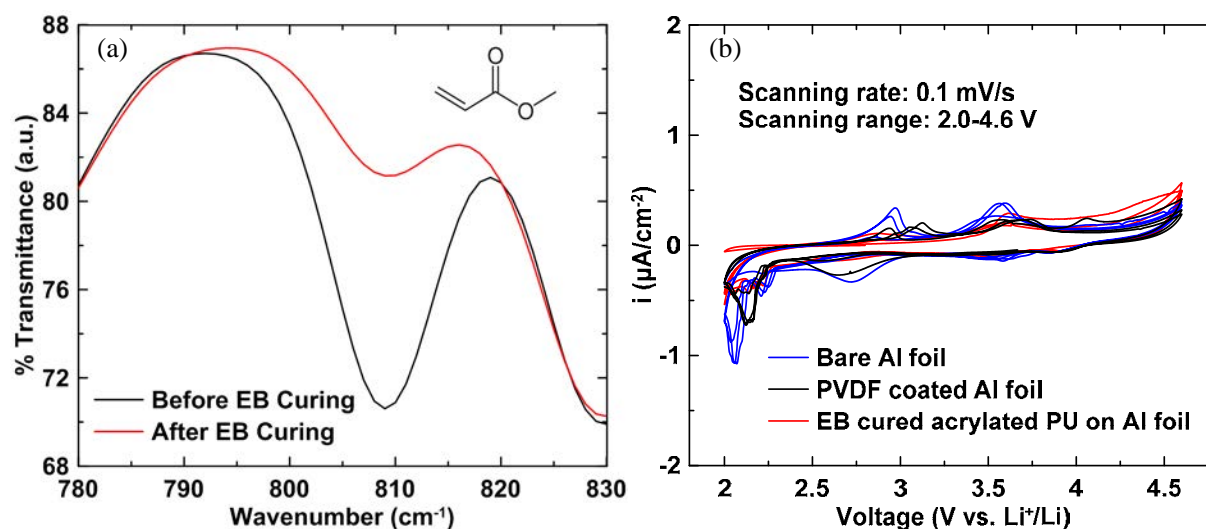
Figure IV-296: (a) FTIR spectroscopy around 810 cm-1 of acrylated PU before and after EB curing; (b) CV of bare Al foil, PVDF coated Al foil and acrylated PU coated Al foils after EB curing

Figure IV-297 shows the voltage curves of NMC composite electrodes using PVDF and several waterborne acrylated polyurethanes (EB cured) as binders. The voltage curves showed typical NMC features indicating EB cured resins do not affect the lithiation/delithiation process of the active solid particles. Typical first Coulombic efficiencies were about 87% with reversible capacity of 150 mAh/g, which is comparable to the NMP/PVDF processed coatings (baseline). Coatings based on resin C and F had slightly higher hysteresis in charge/discharge voltage compared to other EB resins and the baseline coating. The following discussion is based on the electrodes using resin B as binders.

Figure IV-298a shows the voltage profiles of NMC electrodes using conventional PVDF binder and an EB-cured acrylated PU binder in Li half-cells. Both electrodes show sloping charging/discharging curves which is typical for NMC cathode materials. The first charge capacities of electrodes using PVDF and EB-cured acrylated PU as binders are 179 and 178 mAh/g with Coulombic efficiencies of 84% and 85%, respectively. The voltage hysteresis of the electrode using the EB-cured acrylated PU binder is slightly higher for the first cycle compared to the electrode that used PVDF as the binder. However, the hysteresis decreases with cycling and becomes very similar compared to the PVDF.
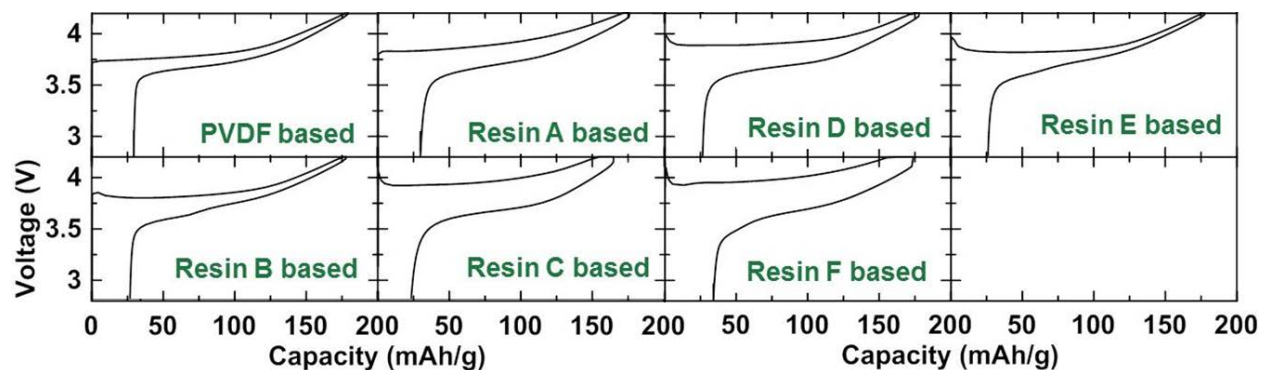
Figure IV-297: Voltage curves of NMC532 composite electrode using different binder system in Li half cells
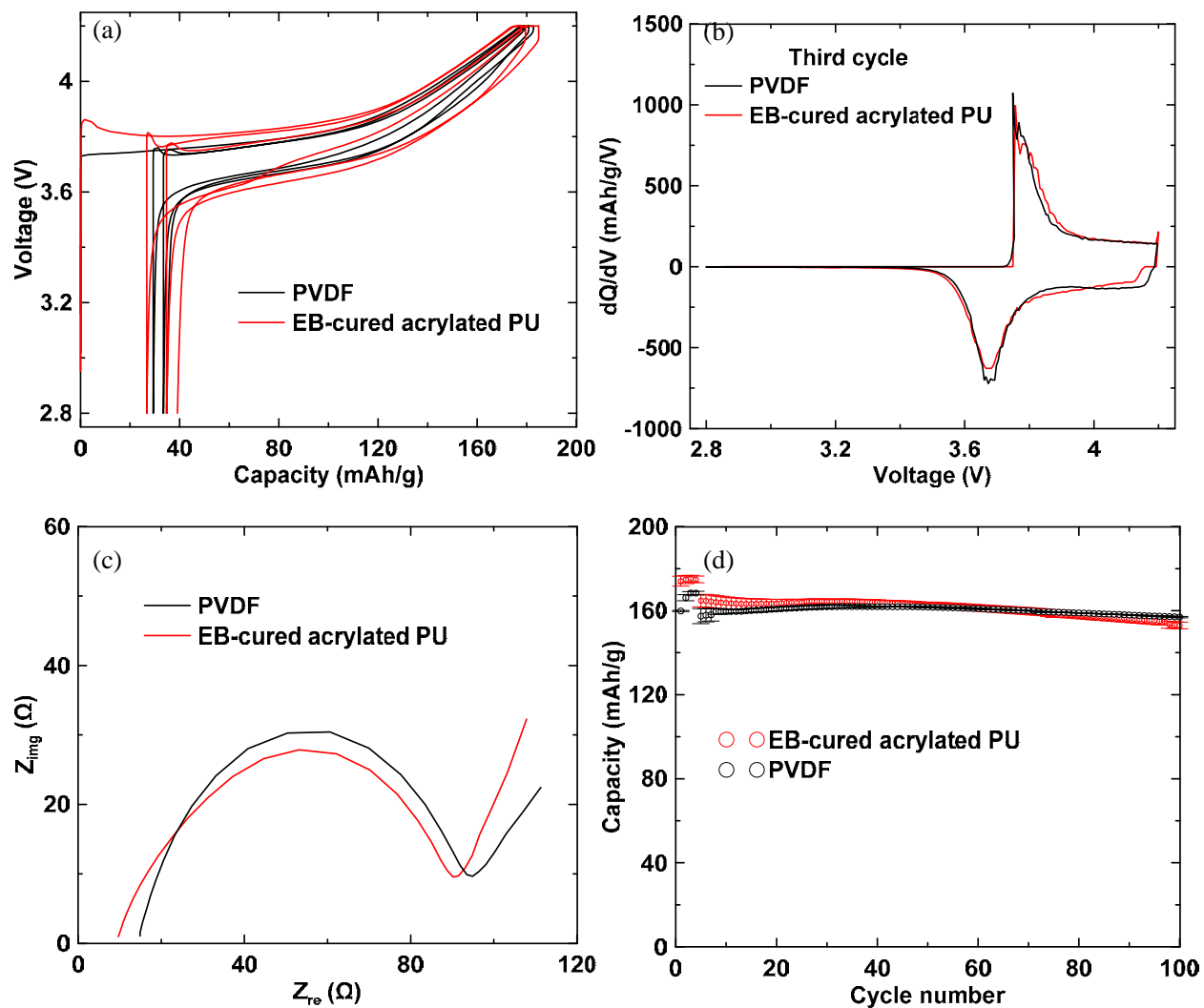
Figure IV-298: (a) Voltage profiles of NMC electrodes using PVDF and EB-cured acrylated PU as binders in Li half-cells; (b) Differential capacity curves of the third cycle for electrodes using different binders; (c) Electrochemical impedance spectra after 3 charge/discharge cycles for electrodes using different binders; (d) Cycling performance of NMC electrodes using PVDF and EB-cured acrylated PU as binders in full coin cells at C/3.

The differential capacity curves of the two electrodes during the third cycle are shown in Figure IV-298b with two broad redox peaks at 3.8 V during charge and 3.7 V during discharge. The similar overlapping curves indicate that the EB-cured acrylated PU functions identically to the PVDF binder, which does not affect the electrochemical reactions of Li+ intercalation/de-intercalation into the NMC particles.

The electrochemical impedance spectra (EIS) of NMC electrodes with different binders after 3 cycles at 2.8 V are shown in Figure IV-298c. Both spectra are comprised of compressed semicircles at high-medium frequency followed by slopes at low frequency, corresponding to the charge-transfer at the electrode/electrolyte interface and subsequent Li^+ diffusion in the NMC phase. It can be seen that the diameter of the semicircles using different binders are similar, indicating the charge-transfer resistance of NMC is not impaired by using EB-cured acrylated PU binders in comparison to PVDF binders. This is in accordance with the discussion on voltage curves.

Figure IV-298d shows the cycling performance of the discharge capacity for both NMC electrodes paired with graphite electrodes. The capacity ratio of the negative electrode to the positive electrode is set to be around 1.2. The use of full-cell, instead of half-cell, can provide more accurate cycling performance. The capacities in the plot are the averaged values from three duplicate cells. The error bar is barely observed in the figure, indicating the good repeatability of the electrode performance. The NMC electrodes using the PVDF as the binder shows excellent cycling stability with 157 mAh/g capacity maintained after 100 cycles. A similar cycling performance is observed for the NMC electrodes using the EB-cured acrylated PU as binder. The discharge capacity is 153 mAh/g after 100 cycles. This demonstrates that using the EB-cured acrylated PU as the binder can achieve equally good cycling life as compared to the conventional PVDF binder.
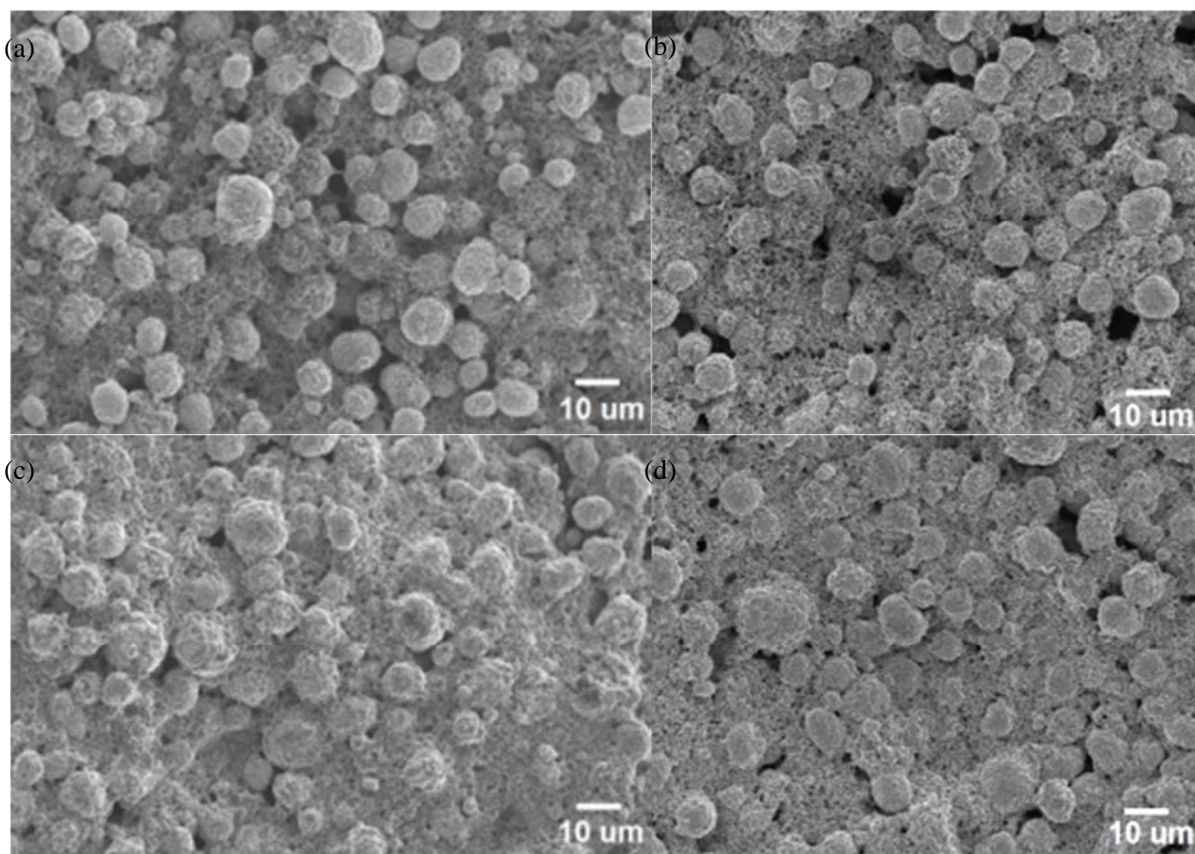
Figure IV-299: SEM images of the electrodes using (a, before cycling; b, after cycling) PVDF and (c, before cycling; d, after cycling) EB-cured acrylated PU as binders

Figure IV-299 shows the morphology of the electrodes using different binders before and after cycling. NMC particles used in this study were composed of tiny primary particles (0.5-2 μm) agglomerated into larger secondary particles (5-10 μm). The NMC particles and carbon black are uniformly dispersed in both electrodes without any appreciable defects such as agglomeration or cracks. They showed very similar morphologies to each other. The integrity of the electrode is also examined by passing it through a 5 mm pin 20 times. No cracks or delamination can be observed in the electrode, demonstrating excellent flexibility and adhesion using EB cured polymers as binders. Both electrodes after 100 cycles show no significant change in morphology compared to the pristine electrodes. No crack or delamination can be seen in the electrodes. The good integrity maintenance of the electrodes indicates that EB-cured acrylated PU binders can provide equally good performance as conventional PVDF binders.

Figure IV-300 presents the rate capability of composite electrodes using different binders up to 3C. Compared to the capacity at the end of the formation cycles (C/20), the discharge capacity retentions at C/3, C/2, 1C, 2C and 3C are 88.1%, 85.8%, 80.8%, 78.1% and 74.0% for the electrode with PVDF binder. The retentions at C/3, C/2, 1C, 2C and 3C are 88.9%, 87.1%, 83.8%, 80.8% and 75.4% for electrodes with EB-cured acrylated PU as the binder. It is clearly seen that the latter electrode has slightly improved rate capability compared to the former one. It is also noticed that the electrode using the EB-cured acrylated PU binder gains higher capacity back than the electrode using the PVDF binder when the C-rate was changed back to C/3. (Table IV-42)
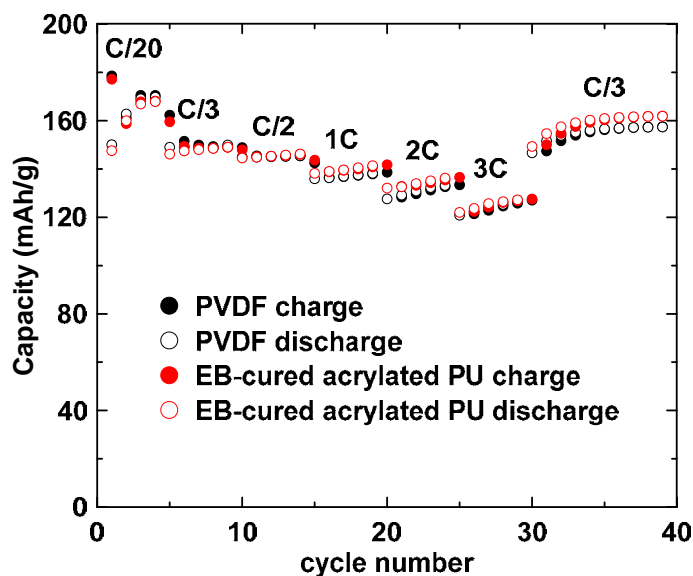
Figure IV-300: Rate performance of NMC composite electrodes using PVDF and EB-cured acrylated PU as binders

Table IV-42: Capacity Retention Rate of NMC Composite Electrodes Using PVDF and EB-Cured Acrylated PU as biNders at Different C Rate

Capacity retention	C/3	C/2	1C	2C	3C
PVDF based	88.9%	85.8%	80.8%	78.1%	74.0%
EB cured	88.1%	87.1%	83.8%	80.8%	75.4%

ORNL selected PCT Engineered Systems, LLC Davenport, Iowa to produce the NMC 532 cathode roll using their Electron Beam Pilot Line. Electron beam curing line speed trials were conducted on several of ORNL's cathode electrodes. PCT's Electron Beam Pilot Line has tunable energies from 100 to 300 keV and is capable of line speeds exceeding 650 fpm (Figure IV-301). During this visit we were able to process ORNL's cathode electrodes at line speeds of 300 to 450 fpm. Preliminary processing trials at even higher line speeds of ~ 450 fpm resulted in the foil material becoming unstable and tearing apart (~ 500 fpm), however this issue can be resolved by optimization of the web handling parameters.
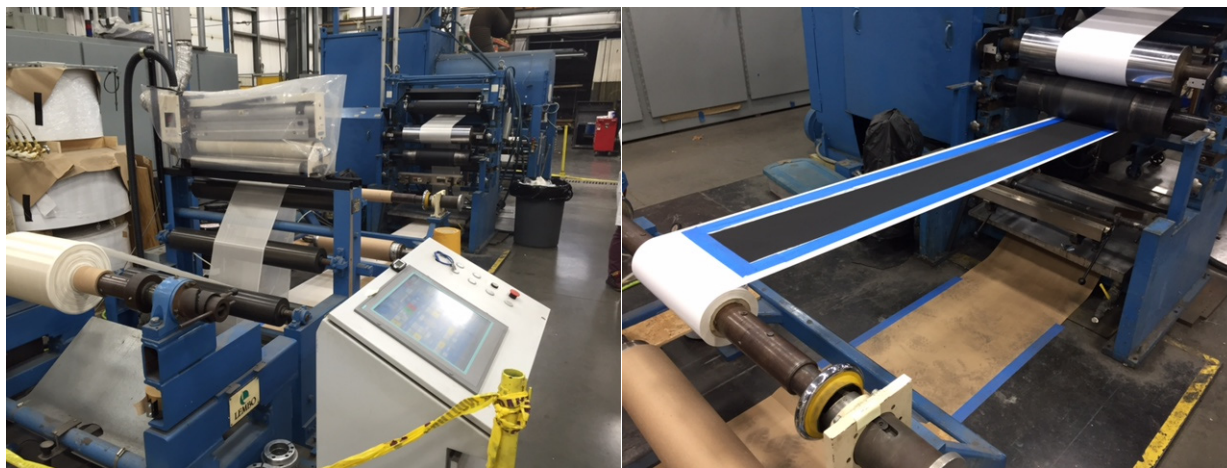
Figure IV-301: Pilot scale, high speed curing process trial run at PCT Engineered Systems, LLC Davenport, Iowa

Conclusions

Electron beam curable acrylated polyurethanes have been demonstrated to be excellent aqueous binders for use as positive electrodes in lithium-ion batteries. Carbon-Carbon double bonds in the binder are cross-linked with each other during electron beam curing to form a three-dimensional solid network structure. The good electrochemical stability of the binder in the electrolyte is verified in a potential window from 2.0 V to 4.6 V. The electrode using the EB-cured acrylated polyurethane binder shows equally good performance compared to the conventional PVDF binder in terms of electrode morphology and electrochemical performance. They also have similar voltage hysteresis during charge/discharge, charge-transfer resistance and cycling stability.

Products

Presentations/Publications/Patents

1. "Towards Solventless Processing of Thick Electron-Beam (EB) Cured LIB Cathodes", es207_wood_2016, US DOE Vehicle Technologies AMR, 2015.
2. "Electron Beam Curing of Acrylated Polyurethanes and Associated Applications in Lithium-ion Batteries", Zhijia Du, Chris J. Janke, Jianlin Li, Claus Daniel, and David L. Wood, III, 18th ISCST Symposium, September 20, 2016, Pittsburg, PA.
3. Du, Zhijia, C. J. Janke, Jianlin Li, C. Daniel, and D. L. Wood. "Electron Beam Curing of Composite Positive Electrode for Lithium-ion Battery." Journal of the Electrochemical Society, 163, no. 13 (2016): A2776-A2780.

IV.E.5. Thick Low-Cost, High-Power Lithium-Ion Electrodes Via Aqueous Processing (Oak Ridge National Laboratory)

Jianlin Li
Oak Ridge National Laboratory
One Bethel Valley Road
P.O. Box 2008, MS-6479
Oak Ridge, TN, 37830
Phone: 865-946-1561; Fax: 865-946-1568
E-mail: lij4@ornl.gov

Peter Faguy, DOE Program Manager
U.S. Department of Energy
Vehicle Technologies Office
1000 Independence Avenue, SW
Washington, DC 20585
Phone: 202-586-1022
E-mail: Peter.Faguy@ee.doe.gov

Start Date: October 1, 2014
End Date: September 30, 2019

Abstract

Objectives

To improve cell energy and power density and reduce battery pack cost by manufacturing thick electrodes via aqueous processing

- Replace NMP processing with water-based chemistry at scale.

- Understand limiting performance factors in thick electrodes towards high energy and power density.

- Investigate processibility of thick electrodes (coating integrity, substrate adhesion, particle/agglomerate cohesion, etc.).

- Characterize electrolyte wetting.

- Correlate electrode structure with cell performance.

- Optimize power density by controlling particle size distribution, electrode porosity, pore size distribution, and porosity gradients

Accomplishments

- Significant revision in energy consumption of electrode primary drying via aqueous and NMP-based processing (with B&W MEGTEC and ANL).

- Completed 1000 high-rate (accelerated durability) cycles of 1.5-Ah pouch cells with both anodes and cathodes for both aqueous and NMP-based processing.

- Numerical modeling on benefit of thick electrodes to energy-power density.

- Built a custom experimental apparatus for electrolyte wetting study.

- Started calendar life study of 1.5-Ah pouch cells with INL
  - Obtained 1.5 Ah pouch cell data for aqueous and NMP processed NMC 532 cathodes through 1000 1C/-2C cycles.
  - Numerically simulated correlation of energy and power density with electrode thickness.
  - Doubled NMC532 thickness with 2 separate coating methods.
  - Pre-screened processibility of different graphite materials for thick graphite anodes.

Future Achievements

- Characterize pore structure and electrolyte wetting in electrodes via aqueous and NMP-based processing.

- Begin obtaining 2000 USABC capacity fade cycles at 0.33C/-0.33C for baseline PVDF/NMP and all-aqueous processed pouch cells.

- Characterize the contribution of interfacial resistance between electrode layers to the overall polarization.

- Develop initial formulations for dual slot-die coated (graded) thick electrodes.

- Fabricate thick electrodes with various active material particle size.

- Characterize stability of high-nickel content NMC (NMC622, NMC811) in aqueous suspensions.

- Improve gravimetric energy density of baseline cell design to ≥200 Wh/kg (cell level) and demonstrate no more than 20% capacity fade through 200 additional 0.33C/-0.33C cycles in 1.5-Ah full pouch cells.

Technical Discussion

Background

Researchers at the DOE Battery Manufacturing R&D Facility at ORNL (BMF) have been working since early 2010 to raise the energy density and lower the cost of advanced lithium-ion batteries for transportation applications with support from VTO. Key areas that have been investigated include low-cost electrode processing, coating non-destructive evaluation (NDE), and pouch cell assembly scale-up and manufacturing science. These research areas support DOE and USDRIVE Electrochemical Energy Storage Tech Team ultimate targets of $125/kWh-usable system cost, 400 Wh/kg cell energy density, and 800 W/kg cell power density.

Introduction

The driving range of electric vehicles is limited by the energy density of lithium-ion batteries (LIBs). One effective way to increase energy density is through electrode engineering, which accounts for the major improvement even since 1990s. This project will focus on at least doubling the calendered cathode (conventional NMC and next-generation high-voltage cathodes) thickness to ≥200 microns using aqueous electrode processing through advanced colloidal chemistry implementation, functional binder development, binder content optimization, dual slot-die coating, rheology control for controlled dispersion settling, graded pore structures, graded particle-size distributions, and advanced drying protocols. Similar activities will be undertaken for next-generation high-capacity anodes (HCAs), such as the Si-C nanocomposites, for capacity balancing. The end result will be electrode coatings that do not just give higher energy density at low C rates, but that have sufficient lithium ion mass-transport rates in the liquid phase to give high power performance as well and are produced at lower cost (wetting and formation time reduction, etc.)

Approach

There are two parallel approaches being followed, simulation and experiment. We work with Argonne National Laboratory and B&W MEGTEC to analyze benefits in cost saving and energy consumption reduction from aqueous processed thick electrodes. The correlation between energy and power density and electrode thickness is also investigated via simulation. Experimentally, surface chemistry, colloidal science and manufacturing science are integrated in manufacturing thick electrodes via aqueous processing. The thick and graded electrodes are characterized by electrode architecture, electrolyte wetting and electrochemical performance.

High Solids Loading in Aqueous Slurry Enabling Shorter Drying Time

The slurry solids loading in the LIB electrode material can have an effect on the rate at which water or NMP is dried from a LIB electrode coating, which is a result of the change in the amount of water or NMP that is needed to be dried from the coating. Figure IV-302 shows the relationship between slurry solids loading and the dryer residence time or required drying time for a constant LIB electrode coating. With same solids loading in the slurry and same areal loading in the dry electrode, it requires longer dwell time to dry the water based electrode. However, the water borne binder solutions could have lower viscosity than the PVDF-NMP solution, which allows higher solids content in the water based slurry and enables a shorter dwell time.

For example, ORNL has shown that the solids loading for a water-based $LiNi_{0.5}Mn_{0.3}Co_{0.2}O_2$ (NMC 532) cathode slurry may be raised up to 60%, while NMP-based slurries are typically 45%.[7] Similar rheological properties were maintained for high coating quality between the two slurries. If this same difference in slurry solids loadings were applied to the graphite anode data in Figure IV-302, a dwell time of 38 s for the water-based slurry would be realized as compared to a dwell time of 52 s for the NMP-based slurry (a 37% longer residence time).
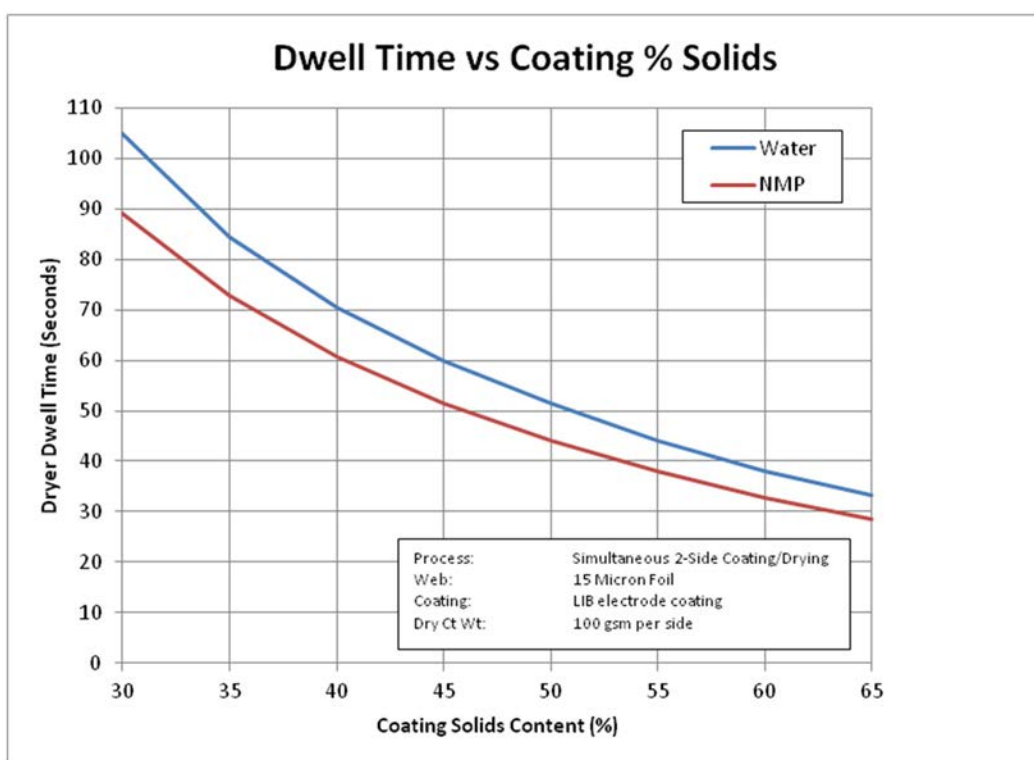
Figure IV-302: Relationship between slurry solids and resulting drying residence time

Outstanding Cyclability from Aqueous Processed Cells

The capacity retention is 86% when discharged at 1C (1C=1.5 A) at 25°C. The comparison in long term cyclability between NMP and water-based processed NMC532 and A12 graphite electrodes is shown in Figure IV-303. The pouch cells with NMP based processed electrodes (red curve) were cycled at 0.2C/-0.2C at 25°C and the temperature was increased to 30°C at 548th cycle. The temperature increase resulted in 4% capacity increase. The pouch cells with water based electrodes were cycled at 0.33C/-0.33C at 30°C. Although the water based processed electrodes showed faster capacity fade at the beginning which could be ascribed to the non-optimized formation protocols, the capacity fade slowed down after the first 50 cycles. Both cells demonstrated identical capacity retention of 83.7% after 668 cycles. Considering the water based processed

---

[7] D.L. Wood, III, J. Li, C. Daniel, D. Mohanty, and S. Nagpure, "Overcoming Processing Cost Barriers of High-Performance Lithium-Ion Battery Electrodes," DOE Annual Merit Review, June 18, 2014.

electrodes were cycled at higher C-rate, their long term cyclability is comparable or even better than the NMP based processed one. The capacity retention after 886 cycles is 79.5%. The results will be discussed in greater detail in a future publication.

Figure IV-303: Comparison in long term cyclability

Correlation Between Energy and Power Density and Electrode Thickness:

Increasing electrode thickness, thus increasing the volume ratio of active materials, is an effective method to enable the development of high-energy-density LIBs. We use NCA/graphite cell stacks as an example to optimize their energy density versus power density via mathematical modeling. Three different approaches were studied to further improve the energy/power density of the cell stack. Approach (a) is decreasing NCA particle size to 500 nm while maintain other parameters unchanged. Approach (b) is increasing initial electrolyte concentration to 1.5 mol/L while maintain other parameters 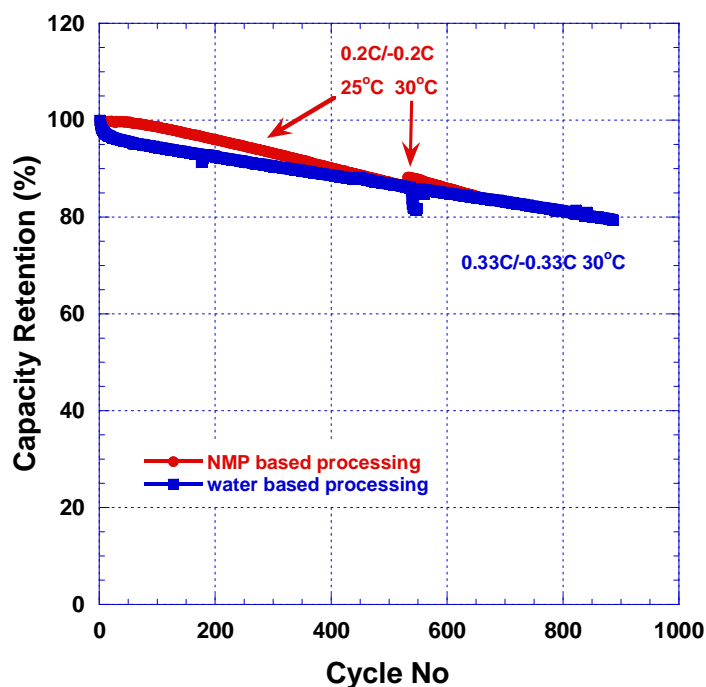unchanged. Approach (c) is decreasing NCA particle size to 500 nm and increasing initial electrolyte concentration to 1.5 mol/L while maintain other parameters unchanged. Several different porosity gradients in NCA electrode were also modeled to study their effects on battery performance. In this part of study, the electrode thickness and areal loading was unchanged. On the x-axis, "0" represents the interface between the separator and the cathode; "1" represents the interface between the cathode and the Al foil.

The lithiation concentration of NCA particles in thick electrodes is shown in Figure IV-304A. The dashed lines are the Li$^+$ concentration at the surface layer of NCA particles ($c_{s,s}$) and the solid lines are the averaged Li$^+$ concentration of NCA particles ($c_{s,a}$) at the end of the discharge process. It is well known that the cathode potential (cut-off voltage) is determined by $c_{s,s}$, and that the specific capacity (utilization ratio of active materials) is determined by $c_{s,a}$. For cells discharged at C/5, the difference between $c_{s,s}$ and $c_{s,a}$ is negligible for all the thicknesses. This is in accordance with Figure IV-303. The capacity of NCA is almost the same for different thicknesses from 60 to 240 μm. The $c_{s,s}$ barely changes for cells with the same thickness regardless of C rates. However, the $c_{s,a}$ gradually decreases because $c_{s,s}$ increases rapidly to the saturation value at higher current density and causes the cell to reach the cutoff voltage. The concentration gradient between the surface and the interior of NCA particles for Li$^+$ diffusion results in underutilization of the active materials. The y-axis scale on the right side of Figure IV-305a shows the normalized utilization of the NCA phase with the fully lithiated state as 1 and the fully delithiated state as 0. The difference between $c_{s,s}$ and $c_{s,a}$ at the back of the electrode (near the Al foil) is greater than that at the front of the electrode (near the separator) because the reaction is uneven across the thickness of the electrode. The region at the front reacts first, and the region at the back reacts later. Both $c_{s,s}$ and $c_{s,a}$ drop rapidly at the back of the electrode for 240 μm at C/2, 180 μm at 1C,

and 120 μm and 150 μm at 2C. This is because the lithium-ion concentration in the electrolyte phase ($c_{l,s}$) reaches zero at the back of electrode before $c_{s,s}$ reaches the saturation value. It was notice that $c_{s,s}$ and $c_{s,a}$ converge near Al foil because the lithium ion concentration in the particle levels off while part of the electrode near separator is still under discharging. Since no lithium ions are available for solid-phase intercalation, the voltage drops rapidly to the cutoff value. This can be clearly seen in the 2C discharge of Figure IV-303, which shows that the voltage profile below 3.0 V has a steeper slope for 150 μm than it has for 120 μm.

Figure IV-304B shows the electrolyte concentration across the thickness direction in the cell stack. During discharge, the concentration gradient gradually builds up beside the electric field to drive the Li⁺ transport from the negative electrode to the positive electrode. The concentration gradient becomes steeper under higher C rates for a given cell thickness and in thicker cells for a given C rate. It can be clearly seen that $c_{l,s}$ reaches zero near the Al foil for 240 μm at C/2, 180 μm at 1C, and 120 μm and 150 μm at 2C in Figure IV-304B, which is in accordance with the observation in Figure IV-304A.
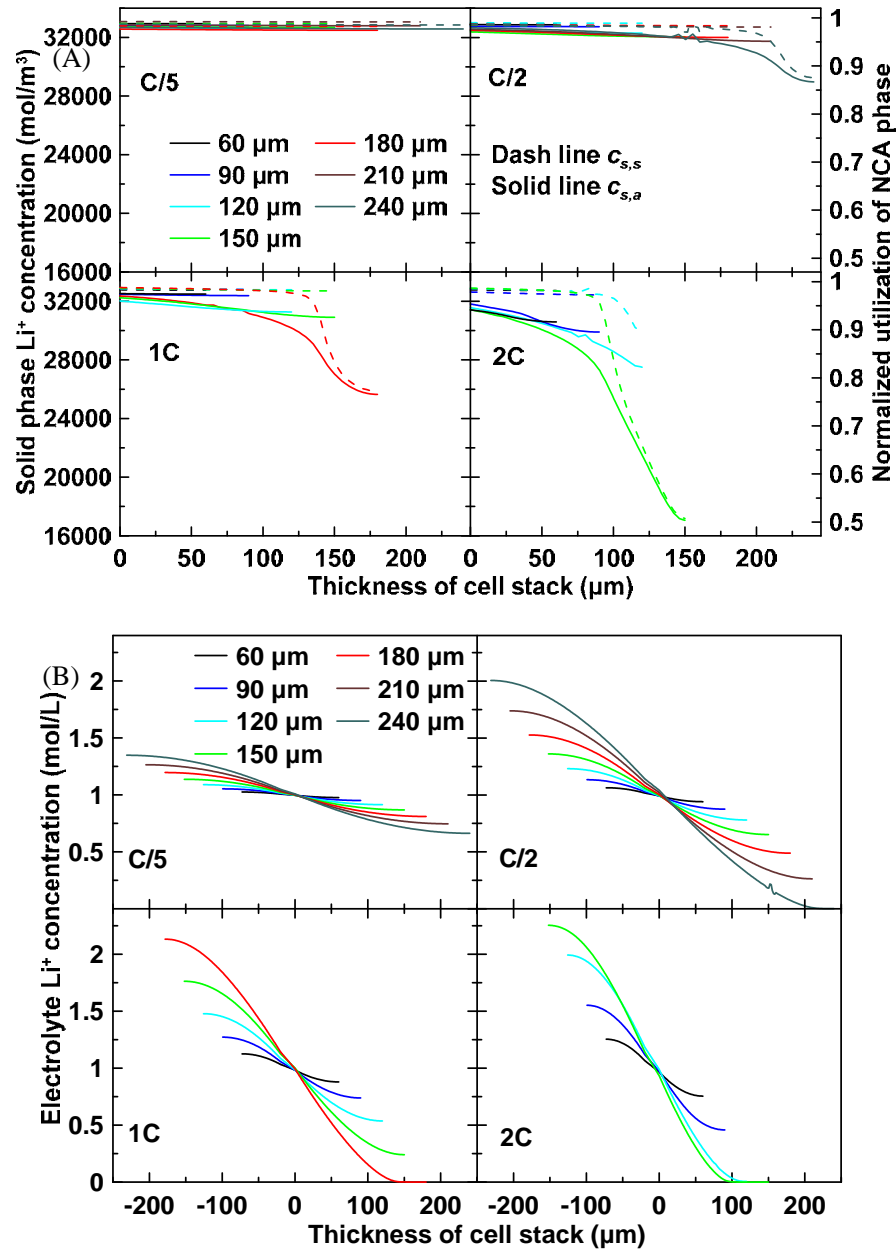

Figure IV-304: (A) Surface and averaged lithium ion concentration of NCA particles across the cathode thickness direction upon reaching 2.8 V; (B) Li ion molarity profiles in the electrolyte across the cell stack thickness direction upon reaching 2.8 V

The underutilization of active materials in thick electrodes can be attributed to the Li$^+$ diffusion gradient in the solid phase and/or Li$^+$ depletion in the electrolyte phase. Therefore, all the factors that could improve the above issues can be considered during cell engineering. For the solid phase, possible approaches include but are not limited to increasing Li+ diffusion coefficient (D_s) and/or decreasing particle size (R). For the electrolyte phase, possible approaches include but are not limited to increasing Li$^+$ diffusion coefficient (D_l), increasing molarity (c_0), and/or decreasing Bruggeman factor (α).

Figure IV-305A shows the molarity gradient inside the cells for thicknesses of 150 µm and 180 µm under 1C discharging. The increase in initial electrolyte molarity raises the whole gradient profile and thus avoids electrolyte depletion in the 180 µm electrode. The decrease in particle size slightly increases the slope of the gradient because more lithium ions are intercalated into the solid phase. Figure IV-305B shows the $c_{s,a}$ in NCA electrodes under the same conditions as Figure IV-305A. For approach (a) and (c), the value of $c_{s,a}$ near the Al foil in the 180 µm electrode is significantly increased due to the abundant availability of lithium ions in the electrolyte. Little effect on $c_{s,a}$ is observed in the 150 µm electrode because no depletion occurs in the cell for baseline molarity. The decrease in particle size can increase $c_{s,a}$ in the whole 150 µm and 180 µm electrodes near the separator, where no electrolyte depletion occurs. The value of $c_{s,a}$ is improved across the whole 180 µm electrode for decreased particle size and increased electrolyte molarity.
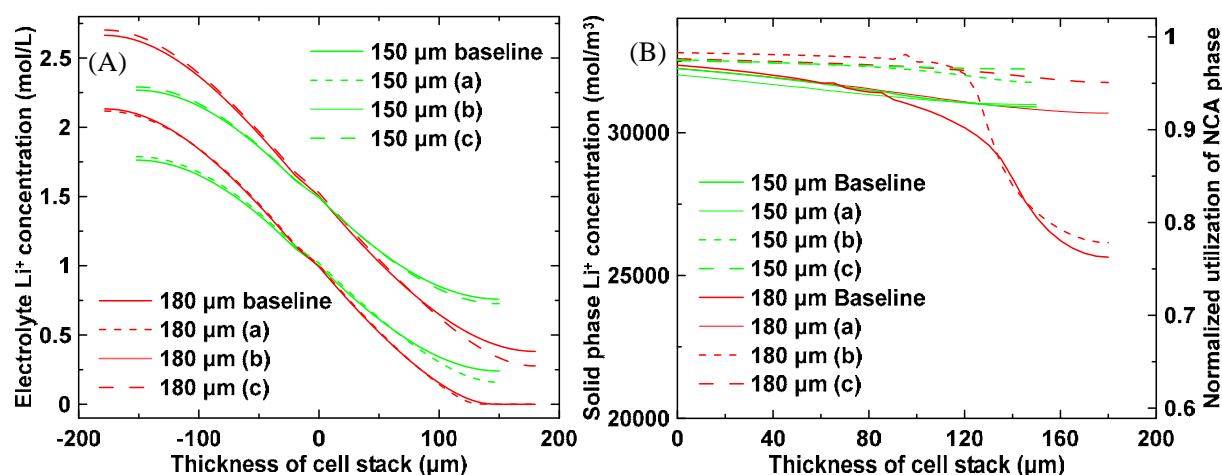

Figure IV-305: The effect of approaches (a) increasing initial molarity, (b) decreasing particle size, and (c) both increasing initial molarity and decreasing particle size on (A) lithium ion molarity profiles in the electrolyte and (B) averaged lithium ion concentration of NCA particles, c_(s,a), at 1 C discharge upon reaching 2.8 V

Figure IV-306A shows the volumetric energy densities of cell stacks versus the thicknesses of their NCA electrodes under different C rates. The energy density increases with the increase of NCA electrode thickness, rapidly at first, and gradually plateaus at around 728 Wh/L under C/5. The maximum points of the energy density are 692, 643, and 563 Wh/L, occurring at 210, 150 and 120 µm under C/2, 1C, and 2C rates, respectively. As the electrode thickness increases beyond the maximum point, the volumetric energy density decreases rapidly. Gravimetric energy density versus thickness follows the same trend and is therefore not shown here. This is in accordance with battery manufacturing practices: thin electrodes are used to meet high power requirements, and thick electrodes for applications requiring low power but high energy density. Figure IV-306A shows the effect of approaches (a), (b), and (c) on the improvement of cell energy density. The energy density improvement is based on the increased utilization of active materials and decreased cell polarization. Also, the critical thicknesses are increased to 240 µm under C/2 and 180 µm under 1C.

The total volume of an 18650 lithium-ion cell is 17.7 mL. The cell stack occupies a volume of 15.9 mL. Figure IV-306B is a practical energy-power Ragone plot in which the values are comparable to those of commercial 18650 cells. The energy-power values of the baseline cell stacks are constrained by the curves due to cell polarization and underutilization of active materials near the current collectors. The cell polarization could be addressed by reducing the resistance associated with electrolyte conductivity, charge-transfer resistance, and Li+ diffusion impedance in the solid phase. To maximize the utilization of active materials in thick electrodes, approaches should focus on avoiding electrolyte depletion and improving Li$^+$ diffusion in the solid phase

particles. The dashed lines in Figure IV-306B, which correspond to approach (c), show that improvement can be achieved by the strategies discussed in this paper.
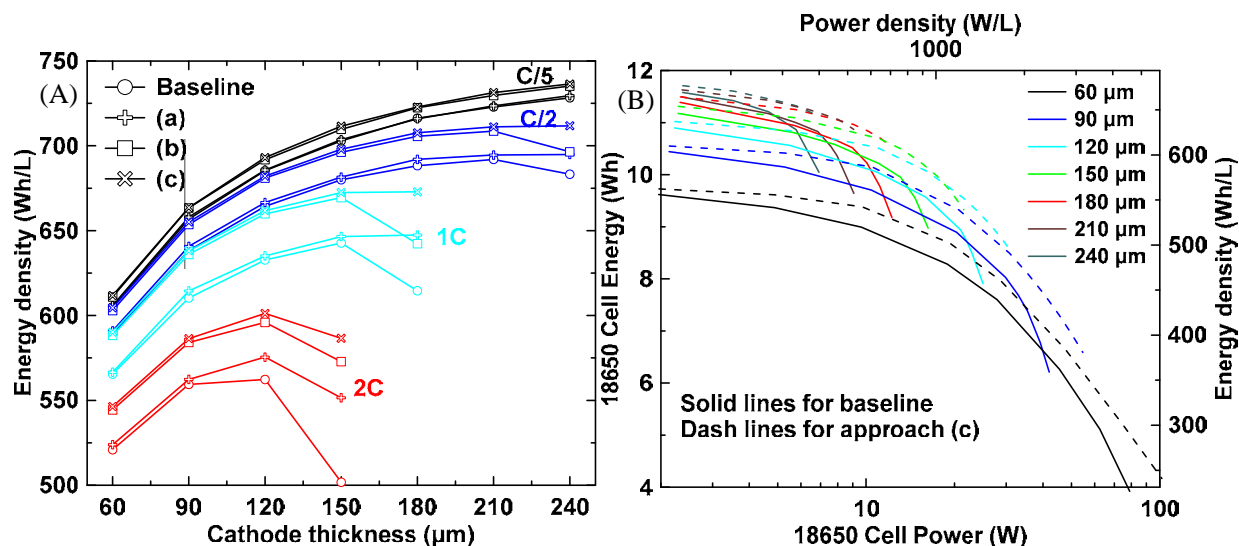
Figure IV-306: (A) the effect of approaches (a), (b) and (c) on (a) average discharge voltages of cell stacks and (b) energy density of cell stacks; (B) The effect of both increasing initial molarity and decreasing particle size on the energy-power Ragone plot of 18650 cells

SCMG-BH graphite preferred for thick anode fabrication

Different graphite materials were screened for negative electrodes to pair with the thick positive electrode. It was found that the flexibility of the negative electrode with higher loading (14 mg/cm^2) varied when different types of graphite materials were used. Flexibility is defined here as the ability of a coating to pass a 5 mm diameter rod without cracking or losing adhesion to the current collector, which is a critically important mechanical property for electrode coatings. During cell manufacturing, many steps require good flexibility such as coating, drying, punching, stacking, and jelly roll winding. Figure IV-307 shows the electrodes after passing over a 5 mm diameter rod. For the A12 graphite, the coating developed repeating cracks with 2-3 mm gaps, and it nearly delaminated from copper foil. For the Superior graphite, periodic cracks were observed, but the cracked coating remained adhered to the copper foil. The SCMG-BH graphite exhibited the best flexibility with no cracking or delamination observed after repeated bending on the rod.
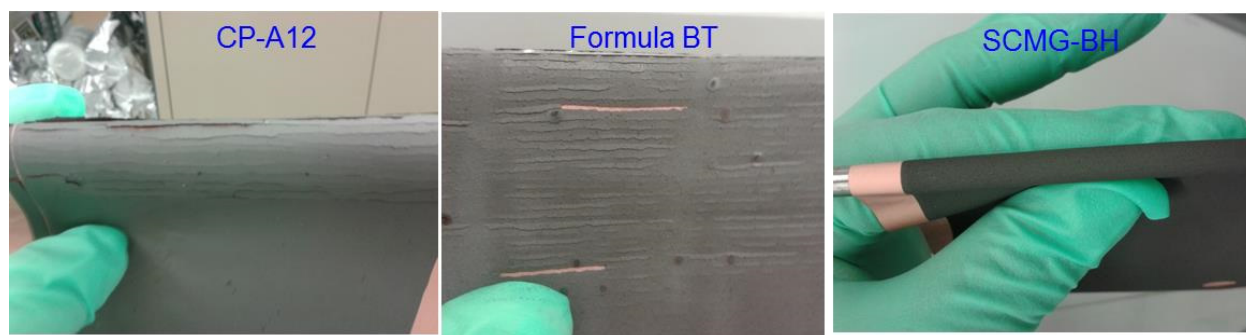
Figure IV-307: Negative electrode flexibility test where electrodes were bent over a 5 mm diameter cylindrical mandrel

First design of thick graded cathode

In the experimental section, first design of aqueous, graded cathode architecture with NMC 532 was performed as shown in Figure IV-308A. A denser layer with 27% porosity was close to the current collector and a second layer was coated on top of the former layer with a porosity of 40%. Figure IV-308B shows the cross-section of the cathode. An interfacial border can be clearly seen from the processing and this interface between the two layers may lead to an additional electron and lithium-ion "transport barrier".

(A)

(B)
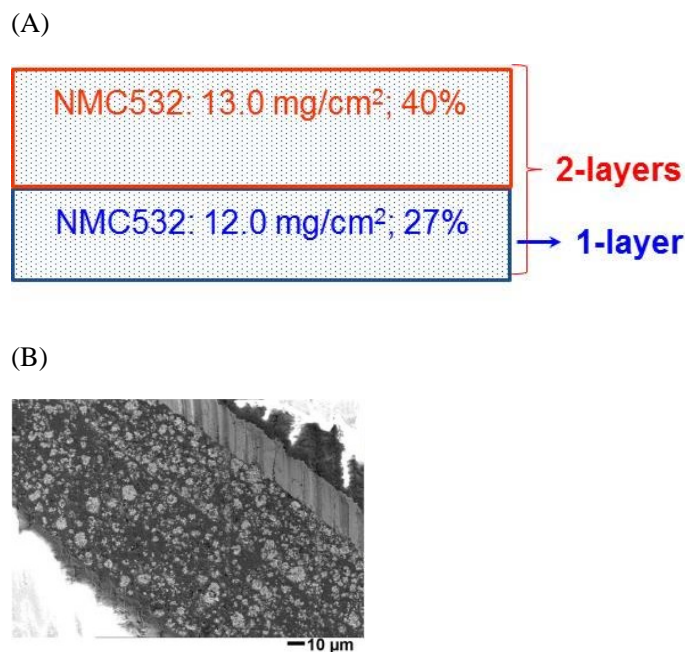
Figure IV-308: (A) illustration of the first design of graded cathode and (B) cross-section image of the electrode

The electrodes were assembled in ORNL BMF dry room into 1.5 Ah pouch cells. The cells were found to have poor rate capability as shown by the huge polarization in the cell during charge/discharge in Figure IV-309A and Figure IV-309B. Figure IV-309C shows the capacity and average discharge voltage variation at different C-rates. Cell capacity drops quickly with increasing C-rate. The average discharge voltage also decreases with increasing C-rate. Figure IV-309D shows the energy density of the cell at different discharge C rate. The cell has 191 Wh/kg discharge energy density at C/20, which decreases quickly with increasing C-rate. Figure IV-309E and Figure IV-309F show the cycling performance of the 1.5Ah cells at ±C/5 and ±C/3 rate. The cells had no capacity at +1C/-2C rate. The cells were found to have 95% capacity retention after 50 cycles at C/5 and 90% capacity retention after 100 cycles at C/3.

Conclusions

It has been demonstrated that a dwell time of 38 s for the water-based slurry would be realized as compared to a dwell time of 52 s for the NMP-based slurry (a 37% longer residence time) with 45% and 60% solids loading in the NMP and water-based slurry, respectively. Majority of cost saving from aqueous processing is from capacity investment and environmental effect. Aqueous processed electrode delivered 80% capacity retention after 886 cycles at 0.33C/-0.33C at 30C. Increasing electrode thickness improves battery energy density. However, it saturates at certain thickness. Further improvement in energy density relies on novel electrode design to reduce polarization in electrode and electrolyte depletion.
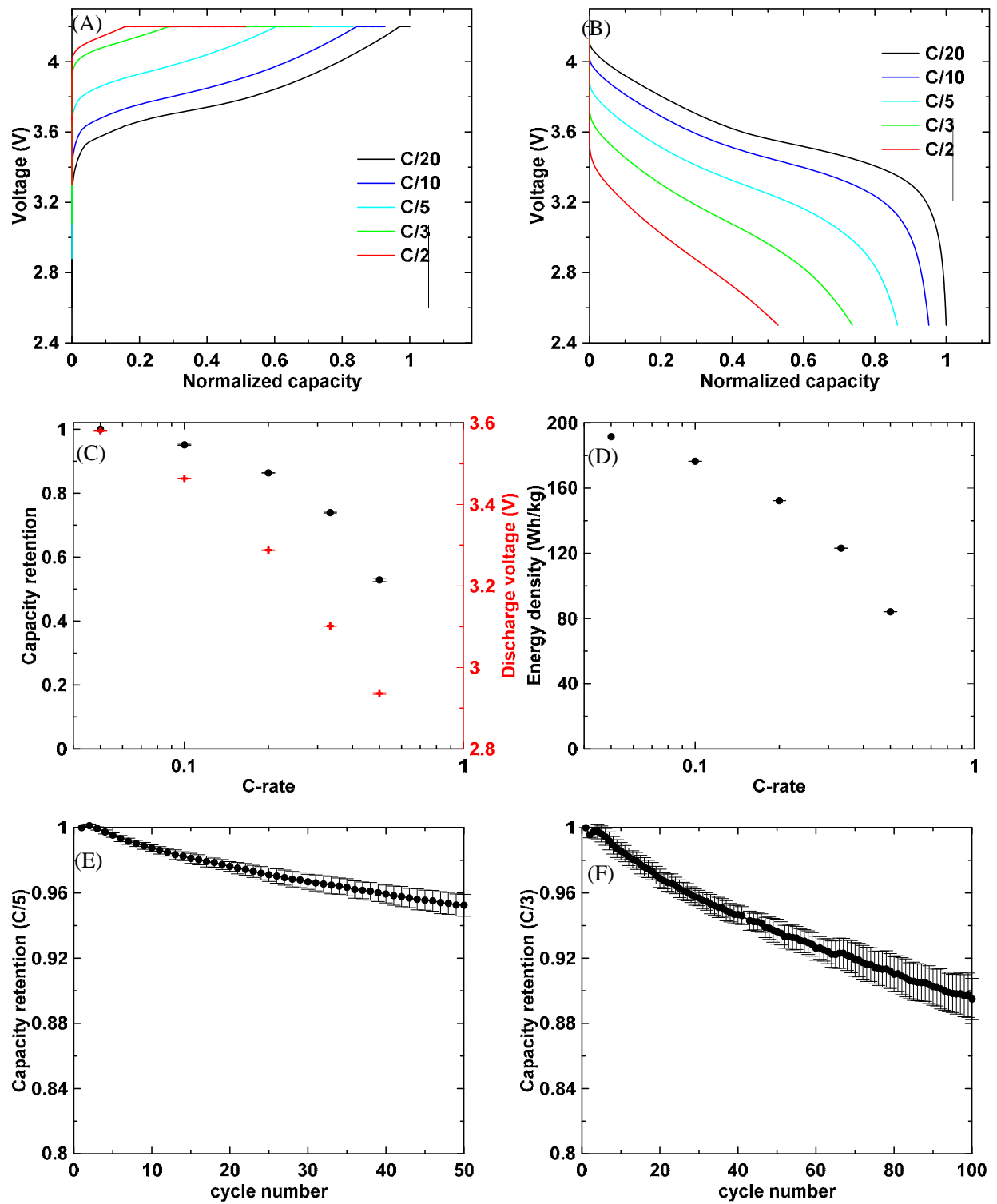
Figure IV-309: (A) charge and (B) discharge voltage curves of 1.5 Ah cells. (C) discharge capacity and average discharge voltage and (D) energy density of the 1.5 Ah cells at different C rate. Cycling performance of the 1.5 Ah cells at (E) ±C/5 and (F) ±C/3

Products

Presentations/Publications/Patents

1. Grid indentation analysis of mechanical properties of composite electrodes in Lithium-ion batteries, Extreme Mechanics Letters, In Press.

2. Evaluation of residual moisture in lithium-ion battery electrodes and its effect on electrode performance, MRS Advances, 1(15) (2016) 1029-1035.

3. Understanding limiting factors in thick electrodes towards high energy density Lithium-ion batteries", Journal of Applied Electrochemistry, Submitted.

4. Technical and economic analysis of solvent-based lithium-ion electrode drying with water and NMP, Drying Technology, Submitted.

5. Coating of $LiNi_{0.5}Mn_{0.3}Co_{0.2}O_2$ cathode on various substrates via slot-die coating and their performance", European Coating Symposium 2015, Eindhoven, Netherlands, September 9-11, 2015.

6. Aqueous processing for $LiNi_{0.5}Mn_{0.3}Co_{0.2}O_2$ cathodes", Materials Research Society Conference 2015 Fall, Boston, MA, November 30- December 4, 2015.

7. *In situ* characterization of stress evolution and volume expansion associated with cycling of prismatic lithium-ion batteries", Materials Research Society Conference 2016 Spring, Phoenix, AZ, March 28- April 1, 2016.

References

1. D.L. Wood, III, J. Li, C. Daniel, D. Mohanty, and S. Nagpure, "Overcoming Processing Cost Barriers of High-Performance Lithium-Ion Battery Electrodes," DOE Annual Merit Review, June 18, 2014.

IV.E.6. Development of Industrially Viable Electrode Coatings (NREL)

Robert Tenent, Principal Investigator
National Renewable Energy Laboratory
16253 Denver West Parkway
Golden, Colorado, 80402
Phone: 303-384-6775; Fax 303-384-6490
E-mail: robert.tenent@nrel.gov

Peter Faguy, DOE Program Manager
U.S. Department of Energy
Vehicle Technologies Office
1000 Independence Avenue, SW
Washington, DC 20585
Phone: 202-586-1022
E-mail: Peter.Faguy@ee.doe.gov

Start Date: October 1, 2015
End Date: September 30, 2018

Abstract

NREL and the University of Colorado at Boulder (CU) have collaborated previously to demonstrate that Atomic Layer Deposition (ALD) can provide thin, uniform, conformal coatings on lithium-ion battery electrodes. Earlier work has shown that these coatings can improve cycle life, abuse tolerance, and safety for a variety of lithium-ion battery technologies. In addition to developing extensive capabilities for performing ALD coatings of standard flat substrate and powder materials samples, the NREL/CU team has designed a new developmental in-line ALD coating prototype reactor that is suitable for integration with Roll to Roll (R2R) manufacturing processes commonly used in the lithium-ion battery space.

The work presented here highlights the development of an ALD coating process using our developmental R2R reactor on lithium cobalt oxide(LCO) cathode materials. Comparative experimental and process development efforts were conducted using both the new R2R format as well as with more traditional "static" ALD systems to demonstrate performance of the new reactor. In addition, work focused on early stage assessment of the coating of NMC 532 materials in conjunction with the High Energy – High Voltage project led by Argonne National Laboratory.

Objectives

- Development and demonstration of an ALD coating process for aluminum oxide on a commercially relevant cathode material.
- Assessment of coating performance of ALD aluminum oxide on NMC 532 cathode materials.

Accomplishments

- Demonstration of R2R ALD alumina oxide coatings on lithium cobalt oxide (LCO) materials showing improved cycling performance over uncoated samples.
- Initial ALD alumina coating and assessment of NMC 532 cathode materials.

Future Achievements

- Integration of web-handling system with earlier demonstrated R2R ALD coating system to allow "true R2R" functionality for electrode samples greater than 1 m in length.
- Assessment of the performance of ALD alumina coatings on the high nickel content NMC materials (532, 622 and 811) on both electrode laminates as well as active material powders in support of a

Go/No-Go decision point for these types of coatings. This work will be conducted in conjunction with the aforementioned HE-HV effort.

Technical Discussion

Background

The work presented here is focused on improving the cycle-life, abuse tolerance and safety of lithium-ion battery materials. Earlier efforts have shown that extremely thin, conformal coatings produced using the Atomic Layer Deposition (ALD) method on lithium-ion battery materials can improve cell performance. However, ALD is currently not accepted as suitable to integrate within current lithium-ion battery manufacturing. This effort seeks to demonstrate that impactful ALD coatings can be developed through practical manufacturing methods. Work here includes demonstration of a new ALD reactor format with current commercial cathode materials (LCO) as well as preliminary studies of coatings performance on emerging cathode materials (NMC532). Focus is placed on standardization of electrode materials, processing and testing to ensure a thorough understanding of the ALD coating performance.

Introduction

In previous work, NREL has shown, in partnership with the University of Colorado, that extremely thin, conformal coatings deposited with the Atomic Layer Deposition (ALD) technique can dramatically improve the performance of lithium-ion cells. Current technology for performing ALD is likely not amenable to high-throughput manufacturing methods and thus represents a high-priced bottleneck in the implementation of ultrathin electrode coatings at a commercial scale. This project had dual purposes in fiscal year 2016. Initially, the focus was on completing development and demonstration of an ALD coating process for an industry relevant cathode laminate material using our developmental R2R ALD reactor. This effort sought to demonstrate that ALD coatings could be employed in a fashion similar to current manufacturing processes. The key goal of this effort was to demonstrate to commercial entities that ALD coatings could be integrated with manufacturing in a practical manner.

The expanded goal of this effort was to provide more broad support for assessing the performance of ALD coatings under the High Energy-High Voltage (HE-HV) effort led out of Argonne National Laboratory. Through this effort, described elsewhere in this document, NREL assessed the performance of ALD coatings on electrode laminates of the NMC 532 material. This effort was conducted under a multi-lab consortium including Argonne National Laboratory, Oak Ridge National Laboratory and Lawrence Berkeley National Laboratory. The NREL team performed ALD coating experiments using multiple ALD reactors and performed cell testing both at NREL and also supplied samples to collaborators at Argonne for further verification testing.

Approach

Typical ALD coating processes are conducted by sequential and separate exposure of a sample substrate surface to gas phase precursors that react to form a film. Deposition is typically performed in a closed reactor system at mild vacuum as shown in Figure IV-310A. Precursor exposure steps are conducted in a single chamber and are separated *in time*. In a typical exposure "cycle," a sample is exposed to one precursor. The chamber is then purged with inert gas prior to exposure to the second precursor that completes the coating reaction. The "cycle" ends with another extensive inert gas purging step before the process can be started again. Film growth takes place by repeating this cycling precursor exposure process multiple times. The sequential and separate exposures are key to achieving the excellent conformal film deposition on highly textured substrates for which the ALD technique is known.
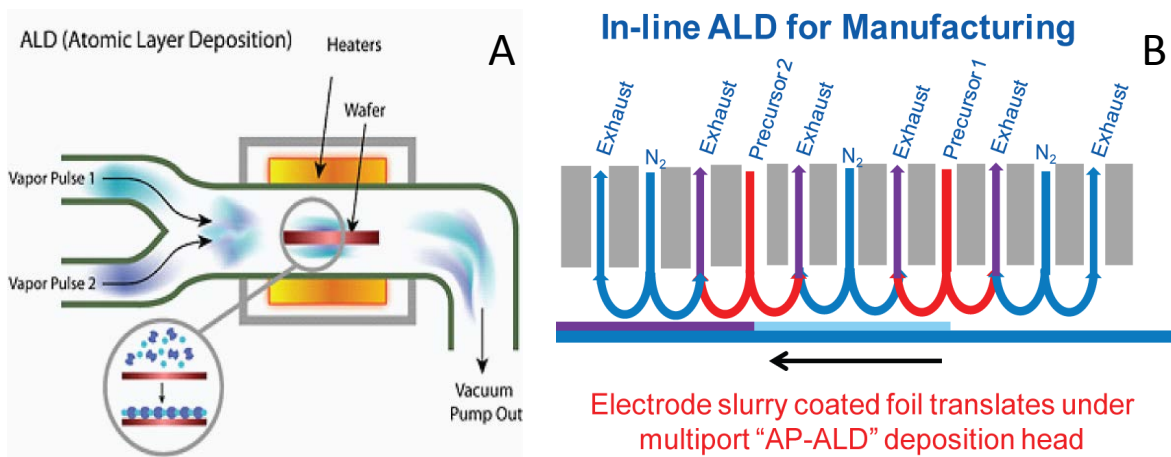
Figure IV-310: (A) Standard "static" or temporal ALD reaction chamber. The coating substrate remains stationary and precursor exposures are separated in time. (B) A conceptual sketch of "spatial" ALD in which a substrate to be coated moves through spatially separated reaction zones

As an alternative to the temporal separation of precursor exposure in the same reaction chamber, our work proposes a spatial separation of precursor exposure steps that is more consistent with "in-line" processing techniques. Figure IV-310B shows a simplified conceptual schematic of our proposed apparatus. Our "spatial" ALD approach employs a multichannel gas manifold deposition "head" that performs sequential exposure of precursor materials as an electrode foil translates beneath it. It is important to note that similarly designed deposition heads are currently employed by glass manufacturers for production of a variety of coated glass products using high-volume, in-line atmospheric pressure chemical vapor deposition (AP-CVD). Our approach leverages this existing knowledge base as well as our ALD expertise to enable in-line ALD coating that will allow the transfer of our previously demonstrated ALD-based performance improvements to larger format devices.

A generalized schematic of the developmental R2R reactor is shown in Figure IV-311. In brief, the reactor employs a "drum in drum" design. The outer drum cylinder is designed to allow mating with gas delivery and extraction modules in a high flexible fashion. This design was chosen to facilitate easy re-configuration in order to enable a wide variety of experimental conditions to be explored for coating process development. For our initial examinations, the reaction of trimethyl-aluminum (TMA) with ozone was chosen. The more traditional TMA-water ALD process was abandoned due to excessively long purge times required to remove residual water from the reactant zone. It is important to note that in work to date, the reactor shown in Figure IV-311 was employed in a "rotary" rather than a fully functional R2R format. This means that substrates for coating are placed on the outer surface of the inner drum cylinder. The inner cylinder is then rotated to translate the sample substrate through the two reactant zones to drive the ALD deposition process. In on-going work, the NREL/CU-Boulder team are currently integrating a "wind-unwind" web handling system with the developmental R2R coater to enable true R2R demonstrations.
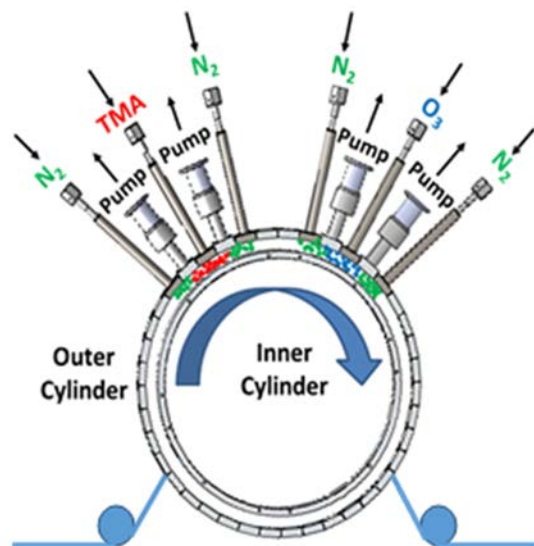
Figure IV-311: Generalized schematic of the developmental R2R ALD reactor

In previous efforts, the NREL/CU-Boulder team focused on designing, constructing and demonstrating initial functionality of a the developmental R2R compatible ALD reactor. In FY16, our focus shifted to development and demonstration of functional coatings on industrially relevant cathode materials. Based on previous work as well as commercial prevalence, a lithium cobalt oxide (LCO) material was chosen for initial demonstration purposes. In early work, we have shown that ALD alumina coatings can improve capacity retention for LCO even when cycled to high voltage. For this reason, our approach was to confirm earlier results with temporal ALD methods and perform comparison experiments with coatings on the same materials performed under the R2R format.

In addition to demonstrating the functionality of the R2R coating system on a relevant electrode material, NREL, in conjunction with our national laboratory partners has initiated studies on the impact of ALD alumina coatings on the NMC532 material under the HE-HV project. Assessment of coatings performance on NMC532 was focused on laminate samples as supplied by the Cell Analysis, Modeling, and Prototyping (CAMP) facility at Argonne. Coating processes were attempted using both temporal as well as R2R spatial ALD methods. Efforts related to both temporal and spatial ALD were maintained throughout this work in order to assess both industrially relevant manufacturing conditions as well as allow flexibility in experimental coating processes.

Figure IV-312: Discharge capacity for LCO/graphite coin cell samples with and without R2R and Static ALD coatings

As discussed earlier, in previous results the NREL/CU-Boulder team demonstrated the impact of ALD alumina coatings on LCO materials. For this reason as well as industrial prevalence of this material, LCO was chosen as our initial demonstration sample for the R2R ALD process development. Samples of LCO cathode materials were supplied by the CAMP facility at Argonne National Laboratory. LCO materials were coated with both the R2R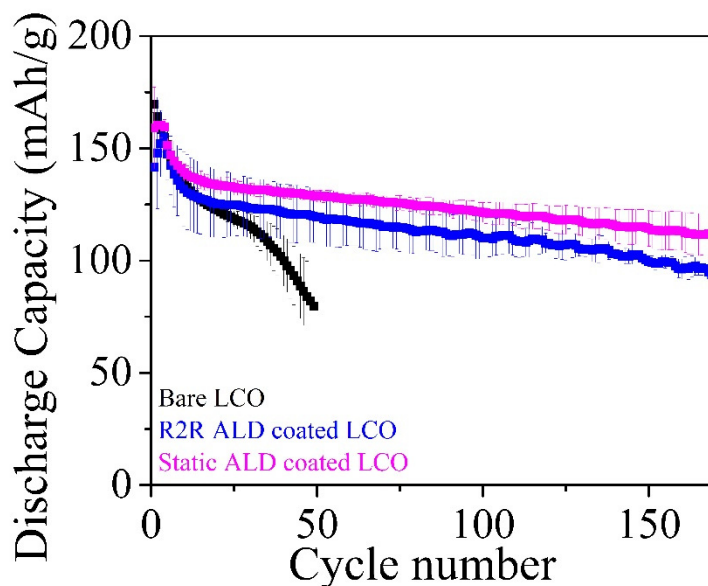 and a more traditional temporal ALD reactor. The initial conditions for the R2R deposition process was determined based on previously published studies on coating of model porous substrates (anodic aluminum oxide). In brief, the R2R ALD process was conducted using the aforementioned TMA/ozone chemistry at a temperature of 60°C and an inner cylinder rotation rate of 10 RPM. This rotation rate would roughly translate to a 30 foot/minute line speed in a full R2R system. Each sample was translated through precursor reaction zones for TMA and ozone sequentially four times, leading to a total of four "cycles" of the ALD process. Temporal ALD processing was modeled on earlier results and consisted of a total of four sequential exposure cycles to TMA and water conducted at 120C. Both processes were designed to saturate surface exposure of reactants to drive the ability to demonstrate surface coating. Figure IV-312 shows cell discharge capacity for LCO/graphite full cells cycled between 3V and 4.5V at a 1C rate for coin cell samples using untreated LCO as well as LCO cathodes coated with aluminum oxide using both the static and R2R ALD formats. A total of five coin cells were fabricated for each sample condition and statistical data obtained. While these cycling conditions are considered abusive for the LCO material, the choice of conditions was based on earlier literature data that had demonstrated the impact of alumina coatings on LCO. As can be see in the data from Figure IV-312, under these cycling conditions, the uncoated LCO cells clearly degrade rapidly while both ALD coated samples retain significant cell capacity. It appears that the static ALD coated materials may show slightly higher capacity retention this could be due to insufficient reaction within the porous materials under the R2R format. Under the static ALD conditions, precursor materials have a higher potential to penetrate the porous electrode structure thereby possibly leading to improved coating performance. Multiple further experiments are being conducted to understand this initial result more fully including additional surface analysis to determine how the ALD alumina coats the sample surface and may react with varied parts of the electrode laminate. Also, there is potential that the different precursor (ozone vs. water) and deposition temperatures (60C vs. 120C) could lead to changes in sample performance. These concerns are being addressed through further experiments focused on employing the ozone precursor into the static ALD format and will be reported at at a later date. Despite the remaining questions, the data in Figure IV-312 shows a clear impact of the ALD coating process for both the R2R and static ALD processes.

While LCO appears to serve as a suitable demonstration material for qualifying our R2R processing capabilities, significant future focus in this effort will be placed on understanding the impact of ALD alumina coatings on high nickel content NMC cathode materials. This work, as discussed earlier is part of the High Energy- High Voltage (HE-HV) effort lead by Argonne National Laboratory focused on understanding how to stabilize these materials at up to 4.5V. Initially, our work focused on coating of the NMC 532 material that was chosen as a baseline material for the HE-HV effort. NMC 532 electrode laminates were supplied by the CAMP facility at Argonne and ALD coatings were examined with both the R2R and static ALD reactor systems. Samples were coated at NREL and CU-Boulder with testing performed at NREL and Argonne. ALD alumina deposition conditions we the same as employed earlier for LCO cathode coatings. Figure IV-313 shows discharge capacity for as received as well as ALD coated NMC532 tested in a full cell format. Testing for these cells was conducted using the standardized HE-HV project protocols at a rate of C/3 with periodic HPPC testing. For this data, ALD coatings were performed with the static ALD reactor system as described earlier. The only noticeable difference between the coated and uncoated materials is a slight decrease in cell capacity for the ALD coated materials. Outside of this observation, the overall cell capacity appears to degrade at an identical rate to the ALD coated materials. Similar results were observed for R2R ALD coated materials with testing confirmed by both NREL and Argonne. These results are also consistent with earlier observations from the Argonne team indicating little impact of coatings on the NMC532 material when tested under standardized HE-HV protocols.

Both the NREL and Argonne teams are pursing multiple on-going efforts in an attempt to understand why these and other coatings are not impacting the performance of the NMC532 materials. Efforts in fiscal year 2017 are focused on understanding the potential for alumina coatings to impact not only the NMC532, but also the NMC622 and NMC811 materials.
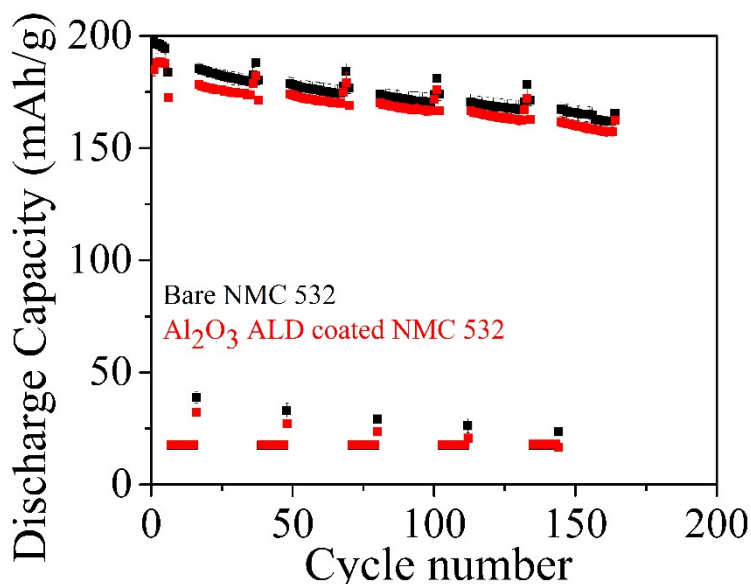
Figure IV-313: Discharge capacity for NMC532/graphite cells with and without static ALD coatings

Conclusions

The NREL/CU team has demonstrated a manufacturing compatible method for performing ALD coating on commercially relevant cathode laminate samples. This effort will continue to further characterize the ability to coat materials effectively under varied conditions to achieve higher deposition rates. Data presented here indicated the ability to coat LCO cathode materials effectively at an estimated 30 ft/minute sample translation rate. Earlier results have shown excellent control of the ALD coating process at rates as high as 300 ft/minute on flat substrates and work will continue to test the ultimate limit with respect electrode coating speeds.

In conjunction with partners at Argonne National Laboratory, Oak Ridge National Laboratory and Lawrence Berkeley National Laboratory, NREL has also initiated studies related to the stabilization of high nickel content NMC cathode materials (532, 622 and 811) and will continue this work as part of the broader HE-HV

effort. Early results appear to show limited impact to NMC532 from ALD alumina coatings when tested at low cycling rates, however early results appear to indicate improved performance for ALD coated materials when tested at higher cycling rates. Investigations into this effect will continue as a part of future work.

Products

Presentations/Publications/Patents

1. Sharma, K. et al, J. Vac, Sci. Technol. A 34(1) Jan/Feb 2016, 01A146.
2. Vehicle Technologies Office, Annual Merit Review, June, 2016 (presented as part of HE-HV).

References

1. Jung, Y.-S. et al., Journal of The Electrochemical Society, 2010, 157, A75-A81.
2. Sharma, K. et al, J. Vac, Sci. Technol. A 34(1) Jan/Feb 2016, 01A146.

IV.F. Process Development and Manufacturing R&D with U.S. Industry

IV.F.1. Low Cost Manufacturing of Advanced Silicon-Based Anode Materials (Group14 Technologies, Inc.)

Henry R. Costantino, Ph.D., Principal Investigator
Group14 Technologies Inc.
100 NE Northlake Way
Seattle, WA 98104
Phone: 206-547-0445; Fax: 206-546-5304
E-mail: rcostantino@group14technologies.com

Walter G. Parker, Technical Project Officer
U.S. Department of Energy
National Energy Technology Laboratory
626 Cochrans Mill Road
Pittsburgh, PA 15236
Phone: 412-386-7357
E-mail: walter.Parker@netl.doe.gov

Start Date: January 2016
End Date: March 2017 (Budget Period 1), December 2017 (Budget Period 2)

Abstract

Objectives

- Develop a new low-cost production process to produce silicon-based lithium-ion battery (LIB) anode material that achieves a gravimetric capacity of 1000 mAh/g, cycle stability of 1000 cycles, and a cell level cost target of < $125/kWh.

- Validate the capacity and cycle life projection in LIB full cells.

- Prove the above cost basis at pilot scale.

Accomplishments

- Suppliers have been identified for feedstock materials to produce silicon-carbon composite materials supporting < $125/kWh at full scale volume.

- Materials and processes to produce silicon-carbon composite materials have been down-selected.

- Synthesized composite at lab scale achieving > 1000 mAh/g for composite material.

- Achieved stability of ~500 cycles for composite materials when tested as an anode additive in lithium-ion full cell.

Future Achievements

- Establish pilot scale manufacturing of Si-C composite materials.

- Synthesize pilot quantities of Si-C composite materials.

- Validate performance and cost targets (1000 mAh/g, 1000 cycles, <$125/kWh) for Si-C materials in LIB full cells.

Technical Discussion

Background

Despite substantial investment in Lithium-Ion Battery (LIB) technology, most commercial cells still rely on graphite anodes – originally deployed in the 1990's, because of their low cost and acceptable lithium capacity. A shift is underway to replace the graphite anode with a silicon containing material, but due to elaborate manufacturing techniques current costs exceed $100/kg. It is our vision to develop new anode materials that are high performance, and also easily scalable, employing low-cost materials and manufacturing processes. To this end, we have launched Group14 Technologies, spun out of EnerG2 Inc., a leader in carbon materials development, manufacturing, and commercialization. Group14's strategy is to develop low cost processes for manufacturing silicon-carbon (Si-C) composite materials that will enable a dramatic reduction in the cost structure of silicon-carbon anodes, i.e., by an order of magnitude, while maintaining the high performance that the LIB industry demands of these advanced anodes.

Introduction

Group14 is developing a Si-C composite material with a focus on low-cost manufacturing that builds upon the carbon technology innovated by EnerG2. Since it's founding in 2003 at the labs of the University of Washington, EnerG2 has emerged as a world leader in carbon-based energy storage materials. EnerG2 uses polymer chemistry to engineer carbon precursors for energy storage applications including ultracapacitor electrode materials (best in its class for capacitance and pulse power) and lead-acid battery additives (improved charge acceptance and cycle life). Such products were all developed in EnerG2's 7000 sq-ft state-of-the-art R&D lab in Seattle and are manufactured at commercial scale in our Albany, OR production facility. Group14 was spun out of EnerG2 to develop Si-C composite materials as anode materials for lithium-ion batteries. As such, Group14 builds upon EnerG2's commercial traction, manufacturing capability and R&D prowess through both privately and publicly funded work, which all contribute as the technical foundation for the current project.

Approach

At Group14, we are leveraging EnerG2's carbon technology as our foundation to develop new approaches for low-cost manufacturing of high-performing Si-C composites. These Si-C composites comprise nano-sized and/or nano-featured silicon. Our approach focuses on raw materials that are low cost and readily sourced. Likewise, our approach focuses on manufacturing processes that are low-cost and readily scalable. For example, the carbon component within the Si-C composite is based on low-cost polymeric carbon precursors.

Our approach is to develop Si-C composite material at lab-scale, supported by robust characterization, including electrochemical characterization with a focus on electrochemical testing of the Si-C composite anode materials in full cell lithium-ion batteries such as coin cells or pouch cells. Our philosophy for the electrochemical characterization is to employ relatively standard procedures and materials, i.e., industry-standard electrolyte, cathode, and battery cycling conditions. While we are interested in potential synergies with our Si-C composite materials and the next generation of other battery materials (cathodes, electrolyte, etc.) our current intent is that our Si-C composite materials are a "drop-in" replacement for graphite powder as an anode materials, compatible with current commercial anode and lithium-ion battery manufacturing lines.

Consistent with our project plan, the next step in our approach is scale-up of down-selected materials and manufacturing process, as determined from the lab-scale screening. The purpose of this next stage is to prove the cost basis at pilot scale, as well as validate the performance of the scaled-up Si-C composites in lithium-ion battery full cells.

Results

To date, the project has remained on track with regards to achieving the results and milestones set out per the project plan. For the period corresponding the first quarter of the project (Jan 1 – Mar 31, 2016), the work focused on identifying suppliers for each feedstock material required for the Si-C composite, wherein said materials must be available at full scale volume supporting < $125/kWh. This objective was met, and the

information was shared with the DOE via telecon. To achieve this objective, the major activities undertaken included the identification of critical components, materials types, and suppliers of material for producing Si-C composites. For each component, at least three material types/species were evaluated, and for each material, at least two suppliers were identified.

In addition to achieving the above milestone related to the feedstock materials, we also gained mechanistic insight into the improved stability afforded by our Si-C composite systems compared to base silicon. Specifically, we have collected data in support of the hypothesis that our Si-C compositing process allows for substantial reduction in anode volume expansion upon lithiation. This finding is highly significant, since it is well described in the field that anode expansion is a major pathway for deterioration of performance in lithium batteries. This finding is exciting, since the observed decrease in volume expansion is anticipated to provide improved cycle life in a lithium-ion battery, and our data thus far are consistent with this view.

Figure IV-314 provides an example of the measured volume expansion of an electrode comprising a bare nano-silicon material compared to an electrode comprising the same material as a silicon-carbon composite material. The data are shown for anode expansion (% of initial) of lithiated bare nano-silicon compared to the same material incorporated into a Si-C composite. The data were collected in coin cell, half cells, wherein the anode also comprised graphite blended to achieved capacity in the range of ~ 450 – 650 mAh/g. For reference, data are also depicted for graphite, whose data fall roughly within the extrapolation of the trendline. As can be seen, the anodes comprising bare nano-silicon demonstrated a relative large volume expansion, with about 100% expansion observed for an anode exhibiting about 600 mAh/g. In contrast, there was a dramatic reduction in volume expansion observed for the case where the nano-silicon was incorporated into Si-C composite, with only about 60% expansion observed for an anode exhibiting about 600 mAh/g.
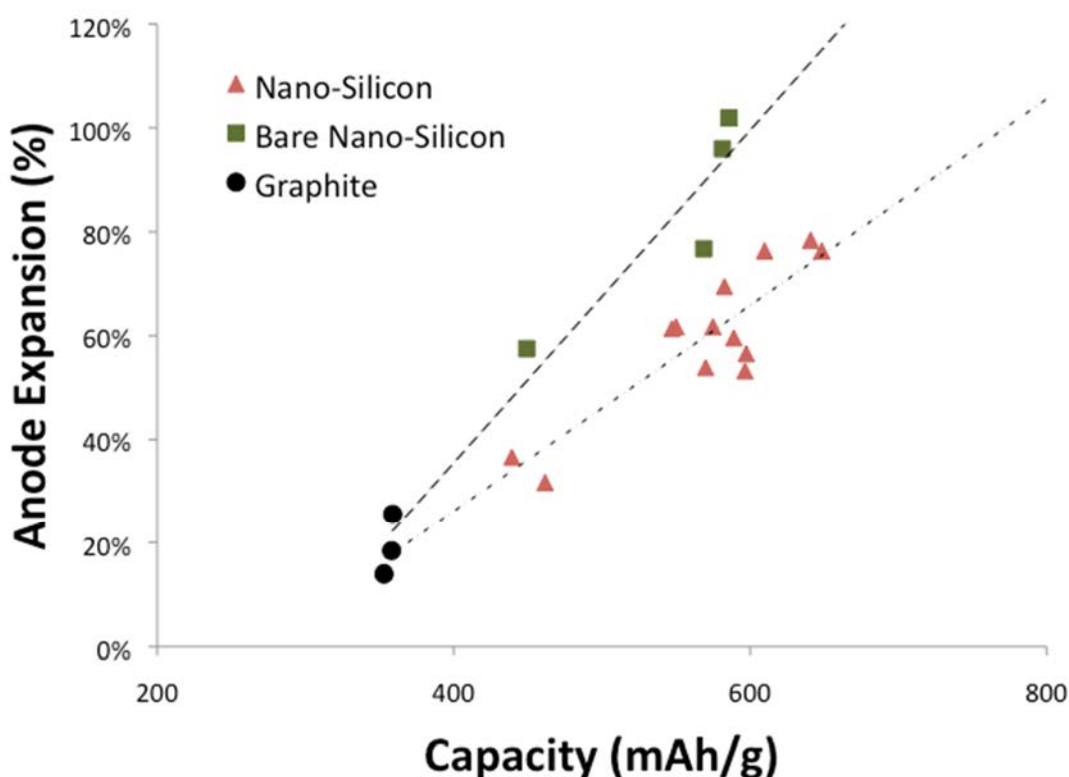
Figure IV-314: Anode volume expansion for bare nano-silicon compared to the same material in Si-C composite

The same analysis was conducted for a variety of Si-C composites produced from a variety of different silicon types (Figure IV-315). We measured volume expansion of an electrode comprising Si-C composites incorporating nano-silicon, in addition to Si-C composites incorporating nano-featured silicon, and Si-C composites incorporating silicon oxide, denoted SiO_x. The data were collected in coin cell, half cells, wherein the anode also comprised graphite blended to achieve capacity in the range of ~ 450 – 650 mAh/g. Interestingly, all of these Si-C composites exhibited a similar volume expansion with increasing capacity, for

example the volume expansion for these anode materials was in the range of about 60-80% when blended in graphite to achieve a capacity of about 600 mAh/g. For reference, data are also depicted for graphite, whose data fall roughly within the extrapolation of the trendlines. Also included in Figure IV-315 are data for Si-C composites wherein we have synthesized the silicon within the confines of the Si-C composite production process (this sample is denoted "Group14 composite"). As can be seen, the Group14 Si-C composites exhibited extremely low volume expansion.

Figure IV-315: Anode volume expansion for various Si-C composites comprising different silicon types

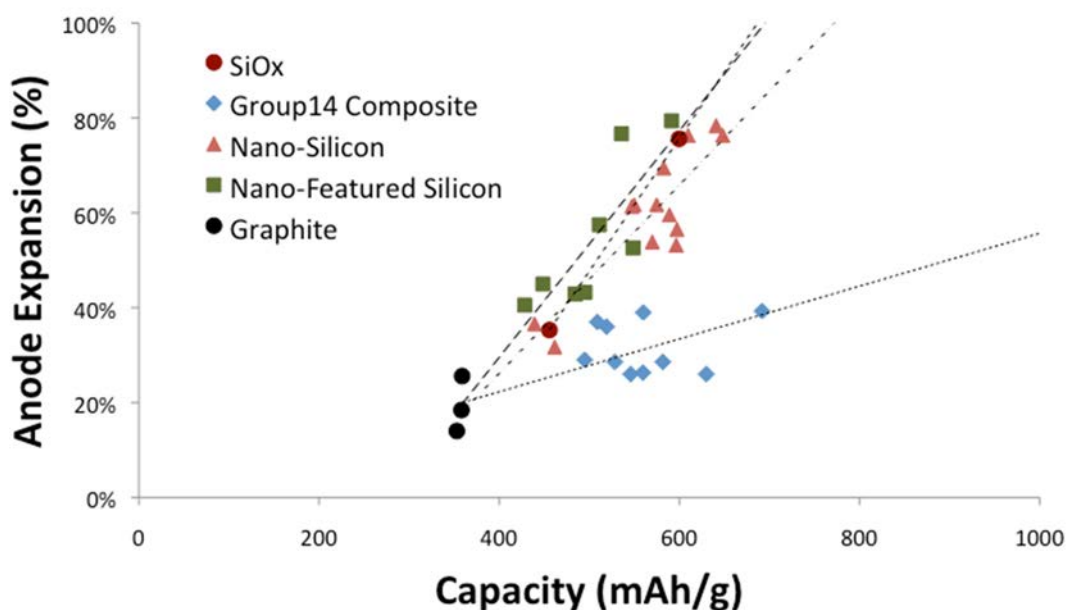For the period corresponding the second quarter of the project (Apr 1 – Jun 30, 2016) the work focused on down selection. Specifically, we met the objective of choosing three down-selected samples, and the information was shared with the DOE via telecon. Major activities included physicochemical and electrochemical evaluation of a large variety of silicon-carbon composites representing a wide variety of formulation and process variables. The surface area and pore volume for the three down-selected samples were as low as 2-8 m^2/g and <0.001 – 0.011 cm^3/g, respectively. The gravimetric capacity and Coloumbic efficiency as measured in half cells were as high as ~1100 mAh/g and ~0.9980, respectively. The cycle stability as measured in full cells was as high as ~300 cycles, as depicted in Figure IV-316(volumetric basis) and Figure IV-317(gravimetric basis). Gravimetric capacity was calculated based on the total active mass of the anode and cathode (minus current collector, binders, conductive enhancers). Volumetric capacity was calculated based on the total volume of anode and cathode (minus current collector) including binders and conductive enhancer. These data were obtained in full cell coin cells, employing LiNiCoAlO cathode and 1 M LiPF$_6$ in EC:DEC w/10% FEC electrolyte, cycled at C/2 rate between 2.0 -4.2V with an I/2 hold at 4.2V. Our anodes were paired with LiNiCoAlO cathode, typically with 5-15% anode excess. Anode comprised CMC-SBR, Super-P, graphite, and Si-C composite suitable to achieve ~ 650 mAh/g on an anode basis. Notably, we demonstrated a doubling in stability over only the first six months of our project (compare down-selected sample 3 (DDS-3), presented at the end of the second quarter vs. the baseline presented in January). Since that time, further improvements in stability have been achieved; over the last few months we have demonstrated at least a tripling in the stability of our Si-C composite compared to the January baseline (vide infra).
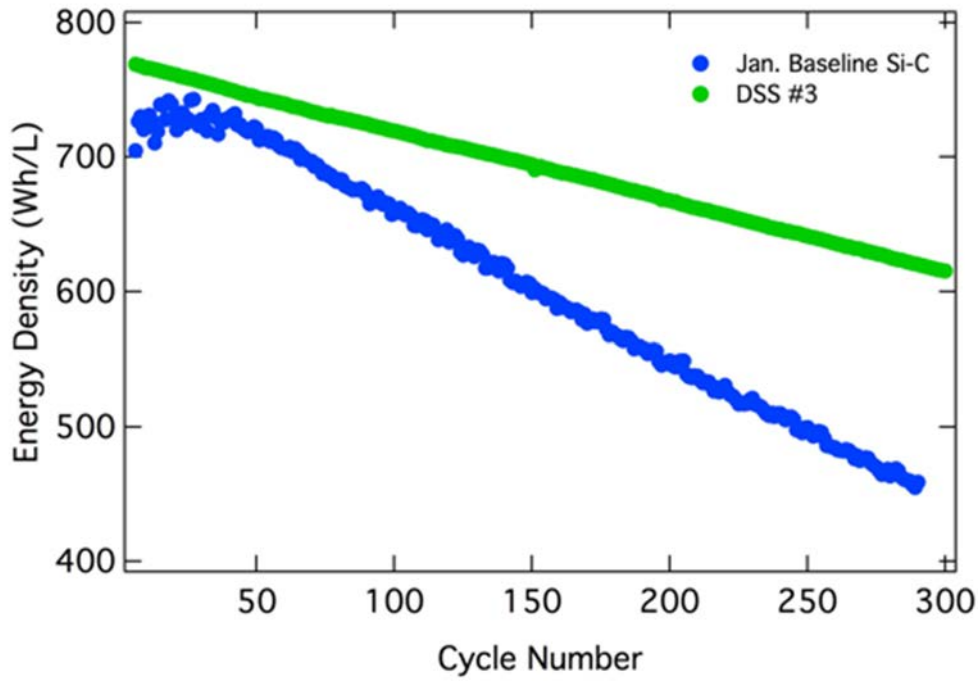
Figure IV-316: Example of volumetric capacity (Wh/L) for down-selected sample 3 ("DSS-3") presented at end of second quarter of the project as compared to baseline presented six months earlier ("January Baseline Si-C")
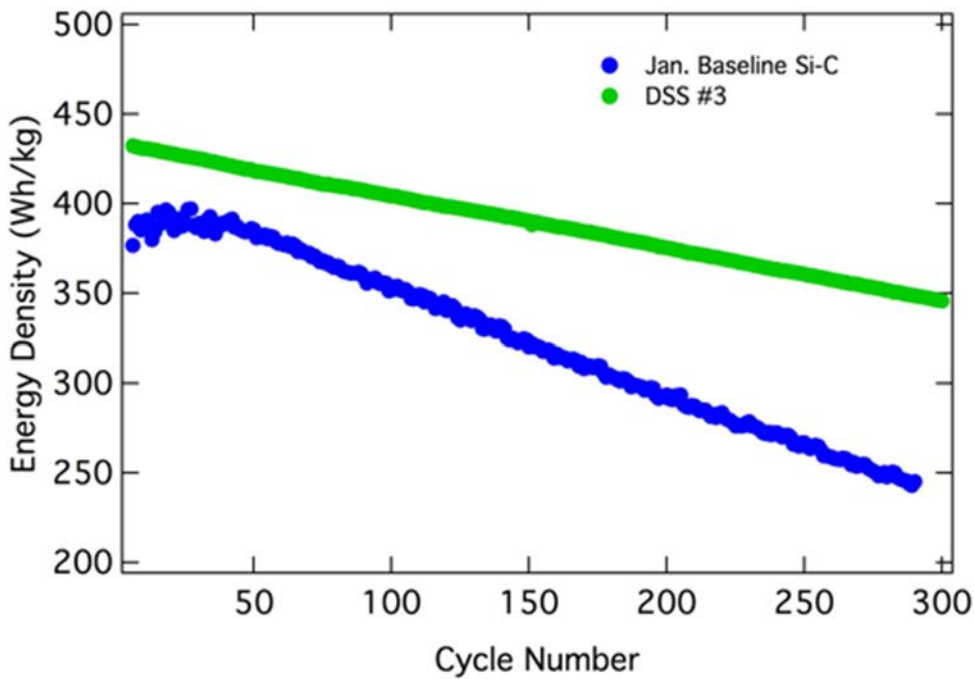
Figure IV-317: Example of gravimetric capacity (Wh/kg) for down-selected sample 3 ("DSS-3") presented at end of second quarter of the project as compared to baseline presented six months earlier ("January Baseline Si-C")

In addition to achieving the aforementioned milestone of down selection, we also accomplished substantial progress in other important areas. Importantly, we continued to gain mechanistic insight into the improved stability afforded by our Si-C composite. Specifically, we initiated two collaborations, one with Pacific Northwest National Laboratories (PNNL) and the other with the University of Washington (UW), both of which are focused on materials characterization and mechanistic insights into Si-C composite stability.

Our key collaborators at PNNL are Dr. Chongmin Wang and Dr. Langi Luo. Data were presented to Group14 indicating that our Si-C composites exhibit very low expansion compared to other silicon-containing materials. For example, data presented for DSS-3 exhibited a very low expansion when examined via TEM during lithiation. Specifically, DSS-3 exhibited as low as 24% volume expansion upon lithiation (see Figure IV-318). For comparison, Dr. Wang communicated data for a comparator Si-C composite (not provided by Group14) wherein 200% volume expansion was observed.

Non-Lithiated	Lithiated
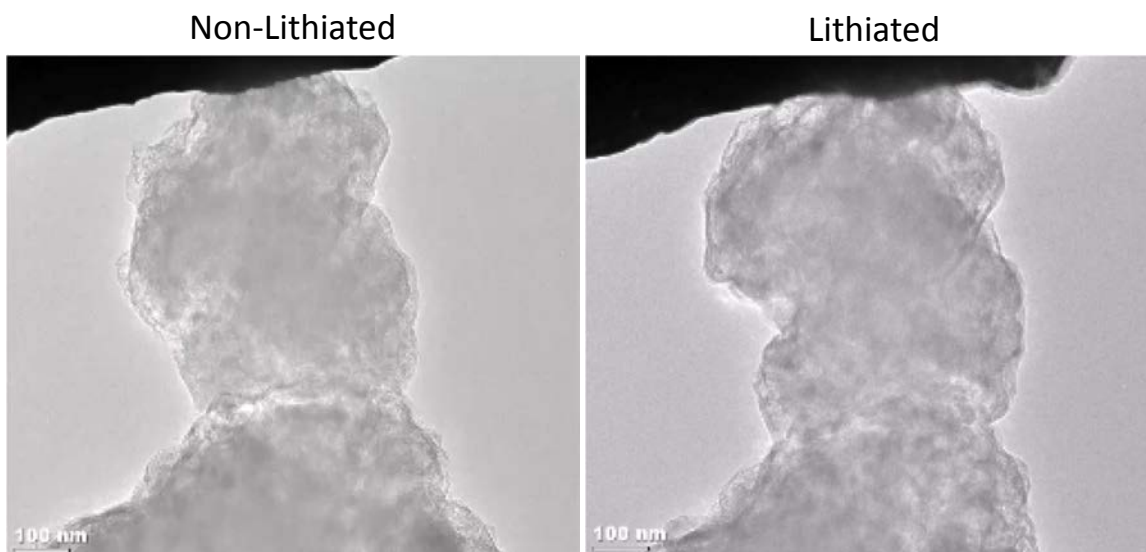
Figure IV-318: TEM observation of down-selected sample 3 (DSS-3) expansion before lithiation (left) and after lithiation (right); the observed expansion was 24%
Credits/Source: Chongmin Wang & Langli Luo, PNNL, "Diagnosing failure mechanisms of Si-C nanocomposite anode materials", PowerPoint presentation to Group14 Technologies on 6/16/2016.

For the period corresponding the third quarter of the project (Jul 1 – Sep 30, 2016) the work focused on process assessment and production of Si-C composite material beyond lab quantities. We met the related quarterly milestone, and the information was shared with the DOE via telecon. During this period, activities included process assessment, production of larger quantities of composite, and continued physicochemical and electrochemical evaluation of various silicon-carbon composites. Several key parameters were evaluated, including different, scalable reactor types and temperature, time, and reactant mixing conditions.

We also demonstrated continued improvement in stability for the Si-C composite. For example, Figure IV-319 (volumetric basis) and Figure IV-320 (gravimetric basis) compare the improvement in full cell stability (coin cells) for down-selected sample 1 (DSS-1) achieved between the end of the second and third quarter of the project. The cells were cycled at 1C between 2.5 – 4.2 V with I/2 hold, with a rate change to C/10 every 20th cycle, employing an electrolyte of 1 M LiPF6 in EC:DEC w/10% FEC, and LiNiCoAlO cathode. Typically, the anode was 5-15% excess, and comprised CMC-SBR, Super-P, graphite, and Si-C composite suitable to achieve ~ 650 mAh/g on an anode basis. Importantly, the data show an improvement from ~250 cycles to ~ 450 cycles (comparison of samples presented to DOE on 7-28-2016 and 10-27-2016).
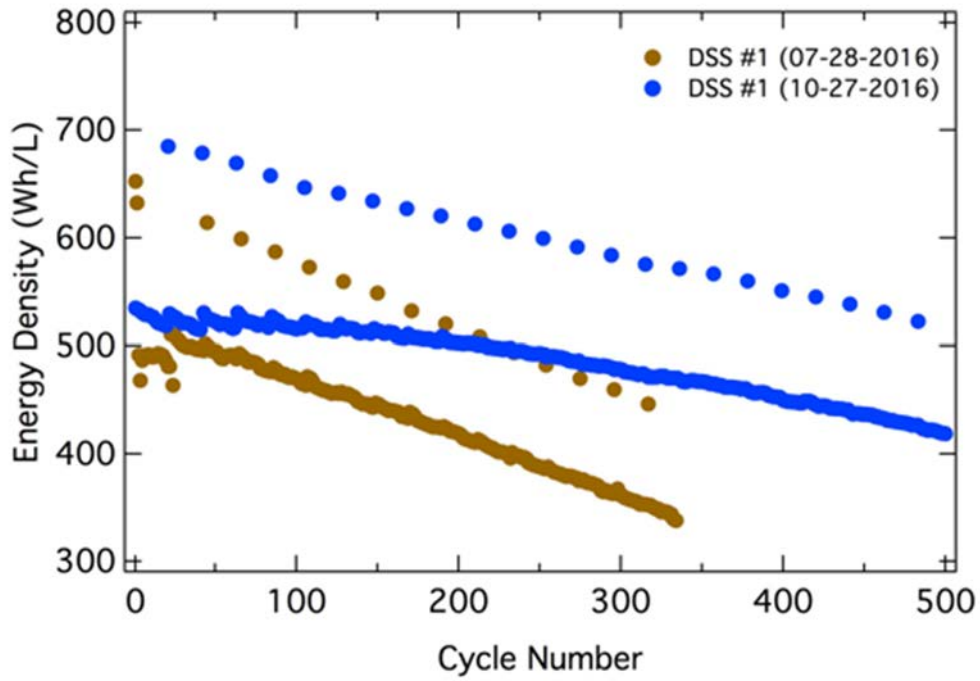
Figure IV-319: Example of volumetric capacity (Wh/L) for down-selected sample 1 ("DSS-1") presented on 7-28-2016 compared to the data presented on 10-27-2016
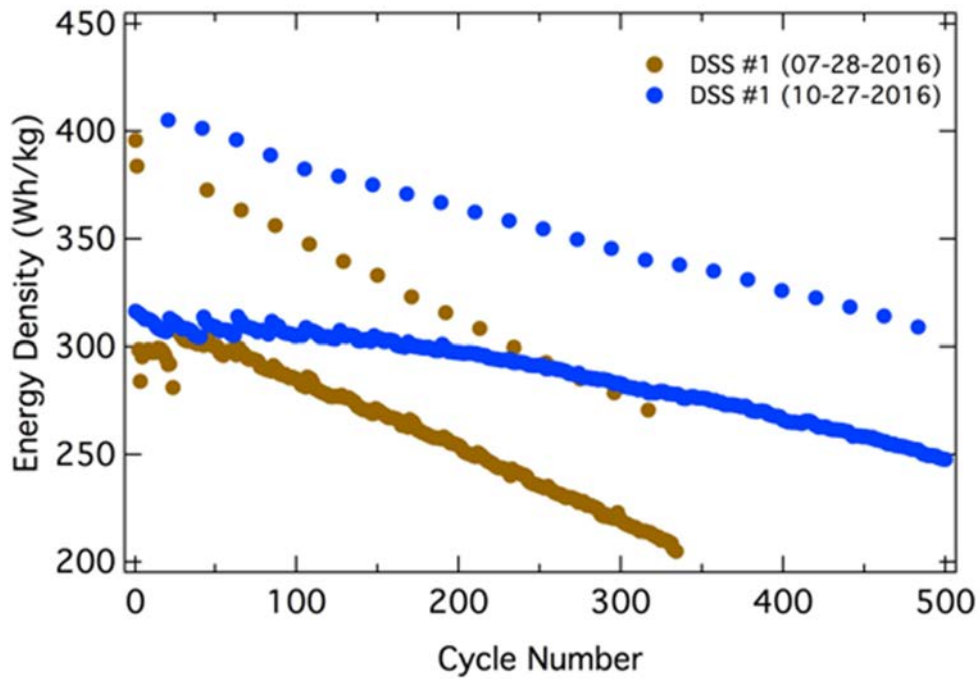
Figure IV-320: Example of gravimetric capacity (Wh/kg) for down-selected sample 1 ("DSS-1") presented on 7-28-2016 compared to the data presented on 10-27-2016

Conclusions

Group14 Technologies is developing low-cost, high-performing Si-C composite materials suitable as a drop-in for lithium-ion battery anodes. For the first three quarters, the project has remained on-track and met project milestones, as presented to the DOE. We have successfully down-selected samples for scale up, and demonstrated ongoing performance improvements. We are also conducting mechanistic investigations into the stability afforded by our Si-C composites; in particular, our collaboration with PNNL has confirmed very low volume expansion for our materials.

Products

Presentations/Publications/Patents

1. "Enabling Exceptional Cycle Life and Energy Density in Silicon Based Lithium-ion Anode Materials," presented by Dr. Henry Costantino on March 23, 2016 at the 33rd Annual International Battery Seminar & Exhibit held in Fort Lauderdale, FL.
2. "Low Cost Manufacturing of Advanced Silicon-Based Anode Materials," presented by Dr. Aaron Feaver on June 9, 2016 in Washington, DC at the 2016 DOE Annual Merit Review and Peer Evaluation Meeting.
3. International patent application PCT/US2016/049025, "Novel Materials with Extremely Durable Intercalation of Lithium and Manufacturing Methods Thereof," A Sakshaug, HR Costantino, AM Feaver, LA Thompkins, K Geramita, BE Kron, S Frederick, F Afkami, A Strong.

References

1. Chongmin Wang & Langli Luo, PNNL, "Diagnosing failure mechanisms of Si-C nanocomposite anode materials", PowerPoint presentation to Group14 Technologies on 06/16/2016.

IV.F.2. Commercially Scalable Process to Fabricate Porous Silicon (Navitas Advanced Solutions Group, LLC.)

Peter Aurora, Principal Investigator
Navitas Advanced Solutions Group, LLC.
4880 Venture Drive, Suite 100
Ann Arbor, MI 48108
Phone: 734-205-1447
E-mail: paurora@navitassys.com

Subcontractor
Matthew Seabaugh
Nexceris, LLC
404 Enterprise Drive
Lewis Center, OH 43035
Phone: 614-842-6606 Ext.107
E-mail: m.seabaugh@nexceris.com

Wenquan Lu
Argonne National Laboratory
9700 S. Cass Avenue
Argonne, IL 60439
Phone: 630-252-3704
E-mail: wenquan.lu@anl.gov

Walter G. Parker, DOE Program Manager
National Energy Technology Laboratory
Phone: 412-386-7357;
E-mail: walter.Parker@netl.doe.gov

Start Date: January 1, 2016
End Date: June 30, 2017

Abstract

Objectives

Navitas Advanced Solutions Group proposes a novel, commercially scalable approach to supply microporous silicon (μpSi) to lithium-ion battery manufacturers. The objectives for this program are:

- Qualify low-cost precursor materials for production of μpSi powder.

- Optimize at bench scale the processes used to manufacture μpSi powder

- Transfer technology to Nexceris (scale-up partner) and establish pilot scale μpSi production (>1.0kg/batch).

- Validate materials performance in an open-source baseline prototype cell design. (Irreversible capacity loss <25% and 4-week self-discharge < 15% at 60°C)

- Establish the economic feasibility of μpSi manufacturing process (<25 $/kg)

Accomplishments

- Text Lab scale process optimization has been accomplished. Parameters for mechanical milling, thermal treatment and metal oxide removal have been down selected.

- Current μpSi powder (at 10g scale) has $30 m^2/g$ BET surface area, 10-40μm particle size, and $1.4 g/cm^3$ tap density, meeting the set targets.

- Navitas has started milling scale-up in collaboration with an industrial partner. Navitas has set up an intermedium mill to increase the synthesis scale to > 200g per batch.

- ANL has been conducting extensive material characterization for fundamental understanding of the microstructure. Electrochemical characterization showed ~3600 mAh/g and 7% initial capacity loss (ICL) of the pure µpSi.

- Silicon anode composites made with µpSi have shown 950 mAh/g reversible capacity with 17% ICL, and reached over 250 cycles at 80% capacity retention in a half cell (2.0 mAh/cm^2 at 0.5C).

- Nexceris has started to analyze safety requirements to scale up the µpSi process. Additionally, they will review the process to identify opportunities for reducing cost and manage potential hazards associated with scaling-up.

Future Achievements

- Navitas and ANL will work closely to optimize material composition and process towards scale-up.

- Nexceris will continue to identify opportunities for cost reduction using initial economic assessment and to manage potential hazards associated with scaling-up the processes.

Technical Discussion

Background

Advanced battery researchers have identified silicon nanocomposite materials as a viable anode technology for EV batteries. Presently, high capacity silicon-based anodes rely either on materials that are expensive (e. g., silane or nano-silicon powder) or on processes that are limited by low yield methods (e.g., chemical vapor deposition). Microporous silicon potentially avoids these limitations and is attracting increasing attention as a lower cost alternative for the manufacture of high capacity silicon-based anodes. Microporous silicon suitable for EV batteries is not currently available as a commodity material. Microporous silicon can be produced at lab scale through a metal catalyzed hydrofluoric acid etching process. However, this process is expensive and hazardous.

Introduction

Navitas proposes a novel, commercially scalable approach to supply microporous silicon (µpSi) to lithium-ion battery manufacturers (Figure IV-321). If successful, this project will result in a significant reduction in the cost and environmental impact of high capacity anodes that are needed to meet EV battery goals. Our proposed production route will facilitate the availability of µpSi to lithium-ion battery producers and developers at a scale and cost able to support EV battery production.

The critical success factors to achieving this goal are:

- Use low-cost raw materials.

- Eliminate the use of hazardous materials such as silane and hydrofluoric acid.

- Reduce process cost through higher intensity and throughput.

- Retain desired electrode powder morphology.

- Control impurity level and nature of the product throughout the manufacturing process.

Approach

To accomplish the above goals, Navitas is teaming with Nexceris and Argonne National Laboratory (ANL) to establish a reliable domestic source of µpSi. Nexceris provides powder manufacturing scale up development and expertise. ANL performs material characterization and gives input to improve material design and process optimization. The Navitas' process is expected to transition this process from MRL 3 to MRL 6, providing the ability to deliver µpSi in adequate quantity to support pilot scale electrode coating by EV battery OEM's at the scale needed to support cell design validation (typically 500 – 600 cells in the EV battery cell format).

The proposed µpSi production comprises a three-step process involving the usage of inexpensive commodity grade silicon oxide (refer to Figure IV-321, Figure IV-322, Figure IV-324 and Figure IV-326). Each step employs scalable industrial processing methods (i.e. mechanical mixing, thermal reduction, and etching). The combination of these steps will reduce process temperature and times for the complete reduction silica, reducing operating cost compared to other methods. In addition, by avoiding usage of hydrofluoric acid, the proposed process also has environmental and non-hazardous advantages over the conventional route.

Results

Lab-scale Process Optimization: Powder Milling (Step 1)

The mechanical milling parameters including rotational speed, milling time, ball to powder ratio (BPR), and relative proportion of the reactants have been down-selected at lab scale (Figure IV-322). These factors play important roles on the nature and kinetics of the product phase as well as the powder mixture composition.
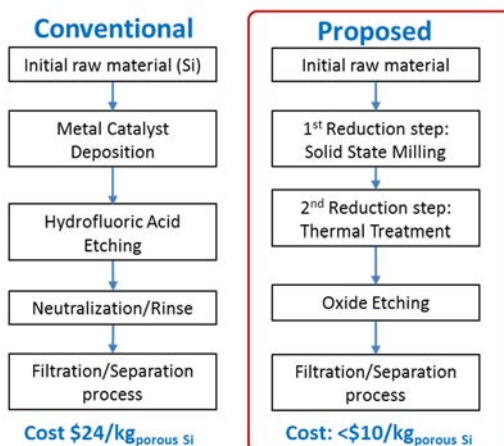
Figure IV-321: Conventional production of porous silicon uses hazardous hydrofluoric (HF) acid and expensive metal catalyst. Navitas route reduces cost and impact, using SiO₂ raw material and no HF

Navitas proof of concept data were used as starting point for the µpSi manufacturing process optimization. Initial experiments have shown that porous silicon can be produced using a combination of a mechanical milling activation step, a thermal reduction step, and a final etching process. The mechanical milling step provides activation and partially reduces silica. The temperature of chemical reduction of SiO_2 can be reduced to < 800°C when mechanical activation is employed, which otherwise requires T > 1000°C.

Step-1: Mechanical milling pretreatment
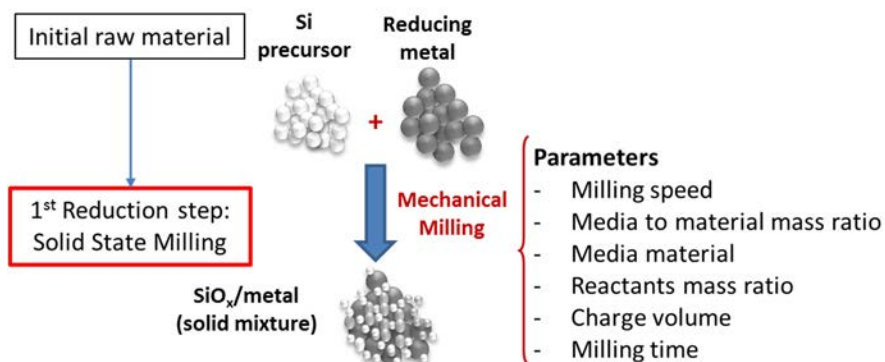
Figure IV-322: Schematic diagram of the 1st step reduction/activation. SiO₂ and reducing metal are mechanically milled to pre-activate the solid system and partially reduce the oxide

Lab-scale Process Optimization: Thermal Reduction (Step 2)

Thermal reduction of silicon oxide using a reducing metal initiates at temperatures below the metal melting point. The phase and composition of the Si/metal oxide composite varies with process conditions. Heating rates, soaking temperature and holding times influence the final structure of the result composite. The structure of the resulting particles is critical to the formation of porous silicon structures by the removal of metal oxide in the later step. A schematic representation of this process is shown in Figure IV-323.

Step-2: Thermal treatment
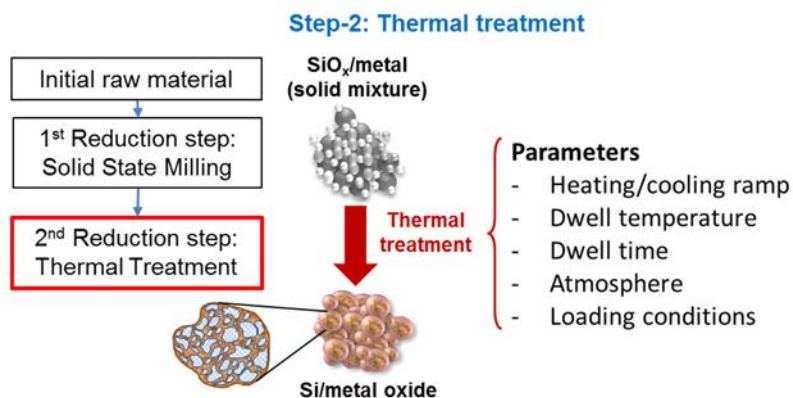
Figure IV-323: Schematic diagram of the 2nd step-thermal reduction. Ball milled SiO₂ /metal composite is thermally treated under inert atmosphere and converted to Si/metal oxide. The magnified particle scheme indicates the desirable microstructure for porous silicon formation, where orange is the reduced silicon

Thermal reduction parameters has been selected at lab scale. Reduction holding temperature has been kept under 800°C, which is preferred for production. After thermal treatment a Si/metal oxide composite particle with a pomegranate-like structure (inset Figure IV-324a.) is desirable for the formation of porous silicon structure (after metal oxide removal).
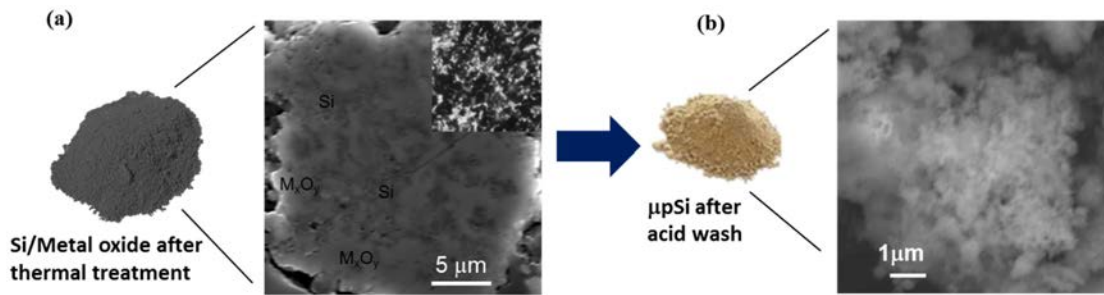
Figure IV-324: SEM micrographs for (a) Si-metal oxide composite structure after thermal treatment, inset shows the microstructures of the metal–SiO_2; (b) final microporous Si structure

Lab-scale Process Optimization: Metal Oxide Removal (Step 3)

The objective of this step (Figure IV-325) is to develop and optimize a wet chemistry process, safer and lower cost than HF etching, to remove the metal oxide and produce a microporous silicon powder. The task focuses on etchant type, etching solution concentration, digestion time, and etching temperature.

A non-HF acid was selected as the metal oxide etchant. The concentration, reaction time and temperature during etching is influenced by the composition of the Si/metal oxide mixture after thermal treatment. Usage of optimized thermal treatment parameters led to the reduction of etchant concentration, reaction time, and temperature.
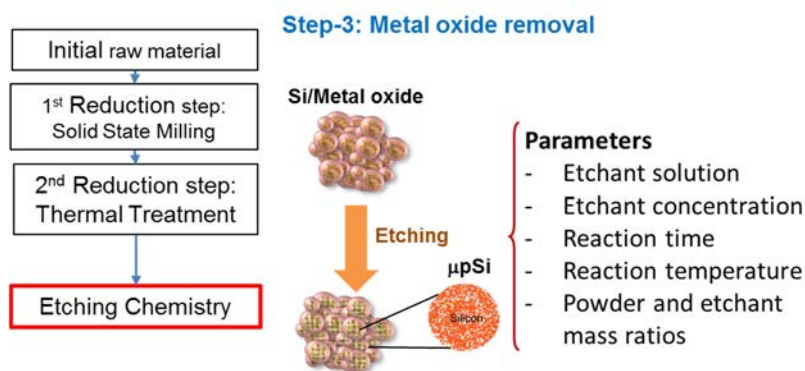
Figure IV-325: Schematic diagram of the metal oxide removal process. The Si/metal oxide is treated using acidic solution to remove the oxide leaving a porous structure

ANL conducted morphological and electrochemical characterization using the latest μpSi sample. The SEM micrograph in Figure IV-324.b confirms the high porosity of the Si material. X-ray diffraction studies, shown in Figure IV-326, confirmed the presence of crystalline Si. The measured physical properties of the μpSi powder are in line with the proposed targets. A summary of these properties are presented in Table IV-43.
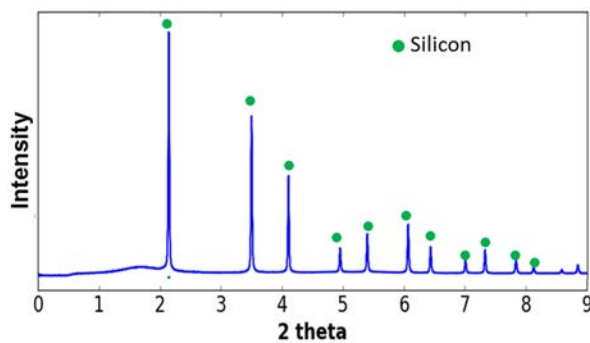
Figure IV-326: X-ray diffraction pattern for μpSi sample tested at ANL confirming the powder composition consists of crystalline Si and small traces of metal oxide

Nexceris has started to search for etchants including alternatives to sulfuric acid, focusing on safety assessment and cost reduction. Their experiments include dissolution studies of metal oxide transition phases at room and higher temperatures.

Table IV-43: Physical Properties of Current μpSi Powder

Property	Target	Actual
Particle size (μm)	5 - 50	10 - 30
BET surface area (m^2/g)	< 200	30
Tap density (g/cm^3)	> 0.8	1.4
True density (g/cm^3)	2.0 – 2.4	2.2

Lithium-ion Battery Grade Material Demonstration

Electrochemical performance evaluation was done using an 'open source' cell design, i.e. not involving proprietary designs or components. The intent is to demonstrate that the μpSi powder produced by our low cost process is a functional and compatible component in the anode, rather than to optimize the overall anode design and performance. Electrochemical validation of the μpSi material was carried out in half-cell (CR2025) and full lithium ion (single layer pouch) cell configurations.

Electrochemical characterization at ANL was targeted to measure the μpSi true reversible capacity and ICL. Figure IV-327 shows the voltage-capacity profiles for the μpSi anode electrodes. The voltage range used was 0.01-1.5V at 0.1C rate. The first delithiation capacity was 3610mAh/g with a 7% ICL.

In addition, Navitas has performed electrochemical experiments to qualify the μpSi as a precursor for the fabrication of Si anode composites. Commercially available micron size Si powder was used to make a baseline composite. In order to fabricate electrodes the Si powders were made into a composite with 50% graphite. Both types of composite electrodes were hand-casted to a 2mAh/cm2 reversible loading.
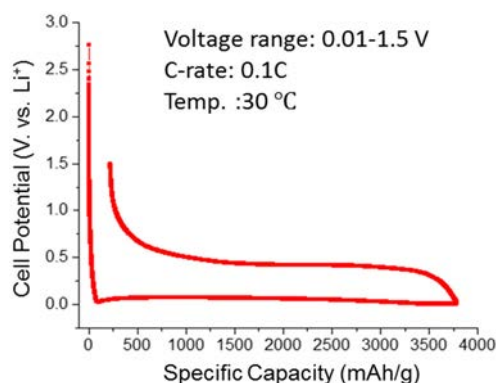
Figure IV-327: Voltage-capacity plots for μpSi electrode formation, with ~3600mAh/g reversible capacity and 7% ICL

Half-cell formation cycles were carried out at 0.05C rate from 0.01V to 2.0V. Cycle life test was run at 0.01 – 1.0V and at +0.5C/-0.5C lithiation/delithiation rate. Table IV-44 summarizes formation values. The composites have reversible capacities of ~950 mAh/g (Figure IV-328a). The ICL are 15% and 17% for the commercial Si and μpSi based composites respectively. The μpSi/graphite composite electrode shows promising cycle life (Figure IV-328b). These results suggest that the μpSi is a good precursor to make Si anodes with improved cycle life while maintaining high reversible capacities.

Table IV-44: Formation Summary Values for Half Cells Build with Navitas μpSi and Natural Graphite

Anode	Precursor	Capacity at C/20 (mAh/g)		ICL (%)
		Lithiation	Delithiation	
Si composite	1-5μm commercial Si	1115	955	15%
μpSi composite	Navitas μpSi	1170	946	17%
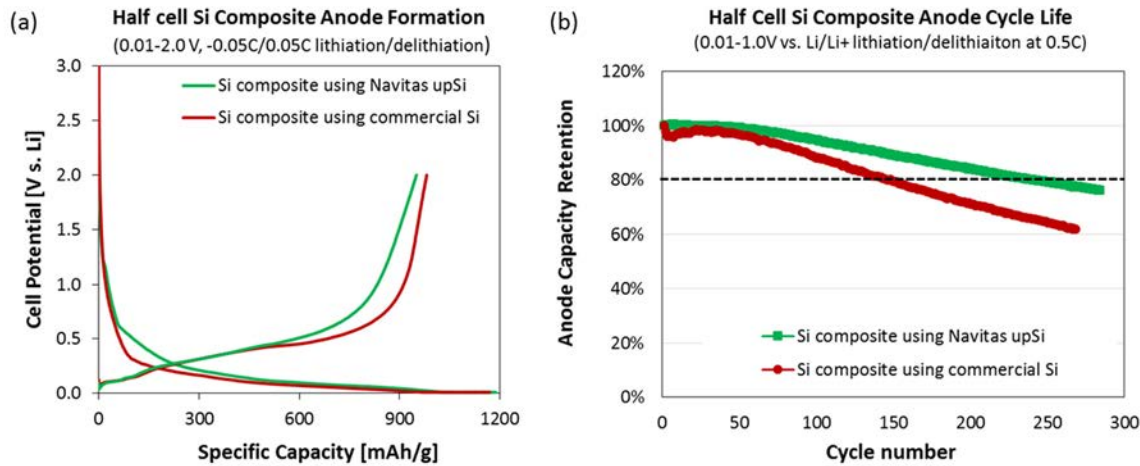
Figure IV-328: Silicon composite made with commercial Si and μpSi (a) half-cell anode formation data (b) cycling performance with 2.0 mAh/cm² loading

Furthermore, single layer pouch (SLP) lithium cells have been fabricated with the μpSi composite anodes and NCM523 cathodes (2.5 mAh/cm²). The anode and cathode were matched using an A/C ratio of 1.1. The cell shows high rate capability, retaining 90% capacity at 2C (Figure IV-329). Life cycle testing is ongoing and results will be presented in the next reporting period.
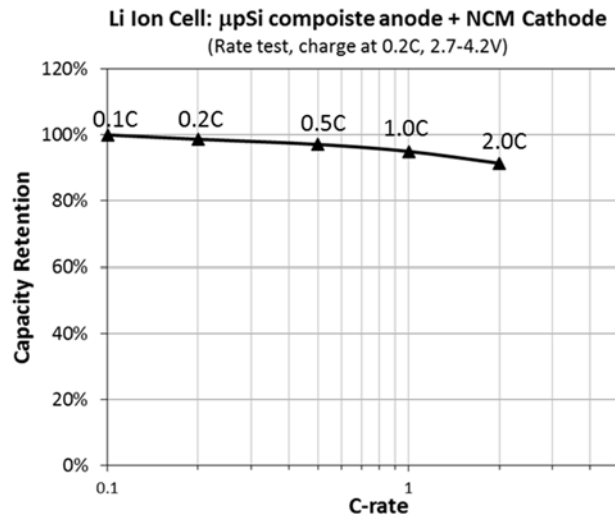
Figure IV-329: Rate capability of a lithium-ion single layer cell with μpSi composite anode and NCM 523 cathode, charged at 0.2C, and discharged at 0.1, 0.2, 0.5, 1.0, and 2.0C

Cost Analysis

Navitas has started working on mechanical milling scale up using larger milling system. Initial transition from lab-scale to medium scale (≥200 g per batch) will be done at Navitas facilities. Final milling for pilot scale demonstration will be performed at toll milling facility. Ball milling process cost model will be based on large scale mill equipment. To make the process cost-effective, the most important issue is to balance the time and labor requirements with capital costs and operator risk. Nexceris has begun trials to determine the lowest cost and safest method for extracting the metal oxide from the aggregate powder. Heat treatment evaluation focusing on effect of batch size and atmosphere is also in the process at Nexceris. Nexceris will develop a preliminary cost model for the thermal and etching processes, defining process and safety equipment by the end of Year 1.

Conclusions

Optimization at lab-scale for the process to fabricate micro porous Si has successfully completed. The material quality was obtained by characterization studies performed by the ANL investigators. The synthesized μpSi powder has met the physical property targets, including BET surface area, particle size, and tap density.

Navitas and ANL conducted electrochemical validation of the μpSi powder in half and full cell configuration. ANL characterization focused on fundamental understanding of the microstructure and measurement of the true reversible capacity of the μpSi (~3600 mAh/g) and initial capacity loss (7%). Navitas has used μpSi as a precursor for the fabrication of Si composite anodes. Half and full cell results suggest that the μpSi is a promising precursor to make Si anodes with improved cycle life while maintaining high reversible capacities.

Navitas has started milling scale-up in collaboration with commercial milling company. While, Nexceris has initiated the large scale process analysis and cost modeling.

Products

Presentations/Publications/Patents

1. "Commercially Scalable Process to Fabricate Porous Silicon", ES216_Aurora_2016_O, US DOE Vehicle Technologies AMR, 2016.
2. "Processes to Fabricate Porous Silicon and its use as feedstock for Secondary Battery Electrodes", Aurora et al., US Provisional Patent Application, filed July 2016.

IV.F.3. An Integrated Flame Spray Process for Low Cost Production of Battery Materials for Lithium Ion Batteries and Beyond (University of Missouri)

Yangchuan Xing, Principal Investigator
University of Missouri
Department of Chemical Engineering
Columbia, MO 65211
Phone: 573-884-1067; Fax: 573-882-4940
E-mail: xingy@missouri.edu

Walter G. Parker, DOE Program Manager
National Energy Technology Laboratory
Phone: 412-386-7357
E-mail: Walter.Parker@netl.doe.gov

Start Date: January 2016
End Date: December 2018

Abstract

Objectives

The objective of this project is to develop an advanced manufacturing technology for battery materials production at low cost and in a green chemical process. The work for 2016 was on chemical precursor (deep eutectic solvent or DES) development and flame spray reactor development. This included:

- Achieve a precursor DES formulation to make $Li(Ni_{1/3}Mn_{1/3}Co_{1/3})O_2$.

- Achieve a precursor DES formulation to make $Li(Ni_{0.80}Co_{0.15}Al_{0.05})O_2$.

- Establish physical and chemical properties of feasible DES formulations.

- Fabricate an operational flame spray pyrolysis reactor that can spray the DES precursors.

- Demonstrate a production capacity of 1.5 kg/day with the spray technology.

Accomplishments

- Achieved understanding of DES precursors to make $Li(Ni_{1/3}Mn_{1/3}Co_{1/3})O_2$.

- Achieved understanding of DES precursors to make $Li(Ni_{0.80}Co_{0.15}Al_{0.05})O_2$.

- Formulated DES precursors for cathode materials.

- Designed and fabricated improved version of the iFSP reactor (Gen 2.0).

- Demonstrated high throughput spray rate.

Future Achievements

- To further demonstrate powder materials production capacity.

- To control powder morphology and size.

Technical Discussion

Background

Advanced automotive battery research has the aggressive goal of cutting battery cost from the current $500/kWh to $125/kWh by 2022. This 75% reduction can only be achieved with an array of technological innovations and process integrations. Active cathode materials of transition metal oxides account for more than 30% cost of lithium-ion batteries. Reducing the cost of such materials is needed to achieve the overall battery cost target and enable wide-spread commercialization of electric vehicles. New cost-effective manufacturing processes have to be developed to meet the challenges.

Introduction

Flame (combustion) processes have been proven to be the most economic ways to produce fine powders. Pigment titanium oxide and fused silica are produced in millions of tons per year worldwide using flame processes. One of the challenges in these gaseous flame processes is that multiple metal oxides, like those used for lithium-ion batteries, are difficult to produce due to the lack of appropriate gasified chemical precursors. Oxides of multiple metals are often produced in flame spray pyrolysis processes in which liquid precursors (mostly dissolved metal salts) are used. Precursor salt solutions are atomized and sprayed into a flame to make metal oxide powders. Unfortunately, the current flame spray technologies have problems in high throughput manufacturing. They also use a large amount of water and are prone to producing pollutants.

This project is to develop a battery material manufacturing technology using an integrated flame spray process (iFSP). It is a green chemical process and has the potential to significantly reduce manufacturing cost of battery materials. The technology is based on our innovations in spray processes, chemical precursors, and process integrations. The three-year R&D project will take the proposed iFSP to a new technology readiness level, with a goal to achieve a 25% cost reduction for the cathode active materials. Further full-scale production development beyond the performance period is expected to reduce the cost by 50% by 2020.

Approach

Our approach to solving the manufacturing problem is to develop the iFSP technology. The innovations of the proposed technology can be summarized in the following three technical aspects:

(1) DESs as novel chemical precursors.
(2) Innovative spray process.
(3) Integrated downstream processing.
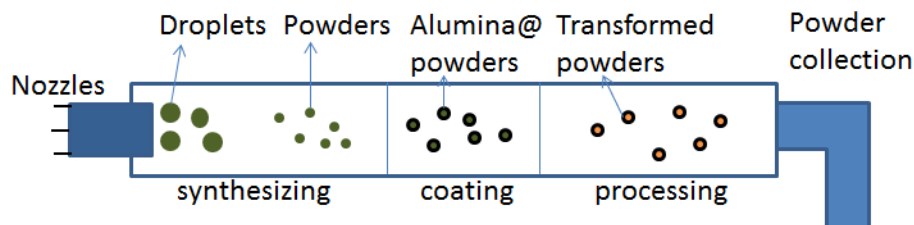
Figure IV-330: Schematic illustration of the iFSP technology in manufacturing cathode powders with synthesizing, coating (e.g, alumina), and processing processes integrated

As shown in Figure IV-330, there are two downstream processes (surface coating and materials processing), integrated into the flame reactor apparatus. Spray droplets of DESs will combust to produce the metal oxide powders. The process following it has an aluminum source introduced to make an alumina surface coating on the metal oxide powders to prevent degradation (dissolution) of the active materials and increase operation voltages. Carbon black (soot) may be produced *in situ* to achieve good electronic conductivity if needed and save another blending process in cathode fabrication. Another process is for processing of the powders to achieve desired crystalline phases through *in situ* annealing. The annealing process may be put before the

coating process. These innovations, if fully realized, would make manufacturing of battery materials at unprecedented low cost. This project is aimed to further develop the iFSP technology with the innovations, and move the work to a pilot scale production line.

Results

Formulation of metal containing deep eutectic solvents (DESs)

DESs have been studied in their formulations and properties. Room temperature DESs of different metals for battery materials have been made by using metal acetate hydrates and glycerol (a byproduct from biodiesel production). One of the most important factors affecting spray droplet characteristics is the viscosity of the DESs. Glycerol has a very high viscosity. After the DES formation, the DESs become more viscous. Their viscosities were studied so that a spray nozzle can be designed and used to make sprays. Figure IV-331 shows the viscosity measurements of the DES precursors to make the material $Li(Ni_{1/3}Mn_{1/3}Co_{1/3})O_2$ (LNMC). The DES has a viscosity of a Newtonian fluid at temperatures above room temperatures (25°C), but they generally display larger viscosities than glycerol (GL) at temperatures of 20-100°C.
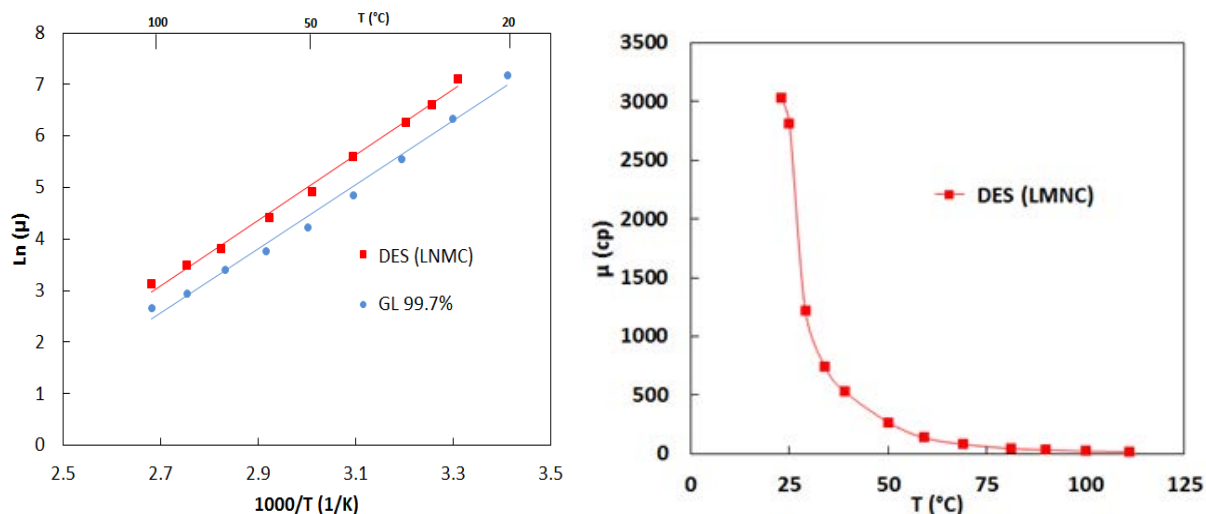
Figure IV-331: Left: Arrhenius plot of the GL and LNMC DES showed a Newtonian fluid behavior of the liquids. 99.7% GL is a product from biomass. Right: The viscosity of the DES precursor for LNMC materials measured within the temperature range

The DESs shown in Figure IV-332 are made with 1:5 molar ratios, displaying clear solutions at room temperatures, which are the precursors for making LNMC powders.

Figure IV-332: DESs of different metal acetate hydrates and that of a mixture to make LNMC materials

Room temperature DESs containing relevant metals for battery materials have been made by using nickel and cobalt acetate hydrates and aluminum nitrate, together with glycerol for $Li(Ni_{0.80}Co_{0.15}Al_{0.05})O_2$ (LNCA). The aluminum nitrate was used for aluminum source in the materials because aluminum basic acetate or aluminum dibasic acetate does not form a DES with glycerol. The 5% in moles of aluminum nitrate is a small fraction in the DES, and account for only about 2% in weight in the DESs. Figure IV-333 shows the viscosity measurements of the DES precursor to make the powder material LNCA. The DES also has a viscosity of a Newtonian fluid at temperatures above room temperatures (25°C).
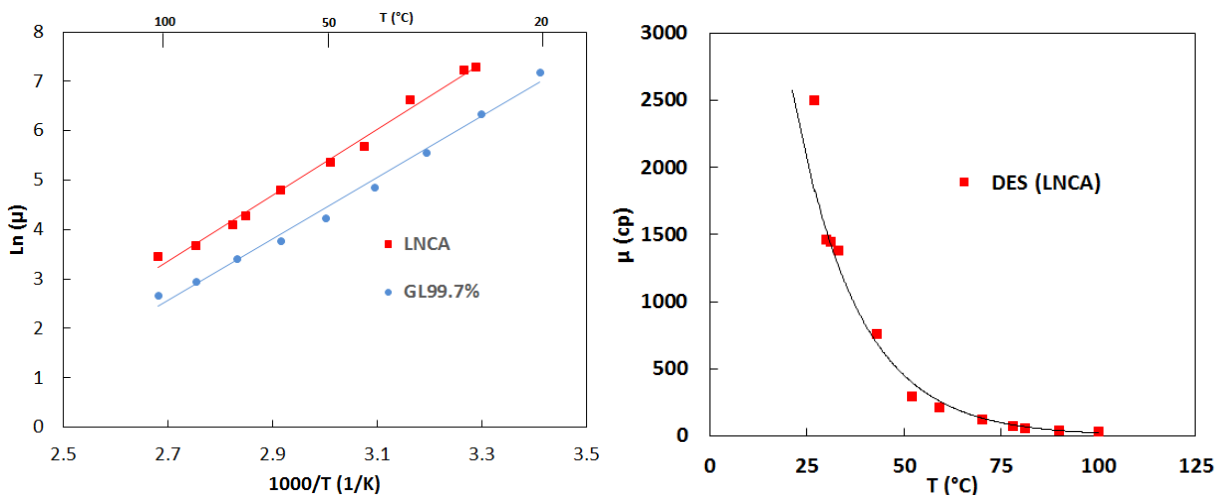
Figure IV-333: Left: Arrhenius plot of the GL and LNCA DES showed a Newtonian fluid behavior of the liquids. 99.7% GL is a product from biomass. Right: The viscosity of the DES precursor for LNCA materials measured within the temperature range

Spray process development and powder production

Process developments include nozzle and flame reactor design and development. The factors affecting the process are multifaceted. Process control include precursor feeding rates, flame temperatures, droplet flow, and residence time, which are all playing an important role in the powder morphology and structures. Work has been focused on improving all aspects of these factors with the goal to produce desired powder materials.

Powders were produced in the first generation process and powders of LNMC have been synthesized with the formulated DES precursors described above. The LNMC powders produced have a size of ~50 microns, as shown in Figure IV-334. These powders showed porous structures with low tap density that can be increased by making the powders less porous.
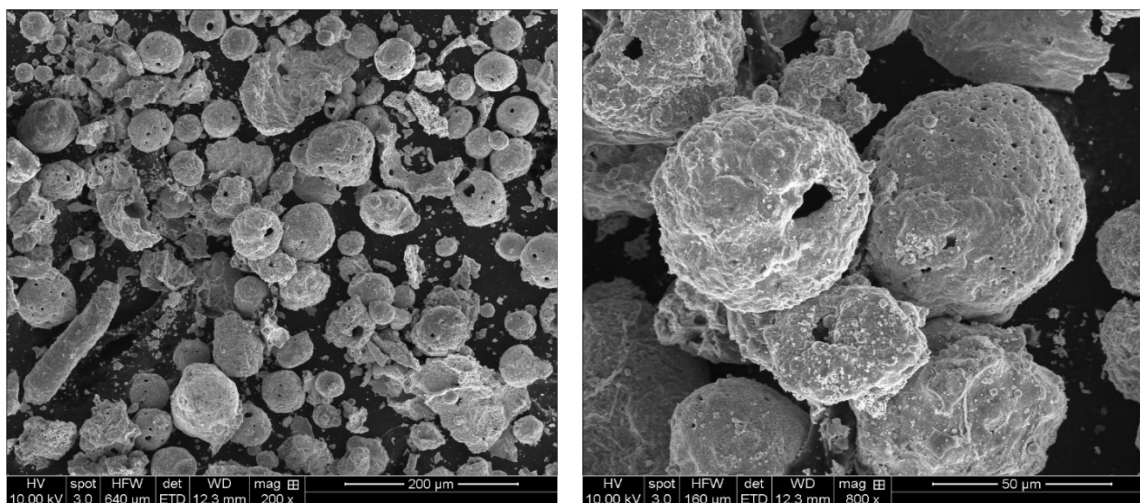
Figure IV-334: The LNMC powders produced in Gen 1.1 reactor

Conclusions

We started the project in January 2016. Our work has been focused on developing green chemical precursors based glycerol, a byproduct from biomass processing. We have also been developing a flame spray reactor to make powder materials. On chemical precursors, we have selected and studied salts of transition metals and lithium for the making of the active cathode materials. Acetate salts were selected that can form DESs with glycerol, and DESs from them were prepared. The DESs were studied for their fluid properties. It was determined that their viscosities are higher than pure glycerol but follow Newtonian fluid characteristics in the test range. It was also determined that the chemical precursors have to be sprayed at an elevated temperature (e.g., >100°C). The flame spray reactor has been designed and fabricated to spray the DES precursors at elevated temperatures. The reactor has a high throughput flow rate of the precursors, reaching the target of production rate set for this period of work.

Products

Presentations/Publications/Patents

1. Y. Xing, "Synthesis of Deep Eutectic Solvent Chemical Precursors and Their Use in the Production of Metal Oxides". Patent filed on 08/08/2016. PCT/US 16/45963.
2. J. Liao, J. Rana, K. Hamad, T. Smith and Y. Xing, "A Flame Spray Process for Cathode Materials Manufacturing for Lithium Ion Batteries", presented at the 230th Electrochemical Society meeting, Honolulu, HI. October 2-7, 2016. Abstract #95.
3. J. Rana, T. Smith, J. Liao, K. Hamad and Y. Xing, "Nanostructured Powders Made from Flame Spray Pyrolysis for Lithium-ion Cathode", presented at the 2016 AIChE Annual Meeting, San Francisco, CA. November 12-18, 2016. Abstract #421f.

References

None.

IV.F.4. Low Cost, High Capacity Non-Intercalation Chemistry Automotive Cells (Sila Nanotechnologies, Inc.)

Alex Jacobs, Principal Investigator
Sila Nanotechnologies, Inc.
2450 Mariner Square Loop
Alameda, CA 94501
Phone: 617-953-1548
E-mail: alex@silanano.com

Peter Faguy, DOE Program Manager
U.S. Department of Energy
Vehicle Technologies Office
1000 Independence Avenue, SW
Washington, DC 20585
Phone: 202-586-1022
E-mail: Peter.Faguy@ee.doe.gov

Start Date: October 2014
Projected End Date: May 2017

Abstract

Development of higher energy density electrodes for lithium-ion batteries is needed to greatly enhance cell energy storage characteristics. With this project, we aim to develop stable mixed metal fluoride-based cathodes based on some of the inexpensive, abundant and mass-produced metals. We further plan to produce demonstration high-energy full cells, where high capacity metal fluoride-based cathodes are matched with high capacity silicon-based anodes. Because of its drop-in replacement nature for existing production processes, the proposed technology will offer a smooth path to lower cost automotive cells. Therefore, the proposed project is well aligned with DOE goals: higher battery energy and power density, reduction in cell cost, and enhancement in safety, all to promote EV adoption.

Objectives

The objective of this project is to research, develop, and demonstrate (RD&D) ultra-high capacity alloy-type Si anodes and conversion-type mixed metal fluoride (MF_x) cathodes within lithium-ion cells, capable of achieving the following unit cell performance characteristics by the end of the project:

- Projected Energy Density: ≥1,200 Watt Hour per Liter (Wh/L)
- Projected Specific Energy: ≥580 Watt Hour per kilogram (Wh/kg)
- Projected Discharge Power Density: ≥2,400 Watt per Liter (W/L)
- Projected Specific Power: ≥1,160 Watt per kilogram (W/kg)
- Full Cell Degradation: ≤20% over 200 Cycles
- Projected Cost Reduction: ~3x

Accomplishments

- Novel approaches for synthesis of metal fluoride nanocomposites developed
  - Semi-automated tool has been designed, assembled and put to work
  - New approach provides the ability to utilize very low cost precursor chemistry

- Good performance of selected metal fluoride cathodes demonstrated
  - Iron fluoride cathodes have shown small voltage hysteresis
  - Iron fluoride cathodes have shown good stability when tested against Li anodes
  - Impact of surface coatings and electrolyte compositions explored

Future Achievements

- Higher voltage metal fluoride cathodes will need to be optimized for good performance
- Full cells with metal fluoride cathode and silicon anodes will need to be produced, tested and optimized for performance

Technical Discussion

Background

Commercial lithium-ion batteries built with Ni- and Co-based intercalation-type cathodes suffer from low specific energy, high toxicity and high cost. Further increase in the energy storage characteristics of such cells is challenging because capacities of such intercalation compounds approach their theoretical values and further increase in their maximum voltage induces serious safety concerns. The growing market for portable energy storage is undergoing a rapid expansion as new applications demand lighter, smaller, safer and lower cost batteries to enable broader use of plug-in hybrid and pure-electric vehicles (PHEV and EV), drones and renewable energy sources, such as solar and wind. Conversion-type cathode materials are some of the key candidates for the next-generation of rechargeable Li and lithium-ion batteries. Continuous rapid progress in performance improvements of such cathodes is essential to utilize them in future applications.

Introduction

Development of higher energy density electrodes for lithium-ion batteries is highly needed to greatly enhance cell energy storage characteristics. Sila has already demonstrated successful development of high energy density anodes. Complementary novel high energy density cathodes are needed to enhance the energy characteristics of the entire cell. Such cathodes also need to be both safer and cheaper than state of the art. However, most commercial and exploratory high energy density cathodes (such as lithium cobalt oxide (LCO), lithium nickel cobalt manganese oxide (NCM), lithium nickel cobalt aluminum oxide (NCA), etc.) contain either Ni or Co or both, which are toxic and rare elements. They are additionally relatively expensive, and thus Ni and Co-based cathodes face difficulties in meeting the demand to lower the cost of lithium-ion technology. Finally, these oxygen-containing, high energy density, high voltage cathodes possess significant safety risks (thermal runaway) when used in cells. We propose development and utilization of mixed metal fluoride - based cathodes based on some of the inexpensive, abundant and mass-produced metals. The proposed conversion cathode technology requires only one metal atom to store 2–3 Li atoms (in contrast with the conventional intercalation-type chemistry, where one metal atom stores only ½–1 Li atom, on average). Because of its drop-in replacement nature for existing production processes, the proposed technology will offer a smooth path to lower cost automotive cells.

Approach

The proposed cathode technology features: (1) micron-scale particles will allow "drop-in" replacement of conventional cathode powders (such as lithium nickel cobalt manganese oxide and lithium nickel cobalt aluminum oxide); (2) ultra-high capacity (~400 mAh/g); (3) a composite structure to achieve low volume changes and both mechanical and electrochemical stability during cycling; (4) compatibility with liquid or solid electrolytes and (5) protection of metal fluorides from undesirable interactions with the electrolyte in order for them to achieve long-term cycle stability. Microstructure optimization of such composite particles focuses on achieving low electrical and ionic resistance within the individual particles, which, in combination with slurry/coating optimization, will allow us to achieve low polarization and low voltage hysteresis at high rates. Sila developed and demonstrated a low-cost Si-based composite anode technology offering a unique combination of high volumetric and gravimetric capacity, high rate, low volume changes on the particle level (comparable to that of graphite) and stable solid electrolyte interphase (SEI) in conventional liquid electrolytes. During the project the conversion-type nanocomposite cathodes being developed will be matched with Si-based nanocomposite anodes to achieve ultra-high specific energy and ultra-high energy density in full cells. Electrolyte composition and slurry processing will be pre-optimized to achieve good cycle stability in matched full cells.

Results

Many scientific publications erroneously assign energy density and specific energy to a cathode based on its capacity and potential vs. Li/Li$^+$. This is technically incorrect and may lead to wrong conclusions. It is, therefore, important to estimate practically attainable energy densities of cells with different types of cathodes and anodes for evaluations in specific applications. Because the weight and volume of packaging as well as the inactive edge of a cell depends on its dimensions and configuration, we consider not the whole cell, but an elementary building block or a unit of a lithium-ion battery comprising a cathode coating (one sided), a thin separator, an anode coating (one sided) and half-thicknesses of cathode (Al) and anode (Cu) current collectors (Figure IV-335). The thickest (limiting) electrode (either anode or cathode) was considered to be 100 µm/one side, while the thickness of the other electrode was calculated based on the areal capacity matching. The volume fraction of the active material in each electrode is considered to be 70 vol. % in case of intercalation materials and 60 vol. % in case of conversion-type cathodes and silicon anodes. Material properties in the fully expanded (lithiated) state were used for calculating the volumetric capacities and inactive volume within each electrode. Formation losses on the anode as well as slightly higher areal anode capacity typical in practical cells have not been considered because such losses may, in principle, be compensated and matching could ultimately be improved. For average cell voltage estimations we considered experimental curves of intercalation cathodes and average potentials of conversion-type cathodes being 0.20~0.25 V lower than theoretical ones (the 0.20~0.25 V value was selected based on many experimental studies conducted on Li-S and Li-Se cells). Figure IV-335 compares energy densities (volumetric energy characteristics) of building blocks (units) of cells based on traditional intercalation-type Mn-, Ni-, Co-based cathodes when paired with = graphite with conversion-type cathodes paired with Si anodes. We see that improvements by over 100% are possible. In terms of specific energy (gravimetric energy density), conversion type cathodes may offer even better possibility for improvements with up to 200% better performance (Figure IV-336). We would like to clarify that our estimations of the energy characteristics of the cell building blocks (in Figure IV-335, Figure IV-336) are provided only to serve as guidelines for a direct comparison of opportunities offered by different chemistries when compared to the state-of-the art intercalation materials.

Matched unit stack with the thickest electrode of 100 µm,
9 µm thick separator and 9 µm thick current collector foils
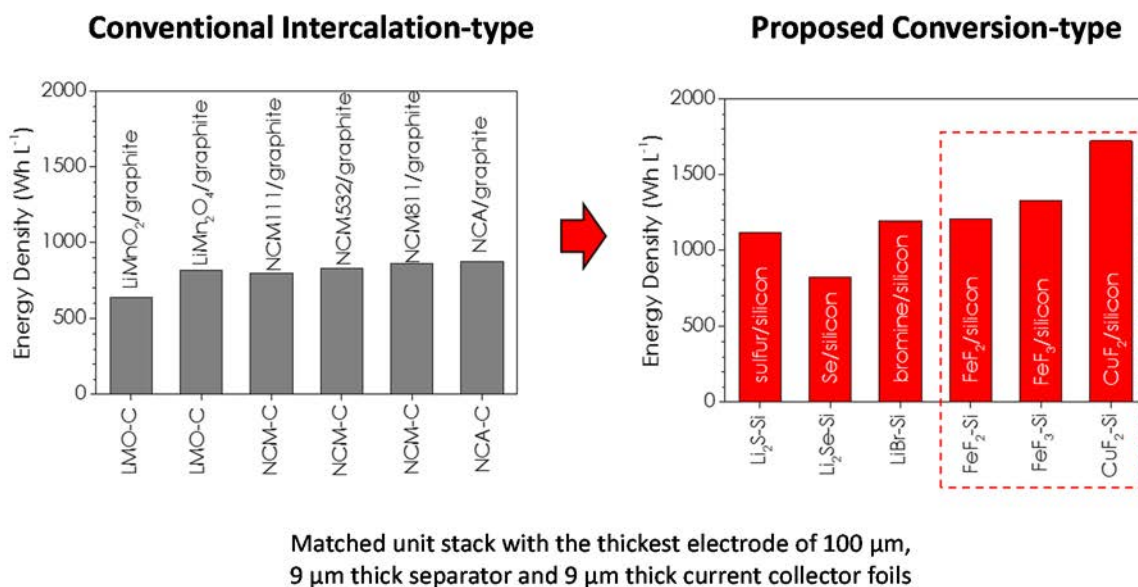
Figure IV-335: Estimation of the volumetric energy densities of unit stacks achievable with commercial intercalation-type electrodes and selected conversion-type electrodes. Areal capacities of anodes and cathodes were matched 1:1 and no extra capacity was considered for the formation losses
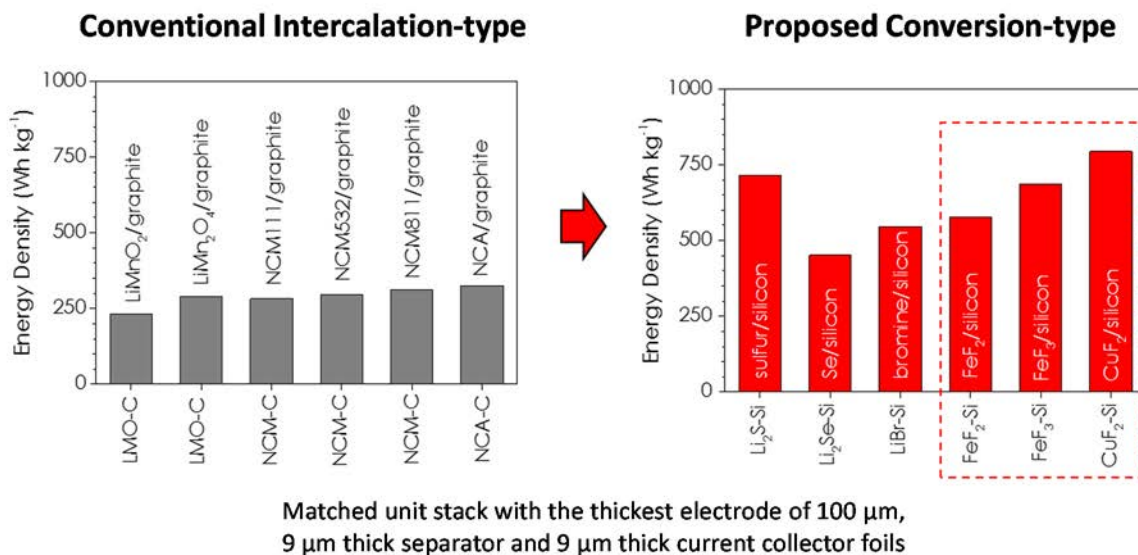
Figure IV-336: Estimation of the specific energy of unit stacks (calculating units) in rechargeable Li batteries achievable with commercial intercalation-type electrodes and selected conversion-type electrodes. Areal capacities of anodes and cathodes were matched 1:1 and no extra capacity was considered for the formation losses

We have designed and commissioned a versatile tool for the formation of metal fluoride cathode powders. All harmful effluent from the fluorination is captured with a custom-designed abatement system (Figure IV-337). As additional engineering controls to prevent exposure to potentially harmful gases or vapors, the tool is located in a fume hood and external sensors for all the harmful gases have been installed. Figure IV-337 shows the complete schematic of the final tool and a close-up view on the electrical components. The tool operation is automated to give precise control of temperature, pressure and gas flow rate. The recorded process parameters are uploaded into the cloud. Such a design facilitates reproducible testing under many conditions efficiently and safely.
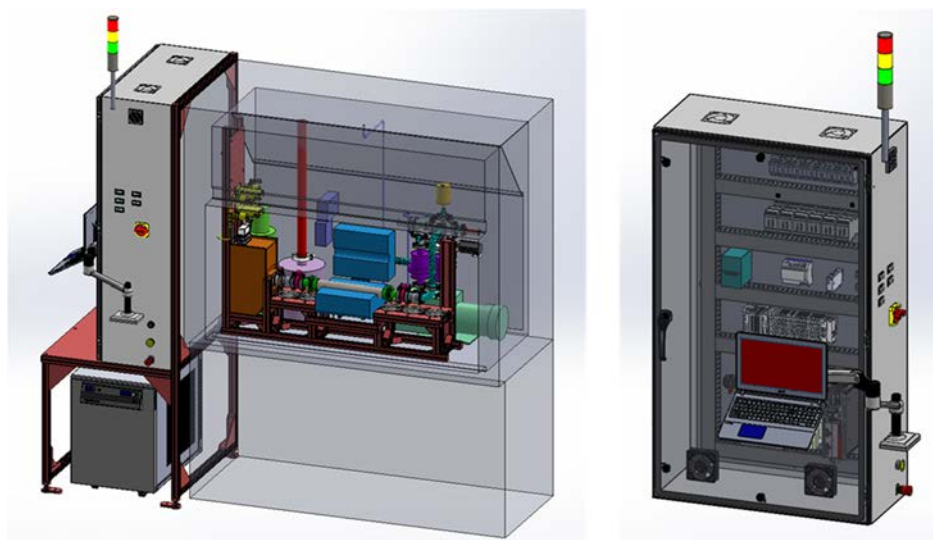
Figure IV-337: Schematic of the designed and assembled tool for use in metal fluoride cathode synthesis: (left) view of the entire system, (right) automation control panel

We have demonstrated good stability of the iron fluoride-based cathodes (Figure IV-338A), which could be matched well with Sila silicon-based anodes, similarly exhibiting good electrochemical stability (Figure IV-338B). Note that Si anodes have been cycled against intercalation-type high voltage LCO cathodes in matched full cells with no pre-lithiation and no excess Li capacity. The work on copper fluoride-based cathodes is still

in progress. The work on full cells with metal fluoride-based cathodes matched with silicon-based anodes is also in progress.
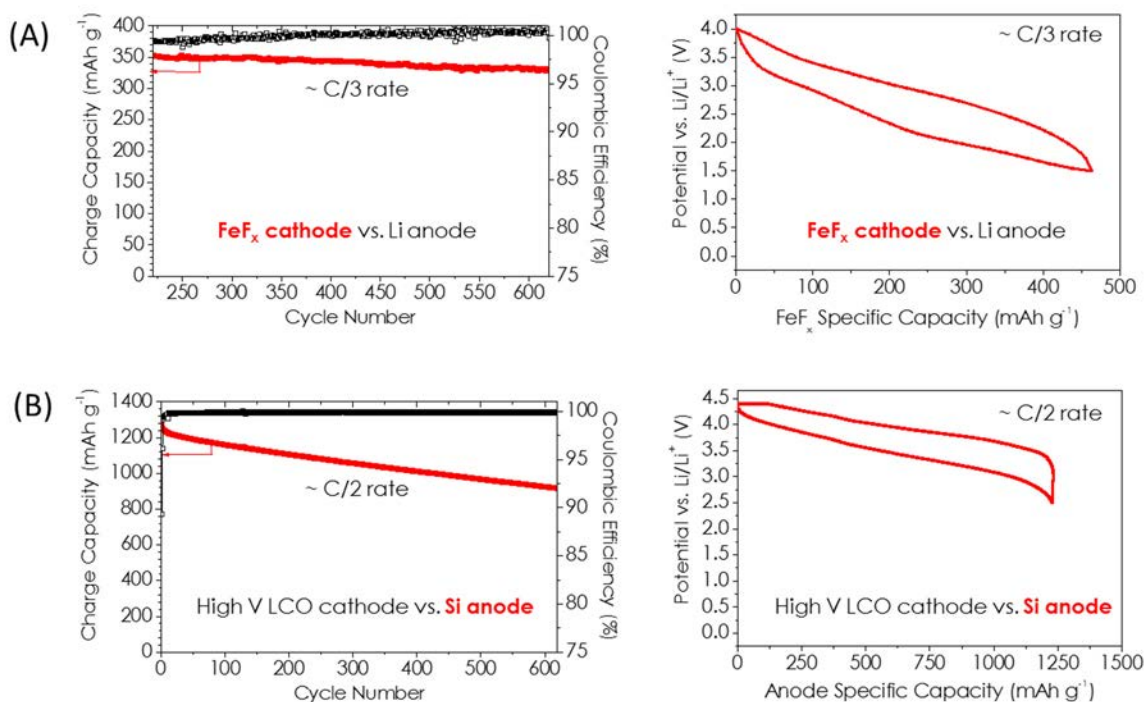
Figure IV-338: Performance of electrochemical cells with conversion-type electrodes: (A) cycle stability and a typical charge-discharge profile of iron fluoride-based cathode cycled against Li anode (capacity is normalized by the mass of the metal fluoride only); (B) cycle stability and a typical charge-discharge profile of Si-based anode cycled against high voltage LCO in matched full cell (capacity is normalized by the mass of the Si-containing composite anode powder)
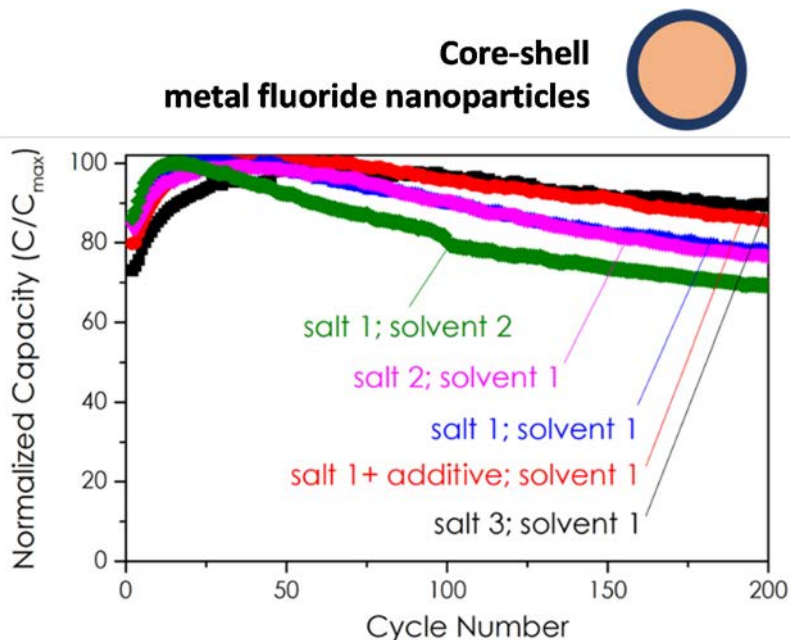
Figure IV-339: Impact of electrolyte composition on electrochemical stability of metal fluoride-based cathode cycled against Li anode

When studying regular metal fluoride nanoparticles coated with the protective shells we revealed a significant impact of both the salt and solvent compositions as well as the additives on the cathode stability (Figure IV-339). Core-shell nanoparticles of the metal fluorides have been utilized in this study as they demonstrate

superior stability. Initial capacity increase in Figure IV-339 is believed to be related to the gradual increase in the shell permeability during cycling.

Conclusions

Replacing conventional intercalation-based lithium-ion cell chemistry by conversion-type anodes and cathodes offers a great potential to boost cell volumetric energy density by ~100% and cell specific energy by ~200%, while simultaneously enhancing cell safety and environmental friendliness. During the last year, we have designed and commissioned a versatile semi-automated tool for the formation of metal fluoride cathode powders. We have further demonstrated that metal fluoride cathodes may exhibit excellent cycle stability when matched with a Li metal anode, while Sila Si-based anode exhibit excellent performance characteristics when tested in full cells with matched intercalation cathodes. In the future we aim to build full cells with metal fluoride cathodes and silicon anodes and optimize their performance by tuning electrolyte chemistry and cathode composition and microstructure.

Products

Presentations/Publications/Patents

1. "Low Cost, High Capacity Non-Intercalation Chemistry Automotive Cells", US DOE Vehicle Technologies AMR, 2016.
2. W. Gu, O. Borodin, B. Zdyrko, H.T. Lin, H. Kim, N. Nitta, J. Huang, A. Magasinski, Z. Milicev, G. Berdichevsky, G. Yushin, "Lithium-Iron Fluoride Battery with *in Situ* Surface Protection", Advanced Functional Materials, 2016, 26 (10), p. 1507-1516.

References

1. F. Wu and G. Yushin, "Conversion Cathodes for Rechargeable Lithium and Lithium-Ion Batteries", Energy & Environmental Science (accepted, in press), 2016.

IV.F.5. FY 2015 Vehicle Technologies Incubator Award: New Advanced Stable Electrolytes for High Voltage Electrochemical Energy Storage (Silatronix)

Peng Du, Principal Investigator
Silatronix
3587 Anderson Street Suite 104
Madison, WI 53704
Phone: 608-661-1964; Fax: 608-661-4630
E-mail: pdu@silatronix.com

Peter Faguy, DOE Program Manager
U.S. Department of Energy
Vehicle Technologies Office
1000 Independence Avenue, SW
Washington, DC 20585
Phone: 202-586-1022
E-mail: Peter.Faguy@ee.doe.gov

Start Date: October 1, 2015
End Date: September 30, 2017

Abstract

Objectives

- Synthesize, characterize, and integrate novel solvents and additives into electrolytes to create the conditions necessary for reliable, long-lasting cells which operate at high-voltages (> 5V). Specific metric: oxidative stability in reference system (Pt electrode)
  - Prevent oxidative breakdown voltage above 6 V.
  - Provide parasitic current below 0.02 mA/cm^2 after 10 hours above 6 V at 50°C.

- Investigate the fundamental mechanisms of complex behavior of new solvent and additive materials within formulations containing commercial electrolyte components (solvents, salts, additives).

- Demonstrate commercially viable performance characteristics using state-of-the-art high voltage electrodes from Argonne National Laboratory (ANL) and US Army Research Laboratory (ARL). Specific metric: cycling performance in 5V LNMO full cells
  - Full cell initial capacity ≥ carbonate control
  - Over 80% initial capacity after 300 cycles at ≥55°C

Accomplishments

- OS3 solvent family shows excellent oxidative stability in Pt reference system with a wider electrochemical stability window and lower parasitic currents above 4.5V compared to the EC/EMC (3/7, %v) carbonate control.
  - Ten OS solvents have been synthesized and evaluated.
  - Several OS solvents met the Go/No Go technical metric (see Objectives).

- Electrolytes with less than 5% OS solvent content show comparable or improved HT cycling stability compared to the EC/EMC (3/7, %v) carbonate control. Low OS content electrolytes were chosen for the 1st pouch build at Argonne National Laboratory.

- Additive selection is an important factor in full cell cycling performance, especially for OS electrolytes. Army Research Laboratory synthesized and screened ten additives for performance improvement. Five additives were shipped to Silatronix for evaluation.

- Solvation studies identified OS3 as a high-affinity Li$^+$ solvent based upon ESI-MS and NMR spectroscopy measurements. Therefore, OS3 could have an impact in SEI formation.

- FEMC was identified as a key solvent for high voltage stability compared to EMC.

- Initial DSC tests performed on de-lithiated LNMO cathodes showed that addition of OS3 reduces the magnitude of the main exothermic peak without a significant change in onset temperature.

- Initial surface analysis found evidence that OS3 participates in cathode surface layer formation.

Future Achievements

- Pouch cell studies at Argonne National Laboratory will examine the full cell performance (cycling stability, gas generation) of OS electrolytes compared to the EC/EMC carbonate control.

- Synthesis efforts continue at Silatronix and Army Research Laboratory to provide new solvents and additives for evaluation.

- Additional surface analysis, including XANES on the cathode material, will investigate the fundamental mechanisms underlying OS performance in the 5V LNMO cell.

- Solvation studies will continue to examine the effect of OS structure on Li$^+$ solvation as well as solvation competition between OS and other carbonate HV solvents.

Technical Discussion

Background

Lithium-ion battery sales are projected to triple in size in the next 10 years, growing the size of the electrolyte market to $1.8 billion in 2025 (Avicenne March 2015). The majority of projected growth is expected to be in non-consumer electronic applications which require larger, more complex batteries operating in broader temperature ranges over longer lifetimes.

To improve the performance, reliability, and safety of lithium-ion batteries, new advanced materials need to be integrated into the cell design. However, a major impediment to improving lithium-ion batteries is the fact that these materials need to be compatible with the electrolyte which is currently a blend of alkyl carbonate solvents, LiPF$_6$ salt, and various additives. This electrolyte formulation has changed little over the last 20 years and is a major disadvantage as it is subject to decomposition, especially at temperatures above 60°C and charge voltages above 4.3 volts. In addition, carbonate electrolytes are highly flammable and a major source of the energy released during an extreme battery failure. As a result, current lithium-ion electrolytes are impeding development of advanced lithium-ion batteries for all applications, including portable, industrial, automotive, and grid scale products. New, more stable solvents are desperately needed to support integration of new electrode materials in future lithium-ion battery designs.

Specifically, new cathodes with higher operating voltages, higher energy density, and reduced cost demand development of new electrolytes with improved electrochemical and thermal stability. Electrolytes with improved thermal stability can enhance battery lifetimes by reducing PF$_5$ degradation processes; while electrolytes with vapor pressures that are lower than carbonate-based electrolytes can also improve the safety of automotive lithium-ion batteries. The development of an electrolyte system with both high-voltage and high thermal stability is a top priority for the development of high energy density lithium-ion batteries required by the automotive industry.

Introduction

High-voltage mixed oxide cathode materials present several challenges due to their high chemical reactivity and their high electrochemical driving force at high cathode potentials. Uncontrolled surface reactions lead to significant decreases in capacity, increased cell resistance, and increased leakage current through the formation of SEI layers and leaching of metal ions from the oxides. In addition, carbonate electrolytes release CO$_2$ under oxidizing conditions, which leads to undesired surface film formation, as well as internal pressurization of the cell that can result in leakage or explosive release of the electrolyte. To date, no solvent system has been

identified that meets all the requirements for compatibility with high-voltage cathodes including high electrochemical stability, low viscosity, wide temperature stability, and low cost.

Silatronix is developing advanced, stable, high-voltage electrolytes to meet the DOE goals for electrochemical energy storage in transportation systems. Early generations of OS solvents have not been on lithium-ion Road Maps, but recent Silatronix innovations have created new OS3 solvents that exhibit exceptional electrochemical stability under the oxidizing conditions associated with high-voltage (HV) cathodes (exceeding 7V vs. Li/Li$^+$ before onset of significant parasitic breakdown current at Pt electrodes) and meet fundamental metrics (conductivity, viscosity) necessary for cell performance (i.e., rate capability, low temperature) in transportation applications and should therefore be considered for the roadmap.

Approach

Silatronix and ARL are synthesizing new materials based upon rational molecular design to achieve the superior oxidative stability required for HV applications. The fundamental electrochemical behavior of these materials is studied in reference cells to determine the oxidative breakdown voltage and mechanism of breakdown to produce a library of materials with superior fundamental oxidative stability for evaluation.

The performance and safety of the new HV solvents and additives in formulated electrolytes are evaluated with the HV cathodes provided by ANL and ARL (5V LNMO, 5V cobalt phosphate). Limited surface analysis is conducted after cycling to identify underlying mechanisms of degradation (i.e., surface film formation, metal dissolution, cathode morphology changes). Differential scanning calorimetry (DSC) is conducted on de-lithiated cathode material to understand the safety impact of the new HV materials. Solvation studies, using ESI-MS and NMR spectroscopy methods, is conducted to understand the Li$^+$ solvation behavior of the new OS solvents. These studies expand the understanding of the fundamental mechanistic behavior and include the relationship between the structure and properties of individual electrolyte components and the performance of a complete system. Top performing HV formulations identified will be tested in 5V LNMO pouch cells (13 layers, 200-300 mAh) at ANL. The pouch cell analysis focuses on cycling stability and pouch swelling.

Results

Evaluation of New Solvents in Pt Reference Cells

Silatronix synthesized 10 organosilicon (OS) solvents and characterized their physical properties and electrochemical behavior. Generally, superior oxidative stability was observed with those OS electrolytes in Pt reference cells by linear scanning voltammetry (LSV) and constant voltage floating tests at 30°C and 50°C. Figure IV-340 compares the parasitic currents for LiPF$_6$ electrolytes using EC/EMC (3/7, %v) and 100% OS3 at 30°C. The OS3 electrolyte showed superior stability compared to EC/EMC between +4.6 V and +6.5 V (vs. Li/Li$^+$) with the Pt working electrode with current at 6V less than 0.02 mA/cm^2.
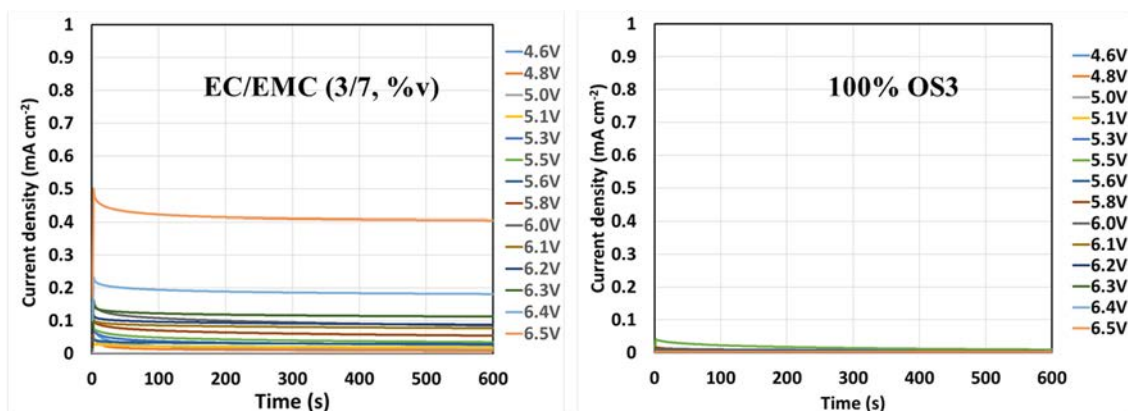

Figure IV-340: Parasitic current results for LiPF6-based electrolytes in a 3 electrode cell (Pt: WE, Li/Li$^+$: CE, RE)

Figure IV-341 summarizes the oxidative stability (vs. Li/Li$^+$) of OS3, carbonate control (EC/EMC, 3/7%v) and the fluorinated electrolyte (FEMC/FEC/HFE, 6/2/2, %v) with LiPF$_6$ at 30°C. The data show that OS3 has the

highest voltage stability. The fluorinated control electrolyte displays a wider window of electrochemical stability than the EC/EMC control. As a result, FEMC and FEC were investigated as replacements for the non-fluorinated EC and EMC solvents in the program.
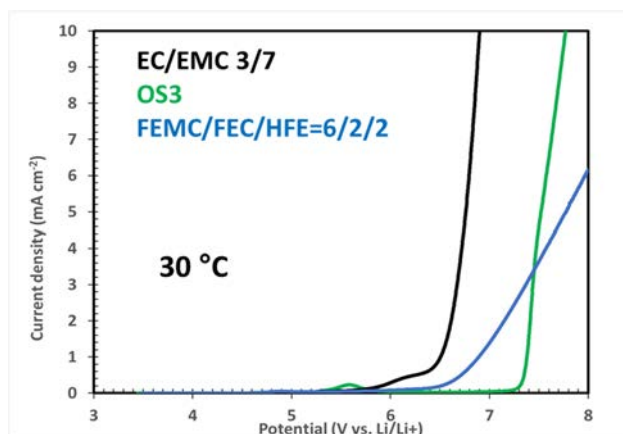
Figure IV-341: Oxidative stability comparison at 30 °C of OS3 vs carbonate control vs fluorinated electrolyte

Four OS3 family solvents with $LiPF_6$ salt satisfied the Go/No-Go Metric #1 (breakdown potentials > 6V at 30°C, shown in Figure IV-342a) and are good candidates for HV systems. Furthermore, Figure IV-342b summarizes the parasitic currents of those OS3 family electrolytes, which showed superior stability and satisfied Go/No-Go Metric #2 (50°C parasitic current <0.02 mAh/cm^2 at 6V).
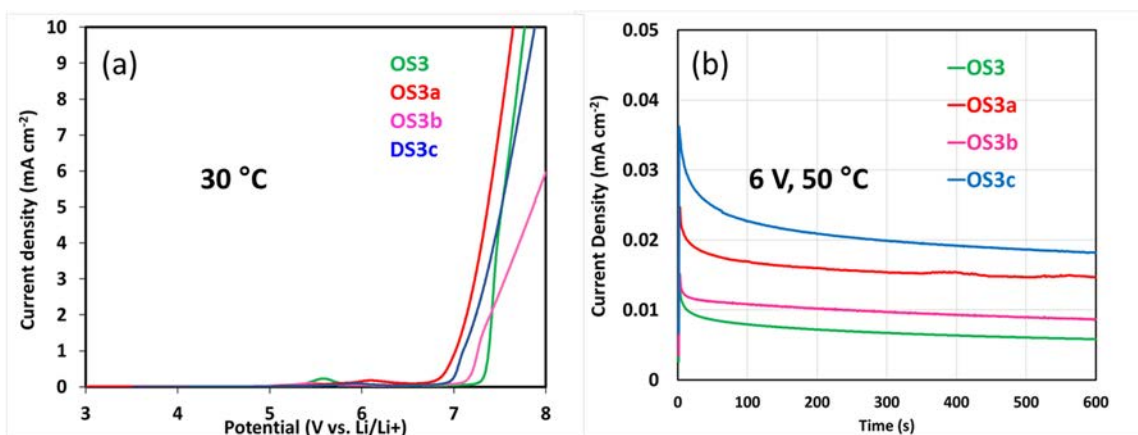
Figure IV-342: a. Oxidative stability comparison at 30 °C; b. parasitic current results at 6 V and 50 °C of OS3 family electrolytes

ARL synthesized 10 new additives with bifunctional groups for protection of both anode and cathode. Most have been characterized with electrochemical characterization and half-cell tests at ARL. Five additives were provided for testing at Silatronix. To date, no clear performance benefit has been observed using these additives.

Full Cell Cycling and Stability Performance

ANL delivered single side coated 5V LNMO and MCMB electrodes to Silatronix and ARL for the evaluation of advanced HV electrolyte materials. Initial screening of OS electrolytes was completed using a refined electrochemical method in both 5V LNMO half cells and full cells. Furthermore, cycling in LNMO half cells and full cells confirmed the importance of additives, especially in electrolyte formulations with higher OS concentration, which showed a lower parasitic current at voltages above 5V compared to carbonate control electrolytes in LNMO cells.

The effect of OS3 concentration on full cell cycling performance was examined in coin cells previously in this program. Formulations containing 2%, 5%, 20%, and 60% OS3 were tested in EC/EMC electrolytes. The EC content was held at 30% for low OS3 concentrations (2%, 5% OS3) and at 20% for high OS3 concentrations

(20%, 60% OS3). Figure IV-343 summarizes the 30°C and 55°C cycling data for the OS3 containing formulations and carbonate control. All electrolytes contain 1M LiPF$_6$ and 0.1M LiBOB and 0.1M LiDFOB additives. Representative data is shown for each formulation. The low OS3 concentration electrolytes (2% - purple, 5% - green) show greater capacity retention compared to the carbonate control after 50 cycles at 55°C. Higher OS3 concentrations (20% - red, 60% - blue) result in greater capacity degradation.

Based upon this cycling data, in Q4 three top performing HV formulations with 2% or 5% OS were tested in 5V LNMO pouch cells (13 layers, 200-300 mAh) at ANL. The pouch cell analysis is focused on cycling stability and pouch swelling.
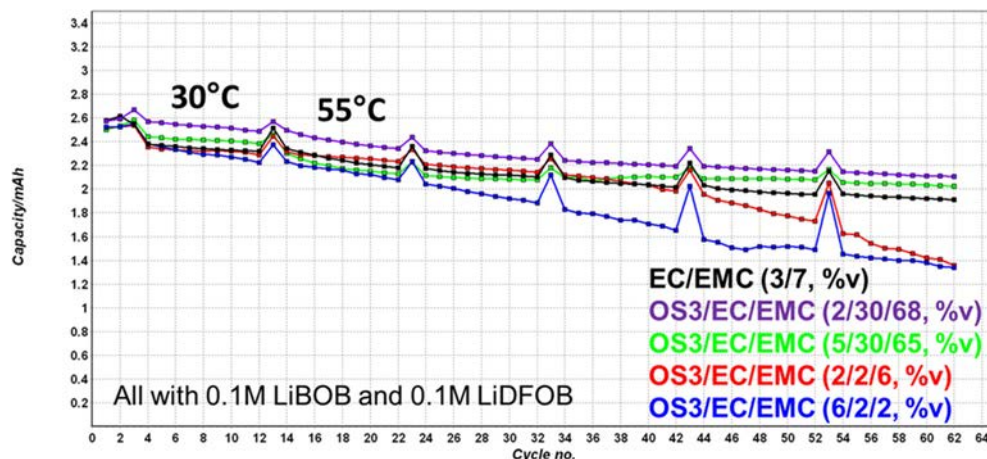
Figure IV-343: Comparison of LNMO full cell performance with control carbonate electrolyte and OS3 containing electrolytes (all with 1M LiPF$_6$). Cells are cycled at C/10 for 2 formation cycles and at C/2 for 10 cycles at 30 °C, then continued 50 cycles at C/2 between 3.5 and 4.9 V at 55 °C
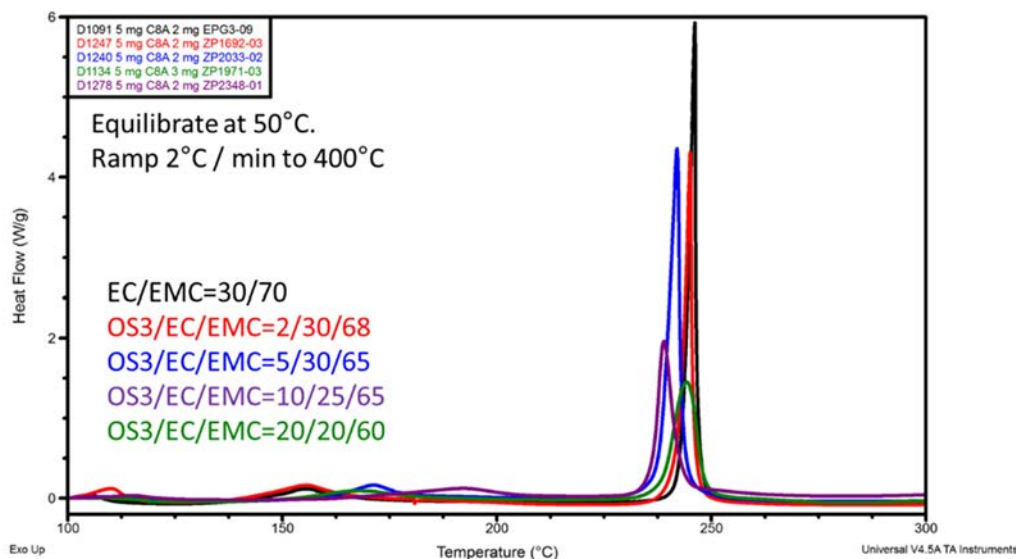
Figure IV-344: Differential scanning calorimetry (DSC) test results for de-lithiated LNMO cathodes formed with various HV electrolyte formulations: Carbonate control (black), 2% OS3 (red), 5% OS3 (blue), 10% OS3 (purple), and 20% OS3 (green)

The effect of OS3 concentration on the safety profile of the charged LNMO cathode was investigated. The carbonate control (black data - EC/EMC – 3/7%v) shows a sharp exothermic peak near 250°C with minor features near 150°C. By comparison, addition of 2% OS3 (red data) or 5% OS3 (blue data) decreases the overall magnitude of this main exothermic peak with little to no shift in the onset temperature. Increasing the OS3 concentration to 10% (purple) or 20% (green) results in over a 60% reduction in the peak magnitude with no onset temperature reduction. The data shown in Figure IV-344 shows that including OS3 in the HV electrolyte formulation improves the safety and stability of the de-lithiated LNMO cathode. No additives were included in the tested formulations to isolate the effect of OS3.

In addition, Post-test degradation analysis has been initiated including XAS measurements at Argonne National Laboratory's Advanced Photon Source on beamline BM20 and SEM and XPS measurements at University of Wisconsin–Madison. This analysis serves to identify the composition of and evaluate the stability of the SEI layer and the bulk structure of the cathode active material.

ESI-MS experiments were performed at ARL to investigate the Li$^+$ solvation behavior for OS3/EC/EMC electrolytes. These formulations were designed to understand the competing solvation between EC and. Formulation A contains 11% OS3 by mole and contains 4 moles of EC and OS3 per Li$^+$. Formulation B contains 4% OS3 by mole and contains only 3 moles of EC and OS3 per Li$^+$. Formulation C contains 25% OS3 by mole and contains 4 moles of OS3 per Li$^+$ and 6.5 moles of EC and OS3 per Li$^+$. Formulation D contains 17% OS3 by mole and represents equal competition between OS3 and EC.

A summary of the results are shown in Figure IV-345. The role of OS3 in the fluorinated electrolyte system can be seen in the relative magnitude of the EC/OS3 and 2OS3 clusters in the low OS3 content electrolytes (A – orange, B – red) compared to the high OS3 content electrolytes (C – blue, D – green). This trend shows that as OS3 concentration increases in the electrolyte, the number of 2OS3 clusters grows compared to the EC/OS3 cluster. This ESI-MS data demonstrates that OS3 is a strong competitor for EC in Li$^+$ solvation. Figure IV-346 shows the fraction of solvent participating in solvation, based upon the relative prevalence of the clusters from Figure IV-345 compared to the bulk composition, for OS3, EC, and EMC solvents as a function of OS3 concentration. This data shows that OS3 participates in solvation at all concentration levels with >50% OS3 participating in the high OS3 concentration electrolytes.
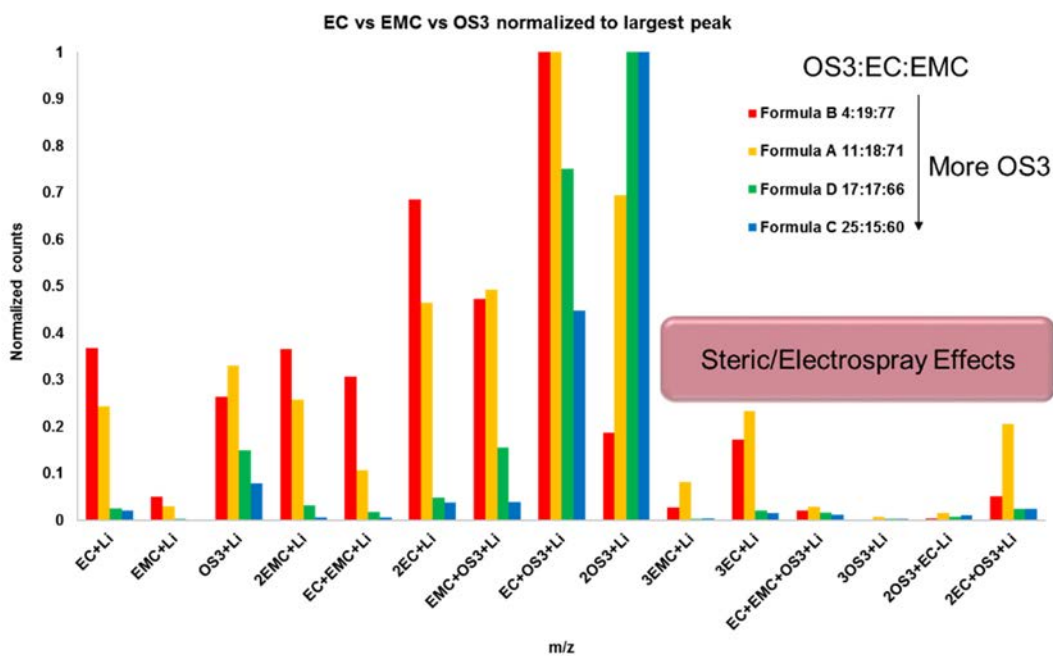
Figure IV-345: Normalized ESI-MS counts as a function of cluster for OS3/EC/EMC electrolyte formulations
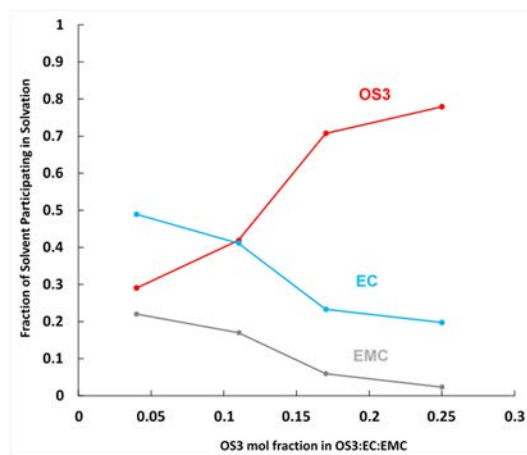
Figure IV-346: Calculated fraction of bulk solvents participating in solvation based upon ESI-MS results in an earlier figure

Conclusions

The focus of this program is the fundamental evaluation of high stability OS solvents and performance of these high voltage (HV) electrolyte formulations in 5V LNMO half cells and full cells. To date, all OS molecules tested in this quarter demonstrate similar properties as other OS molecules, including higher flash points than the carbonate control (EC/EMC, 3/7%v). Superior oxidative stability (above 6V) is observed for these OS molecules in reference cells (Pt) by linear scanning voltammetry (LSV). Full cell testing found that the addition of 2% or 5% OS3 improves the 55°C cycling performance by reducing capacity degradation across 50 cycles compared to the EC/EMC control. Initial DSC tests performed on de-lithiated LNMO cathodes showed that addition of OS3 to the EC/EMC electrolyte reduced the magnitude of the main exothermic peak (near 250°C) without a significant change to the onset temperature. ARL continued the analysis of Li^+ solvation in HV electrolytes using an ESI-MS technique, which demonstrates that OS3 competes well with EC for solvation of Li^+ and may contribute to the formation of SEI layers. Silatronix initiated Li^+ solvation studies using ^{13}C and ^{15}N NMR spectroscopy to evaluate Li^+ solvation behavior in the bulk solution.

Products

Presentations/Publications/Patents

1. "New Advanced Stable Electrolytes for High Voltage Electrochemical Energy Storage", Peng Du. 2016 DOE Hydrogen and Fuel Cells Program and Vehicle Technologies Office Annual Merit Review and Peer Evaluation Meeting, June 6-10, 2016, Washington, D.C.

IV.F.6. A Commercially Scalable Process for Silicon Anode Prelithiation (Amprius)

Ionel Stefan, Principal Investigator (Amprius)
Amprius, Inc.
225 Humboldt Court
Sunnyvale, CA 94089
Phone: 800-425-8803; Fax: 866-685-7420
E-mail: ionel@amprius.com

John Tabacchi, Project Manager (NETL)
National Energy Technology Laboratory
3610 Collins Ferry Road
Morgantown, WV 26505
Phone: 304-285-4764
E-mail: john.tabacchi@netl.doe.gov

Start Date: October 2014
End Date: March 2017

Abstract

Objectives

- Amprius will develop and demonstrate a cost-effective and commercially scalable manufacturing process for silicon anode prelithiation – the insertion of extra lithium from sources other than the cathode. A scalable manufacturing process for prelithiation is a prerequisite for the commercialization of silicon anodes that enable cost competitive, high energy, and long life lithium-ion batteries.

- Numerous prelithiation methods enable the insertion of lithium into silicon, but are not commercially scalable because of cost and process integration challenges with existing battery manufacturing workflows. Amprius' project will develop a prelithiation method that is cost-effective and has minimal impact on existing battery assembly processes.
  - Barriers Addressed:
    - Cost: Impact of prelithiation on the cost of production silicon anodes.
    - Process Integration: Impact on cell build processes, including changes to industrial setups for battery manufacturing
  - Technical Targets:
    - Cost: Develop a prelithiation process that will add no more than 10% to the cost of producing silicon nanowires.
    - Process Integration: Develop a prelithiation method having minimal impact on cell build processes and requiring only limited changes to the industrial setup (dry zones, automatic tools, etc.).

Accomplishments

- Analyzed the cost and scalability of numerous prelithiation methods (six electrochemical methods, five chemical methods and three physical methods).

- Identified five prelithiation methods (three electrochemical, one chemical and one physical) with limited impact on cost and cell build processes. Found that the most of the methods evaluated are not scalable because of their high cost and/or significant impact on existing cell production processes.

- Evaluated the technical feasibility of electrochemical (involving "in cell" and roll-to roll bath type prelithiation), chemical (involving organometallic compounds) and physical (involving the decomposition of lithium salts) methods with limited impact on cost and cell build processes.

- Selected two electrochemical methods (involving "in cell" and "in stack" prelithiation) for further evaluation. Found that the scalable electrochemical (involving roll-to roll bath type prelithiation), chemical (involving organometallic compounds) and physical (involving the decomposition of lithium salts) methods either require a dry environment for the entire assembly process and raise safety issues in handling or irreparably damage the integrity of Amprius' silicon nanowire anodes.

- Tested the impact of an electrochemical method, "in stack" prelithiation," on capacity and cycle life.

- Evaluated the feasibility of new classes of chemical additives that can be used in electrochemical prelithiation but are not suited for full cell operation. These additives are active at low voltages, such as those on prelithiated anodes, and can decompose at higher voltages, such as those at the cathode. Results of initial testing indicate that these additives can substantially increase cycle life in some cases.

- Designed and assembled an eight-cell prelithiation fixture and pressure control setup for "in stack" prelithiation and formation protocol.

Future Achievements

- Optimize the prelithiation formation protocol in the new eight-cell prelithiation fixture.

- Build and deliver 10 cells prelithiated using the new prelithiation "in stack" prelithiation process and fixture.

Technical Discussion

Background

Silicon offers nearly 10 times the theoretical energy of graphite. But silicon – particularly in the nano-dimensions developed by Amprius and others – has higher first cycle loss than does graphite, limiting or negating its energy advantage and accentuating its cycle life challenge.

Introduction

Silicon has higher first cycle loss – and therefore requires significantly more lithium than does graphite – for three reasons.

First, silicon consumes a higher percentage of lithium during solid-electrolyte interphase (SEI) formation (10-25%) than does graphite (5%). Second, silicon traps a higher percentage of lithium during discharge (5-10%) than does graphite (1-2%); the high anode voltage necessary to fully extract lithium from silicon is not practicable (because it would result in an impractically low cell voltage cutoff). Third, nanostructures amplify the material's challenges; nanostructured silicon has more surface area than does micron-sized graphite, further increasing silicon's need for lithium. (See Figure IV-347.)

| Up to 25% of Lithium Consumed During SEI Formation | Up to 10% of Lithium Trapped During Discharge | ~65% of Lithium Available | Up to 35% Extra Lithium Added Through Prelithiation |

Figure IV-347: Silicon anodes consume and trap significant amounts of lithium, reducing first cycle efficiency and cell-level energy. Current lab-scale prelithiation methods add extra lithium and address first cycle loss – but are not scalable

Approach

Before the DOE project, Amprius (and others) experimented—at laboratory scale, in gloveboxes and/or in a dry room – with a number of prelithiation methods to address silicon's first cycle loss. In its DOE Project, Amprius (1) evaluated in depth the advantages and disadvantages of numerous prelithiation methods, (2) considered the challenges of using these prelithiation methods in high-volume manufacturing, and (3) is developing and scaling up to pilot scale volumes the most promising method, "in stack" prelithiation.

Amprius tackled prelithiation's challenges head-on by evaluating cost and manufacturability as *a priori* concerns. For example, before testing specific materials (e.g. lithium salts that are less expensive than Li metals), Amprius initially researched their price and evaluate their impact on cell assembly processes.

Amprius then evaluated the technical and commercial feasibility of several prelithiation processes, including:

1. Electrochemical insertion of lithium from liquid electrolytes,
2. Physical lithiation by direct contact with lithium metal or other Li-containing materials, and
3. Chemical lithiation with lithium containing reactants.

Amprius tested candidate processes on silicon nanowire anodes, which are particularly well suited for research because (a) they are made of pure silicon and (b) do not use any binders or conductive additives. As a result, nanowires enable Amprius to directly study the effects of new prelithiation regimes on silicon anodes, without needing to isolate and/or control for secondary reactions (during formation) with the binders, conductive carbons, and other additives that are common in silicon-carbon composite anodes.

Results

Amprius selected a new electrochemical prelithiation method, "in stack" prelithiation

Amprius found that "in stack" electrochemical prelithiation compared favorably with both the "in cell" prelithiation method Amprius tested during the project's first year and Amprius' pre-project "*ex situ*" prelithiation method. "In stack" electrochemical prelithiation increased capacity without reducing cycle life.

During the project's second year, Amprius steadily increased capacity by increasing the amount of prelithiation charge and optimizing the prelithiation bath chemistry. For example, at a rate of C/20, Amprius achieved higher cell capacity using the new "in stack" method than with its pre-project "*ex situ*" prelithiation method. But at a rate of C/2, and as a result of higher cell internal resistance, Amprius initially achieved lower capacity using "in stack" prelithiation than "*ex situ*" prelithiation. To decrease cell resistance and increase cell capacity at a rate of C/2, Amprius (1) performed a screening design of experiment that optimized the composition (additives) of the prelithiation formulation and (2) designed and tested different mechanical setups that improved electrolyte circulation and bubble removal. After improving performance at a rate of C/2, Amprius selected the "in stack" prelithiation method for scale-up. (See Figure IV-347.)

Amprius evaluated the feasibility of new classes of chemical additives that can be used in electrochemical prelithiation but are not suited for full cell operation

Amprius found that additives that are active at low voltages, such as those on prelithiated anodes, and can decompose at higher voltages, such as those at the cathodes, can in some cases substantially increase cell cycle life. For example, of six classes of additives Amprius tested, two classes showed promising results; they improved cell cycle life from a baseline of 180-250 cycles to more than 300 cycles.
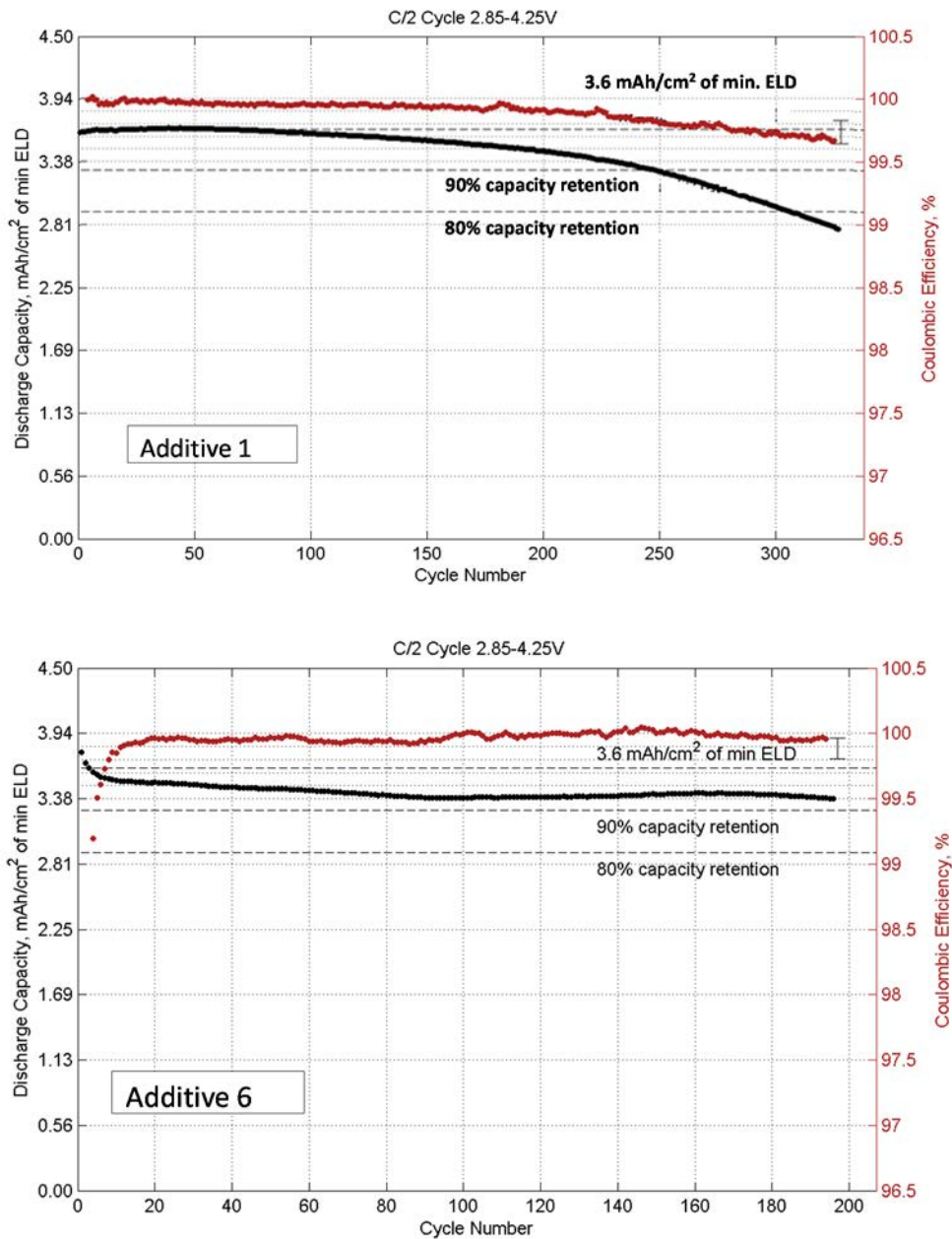
Figure IV-348: Cycle life of Silicon-LCO cells with anodes prelithiated in formulations with different additive classes

Amprius designed an intermediary, two-cell prelithiation fixture and pressure control setup for an "in stack" prelithiation process and formation protocol

Amprius initially designed and sourced the parts and machining necessary for an intermediary, two-cell prelithiation setup. (See Figure IV-349.)The setup enabled Amprius to evaluate (a) the mechanical features needed for multi-call operation, such as pressure control and modulation during prelithiation, and (b) electrical connection handling. The two-cell setup included (1) moving plates that hold the cells under pressure, (2) springs for easy release of the pressure applied to cells, (3) an air flow control valve and (4) a pressure gauge.

Amprius assembled a final, eight-cell prelithiation fixture and pneumatic pressure control setup for the new "in stack" prelithiation process and formation protocol

Amprius later designed and assembled a final, eight-cell prelithiation fixture and pressure control setup for an "in stack" prelithiation process and formation protocol. Amprius' pneumatic control setup enables precise

control of the applied pressure, as well as easy manipulation of the fixture's multiple pressure plates. Testing with control cells (regular electrolyte formulation) and active cells (prelithiation salt added to the electrolyte)
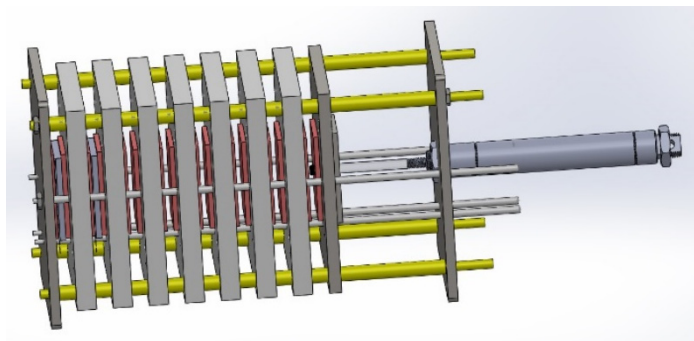
Figure IV-349: Amprius designed a fixture capable of prelithiating eight silicon nanowire anode-based cells "in stack"

Conclusions

During the project's second year, Amprius continued to make significant progress in developing and evaluating the feasibility of electrochemical prelithiation by electrolyte salts, successfully compensating losses to SEI formation. Automation and scale-up tasks are underway.

Products

Presentations/Publications/Patents

1. "A Commercially Scalable Process for Silicon Anode Prelithiation", ES250_Stefan_2016, US DOE Vehicle Technologies AMR, 2016.

References

None

IV.F.7. Dramatically Improve the Safety Performance of Li Ion Battery Separators and Reduce the Manufacturing Cost using Ultraviolet Curing and High Precision Coating Technologies (Miltec UV International)

Gary Voelker, Project Director
Dr. John Arnold, Principal Investigator
Miltec UV International
146 Log Canoe Circle
Stevensville, MD 21666
Phone: 410-604-2900; Fax: 410-604-2906
E-mail: gvoelker@miltec.com; jarnold@miltec.com

Colleen Butcher, DOE Program Manager
National Energy Technology Laboratory
626 Cochrans Mill Road
P.O. Box 10940
Pittsburgh, PA 15236-0940
Phone: 412-386-4984; Fax: 412-386-4604
E-mail: Colleen.Butcher@netl.doe.gov

Subcontractors:
Argonne National Laboratory
Celgard LLC

Start Date: October 2014
End Date: June 2017

Abstract

Objectives

- To further develop and demonstrate the use of Ultraviolet (UV) curing technology to reduce the cost of manufacturing Lithium ion battery ceramic coated separators by more than 50% while improving the porosity of the ceramic coating and retaining or improving the safety attributes.

- Previously identified UV curable binders and associated curing technology will be shown to reduce the time required to cure separator ceramic coatings from tens of minutes to less than one second. This can result in increases in process speeds and significantly reduced capital cost, operating cost, and energy consumption.

- Investigate the use of patterns applied with high speed coating technology to improve the safety performance of ceramic coated separators as well as reduce the cost of separators in a Lithium ion battery.

- Investigate the feasibility of manufacturing thinner (6-10 µm) base separators.

Accomplishments

- Miltec UV continues to make significant progress using a laboratory scale flexographic printing unit modified to accommodate the coating and UV curing of ceramic coated separators with and without printed patterns at thicknesses of 2-6 µm.

- Ceramic coated separators on a base trilayer, PP, UHMWPE, and PE have been made with <10% increase in air permeability measured with a Gurley meter. The <10% increase in air permeability meets the overall project goal. Test results on C210 trilayer, UHMWPE, and PP base material coated with a nominal 3 µm coating has resulted in Machine Direction shrinkage of 1.0%, 0.7%, and 0.4%, respectively at 150°C for 1 hour which also exceeds the project goal.

- A full scale coating unit with UV curing (Miltec UV CX400) has been designed, fabricated and is now operational at Miltec UV. The unit is capable of coating and curing a 2-6 µm ceramic layer on polyolefin base separator in widths up to 450 mm and processing speeds of 400 fpm. The unit occupies a space of approximately 8' x 4'.

- A detailed cost model has been developed to estimate the cost of coating and UV curing a ceramic layer using UV curing technology. The project goal is $0.20/m^2.

Future Achievements

- Until the contract end in June 2017, Miltec UV will conduct extensive performance calibration on the Miltec UV CX400 full scale coating and UV curing unit with multiple base separator materials; with and without printed patterns.

- Expand efforts to achieve battery shutdown with ceramic coated PP.

- Complete and exercise the cost model to estimate the cost of single and double layer ceramic coatings on base separator material as a function of coating thickness, coating material, shifts of operation and operating speed.

Technical Discussion

Background

Placing a coating of fine ceramic particles such as aluminum oxide on the surfaces of a polyolefin base separator in Lithium ion batteries has been shown to reduce shrinkage of the separator at elevated temperatures and reduce the risks of thermal runaway. (See Figure IV-351.) The overall objective of this cost shared contract is to develop safer coatings and better processes for ceramic coated separators. We are developing and demonstrating the use of Ultraviolet (UV) curing technology to reduce lithium-ion battery manufacturing costs. In this project, we apply and cure ceramic coated separators with an environmentally clean UV process. The performance of these coatings must meet current industry standards and be ready to meet tomorrow's standards as well. It is the intent of this project that the development of this technology will lead to safer vehicle batteries and faster incorporation and acceptance of hybrid and electric vehicles.

Introduction

The objective of this project is to further develop and demonstrate the use of Ultraviolet (UV) curing technology to reduce the cost of manufacturing lithium-ion battery ceramic coated separators by more than 50% while improving the porosity of the ceramic coating and retaining or improving the safety attributes. Previously identified UV curable binders and associated curing technology will be shown to reduce the time required to cure separator ceramic coatings from tens of minutes to less than one second. This revolutionary approach can result in dramatic increases in process speeds and significantly reduced capital cost, operating cost, energy consumption and environmental concerns as well as costs due to the elimination of volatile organic solvents. In addition, the use of patterns applied with high speed coating technology coupled with thinner separator bases has the potential to significantly improve the safety performance of ceramic coated separators as well as reduce the cost of separators in a Lithium ion battery.

Cost reduction will largely come from simplification, line reduction, and improved throughput. Thin separator film is fragile. It is difficult to handle this material on a web. Separator film wants to kink, crinkle, shred, and tear. Market and technical forces push the separator film to be thinner and more fragile every year.

For a given speed, a UV process can exponentially reduce the length of the line. Reducing the length of the line, reduces web handling. A shorter web will lead to greater yields; increase yield reduces the largest hidden coating cost. Likewise, for a set press size, UV curing is exponentially faster than a drying web process. Faster webs, reduce manufacturing costs. Faster webs also increase coated separator capacity that the automotive industry will demand as EV vehicles grow.
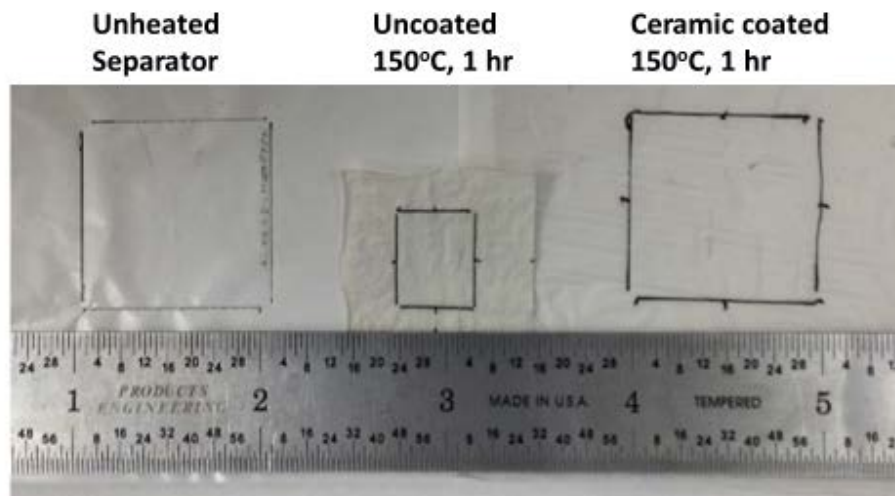
Figure IV-350: UV Ceramic coating affords the separator dimensional stability when heated to dangerous temperatures, like 150oC for 1 hour

Approach

In addition to a UV curing process, we are developing a flexographic coating process. The flexographic process has many advantages 1) higher viscosity than gravure (so less drying), 2) ability to print and change patterns at a fraction of the cost, 3) less down time. Less downtime comes from the fact that a gravure cylinder cannot be removed while the line is running. Aluminum oxide is abrasive and will wear and clog a Gravure plate as well as a flexo plate. The difference is the flexo plate can be removed while the press runs—and if one used 2 flexo stations—cheaper than one gravure station—the plate can be changed without ever stopping. So in essence, if equipped with the correct accumulators the flexo press never needs to stop. The ability to print patterns, is another innovation of this project. By printing patterns, we should be able to maximize ionic flow through the separator while still providing the protection of a ceramic layer and still reinforcing the separator against thermal shrinkage.

This project employs an iterative process of technology evaluation, implementation, testing, and resulting optimization. Multiple samples of ceramic coated separators are prepared using a combination of various UV curable binder chemistries and printing patterns. Multiple analytical tests are conducted to determine characteristics such as: porosity, tear strength, thermal transfer, puncture strength, thermal shrinkage, and permeability. At the end of this iterative development, printing patterns and optimum UV chemistries and base separator materials will be coated using the Miltec UV CX400 and ceramic coated separators will be prepared for extensive evaluation.

Miltec receives separator base material from various vendors; including Celgard, and applies either single or double sided ceramic coatings using the full scale Miltec UV CX400 unit. After in-house testing, the coated samples are submitted to the vendors for extensive further evaluation. ANL conducts electrochemical and physical tests on the cells as well as the analytical tests

Results

As a result of extensive efforts to develop improved UV curable binder chemistry and improved mixing techniques for the UV binder and ceramic particles and improved coating techniques, we have achieved the performance goals of the project. As shown in Table IV-45, we have exceeded both the shrinkage goal of <5% MD at 150°C and the goal of not increasing the Gurley >10% above the base with a ceramic coating.

Table IV-45: UV Ceramic Coatings Pass Basic Specifications for Coated Separators

	Celgard C210 Trilayer		Entek UHMWPE		JNC PP	
	Uncoated	Coated	Uncoated	Coated	Uncoated	Coated
Coating Thickness	0	3+ µm	0	3.5 um each side	0	3 µm
MD Shrinkage 1 hr@150°C	33.0%	1.0%	72.0%	0.7%	36.0%	0.4%
HP Gurley (seconds)	20	22	12	16	7	10
Separator Film Thickness	16 µm	16 µm	16 µm	16 µm	16 µm	16 µm

All coated with Sohn Flexo benchtop press.
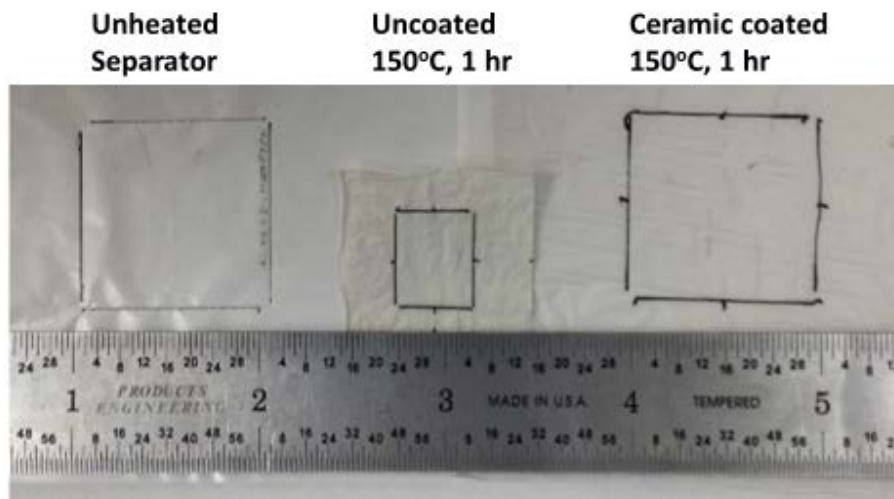
Figure IV-351: UV Ceramic coating affords the separator dimensional stability when heated to dangerous temperatures, like 150 °C for 1 hour

Conclusions

The Miltec UV team has made very good progress in demonstrating the use of UV curing and printing technology to apply a ceramic coating on PE, PP, UHMWPE, and trilayer (PP/PE/PP) separator stocks and for these coatings to achieve performance goals of shrinkage, adherence, porosity, and safety performance. During the final months of this effort we will demonstrate the performance as well as cost savings of this technology on a commercial scale coating and UV curing system, the Miltec UV CX400.

Products

Presentations/Publications/Patents

1. Arnold, Dr. John, DOE Annual Merit Review Presentation (June 2016, Washington, D.C.)

IV.F.8. Advanced Drying Process for Low Cost Manufacturing of Electrodes (Lambda Technologies)

Iftikhar Ahmad, Principal Investigator
Lambda Technologies
860 Aviation Parkway, Suite 900
Morrisville, NC 27560
Phone: 919-462-1919; Fax: 919-462-1929
E-mail: iahmad@microcure.com

Subcontractor:
Navitas Systems
4880 Venture Drive
Ann Arbor, MI 48108

Colleen Butcher, DOE Program Manager
National Energy Technology Laboratory
626 Cochrans Mill Road
P.O. Box 10940
Pittsburgh, PA 15236
Phone: 412-386-7341
E-mail: Colleen.Butcher@netl.doe.gov

Start Date: October 1, 2014
End Date: November 30, 2016

Abstract

Objectives

- To develop a roll-to-roll (R2R) pilot oven for the Advanced Drying Process (ADP) of high loading electrodes for lithium-ion batteries. The ADP pilot oven was anticipated to rapidly dry (5x faster) the casted aqueous slurry, resulting in a 30-50% reduction in the operating cost and hence the overall cost of lithium-ion batteries.

- Evaluate electrodes for physical and electrochemical properties and test fabricated cells for capacity, energy and rate capability. Perform cycle life testing to evaluate that the cells prepared with ADP pilot system are capable of meeting performance (number of cycles, capacity retention) equivalent to the baseline process.

Accomplishments

- Static rapid ADP drying of aqueous anode slurry (5x faster) and NMP based cathode slurry (2x faster) were performed which provided information for the chamber size for continuous electrode coating. Electrode characterization showed identical data when compared to the standard method.

- A major component of the ADP pilot oven was the microwave choke which could accommodate a 150 mm wide web without leaking microwaves. The choke was designed and tested to conform to the international safety standards for microwave emissions in free space.

- The ADP pilot oven components were designed to allow necessary residence time for the slurry coated foil in the process chamber, as well as other features for integration of the equipment at Navitas pilot coating line.

- Custom fabricated components were received from various suppliers and the ADP pilot oven system was completed and checked for electrical functionality. Subsequently, VFM power was delivered to check for any microwave leakage especially at the wide choke openings.

- A temporary web handling setup with variable speed control motor was acquired and installed. A doctor blade and pump to deliver slurry was mounted on the system that would allow casting the slurry on the continuously moving foil.

- Premixed anode slurry from Navitas was received for Go/No-Go demonstration at Lambda. The binder was mixed right before the slurry was casted on the moving copper foil. The high loading aqueous anode slurry was dried in the ADP pilot oven in one minute with the foil moving at 0.5m/min.

- On successful completion of the Go/No-Go demo, the ADP pilot system was packed and shipped to Navitas.

- Lambda personnel visited Navitas for install and training of the ADP pilot oven. Drying tests of aqueous anode and NMP cathode slurries casted on moving foil were successfully performed.

- Material and electrochemical characterization was performed at Navitas, which included binder distribution, adhesion tests, solvent content, SLP formation, rate capability, DCR and life cycling. Testing has shown equivalent or better (detailed results below) performance of the cells made with ADP process when compared to standard drying.

- Power consumption comparison study was conducted on ADP and the standard IR/convection oven. The study demonstrated a > 40% saving in power consumption with ADP while being only a fraction of length, providing a 3 to 5 time advantage over the standard drying systems.

Future Achievements

- Lambda is in communication with end users as well as battery coating line integrators. Discussion with various integrators and battery manufacturers are ongoing about potentially working together to scale VFM systems for high volume manufacturing.

Technical Discussion

Background

High battery cost is a key factor in limiting the rate of adoption of electric vehicles. In the high volume production of electrodes for lithium-ion batteries, drying is the highest cost unit operation.fThe surface heating methods are usually slow. Hence with conventional processing, slurry-cast electrodes are dried under highly controlled conditions in very long furnaces. The furnace length is dictated by the limited rate at which water or NMP can be removed from the slurry without leading to binder/particle segregation, orange peel defects or pore-blocking skin formation. Typical coating lines are limited to operation at speeds of 20 m/min or less, well below the rates of other industrial R2R processing. Practical electrode coating thicknesses can require 2 minutes or more of drying. Therefore the coater footprint can be 40m or more, which is doubled for two-side coating operation. The 40m long furnace drives both high capital equipment and operating expense.

Introduction

The basic operating principle is the use of a novel radiant energy source that enables penetration of the coating and selective coupling of most of the energy instantly with the polar solvent molecules in the entire volume of the electrode. Microwaves have much larger wavelengths than the higher frequency IR radiation, which similar to hot air heats the surface layer. Therefore, heat is transferred from the film surface to the interior with the rate depending on the thermal conductivity of the material. However, most industrial microwave ovens operate at a single fixed frequency (commonly 2.45GHz or 915 MHz). These ovens suffer from temperature uniformity or hot spots and arcing with metals and hence are not compatible with drying slurries cast on metal foils. Lambda employs a proprietary technique of Variable Frequency Microwave "VFM", in which a bandwidth (of 4096 frequencies) is rapidly swept in a fraction of a second (typically 0.1s). The rapid sweep of frequencies provides very good uniformity over a large surface and eliminates the charge build up on metal components. This compatibility with metals has allowed VFM to be used in semiconductor packaging and hence can easily be used for drying slurries casted on metal foils as well.

Approach

The objectives outlined above are accomplished by employing penetrating Variable Frequency Microwave (VFM) which interacts with the polar molecules of the solvent deep in the thickness of the slurry to drive them out to the surface. This Advanced Drying Process (ADP) includes hot air flow on the surface of slurry which collects the vapors and carries them out to the system exhaust thereby resulting in efficient drying of the slurry. The major technology innovations undertaken to accomplish the objectives of this effort include:

1. Perform static specimen drying of anode and cathode slurries to estimate the residence time required in the ADP equipment when the slurry is casted on continuously moving metal foil. Based on the casting speed for each slurry type the residence time in the ADP and thereby the chamber size was determined. The electrodes were tested for physical and electrochemical properties. Cells were evaluated for capacity, energy and rate capability. Cycle life testing was performed to determine that the cells were capable of meeting the performance with respect to the number of cycles and capacity retention when compared to the baseline process.

2. Since a continuous foil width of 150 mm needed to pass through the ADP chamber, microwave chokes had to be designed, fabricated and tested to allow 150 mm wide foil to pass through without any microwave leakage hazard to the personnel working in the area.

3. The ADP pilot oven system was designed to fit into the existing coating line at Navitas. The various designed components were released to vendors for fabrication. As the fabricated parts were received the ADP pilot oven system was assembled and tested. VFM power was delivered to check for any microwave leakage especially at the wide choke openings.

4. A temporary web handling setup with variable speed control was acquired and installed. A doctor blade and pump to deliver slurry was mounted on the system that would allow casting the slurry on the continuously moving foil.

5. Navitas personnel visited Lambda Technologies to perform the continuous casting of electrode and drying of the slurry. On successful completion of the Go/No-Go demo, and upon approval from NETL, the ADP system was packed and shipped to Navitas.

6. Lambda personnel visited Navitas to install the ADP pilot oven and test the functionality of the system. Drying tests of slurries casted on moving foil were performed. The processing parameters were optimized for drying each slurry type.

7. The analytic testing on electrode and cells was conducted on specimens obtained from the continuous casting and ADP drying process. The characterization results are given below after briefly describing the ADP pilot oven system.

Results

The progress on the design and fabrication of the ADP pilot oven and the material and electrochemical characterization has been presented below. The details of this work was presented in the previous annual report, however, the summary of the project and the analytic work follows to allow for the continuity in various aspects of the project.

Design, fabrication of components and assembly of the ADP Pilot oven

The ADP pilot oven chamber and the equipment were designed based on the static sample slurry drying, the casting speed and the space available and integration requirements on the pilot coating line at Navitas in Ann Arbor, Michigan. The most critical component was the wider microwave chokes capable of allowing 150 mm wide metal foil to pass through without any appreciable microwave leakage that could be a hazard to the personnel working in the area. The microwave leakage was maintained within the International Electrotechnical Commission (IEC) emission standard of 5mW/cm2 at 5 cm. At the operator distance the leakage was essentially nonexistent when operated as per intended use.

On fabrication, assembly and testing of the ADP pilot oven, a Go/No-Go demonstration of continuous casting of electrode and drying of the slurry was performed at Lambda in the presence of Navitas personnel. After the successful (Go/No-Go) demonstration of the ADP pilot oven operation and identical analytic results for samples dried with the newly assembled tool, the equipment was packed and shipped to Navitas facilities where it was integrated and installed on their pilot coating line. Figure IV-352 below shows the

digital image of the installed ADP pilot oven equipment. Figure IV-352(a) shows the Power Module, while Figure IV-352(b) shows the Process Module placed in front of the Power Module. VFM power is transmitted and delivered by the waveguide connecting the two modules on top.

(a) Power Module (b) Process Module

Figure IV-352: Digital image of the ADP Pilot oven installed at Navitas. The Power Module (a) delivers VFM power through the waveguide connected to Process Module (b), which is placed between the coater and the standard convection oven

Drying Comparison with ADP Pilot oven

Both anode and cathode films were coated and dried using the ADP system and Navitas IR drying line (baseline). The anode active material was commercial synthetic graphite (97wt. %) combined with water based binder (CMC + SBR). The cathode slurries were prepared with NCM523 (93wt. %), conductive carbon and PVDF binder (NMP solvent). In the case of anode the coating and drying speed used was 500 mm/min for both conventional and ADP drying. For NCM cathode the coating/drying speeds were 350 and 225 mm/min for Navitas baseline and ADP system respectively.

Table IV-46 summarizes the advantage of using ADP over conventional drying system. In the case of water based anodes there is a 5x drying advantage over IR convection drying, while for NMP based cathodes the reduction in drying time has 3x benefit.

SLP Full Cell Testing

After drying the anode and cathode films were calendared to 35% porosity. Anode films were calendared at room temperature, while cathode films were calendar at 120°C and then annealed at 140°C for 2h. Navitas adhesion test were performed on both anode and cathode samples and both samples passed. The films were later punched into electrodes for the fabrication of single layer pouch (SLP) cells.

Table IV-46: Comparison between Conventional Drying and the Advance Drying Process (ADP)

Electrode	Drying Method	Drying speed (mm/min)	Drying length (m)
Anode (graphite, water based binder)	Navitas 2-zone IR system	500	2.5
	ADP (Hot air + VFM)	500	0.5
	ADP Advantage	5X	
Cathode (NCM523, NMP based binder)	Navitas 2-zone IR system	350	2.5
	ADP (Hot air + VFM)	225	0.5
	ADP Advantage	3X	

SLPs were sealed and filled with electrolyte inside of an Argon filled glovebox. Electrochemical performance test (formation, rate capability, cycle life and DCR measurements) were carried out on all cells.

Formation Cycles

Two formation cycles were taken in all cells at C/10 from 3.0 to 4.2V. Figure IV-353 shows the voltage versus capacity plots for cells with electrodes dried with conventional and ADP drying systems. Table IV-47 summarizes numerical values for specific capacities and initial capacity loss (ICL). It is worth emphasizing that no difference has been observed during formation of all cells.
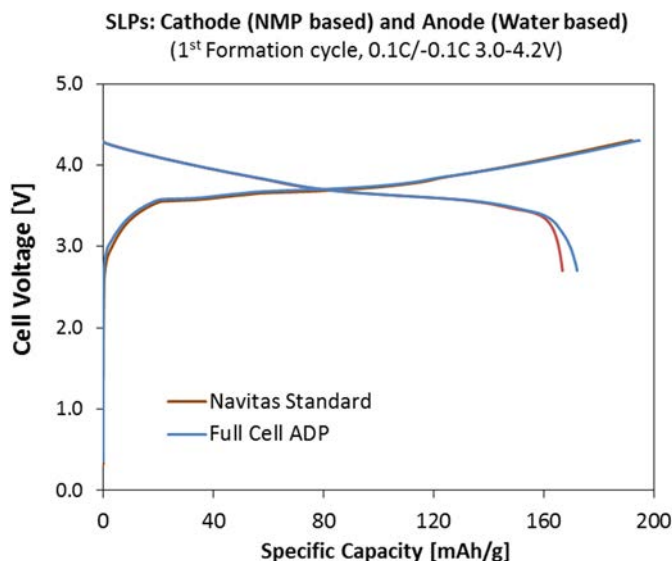

Figure IV-353: First formation cycle for SLP cells with electrodes (anode and cathode) dried using Navitas conventional and ADP drying systems; using CC-CV charge and CC discharge protocols at C/10 from 3.0 to 4.2 V

Table IV-47: Summary of SLP Formation Results

Drying Method		Loading		Reversible Capacity	ICL (%)
Anode	Cathode	(mg/cm^2)	(mAh/cm^2)	(mAh/g)	
Navitas	Navitas	17.2	3.1	166.4	13
ADP	ADP	17.2	3.1	170.5	12

Rate Capability

SLPs were charged at 0.1C and then discharged at different C rates (0.1, 0.2. 0.5, 1.0 and 2.0C) from 2.7 to 4.2V. As expected, rate performance shows no difference between Navitas standard and ADP dried electrodes. In addition, these values are comparable to the ones obtained in previous experiments using static and continuous coatings done at Lambda facilities. (See Figure IV-354.)

SLPs: Cathode (NMP based) + Anode (Water based)
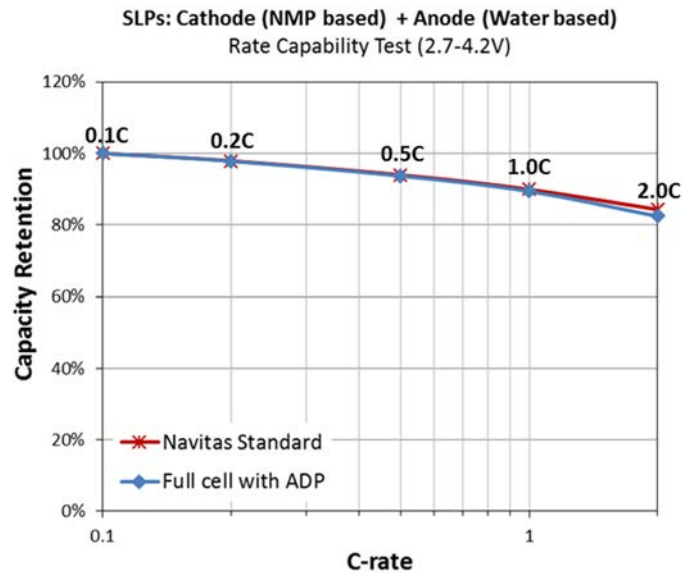**Rate Capability Test (2.7-4.2V)**

Figure IV-354: Rate capability plots for cells with electrodes dried using conventional and ADP drying methods. All cells were charged at 0.1 C, and discharged at 0.1, 0.2, 0.5, 1.0 and 2.0 C

Cycle Life (100% SOC)

Life cycle experiments for SLP cells (both baseline and ADP dried electrodes) with 3.0 mAh/cm2 loadings were performed at 0.5C current rate (100% SOC). Cycle numbers versus discharge capacity retention are shown in Figure IV-355. The plots show comparable performance between the baseline and the cell fabricated with ADP dried electrodes. The summary of life cycling parameters for SLPs fabricated at Navitas (capacities taken at 100%SOC) is shown in Table IV-48.

Cycle Life of Navitas Pouch Cells
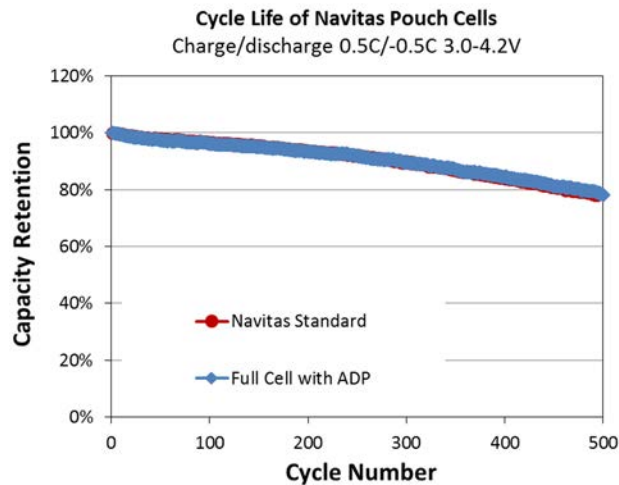**Charge/discharge 0.5C/-0.5C 3.0-4.2V**

Figure IV-355: Cycle life testing comparison for single layer pouch cells. Baseline cells were dried with Navitas standard system. Experiments were carried out at C/2 current from 3.0 to 4.2 V

Table IV-48: Summary of life Cycling Parameters for SLPs Fabricated at Navitas, Capacities were Taken at 100%SOC

Drying Method		Loading (mAh/cm^2)	Initial Capacity (mAh/g)	Capacity Retention @ 500 cycles (mAh/g)
Anode	Cathode			
Navitas	Navitas	3.1	141.9	78%
ADP	ADP	3.1	142.6	79%

2.0Ah High Energy (HEC) Prismatic Lithium Ion Testing

After drying, the anode and cathode films were calendared to 35% porosity. Navitas adhesion test and binder distribution were performed on both anode and cathode samples and all samples passed. The films were later punched into electrodes for the fabrication of HEC prismatic cells. HEC batteries were sealed and filled with electrolyte inside an Argon filled glovebox.

Adhesion & Binder Migration

Standard adhesion tests were carried out on sample electrodes (anode and cathode) dried using standard and Advanced Drying Processes. Binder distribution measurements were done using elemental mapping (EDX: Energy Disperse X-ray spectroscopy) on 4-6 sections of the (anode and cathode) film cross-section (from top to bottom). Binder distribution ratio, from electrode surface and near the metal foil substrate, should be under 1.3. Table IV-49 summarizes adhesion and binder distribution results.

Table IV-49: Summary of Adhesion Testing and Binder Migration Data for Standard and ADP Drying of Anode and Cathode

Electrode	Drying Method	Binder Solvent	Mass Loading (mg/cm^2)	Adhesion	Binder Distribution
Anode	Navitas	Water	10	Pass	1.19
	ADP	Water	10	Pass	1.07
Cathode	Navitas	NMP	18	Pass	1.09
	ADP	NMP	18	Pass	1.03

Cathode Binder Distribution

Cathode electrodes dried with and without ADP were analyzed under SEM (cross-sectional view) to study the binder distribution (fluorine) across the thickness of the electrode. Figure IV-356 shows the SEM and EDX micrographs and fluorine mapping (blue shades on EDX pictures). The ratio of binder content (weight %) between surface (top) and foil (bottom) interfaces is 1.10 for the conventional dried electrode. Conversely, the electrode dried under ADP has a ratio of 1.03. This confirms earlier observations, indicating less (or no) binder migration to the electrode surface when ADP is used to dry the electrodes.

Anode Binder Distribution

Anode electrodes dried with and without ADP were analyzed under SEM (cross-sectional view) to study the binder distribution. Samples were stained with osmium tetroxide prior to SEM studies. Backscattered electron (BSE) microscopy was used to map osmium through the anode cross sections. The metal shows as white bright spots on cross section micrographs. Figure IV-357 shows the BSE micrographs for both sets of samples. The

ratio of binder (Figure IV-357c), content between surface (bottom) and foil (top) interfaces, were 1.2 and 1.1 for conventional and ADP dried electrodes.
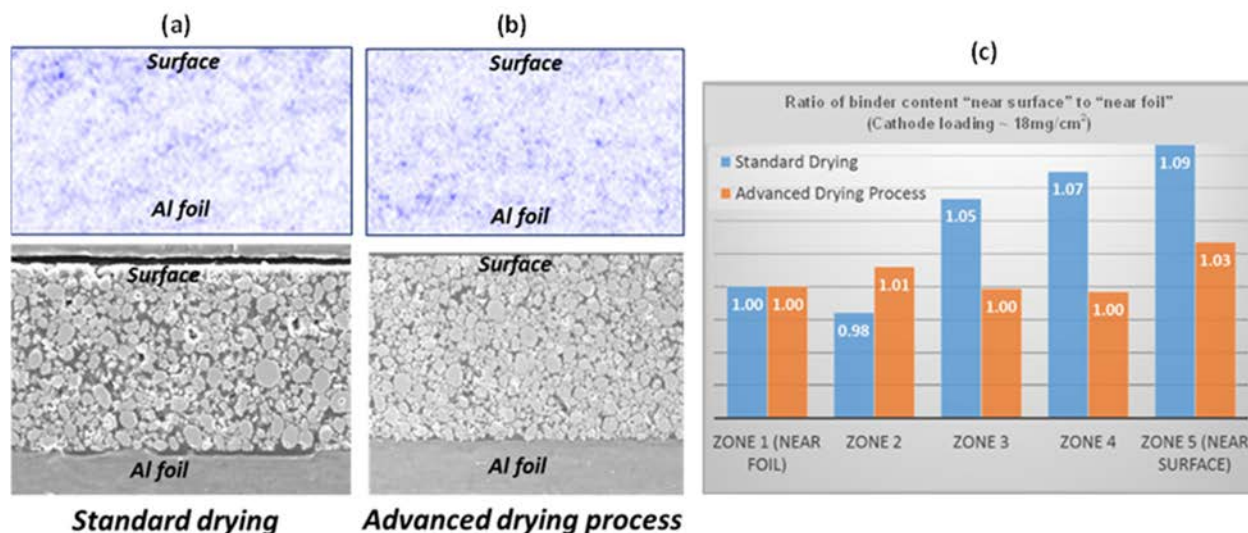

Figure IV-356: Binder distribution for cathode (NCM523) electrodes dried using (a) standard or baseline drying and (b) ADP (hot air plus VFM). (c) Binder ratios measured at various zones across the electrode (from near foil to the electrode surface)
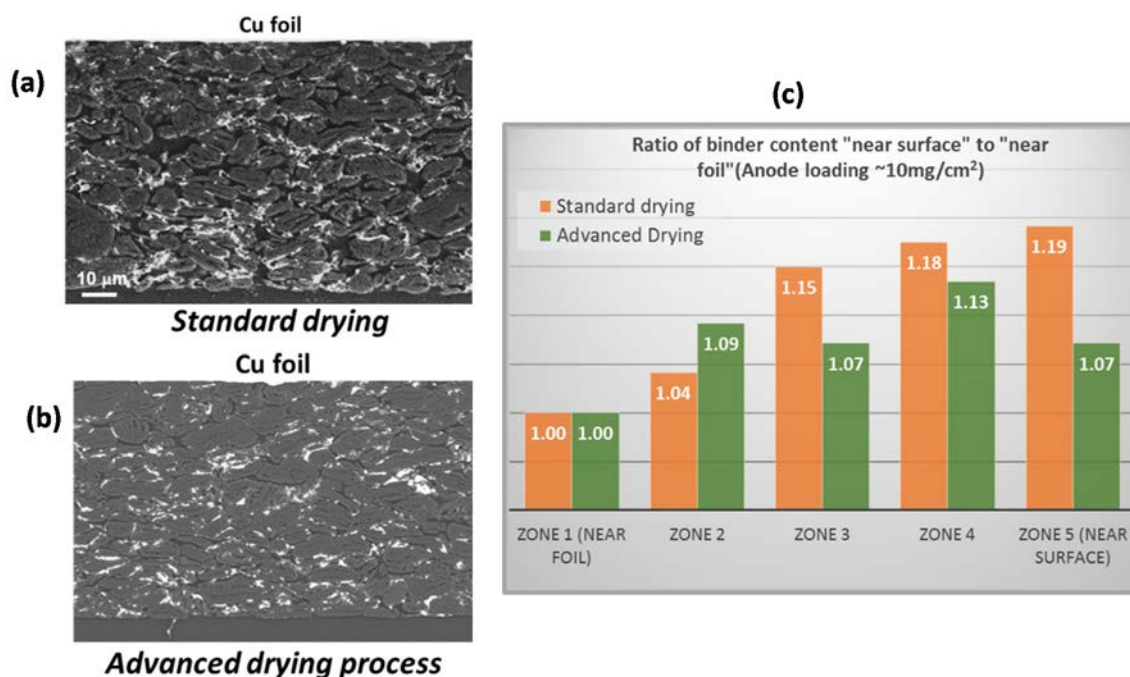
Figure IV-357: BSE micrographs showing binder distribution for anode (graphite) electrodes dried using (a) standard and (b) ADP. (c) Binder ratios measured at various zones across the electrode (from near foil to the electrode surface)

Electrochemical performance

Fifteen (6 baselines, and 9 with ADP) 2.2Ah cells were fabricated. Formation cycles were taken in all cells at C/10 from 3.0 to 4.2V, showing an average of 2.2Ah reversible capacity and 16% ICL for all cells. The cathode electrochemical loadings were set to 3.0mAh/cm^2.

Life cycle experiments for the prismatic cells (both standard and ADP dried electrodes) were carried out at C/3 current rate from 3.5 to 4.2V, at this voltage window the cell discharges to 80% (or 80% depth of discharge, DOD). Cycle numbers versus discharge capacity retention for both methods are shown in Figure IV-358. Both set of cells (with baseline and ADP dried electrodes) have completed 1000 cycles, with capacity retention of

80%. The plots show comparable performance between the baseline and the cell fabricated with ADP dried electrodes. Average numerical values are summarized in Table IV-50.

2.2Ah Li Ion cell (Gaphite anode + NCM523 Cathode): Cycle Life at 80% DOD
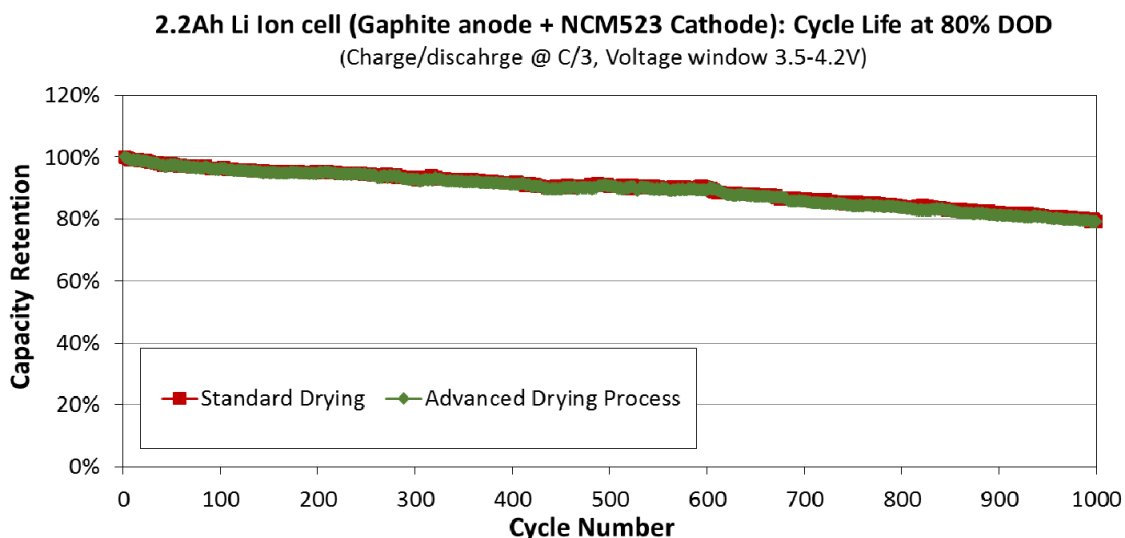(Charge/discahrge @ C/3, Voltage window 3.5-4.2V)

Figure IV-358: Cycle life testing for HEC prismatic cells comparing standard and ADP drying methods. Average values are presented in this plot. Experiments were carried out at C/3 current from 3.5 to 4.2 V

Table IV-50: Summary of 2.2Ah Prismatic Lithium Ion Cells Formation Parameters. Standard Drying (Navitas IR Convection System) and the Advanced Drying Process (ADP) Showing Identical Performance

Drying Method	Capacities (Ah)		Capacity retention at 1000th cycle
	Reversible @ 0.33C, 100% DOD	1st cycle @ 0.33C, 80% DOD	
Standard Drying	2.0	1.6	80%
Advanced Drying Process (ADP)	2.0	1.6	80%

Advanced Drying Process as a Booster to Conventional Drying Systems

The current ADP system was designed to be ~ 50cm in length and the slurry drying speeds were limited to 0.5m/min for graphite/water based binder and to 0.25m/min for NCM cathode/PVDF. However, since most of the bulk drying can be rapidly performed with ADP, the ADP system was explored as a booster module to the convection drying system.

NCM 523 cathode slurry with 55% solid content and NMP solvent was used to perform these experiments. Films were coated with 3.0mAh/cm^2 electrochemical loading. Cathode films were coated and dried at 0.8m/min with this drying configuration and no defects were observed on the dried films.

To further test the advantage of using ADP in this configuration, films with even increased electrochemical loading as high as 4.0mAh/cm^2 were tested. Without VFM surface cracks were observed on these coatings. However, when the VFM (in the ADP) was turned on, the films were completely dried without any surface defects.

Furthermore, the cathode slurry was coated and dried at 1.0m/min. Without ADP there were surface cracks and wet spots. With a slight increase in power and temperatures, the combination of ADP and convection drying made it possible to completely dry the films without any defects. Thus a speed increase of 4X (as compared to ADP standalone) was possible with ADP used as a booster module.

Energy Savings Study

This study on power consumption was performed to evaluate one of the objectives of the project on energy and cost savings. The data collected for the IR/convection Megtec drying oven is compared with the ADP process (Figure IV-359, Figure IV-360).

ADP drying efficiency = 5.789/9.727 = 0.595 or 59.5% of average power used by IR/convection oven.

This study demonstrates a > 40% saving in power consumption with ADP as compared to the convection/IR drying systems. hus one can expect the same saving in the operational cost with ADP. Please note that the objective of the project was a 30-50% reduction in energy and cost.
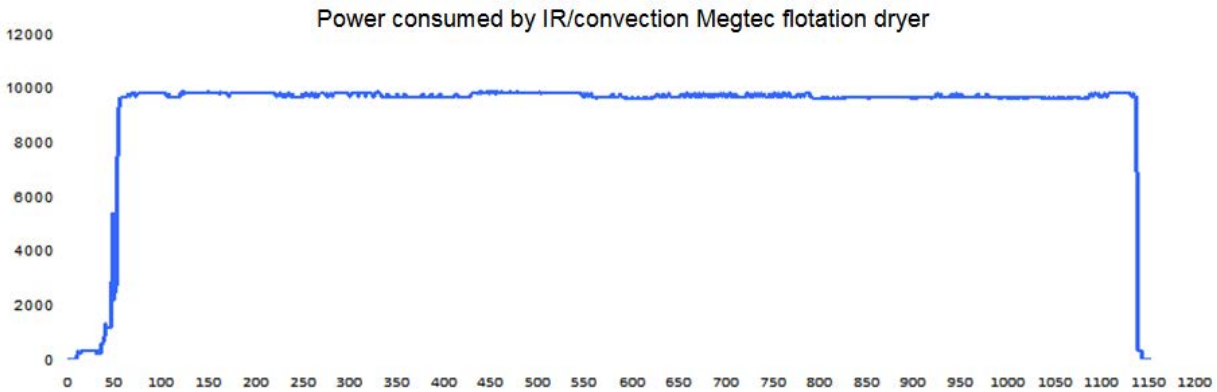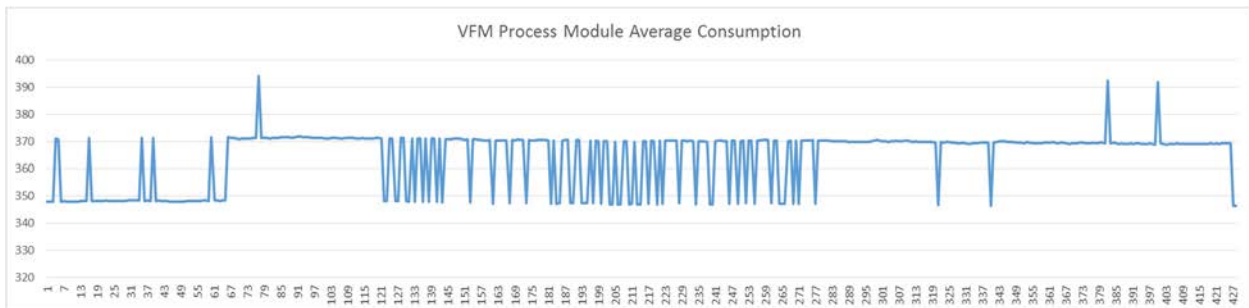

Figure IV-359: The average power consumed by IR/convection dryer during a 500 mm/min drying run = 9.727 kVA
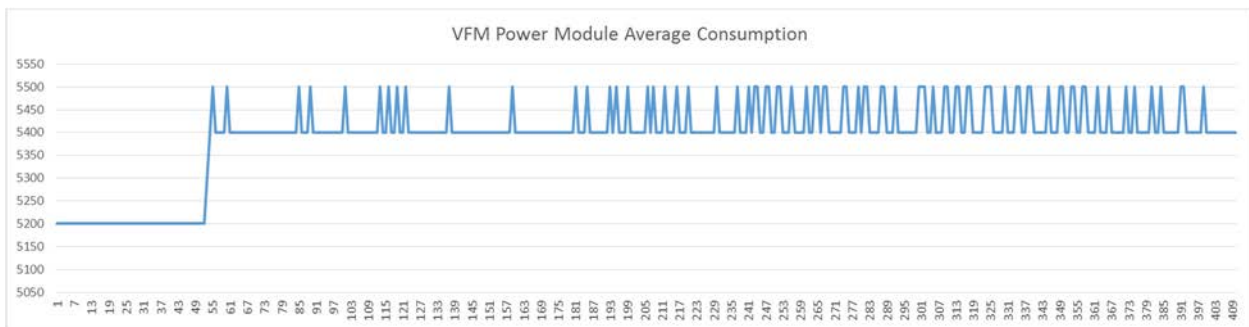
(a)

(b)

Figure IV-360: Average power consumed by the VFM power module = 5.422 kVA, while the average power consumed by the hot air in process module = 367 VA during a 500 mm/min drying run. Total = 5.422 + 0.367 = 5.789 kVA

Conclusions

Drying electrode slurries is a high cost operation for lithium-ion batteries. ADP (hot air plus VFM) can rapidly dry electrode slurries on metal substrates. With the ADP system VFM penetrates into the slurry and targets the polar solvent molecules deep in the electrode and drives the solvent out. With the penetrating nature of microwaves more advantages are expected when drying thick electrodes. The hot air flow will then exhaust the solvent vapors out of the ADP chamber.

The ADP pilot oven system was design, assembled, tested and shipped to Navitas for extensive casting and rapid drying of aqueous anode and NMP based cathode slurries. The material and electrochemical characterization have shown that the faster drying process using ADP did not change the overall properties of the dried electrodes, as a matter of fact the rapid volumetric VFM heating of the slurry minimized binder migration to the surface. HEC prismatic cells were fabricated by drying electrodes with standard and ADP methods. Both set of cells (standard baseline and ADP dried electrodes) have completed 1000 cycles, with capacity retention of 80%. The life cycle testing plots show comparable performance between the baseline and the cell fabricated with ADP dried electrodes.

The ADP equipment has also been explored as a booster module to the convection drying system. Because of the short length (~50cm) of standalone ADP system, the slurry drying speeds were limited to 0.25m/min for NCM cathode/PVDF. However, as a booster module with some optimization it was possible to cast NCM 523 cathode slurry with increased mass loading as high as 4.0mAh/cm2 and completely dry the electrode at 1.0m/min with the combined ADP booster followed with standard convection oven. This has not been possible with the standard convection oven only.

A comparison of the power consumption for ADP and the standard IR/convection oven was performed. The study demonstrated a > 40% saving in power consumption with ADP while being only a fraction of length, providing a 3 to 5 time advantage over the standard drying systems.

Products

Presentations/Publications/Patents

1. "Advanced Drying Process for Low Cost Manufacturing of Electrodes", ES246_Ahmad_2015_p, US DOE Vehicle Technologies AMR, 2015.
2. "Lambda Technologies Develops Rapid Inline drier for Electrode" Posted on August 13, 2015 in The Battery Show Newsletter.
3. "Apparatus and Method for Drying Battery Electrodes", Ahmad et al, Provisional Patent Application September 2015.
4. Rapid, Low-Cost Battery Electrode Dryer, Highlights 2015 US DRIVE.
5. "Advanced Drying Process for Low Cost Manufacturing of Electrodes", ES246_Ahmad_2016_o, US DOE Vehicle Technology AMR, 2016.
6. "Apparatus and Method for Drying Battery Electrodes", Ahmad et al, Utility Patent Application September 2016.

IV.F.9. FY 2015 Vehicle Technologies Incubator Award: New Advanced Stable Electrolytes for High Voltage Electrochemical Energy Storage (Vanderbilt University, LBNL, ORNL)

Peter Pintauro
Vanderbilt University
Department of Chemical and Biomolecular Engineering
PMB 351604
Nashville, TN 37235
Phone: 615-343 3878; Fax: 615-343-7951
E-mail: pn.pintauro@vanderbilt.edu

Gao Liu
Lawrence Berkeley National Laboratory
Energy Storage and Distributed Resources Division
1 Cyclotron Road, MS 70R108B
Berkeley, CA 94720
Phone: 510-486-7207; Fax: 510-486-7303
E-mail: gliu@lbl.gov

Jagjit Nanda
Oak Ridge National Laboratory
Materials Science and Technology Division
P.O. Box 2008 MS6124
Oak Ridge, TN 37831
Phone: 865-241-8361; Fax: 865-574-4066
E-mail: nandaj@ornl.gov

Peter Faguy, DOE Program Manager
U.S. Department of Energy
Vehicle Technologies Office
1000 Independence Avenue, SW
Washington, DC 20585
Phone: 202-586-1022
E-mail: Peter.Faguy@ee.doe.gov

Start Date: October 1, 2015
End Date: September 30, 2018

Abstract

Objectives

- Fabricate, characterize, and optimize the composition/morphology of an entirely new class of Si-based nanofiber anodes for lithium-ion batteries, with high gravimetric and volumetric energy density and minimal capacity fade during charge/discharge cycling.

- Perform pilot-scale-up studies for anode commercialization.

- Improve our understanding of structure/functions correlations in electrospun particle/conducting polymer nanofiber anodes.

Accomplishments

- Identified solution composition and electrospinning conditions necessary to fabricate fiber mats containing Si nanoparticles and an electronically conductive PFM binder.

- Prepared and characterized electrospun fiber mat anodes containing Si nanoparticles, carbon black, and poly(acrylic acid) (Si/C/PAA), to serve as a baseline for anodes prepared with a conductive polymer binder.

- Identified qualitative performance/composition/structure correlations by evaluating the performance of freestanding fiber mats with different compositions, fiber volume fractions, and interfiber connectivities.

- Conducted post-mortem analyses of Si-based anodes using scanning electron microscopy and Raman spectroscopy.

- All project milestones were met on schedule, and future milestones are on track to be achieved within the appropriate time frame.

Future Achievements

- Ink formulation and electrospinning conditions will be identified for the creation of fibers with si nanoparticles and a second electronically conductive polymer binder (PEFM). Various carrier polymers including poly(ethylene oxide) (PEO) and poly(vinylpyrrolidone) (PVP) will be investigated to facilitate fiber formation, if needed.

- Si/PFM/carrier polymer and Si/PEFM/carrier polymer nanofiber mat anodes with average fiber diameters ranging from ca. 300 nm – 1 µm will be prepared and characterized. The effect of fiber diameter on the electrochemical performance of these anodes will be determined.

- Mat processing procedures to form Si/PFM/carrier polymer and Si/PEFM/carrier polymer fiber mats with high fiber volume fractions (e.g., ~0.85) and welded interfiber contacts will be developed.

- The rate capabilities up to 2C of electrospun fiber mats with a range of thicknesses (up to 200 µm) and fiber volume fractions (up to 0.85) will be evaluated.

- Pilot-scale-up studies at a commercial electrospinning facility will be performed using the best fiber mat anode formulations developed during this project.

Technical Discussion

Background

Since their commercial debut in 1991, lithium-ion batteries have revolutionized the functionality of portable electronic devices, and the lithium-ion battery industry continues to grow today due emerging applications such as electric vehicle propulsion.[1-2] Despite the extraordinary success of lithium-ion batteries, many devices are still limited by battery performance, and thus new batteries with higher energy densities and long cycle life must be developed to satisfy the ever-increasing demands of consumers.[3-4]

Si has been widely investigated as a replacement for graphite in today's lithium-ion battery anodes due to its high theoretical capacity (3,600 mAh/g vs. 372 mAh/g for graphite) and low operating potential (< 0.5 V vs. Li/Li$^+$).[5-6] However, Si-based anodes often exhibit poor cycling stability due to large volume changes during charging and discharging. Lithiation of Si is accompanied by a volumetric expansion exceeding 300%, and repeated swelling and shrinking of Si during battery cycling results in capacity fade due to Si pulverization, electronic isolation of Si particles, and irreversible Li consumption associated with repeated formation and rupture of the solid-electrolyte interphase (SEI) layer.[7-8] Although Si pulverization can be eliminated through the use of nanoscale active materials (e.g., Si nanoparticles[9-11] and Si nanowires[12-15]), effective techniques which prevent electronic isolation of Si and stabilize the SEI layer are yet to be identified.[7-8] Furthermore, previously reported nanoscale Si anodes typically contained low active material loadings and densities, resulting in low areal and volumetric capacities. To produce Si anodes which are suitable for commercial applications, new anode designs which can tolerate Si volumetric changes while maintaining high gravimetric, areal, and volumetric capacities over many charge/discharge cycles must be developed.

Introduction

This project investigates a new class of Si-based nanofiber anodes for lithium-ion batteries with high gravimetric, areal, and volumetric capacities and minimal capacity fade during charge/discharge cycling. The successful completion of the project tasks will demonstrate anode fabrication scale-up at a commercial electrospinning facility. These nanofiber anodes can be easily incorporated into the production line of most modern battery manufacturing units to provide Americans with the performance they expect and demand.

This project merges an exciting and important technology for the creation of electrospun hybrid nanofiber structures with recent developments in electronically conductive polymer synthesis. The unique electrochemical characteristics of electrospun nanoparticle/polymer fiber electrodes have been recently demonstrated by Pintauro, Wycisk and co-workers at Vanderbilt University [16-22] while superior performance of n-doped electronically conductive polymer binders in battery applications have been reported by Gao and co-workers at LBNL [23-24]. The achievement of project goals is realized through the intelligent convolution of these two discoveries.

The focus of the present research project is on the fabrication and characterization of electrospun lithium-ion battery anodes containing Si nanoparticles and an electronically conductive polymer binder. The porous electrodes can accommodate the volume changes of Si during charge/discharge cycling without significant capacity losses. An important aspect of this process is the capability to integrate the active anode particles and the functional conductive polymer binder into a robust composite nanostructure with high particle loading, high capacity retention, and resistance to mechanical failure.

It is also important to stress the novelty and uniqueness of particle/polymer nanofiber mats for battery applications. Although nanofiber electrodes have been previously reported with some impressive successes, those studies employed pyrolyzed carbon fibers prepared from polymer precursors. In the present work, there is no pyrolysis; the electrospinning and post-processing are done at room temperature, thus preserving the polymer binder in the final electrode structure.

Approach

This study investigated Si-based anodes containing: (i) Si nanoparticles (50 - 70 nm) and a PFM conductive polymer binder (Si/PFM, electrospun and slurry cast), (ii) Si nanoparticles, carbon powder, and poly(acrylic acid) (Si/C/PAA, electrospun only), and (iii) Si/C/PAA anodes prepared with Si nanowires (electrospun only). 1 wt.% poly(ethylene oxide) (PEO, Mv ~ 1 MDa) was added as a carrier polymer to facilitate the electrospinning process for fibers containing the PFM conductive polymer binder. Electrode inks were prepared by mixing the components in a 1/1 mixture of chlorobenzene/chloroform (for Si/PFM) or n-propanol (for Si/C/PAA).

Slurry cast anodes were prepared by casting the electrode ink onto a copper foil current collector (9 µm, MTI Corp.) and drying at ambient conditions. Electrospun fiber mat anodes were created using a single needle spinneret and a custom-made rotating drum collector as described previously. [21] Fiber mats were spun onto an aluminum foil substrate at the following conditions: (i) 0.25 - 1.00 mL/h solution flow rates, (ii) 5 - 8 kV bias voltage, (iii) 8.0 cm spinneret-to-collector distance, and (iv) 15 – 75% relative humidity. Electrospinning conditions were adjusted for each electrode system to form fibers with uniform particle distributions and fiber diameters. Top-down morphology of the electrospun mats was assessed using scanning electron microscopy (Hitachi S4200 and Zeiss Merlin SEMs).

CR2032 half cells were constructed in an argon-filled glovebox using a Si-based electrode (dried overnight at 70°C under vacuum) as the working electrode and a Li metal counter/reference electrode. The electrolyte was 1.2 M LiPF6 in a mixture of ethylene carbonate and diethyl carbonate (3/7 by volume, BASF Corp.). 30 wt.% fluoroethylene carbonate (BASF Corp.) was added to the electrolyte to ensure formation of a stable SEI layer. Two sheets of Celgard 2500 soaked in electrolyte were used as a membrane separator, and several additional drops of electrolyte were added to completely fill the cell volume. Cells were crimped at 1,000 psi and rested overnight before electrochemical characterization. Galvanostatic charge/discharge experiments were conducted by polarizing the cells between 0.015 – 1.5 V vs. Li/Li+ at 0.1C on an 8-channel battery tester (5 V/1 mA, MTI Corp.). C-rates for the half cells were calculated assuming a theoretical capacity of 3,600 mAh/g for Si and

372 mAh/g for carbon. Except where otherwise indicated, half-cell capacities are normalized with respect to the entire composite anode (i.e., total amounts of Si, conductive additive (if present), and polymer binder).

Selected half cells were disassembled after cycling, and the anodes were rinsed using dimethyl carbonate before conducting post-mortem analysis. Cross-sectional SEM images of pristine (i.e., uncycled) and cycled fiber mat anodes were collected using Zeiss Merlin VP microscope (Carl Zeiss Microscopy GmbH, Oberkochen, Germany). The cross-sectional investigations using both SEM and Raman were carried out on electrodes broken into halves after soaking them in liquid nitrogen. Raman spectra of pristine and cycled fiber mat anodes were acquired using an Alpha 300 confocal Raman microscope (WITec, GmbH) with a solid-state 532 nm excitation laser, 100x objective, and a grating with 600 grooves/mm. Raman maps with a spatial resolution on the order of 1 µm and a pixel density of 9 pixels/µm2 were collected with an integration time of 2 s per spectrum. The laser power was attenuated to 1 mW for analysis of the pristine electrode. The laser power was further reduced to 100 µW for analysis of the cycled sample to prevent crystallization of the amorphous silicon from laser-induced heating. Raman maps were analyzed using WITec Project Plus software.

A CR2032 full cell containing an electrospun Si/C/PAA anode and an electrospun $LiCoO2/C/PVDF$ cathode was assembled and tested. The $LiCoO_2/C/PVDF$ fiber mat cathode was prepared using the ink formulation and electrospinning procedure described in Reference 22. The full cell contained the same electrolyte and separator as used in the half cells. To minimize the irreversible capacity loss in the full cell, the Si/C/PAA anode and $LiCoO_2/C/PVDF$ cathode were preconditioned in half cells for at least 10 cycles at 0.1C. The anode/cathode mass ratio in the full cell was 1/13 to ensure good capacity matching of the electrodes (anode/cathode capacity ratio of 0.89). The full cell was characterized using galvanostatic charge/discharge cycling between 2.50 – 4.20 V at 0.1C, where the C-rate was calculated based on the measured capacity of the cathode. Full cell capacities were normalized with respect to both electrodes (i.e., the combined amounts of the Si/C/PAA anode and $LiCoO_2/C/PVDF$ cathode).

Results

An electronically conductive polymer binder [poly(9,9-dioctylfluorene-co-fluorenone-co-methylbenzoic ester), PFM] was synthesized at LBNL and delivered to Vanderbilt. Slurry cast Si/PFM anodes prepared at Vanderbilt exhibited a high initial capacity of 1,940 mAh/g at 0.1C and showed stable charge/discharge cycling as shown in Figure IV-361.
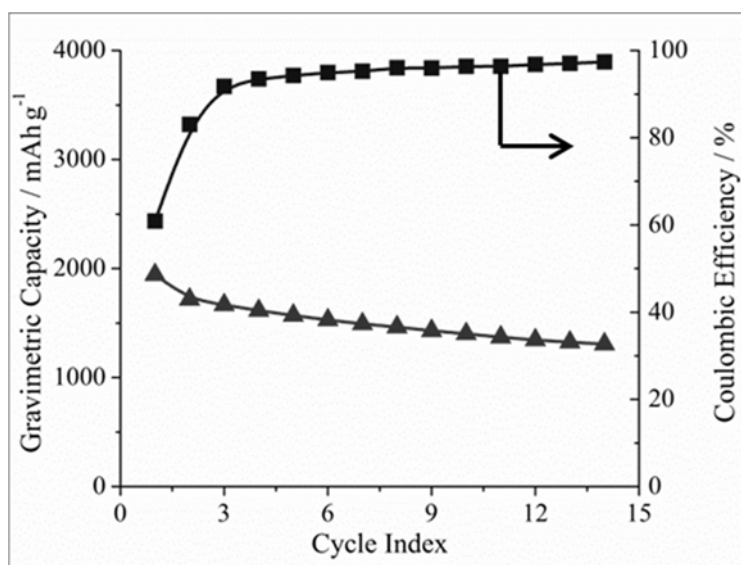
Figure IV-361: Cycling performance of a Si/PFM slurry cast anode over 14 cycles at 0.1 C

Since the slurry cast Si/PFM anode exhibited good electrochemical performance, electrospinning studies were performed to prepare neat PFM and Si/PFM fiber mats. Neat PFM nanofibers had an undesirable bead-on-fiber morphology, so 1 wt.% PEO as a carrier polymer was used to electrospin PFM/PEO fibers with average fiber diameters ~1.5 µm. Relative humidity (rh) had a large impact on the fiber structure during electrospinning; PFM/PEO fibers spun at 15% rh had a smooth surface (see Figure IV-362a) whereas fibers spun at 75% rh

exhibited surface pores ~100 nm in diameter (see Figure IV-362b). Anodes containing 20 - 50 wt.% Si were successfully incorporated into the PFM/PEO fibers as shown in Figure IV-362c-f. The fiber diameters for these Si/PFM/PEO systems ranged from 1.5 – 9 µm depending on the fiber composition. The successful preparation of Si/PFM/PEO fibers containing 50 wt.% Si demonstrates that project milestones M1 and M2 were reached on schedule.
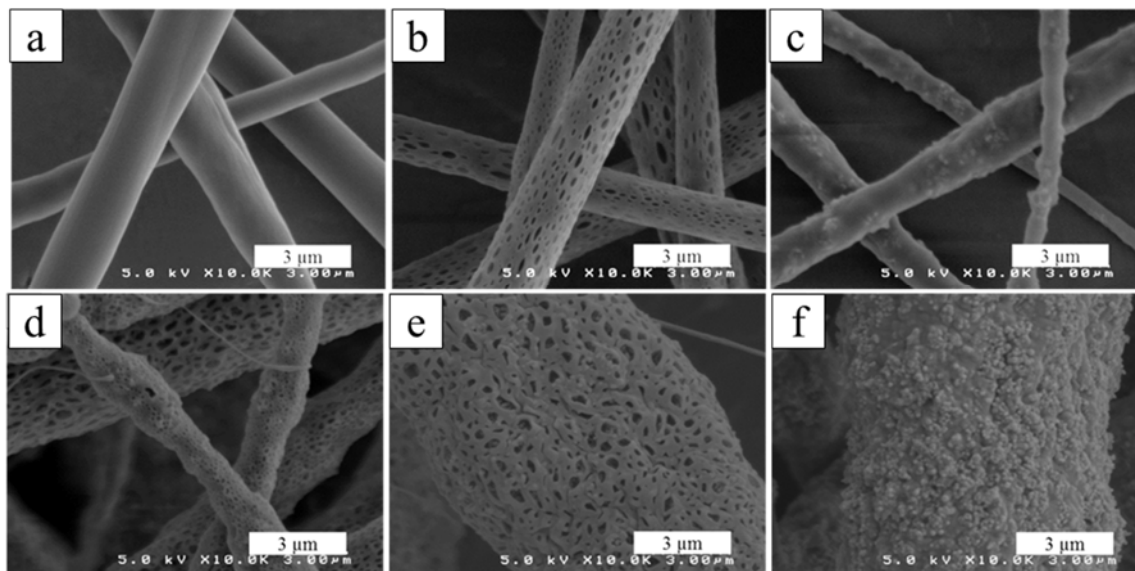

Figure IV-362: SEM images of electrospun (a) PFM/PEO fibers spun at 15% relative humidity, (b) PFM/PEO fibers spun at 75% relative humidity, and (c-f) Si/PFM/PEO fibers containing (c) 20 wt.% Si spun at 15% rh, (d) 35 wt.% Si spun at 75% rh, (e) 50 wt.% Si spun at 75% rh, and (f) 50 wt.% Si spun at 15% rh. The PEO carrier polymer content was 1 wt.% in all samples

To serve as a baseline reference material for the eventual comparison with Si/PFM/PEO fiber mat anodes, electrospun anodes containing Si nanoparticles, carbon black, and a poly(acrylic acid) binder (Si/C/PAA in a 40/25/35 weight ratio) were prepared and evaluated in lithium-ion battery half cells. Mat compaction and welding procedures were developed to improve the mat's interfiber connectivity and mechanical strength. SEM images of as-spun and compacted/welded fiber mats are shown in Figure IV-363a and Figure IV-363b, respectively. Charge/discharge curves collected at 0.1C for these anodes (see Figure IV-364a) show that lithiation/delithiation processes occurred at potentials < 0.5 V vs. Li/Li$^+$, as is expected for Si-based anodes. Figure IV-364b shows that the as-spun mat exhibited an initial capacity of 1,064 mAh/g and rapid capacity fade during cycling at 0.1C, but the compacted/welded Si/C/PAA nanofiber mat had higher gravimetric capacity (1,484 mAh/g) and superior cycling stability (73% capacity retention after 50 cycles at 0.1C). Compacted/welded fiber mat anodes prepared with a high material loading (3.49 mg/cm^2) had high areal and volumetric capacities of 4.5 mAh/cm^2 and 750 mAh/cm^3, which are much greater than that of commercial graphite anodes (~3 mAh/cm^2 and ~430 mAh/cm^3, respectively).
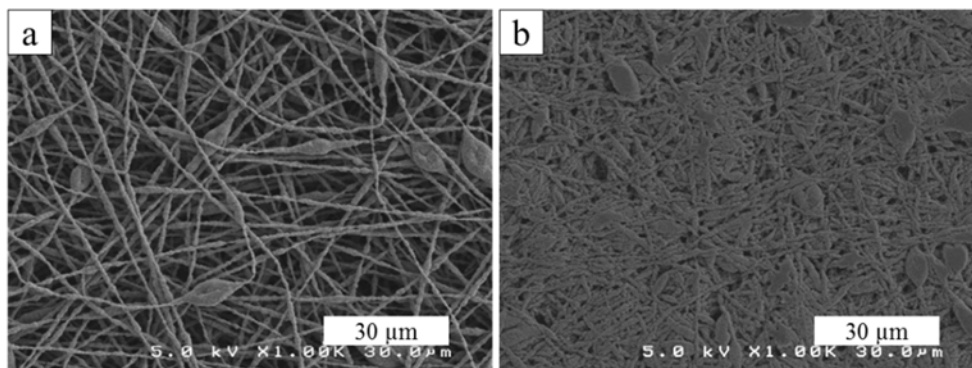

Figure IV-363: SEM images of electrospun mats containing Si nanoparticles, carbon black, and poly(acrylic acid) (Si/C/PAA) in a 40/25/35 weight ratio. (a) an as-spun fiber mat and (b) a compacted/welded fiber mat
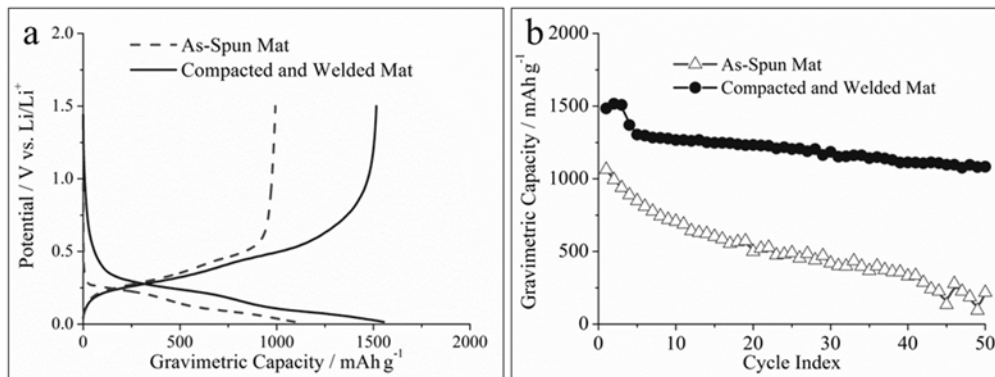
Figure IV-364: Electrochemical characterization of as-spun and compacted/welded Si/C/PAA nanofiber mats: (a) charge/discharge curves and (b) gravimetric capacity over 50 cycles at 0.1 C. The weight ratio of Si/C/PAA was 40/25/35 in both samples

Pristine and cycled Si/C/PAA electrodes tested at Vanderbilt were sent to ORNL for post-mortem analysis using Raman spectroscopy and high resolution SEM imaging. These ORNL results provided important insight on how electrode structure and composition evolved during cycling. Ultimately, these techniques improve our understanding of structure/functions correlations in electrospun particle/polymer nanofiber anodes.

The Raman spectra shown in Figure IV-365 indicate that pristine (i.e., uncycled) Si/C/PAA anodes contained crystalline Si as evidenced by the sharp peak ~520 cm^{-1}, and the crystalline Si transformed to amorphous Si after electrochemical cycling. This transformation was mapped over a large area ~4.5x9 µm^2 as shown in Figure IV-366. These results demonstrate that the pristine electrode had crystalline Si distributed evenly throughout the fiber mat. In comparison, the Si in the cycled electrode was completely amorphous.
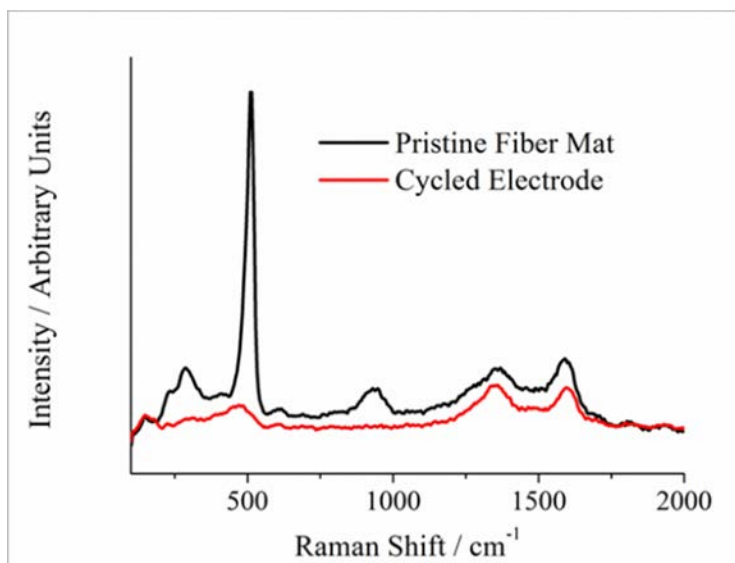

Figure IV-365: Raman spectra of Si/C/PAA nanofiber anodes (a) before cycling and (b) after 50 cycles at 0.1 C. The Si/C/PAA weight ratio in the electrodes was 40/25/35
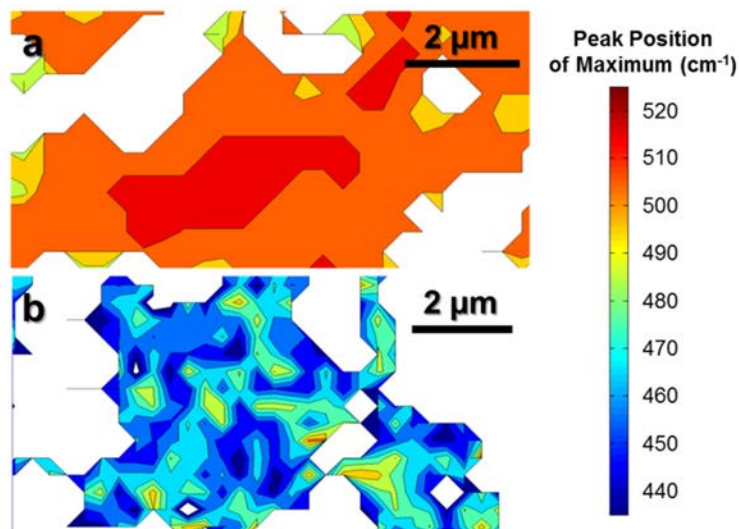
Figure IV-366: Raman maps over an area of ~ 4.5 x 9.0 μm² showing the Raman shift of the maximum peak for Si/C/PAA fiber mat anodes (a) before cycling and (b) after 50 cycles at 0.1 C. White pixels represent regions where the data were omitted due to low spectral intensities (i.e., counts < 10). The electrodes contained Si/C/PAA in a 40/25/35 weight ratio

High resolution SEM images of Si/C/PAA nanofiber anode cross-sections were taken at ORNL. The pristine anode shown in Figure IV-367a contained Si nanoparticles and carbon powder uniformly distributed throughout the fiber diameter. Figure IV-367b shows that the fiber structure and interfiber void space were preserved after 50 cycles at 0.1C, indicating good physical stability of the electrospun nanofiber mats in a battery.
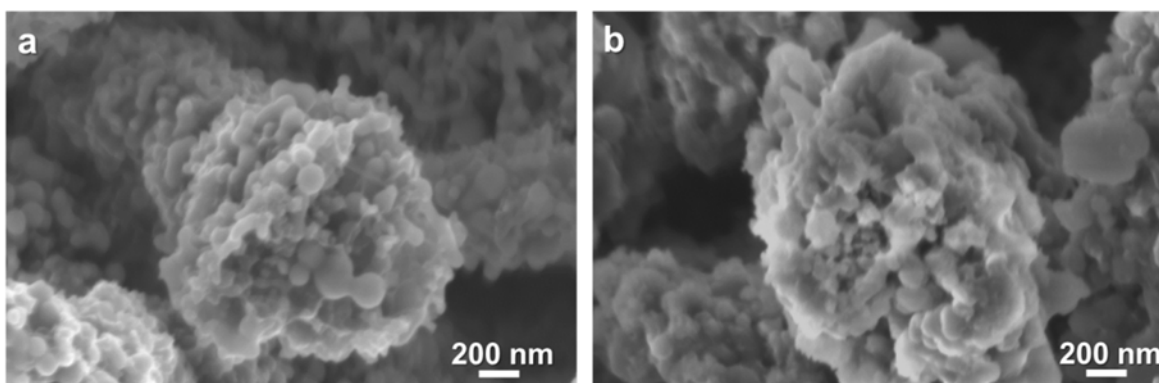
Figure IV-367: Cross-sectional SEM images of Si/C/PAA nanofiber anodes (a) before cycling and (b) after 50 cycles at 0.1 C. The Si/C/PAA weight ratio in the electrodes was 40/25/35.

To evaluate the performance of electrospun particle/polymer nanofiber electrodes under practical testing conditions, full cells containing an electrospun Si/C/PAA anode and electrospun $LiCoO_2$/C/PVDF cathode (developed at Vanderbilt outside of the present DOE-EERE project) were prepared and characterized. As shown in Figure IV-368a, the full cell had a reversible capacity of 75 mAh/g and an average operating potential of 3.6 V which corresponds to an energy density of 270 Wh/kg (normalized to the mass of both electrodes). These are the highest values ever reported for an electrospun full cell. The cell had moderate cycling stability with a reversible capacity of 49 mAh/g after 13 cycles as shown in Figure IV-368b.

Figure IV-368: Electrochemical characterization of a full cell containing an electrospun Si/C/PAA anode and LiCoO₂/C/PVDF cathode. (a) Charge/discharge curve collected at 0.1C and (b) Cycling stability over 13 cycles at 0.1 C

As previously discussed, electrospun Si/C/PAA anodes containing 40 wt.% Si exhibited a high initial capacity (1,484 mAh/g) and good cycling stability (73% capacity retention after 50 cycles) at 0.1C. While the performance of these electrodes was very 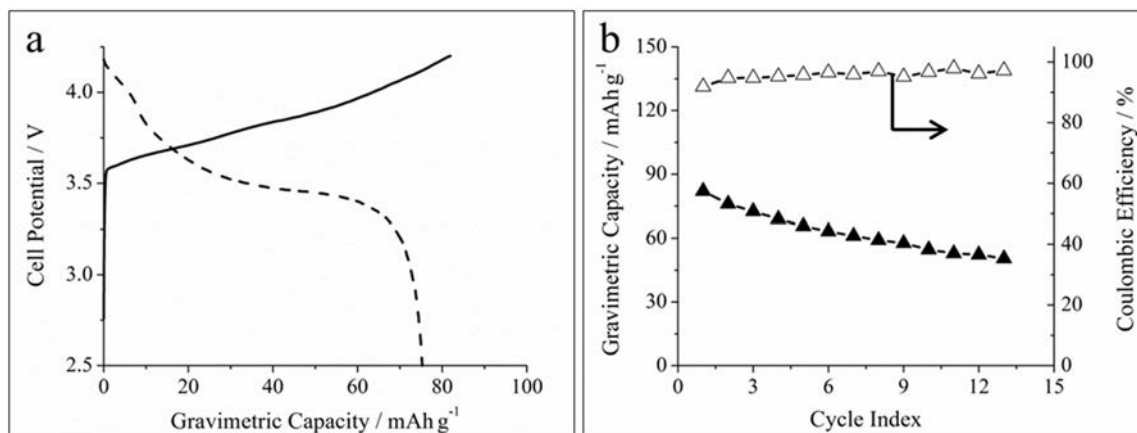encouraging, the material did not meet all the M4 milestone targets (500 mAh/g and 90% capacity retention after 50 cycles). To improve capacity retention while still maintaining a reversible capacity of at least 500 mAh/g, electrospun Si/C/PAA anodes containing 15 wt.% Si were prepared and characterized.

Figure IV-369a shows a representative charge/discharge curve collected at 0.1C for an electrospun Si/C/PAA fiber mat anode containing 15 wt.% Si. Lithiation/delithiation processes occurred at potentials < 0.5 V vs. Li/Li$^+$, as is expected for Si-based anodes. The anode had a reversible gravimetric capacity of 582 mAh/g at 0.1C (corresponding to 3,100 mAh/gist) which indicates good active material utilization. Figure IV-369b shows the performance of the anode over 50 charge/discharge cycles at 0.1C. During the first cycle, the coulombic efficiency was 69% due to formation of a solid-electrolyte interphase (SEI) layer on the anode surface, and the coulombic efficiency rose to > 95% during subsequent cycles. The anode exhibited excellent cycling stability with a reversible capacity of 523 mAh/g and capacity retention of 90% after 50 cycles. This anode's performance exceeded the targets set by the go/no-go milestone M4 (initial capacity of 500 mAh/g and 90% capacity retention after 50 cycles at 0.1C).
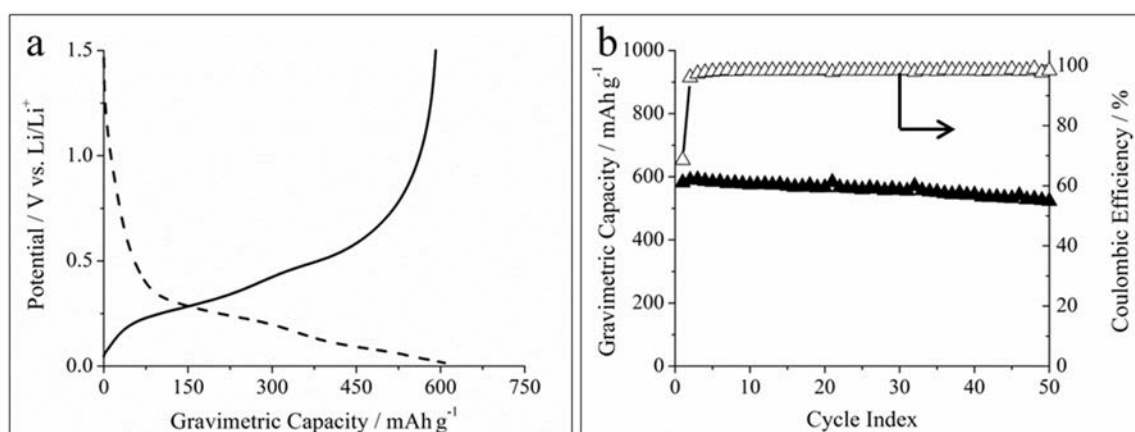
Figure IV-369: Electrochemical characterization of an electrospun Si/C/PAA nanofiber anode containing Si/C/PAA in a 15/50/35 weight ratio. (a) A charge/discharge curve collected at 0.1C and (b) Cycling stability over 50 cycles at 0.1 C

As an alternative to Si nanoparticle-based anodes, Si nanowires (Si NWs, prepared by Professor Sreeram Vaddiraju at Texas A&M University and shown in Figure IV-370a) were also incorporated into a nanofiber structure. Fiber mats containing Si NWs, carbon black, and poly(acrylic acid) in a 40/25/35 weight ratio were successfully electrospun as shown in Figure IV-370b where the Si NWs were well-aligned with the fiber axis. The use of Si NWs rather than Si nanoparticles as an active material offers new opportunities to improve the performance of Si-based anodes.
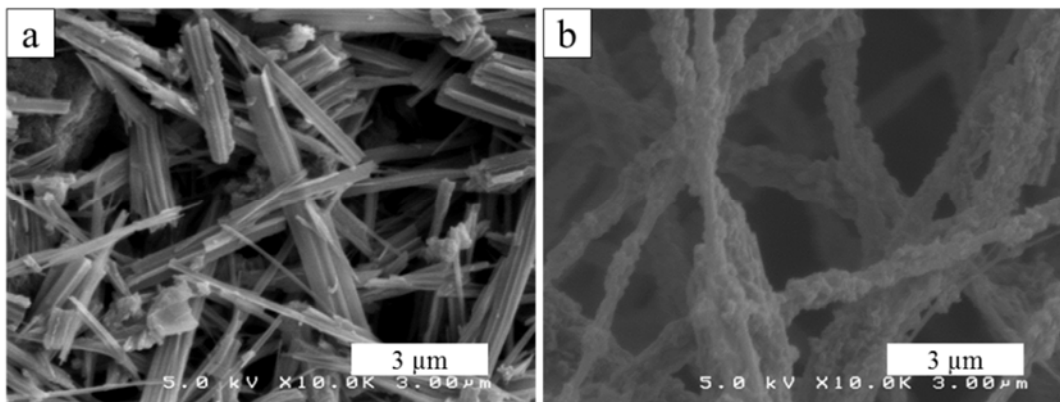
Figure IV-370: SEM images of (a) Si nanowires and (b) electrospun nanofibers containing Si NWs, carbon black, and PAA in a 40/25/35 weight ratio

Electrospun fiber mats containing Si nanowires, carbon powder, and PAA in a 40/25/35 weight ratio were characterized in half cells, and the results are shown in Figure IV-371. Compared to Si nanoparticle-based anodes, as-spun nanofiber mats (no mat compaction or fiber welding) containing Si nanowires exhibited lower capacity (432 vs. 1,001 mAh/g at 0.1C) which was attributed to the 10 nm SiO_x passive layer on the Si nanowires as determined by x-ray photoelectron spectroscopy at ORNL. Despite their lower capacity, the anodes containing Si nanowires exhibited superior cycling stability, retaining 68% of the initial capacity after 50 cycles, as compared to only 21% capacity retention for the Si nanoparticle anode.
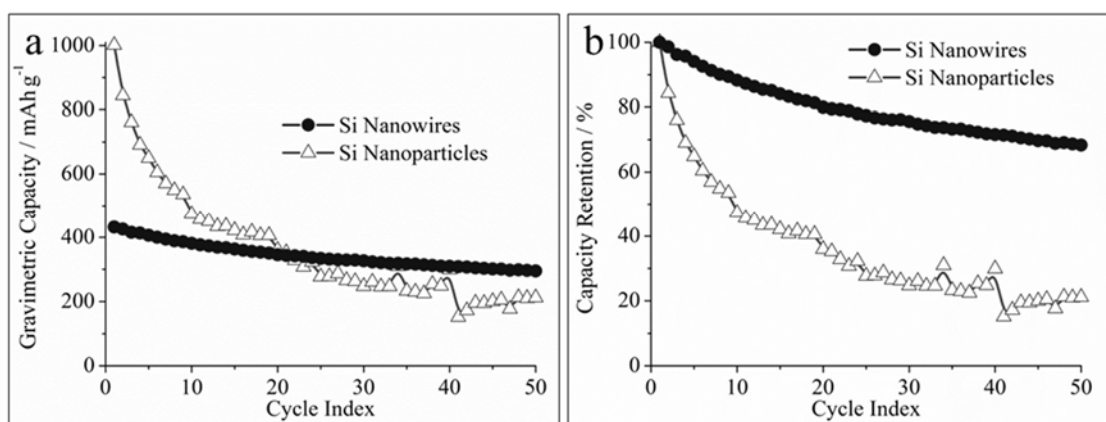

Figure IV-371: Electrochemical performance of as-spun Si/C/PAA nanofiber mats where the Si active material is either in the form of nanoparticles or nanowires: (a) gravimetric capacity and (b) capacity retention over 50 cycles at 0.1 C. The weight ratio of Si/C/PAA was 40/25/35 in both samples

Conclusions

An electronically conductive polymer binder (PFM) was synthesized at LBNL, and electrospinning studies at Vanderbilt were performed to prepare Si/PFM/PEO fiber mats with up to 50 wt.% Si. 1 wt.% PEO was added to the electrospinning ink to facilitate fiber formation. Fiber diameters ranged from 1.5 – 9 µm depending on the Si loading and electrospinning conditions. Relative humidity (rh) had a significant impact on the fiber structure during electrospinning; Si/PFM/PEO fibers spun at 15% rh had a dense surface whereas fibers spun at 75% rh exhibited surface pores ~100 nm in diameter. Si/PFM/PEO fibers containing up to 50 wt.% Si were successfully electrospun; thus project milestones M1 and M2 were reached on schedule.

In a parallel effort, electrospun Si-based nanofiber anodes containing Si nanoparticles, carbon black, and a poly(acrylic acid) (PAA) binder were prepared and then evaluated in a lithium-ion battery half cell as a baseline reference material for the eventual comparison with Si/PFM/PEO nanofiber mat anodes. Mat compaction and welding procedures were developed to improve interfiber connectivity and the mechanical strength of the mat. While the as-spun mat exhibited low Si utilization and rapid capacity fade during cycling, the compacted and welded Si/C/PAA nanofiber mats exhibited a high gravimetric capacity (1,484 mAh/g at

0.1C) and good cycling stability (73% capacity retention after 50 cycles at 0.1C). Nanofiber mat anodes with a high material loading (3.49 mg/cm2) exhibited high areal and volumetric capacities of 4.5 mAh/cm^2 and 750 mAh/cm^3, respectively. A full cell containing an electrospun Si/C/PAA anode and an electrospun LiCoO$_2$/C/PVDF cathode had a high gravimetric capacity of 75 mAh/g and specific energy density of 270 Wh/kg (normalized to the overall mass of both electrodes) at 0.1C.

Electrospun Si/C/PAA anodes where the weight ratio of Si/C/PAA was 15/50/35 exhibited a high reversible capacity of 591 mAh/g at 0.1C and excellent cycling stability with 90% capacity retention after 50 cycles. The cycling stability of these anodes was superior to that of an electrospun Si/C/PAA anode containing 40 wt.% Si due to lower overall volumetric changes of the electrode structure during lithiation/delithiation. The performance of the Si/C/PAA anodes containing 15 wt.% Si met the go/no-go milestone M4 performance target (an initial capacity of 500 mAh/g and 90% capacity retention after 50 cycles).

Post-mortem analyses of electrospun Si/C/PAA anodes containing 40 wt.% Si was conducted at ORNL. Raman spectroscopy indicated that pristine electrodes contained crystalline Si which was transformed to amorphous Si after electrochemical cycling in a half cell. High resolution SEM images of fiber mat cross-sections showed that the Si nanoparticles and carbon powder were uniformly distributed throughout the fiber diameter. After 50 cycles at 0.1C, the fiber structure and interfiber void space were preserved, indicating good physical stability of the electrospun nanofiber mats in a battery.

Overall the results in the present report demonstrate that particle/polymer electrospinning is a viable and attractive technique for the preparation of high performance porous electrodes for lithium-ion batteries. The composition, thickness, fiber volume fraction, and fiber interconnectivity of electrospun mats can be easily controlled to achieve high gravimetric, areal, and volumetric capacities; this flexibility is unique to electrospun particle/polymer mats and is not possible for other electrode fabrication methods. Furthermore, the technique is compatible with a wide range of particle/polymer combinations and thus can be used to prepare nanofiber electrodes with new active materials and binders as they are developed.

Products

Presentations/Publications/Patents

1. E.C. Self, M. Naguib, R. Ruther, E. C. McRen, R. Wycisk, G. Liu, J. Nanda, and P. N. Pintauro. High Rate and Areal Capacity Si-LiCoO2 Batteries from Electrospun Composite Fiber Mats. Manuscript in Preparation.
2. E.C. Self, E.C. McRen, R. Wycisk, J. Nanda, G. Liu, P.N. Pintauro. Si-based Nanofiber Anodes for Lithium-ion Batteries Prepared Using Particle/Polymer Electrospinning. Oral presentation at AIChE Meeting in San Francisco, CA on November 16, 2016.
3. E.C. Self, E.C. McRen, R. Wycisk, P.N. Pintauro. High Performance Nanofiber Electrodes for Lithium-ion Batteries using Particle/Polymer Electrospinning. Poster for International Meeting on Lithium Batteries in Chicago, IL on June 20, 2016.

References

1. M. Armand, J.-M. Tarascon, Nature 2008, 451, 652.
2. J.-M. Tarascon, M. Armand, Nature 2001, 414, 359.
3. J. B. Goodenough, Y. Kim, Chem. Mater. 2010, 22, 587.
4. J. B. Goodenough, Acc. Chem. Res. 2013, 46, 1053.
5. U. Kasavajjula, C. Wang, A. J. Appleby, J. Power Sources 2007, 163, 1003.
6. N. Nitta, G. Yushin, Part. Part. Syst. Char. 2014, 31, 317.
7. H. Wu, Y. Cui, Nano Today 2012, 7, 414.
8. J. Li, N. J. Dudney, J. Nanda, C. Liang, ACS Appl. Mater. Interfaces 2014, 6, 10083.
9. R. C. Guzman, J. Yang, M. M.-C. Cheng, S. O. Salley, K. Y. Simon Ng, J. Mater. Sci. 2013, 48, 4823.
10. L. Hu, H. Wu, S. S. Hong, L. Cui, J. R. McDonough, S. Bohy, Y. Cui, Chem. Commun. 2011, 47, 367.

11. N. Liu, H. Wu, M. T. McDowell, Y. Yao, C. Wang, Y. Cui, Nano Lett. 2012, 12, 3315.

12. C. K. Chan, H. Peng, G. Liu, K. McIlwrath, X. F. Zhang, R. A. Huggins, Y. Cui, Nat. Nanotechnol. 2008, 3, 31.

13. C. K. Chan, R. N. Patel, M. J. O'Connell, B. A. Korgel, Y. Cui, ACS Nano 2010, 4, 1443.

14. N. Liu, L. Hu, M. T. McDowell, A. Jackson, Y. Cui, ACS Nano 2011, 5, 6487.

15. H. Zhou, J. Nanda, S. K. Martha, R. R. Unocic, H. M. Meyer, 3rd, Y. Sahoo, P. Miskiewicz, T. F. Albrecht, ACS Appl. Mater. Interfaces 2014, 6, 7607.

16. W. Zhang, P. N. Pintauro, ChemSusChem 2011, 4, 1753.

17. M. Brodt, R. Wycisk, P. N. Pintauro, J. Electrochem. Soc. 2013, 160, F744.

18. M. Brodt, T. Han, N. Dale, E. Niangar, R. Wycisk, P. Pintauro, J. Electrochem. Soc. 2014, 162, F84.

19. M. Brodt, R. Wycisk, N. Dale, P. Pintauro, J. Electrochem. Soc. 2016, 163, F401.

20. E. C. Self, R. Wycisk, P. N. Pintauro, J. Power Sources 2015, 282, 187.

21. E. C. Self, E. C. McRen, P. N. Pintauro, ChemSusChem 2016, 9, 208.

22. E. C. Self, E. C. McRen, R. Wycisk, P. N. Pintauro, Electrochim. Acta 2016, 214, 139.

23. H. Zhao, Z. Wang, P. Lu, M. Jiang, F. Shi, X. Song, Z. Zheng, X. Zhou, Y. Fu, G. Abdelbast, X. Xiao, Z. Liu, V. S. Battaglia, K. Zaghib, G. Liu, Nano Lett. 2014, 14, 6704.

24. G. Liu, S. Xun, N. Vukmirovic, X. Song, P. Olalde-Velasco, H. Zheng, V. S. Battaglia, L. Wang, W. Yang, Adv. Mater. 2011, 23, 4679.

IV.F.10. Co-Extrusion (CoEx) for Cost Reduction of Advanced High-Energy-and-Power Battery Electrode Manufacturing (PARC, a Xerox Company)

Peter Faguy, DOE Program Manager
DE-EE0007303
U.S. Department of Energy
Vehicle Technologies Office
1000 Independence Avenue, SW
Washington, DC 20585
Phone: 202-586-1022
E-mail: Peter.Faguy@ee.doe.gov

Corie L. Cobb, Principal Investigator
PARC, a Xerox Company
3333 Coyote Hill Road
Palo Alto, CA 94304
Phone: 650-812-4794; Fax: 650-812-5079
E-mail: Corie.Cobb@parc.com

Subcontractors:
David L. Wood, III, Oak Ridge National Laboratory (ORNL)
Kent Snyder, Ford Motor Company

Collaborators:
Daniel Abraham and Bryant Polzin, Argonne National Laboratory (ANL)
Michael Wixom, Navitas Systems

Start Date: December 2015
End Date: December 2018

Abstract

Objectives

- Our overall project objectives are to demonstrate pilot-scale, electric vehicle (EV)–relevant ≥14 Ampere hours (Ah) Co-Extrusion (CoEx) pouch cells with:
  - An estimated ≥ 30% reduction in \$/kWh costs through thick, structured high energy and high power electrodes.
  - A gravimetric energy density improvement of ≥ 20% relative to conventional electrodes of the same chemistry.

- As we progress toward the overall achievement of project objectives, our specific project objectives for FY 2017 are to:
  - Fabricate demonstrator CoEx coin cells with ≥ 20% gravimetric energy improvement over a conventional baseline cell.
  - Optimize the thick CoEx cathode design and matching graphite anode for EV-relevant applications with guidance from Ford.
  - Conduct a technology evaluation and predictive scaling analysis on CoEx to estimate the technology's potential impact at scale.

Accomplishments

- Print feasibility for corrugated CoEx cathode structures has been demonstrated.

- Modeling of different CoEx cathode geometries shows a path towards thick electrodes with higher energy and higher power capabilities.

- Path towards a 6 mAh/cm^2 graphite anode to match the anticipated CoEx cathode design has been experimentally demonstrated.

Future Achievements

- Optimize CoEx cathode and anode for overall capacity improvement.
- Modify PARC's CoEx printhead design for coin cell and 1Ah pouch cell fabrication.
- Increase crack resistance of dried, uncalendered thick CoEx electrodes .
- Optimize and fabricate the necessary matching graphite anode for the CoEx cathode.

Technical Discussion

Background

Most disruptive strategies for increasing the performance and reducing the cost of lithium-ion batteries have focused on battery chemistry, material loading modifications, and electrode thickness. Increasing electrode thickness is a known approach to increase energy density and in turn overall cell capacity. However, practical thicknesses are constrained by ionic transport limitations that occur with increasing thickness, limiting cell power (see Figure IV-372). We believe PARC's Co-Extrusion (CoEx) technology, shown in Figure IV-372, can overcome this limitation, enabling a substantial improvement in the performance of thick electrodes for most lithium-ion chemistries. CoEx has the potential to disrupt current manufacturing processes and enable the DOE 2022 goal of $125/kWh.
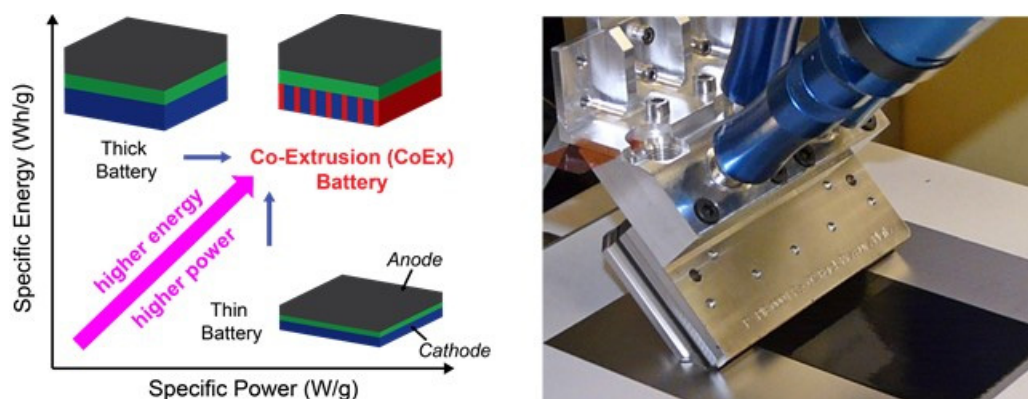

Figure IV-372: (Left) The trade-off space between traditional thick and thin battery electrodes. CoEx can help mitigate the power deficiencies often experiences with thick battery electrodes. (Right) PARC's prototype CoEx battery printhead design for a previous ARPA-E project (DE- DE-AR0000324)
Caption Credits/Source (PARC)

Introduction

Adoption of a new battery manufacturing technology such as CoEx will require extensive scale-relevant demonstration to remove risks, quantify second-order manufacturing characteristics, and to convincingly demonstrate cost and performance benefits. The goal of this project is to move the technology toward manufacturing readiness by accomplishing these tasks. We will leverage ORNL's Battery Manufacturing Facility (BMF) to achieve credible pilot-scale production of CoEx cells and to characterize performance at a pouch cell scale. The BMF will be used to produce the electrode layers needed for EV-format cells (≥14 Ah). The resulting cells will be subjected to ORNL's and Ford's recommended testing protocols, resulting in a documented quantification and validation of the benefits of CoEx cathodes for EV applications. At project completion, we will have an operational CoEx pilot manufacturing line capable of producing automotive format pouch cells with an estimated ≥ 20% energy density improvement (and at least equivalent power density), with a goal of decreasing battery pack costs ($/kWh) by 30%. This will advance the technology to TRL 6-7 and provide a basis for subsequent commercialization investment decisions.

Co-Extrusion (CoEx) Cathode

Co-Extrusion (CoEx) is a deposition technology developed at PARC that uses engineered fluidic channels to cause multiple streams of dissimilar fluids to impart shape to one another [1,2]. The result is a high-speed, continuous deposition process that can create fine structures much smaller than the smallest physical feature within the printhead. By eliminating the small channels necessary for conventional extrusion and injection processes, CoEx is able to deposit highly loaded and viscous pastes at high process speeds under reasonable operating pressures. Depending on particle size, the CoEx process is capable of direct deposition of features as small as 25 μm with aspect ratios of 5 or greater, and print speeds >400 mm/s (~80 ft./min). The physical embodiment of CoEx is a printhead, as shown in Figure IV-372. A CoEx printhead accepts two different battery inks but serves the same function as the slot die printhead in modern battery manufacturing lines, depositing the electrode slurry onto the current collector web in a continuous roll-to-roll process. The thicknesses, widths, and lengths of the deposited CoEx features are dependent on the internal printhead geometry, slurry rheology, and process conditions. The precise flow paths are constructed out of a stack of replaceable printhead layers that can be easily exchanged, allowing for precise tailoring of the final deposited features within a single printhead design.

PARC's scale-up of CoEx batteries for EVs builds on a solid base of experience in applying CoEx to solar cell manufacturing [3]. The technology scale-up for solar cells provided invaluable experience with the nuances of throughput, yield, and maintenance, critical in taking a new technology to the factory floor. PARC has adapted the CoEx process for lithium-ion battery printing, working previously with $LiCoO_2$ and $LiNi_{1/3}Mn_{1/3}Co_{1/3}O_2$ materials. PARC will work with $LiNi_{0.5}Co_{0.2}Mn_{0.3}O_2$ (NCM 523) and further scale the technology from coin cells to 14Ah pouch cells by project completion, focusing on the two cathode structures shown in Figure IV-373. Ford will provide PARC with automotive guidance during the course of the project in addition to EV-relevant cell characterization on the pouch cells developed during the course of the project.
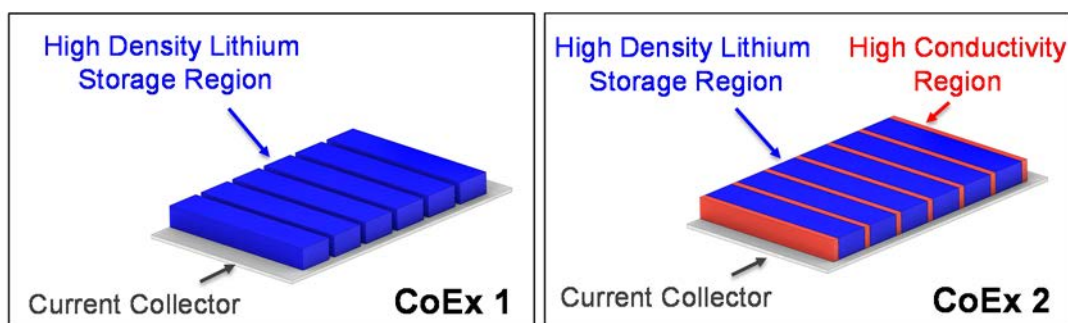
Figure IV-373: Illustrations of proposed CoEx 1 and CoEx 2 structures. CoEx 1 is a corrugated structure with open channels for electrolyte to fill the electrode structure. CoEx 2 is a structure where a more conductive or porous version (red) of the dense blue region will be deposited
Caption Credits/Source (PARC)

High Capacity Graphite Anode

ORNL will develop the thick, high capacity anode that will match the CoEx cathode, fabricate the pouch cells, and assist PARC with technology scale-up on ORNL's roll coater (see Figure IV-374), in addition to running electrochemical rate and cycling tests. As part of the anode development, ORNL will refine graphite-based anode slurries for improved coating adhesion, agglomerate cohesion, and high ionic and electronic conductivity by modifying binder and conductive additive. Below we summarize our approach:

- Method: Anode slurries will be prepared with a NMP/PVDF solvent/binder system and slot-die coated to a sufficient thickness to balance CoEx cathodes. Anode formulations will be adjusted as needed to maintain sufficient anode coating integrity after calendering.

- Baseline Anode: Electrochemical testing of baseline anodes developed at ORNL to quantify electrochemical performance. (Targets: 50-80 μm thick (2.5-3.0 mAh/cm^2) after calendering and capacity >350 mAh/g)

- Thick Anode for CoEx: Demonstrate a 125-200 μm uncracked anode (5-6 mAh/cm^2) with a NMP/PVDF solvent/binder system to match CoEx cathode capacity; Show capability to maintain thick anode coating integrity after calendering to 30-40% porosity.
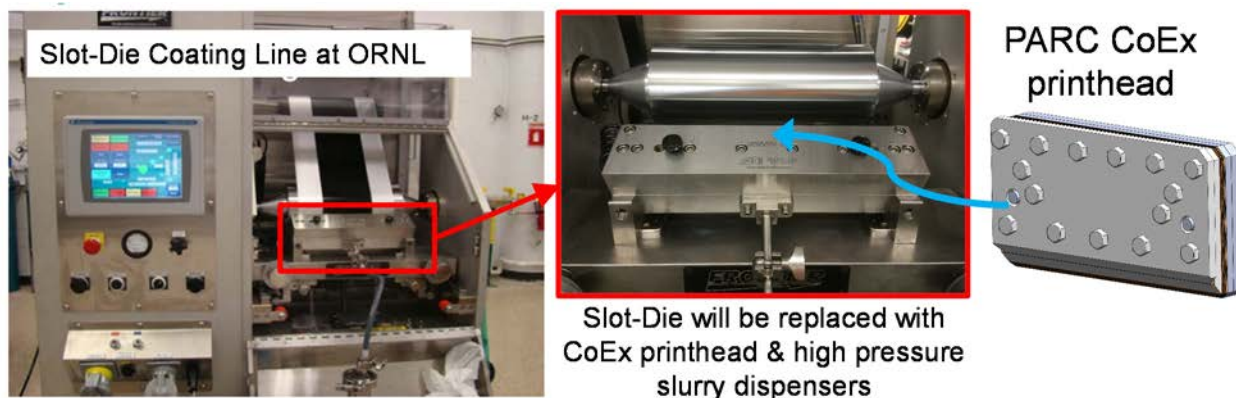

Figure IV-374: Existing electrode coating line at ORNL BMF with planned CoEx integration for this project
Caption Credits/Source (ORNL and PARC)

Results

CoEx Cathode Modeling Results

Figure IV-375 shows the parameterization of the CoEx cathode structures modeled. For the modeled structures, the mass of Region 1 is fixed based on a 90/5/5 composition of NCM523/PVDF/carbon black. For all cases, Region 1 has an active material volume fraction of 0.512, inactive (carbon black and binder) volume fraction of 0.152, and an electrolyte volume fraction of 0.336. Region 2 for the CoEx 1 and 3 cases is pure electrolyte while Region 2 for CoEx 2 consists of a more porous formulation of Region 1. For the CoEx 3 case shown in Table IV-51, h_2 is 50 μm. A standard macrohomogeneous porous electrode model [2, 4, 5] was implemented in COMSOL [6] and extrapolated to two dimensions to capture the cross-section of the CoEx cathode geometry.

The preliminary results for single layer cathodes shown in Table IV-51 have a fixed geometry of $w_{R1} = 100$μm and $w_{R2} = 25$ μm. The CoEx 1 structures showed the best performance on a mAh/g (active material) basis. However, the overall lower cathode densities of the CoEx 1 structures (due to the open channels) affects the total capacity observed when the amount of electrolyte and lack of active material on a g/cc basis is taken into account. The CoEx 2 structures only showed better performance when the porosity of the conductive region was at least 50% or greater. We also modeled a third CoEx structure (CoEx 3) to help compensate the capacity loss of the active material observed in the CoEx1 structure. We believe the CoEx 3 structure can be achieved with our existing printheads and processing and is a promising path if CoEx 1 and CoEx 2 prove to not be sufficiently advantageous at the pouch cell level when we conduct our scale up analysis. A more detailed summary with estimates of potential pouch cell gains is currently in progress.

(a) Half Cell Geometry

(b) Cathode Structure for CoEx 1 and CoEx 2
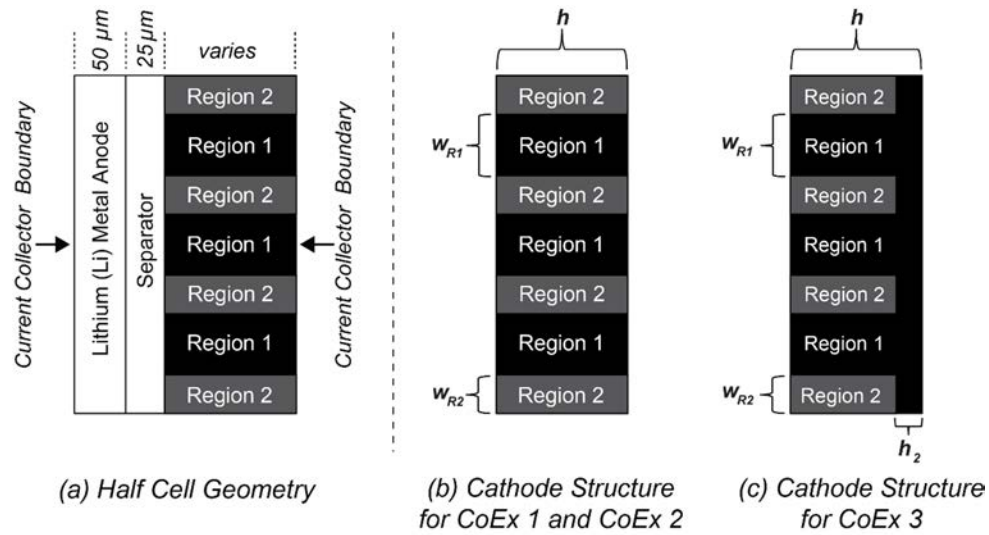
(c) Cathode Structure for CoEx 3

Figure IV-375: Illustrations of the CoEx structures modeled in COMSOL. Region 1 represents a 90/5/5 (NCM523/PCVDF/Carbon Black) Composition with 33.6% porosity while Region 2 represents pure electrolyte for the CoEx 1 and 3 structures and a more porous formulation of the 90/5/5 composition for CoEx 2
Caption Credits/Source (PARC)

Table IV-51: CoEx Modeling Summary

Type	h (μm)	Region 2, Active Volume Fraction, ϵ_s	Region 2, Electrolyte Volume Fraction, ϵ_l	Region 2, Filler Volume Fraction, ϵ_f	C-rate	g/cc (Electrode density - no electrolyte)	Specific Capacity - Cathode (mAh/g, active only)
baseline	60	n/a	n/a	n/a	0.5	2.70	151.7
baseline	60	n/a	n/a	n/a	1	2.70	141.9
baseline	60	n/a	n/a	n/a	2	2.70	134.0
CoEx 1	120	0	1	0	0.5	2.16	151.8
CoEx 1	120	0	1	0	1	2.16	145.4
CoEx 1	120	0	1	0	2	2.16	137.0
CoEx 1	150	0	1	0	0.5	2.16	151.8
CoEx 1	150	0	1	0	1	2.16	145.2
CoEx 1	150	0	1	0	2	2.16	7.4
CoEx 2	120	0.386	0.5	0.114	0.5	2.57	151.8
CoEx 2	120	0.386	0.5	0.114	1	2.57	145.0
CoEx 2	120	0.386	0.5	0.114	2	2.57	7.1
CoEx 3	170	0	1	0	0.5	2.32	151.8
CoEx 3	170	0	1	0	1	2.32	145.1
CoEx 3	170	0	1	0	2	2.32	6.5

CoEx Cathode Printability Results

A series of inks and print tests were conducted to test the print feasibility of two different cathode structures (see Figure IV-373). Prior to this project, PARC had not tested the print feasibility of the CoEx 1 structure in Figure IV-373. The print feasibility of the CoEx 2 structure in Figure IV-373 had been previously demonstrated in an ARPA-E seedling project (DE-AR0000324). PARC was able to successfully print and calender a series of CoEx 1 structures made from a 91/5/4 (NCM523/carbon black/PVDF) ink. Our initial results show that the CoEx cathode pillars maintain their integrity after a moderate amount of calendering (~12%). Figure IV-376 shows a 3-dimensional image of the CoEx 1 structure generated from scanning optical microscopy, along with profilometry measurements before and after calendering. Our CoEx 1 prints have also gone through electrochemical testing and we observed no obvious issues with the initial performance of the cells in a half cell format. The printhead used to print the structures in Figure IV-376 will be modified based on the modeling results. For instance, modeling efforts discussed in the previous section have indicated the need for narrower width electrolyte regions for the CoEx 1 structure to increase the overall cathode density and in turn reduce any potential capacity losses at the pouch cell level. Additionally, with guidance from Ford, ORNL, and ANL, PARC is in the process of making reference cathode half cells which will be used for comparison purposes against the CoEx cathode half cells that will be generated in FY 2017.
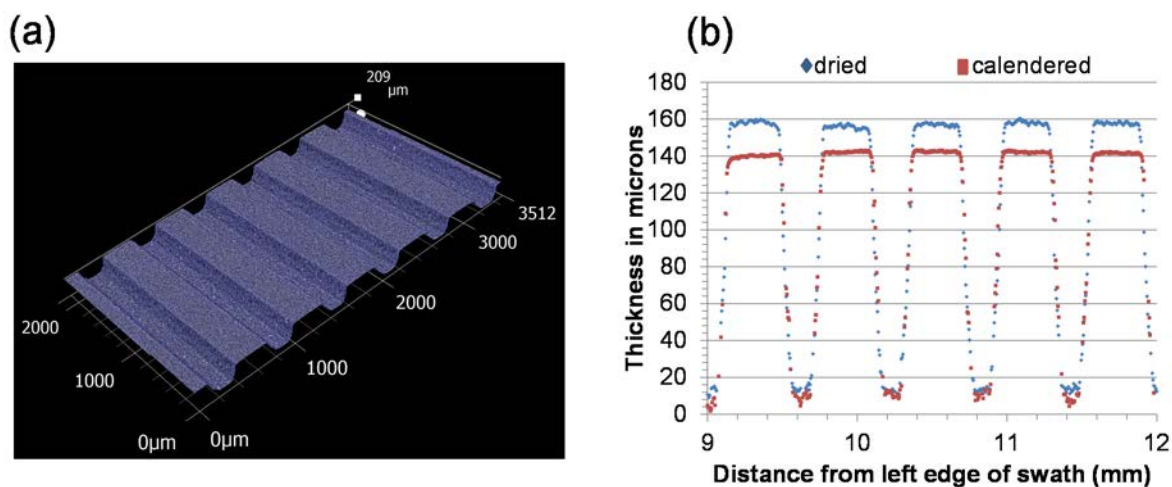

Figure IV-376: CoEx cathode structures. (a) shows the CoEx 1 dried sample print. (b) shows a profile measurement of the dried CoEx 1 print before and after ~12% calendaring. These samples are currently being investigated for electrochemical integrity
Caption Credits/Source (PARC)

High Energy Anode Development

Half cells were made with two different graphite coatings (Showa Denko and Hitachi MAGE 3) at two areal capacities to evaluate the electrochemical rate performance. Results for 2.6 mAh/cm^2 and 6 mAh/cm^2 coin cells made with 1.2 M LiPF$_6$ in 3:7 v/v EC/DEC electrolyte (Electrolyte 1) are shown below in Figure IV-377. Although the Hitachi MAGE 3 graphite shows a higher capacity than the Showa Denko graphite in all cases, both materials demonstrate useful rate performance at 2.6 mAh/cm^2. However, the capacity drops off more rapidly at higher rates for both thicker 6 mAh/cm^2 coatings.

A second set of coin cell tests was also conducted using a different, slightly less viscous electrolyte (1.2 M LiPF$_6$ in 3:7 wt% EC/EMC (Electrolyte 2)) to see if this would help improve the rate performance. A comparison of the results from cells made with both electrolytes is also shown in Figure IV-377. Both the Showa Denko and Hitachi MAGE 3 graphite 2.6 mAh/cm^2 cells showed improved rate performance when Electrolyte 2 was used. Both of the higher loading 6 mAh/cm^2 cells also showed improved rate performance below 1C when Electrolyte 2 was used. We are continuing to work on improving the rate performance at higher loadings.
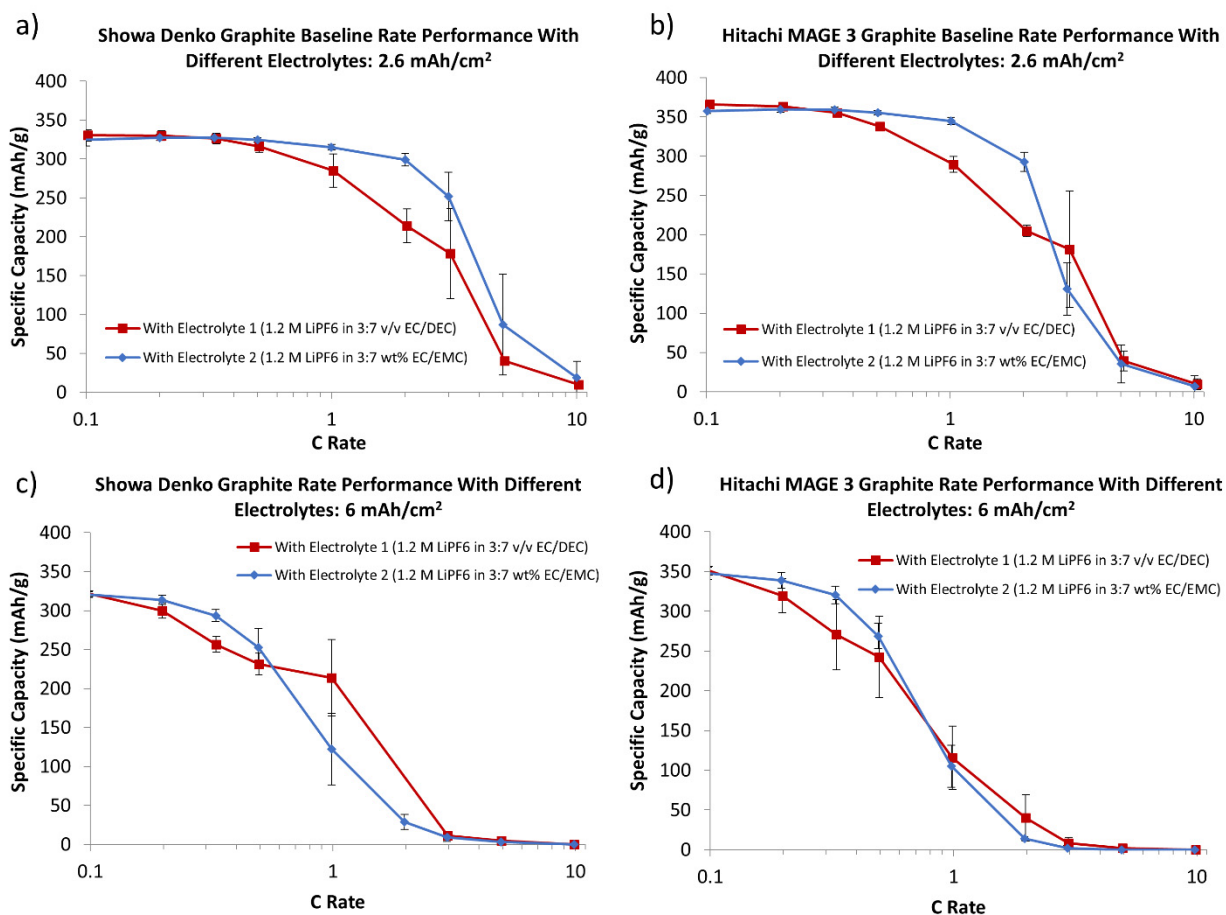
Figure IV-377: Comparison of the electrochemical rate performance of Showa Denko and Hitachi MAGE 3 half coin cells made with two different electrolytes: 1.2 M LiPF6 in 3:7 v/v EC/DEC (Electrolyte 1) and 1.2 M LiPF6 in 3:7 wt% EC/EMC (Electrolyte 2). All cells were made with slot die-coated anodes calendered to ~35% porosity and dried in a vacuum oven overnight before use. a) Showa Denko graphite at 2.6 mAh/cm²; 61 μm thick with a total loading of 8.6 mg/cm²; Data is an average of 3 coin cells for each condition. b) Hitachi MAGE 3 graphite at 2.6 mAh/cm²; 57 μm thick with a total loading of 8.0 mg/cm²; Data is an average of 4 coin cells for each condition. c) Showa Denko graphite at 6 mAh/cm²; 142 μm thick with a total loading of 20.0 mg/cm²; Data with Electrolyte 1 is an average of 3 coin cells. Data with Electrolyte 2 is an average of 6 coin cells. d) Hitachi MAGE 3 graphite at 6 mAh/cm²; 130 μm thick with a total loading of 18.2 mg/cm². Data with Electrolyte 1 is an average of 3 coin cells. Data with Electrolyte 2 is an average of 4 coin cells
Caption Credits/Source (ORNL)

Conclusions

PARC, ORNL, and Ford are collaborating to create a pilot scale demonstration of PARC's CoEx battery manufacturing technology for structured high energy and high power cathodes for cost-effective and long-range EVs. To date, we have completed initial modeling of CoEx cathodes, printability testing of different CoEx structures, and generated data for thick, high energy anodes that will be required to match the CoEx cathodes. By project completion, our goal is to demonstrate CoEx cells with a gravimetric energy density improvement of at least 20% relative to conventional electrodes of the same chemistry and a projected 30% reduction in $/kWh costs.

Products

Presentations/Publications/Patents

1. C.L. Cobb, "Co-Extrusion: Advanced Manufacturing for Energy Devices," 2016 AIChE Annual Meeting, Battery and Energy Storage Technologies, San Francisco, CA, November 14, 2016. (Session Keynote)
2. C.L. Cobb, "Modeling Co-extruded Cathodes for High Energy Lithium-ion Batteries," 229th ECS Meeting, San Diego, CA, June 1, 2016.

References

1. K. Littau, C.L. Cobb, S. Solberg, M. Weisberg, N. Chang, and A. Rodkin, "Developments in MEMS scale printable alkaline and Lithium-ion technology," In Proc. of 2011 SPIE Micro- and Nanotechnology Sensors, Systems, and Applications III, # 80311L, pp. 1-10.
2. C.L. Cobb and M. Blanco, "Modeling Mass and Density Distribution Effects on the Performance of Co-extruded Electrodes for High Energy Density Lithium-ion Batteries," J. of Power Sources, 249: 357-366, 2014.
3. L.P. Richter, G. Fischer, L. Sylla, M. Hentsche, S. Steckemetz, M. Müller, C.L. Cobb, S.E. Solberg, R. Rao, S. Elrod, P. Palinginis, E. Schneiderlöchner, H. Neuhaus, "Progress in Fine Line Metallization by Co-extrusion Printing on Cast Mono Silicon PERC Solar Cells," Solar Energy Materials and Solar Cells, Vol. 142, pp. 18-23, 2015.
4. M. Doyle, T.F. Fuller, and J. Newman, "Modeling of Galvanostatic Charge and Discharge of the Lithium/Polymer/Insertion Cell," J. Electrochem. Soc. 140, 1526-1533, 1993.
5. T.F. Fuller, M. Doyle, and J. Newman, "Simulation and Optimization of the Dual Lithium Ion Insertion Cell," J. Electrochem. Soc., 141, 1-10, 1994.
6. COMSOL v5.1: https://www.comsol.com/

IV.F.11. Electrodeposition for Low-Cost, water-Based Electrode Manufacturing (PPG Industries, ANL, Navitas, ORNL)

Stuart Hellring, Principal Investigator
Senior Scientist
PPG Industries, Inc.
4325 Rosanna Drive
Allison Park, PA 15101
Phone: 412-492-5526
E-mail: hellring@ppg.com

Brian Kornish, Program Manager
PPG Industries, Inc.
4325 Rosanna Drive
Allison Park, PA 15101
Phone: 412-492-5165
E-mail: kornish@ppg.com

Start Date: January 1, 2016 (BP1 Start)
End Date: December 31, 2018 (BP3 End)

Abstract

Objectives

- Identify at least one cathode active material for lithium-ion batteries that is suitable for development of an electrocoat formulation and application process.

- Identify at least one polymeric resin that can be used as a binder in cathode coatings that are applied by an electrocoat process.

- Develop a cathode coating formulation with binder and active material candidates.

- Develop a bench-scale electrocoat process for applying cathode coatings.

- Produce cathodes by electrocoat process and evaluate electrochemical performance in a lithium-ion battery.

Accomplishments

- Identified a commercially available NMC-532 material that has suitable particle size, stability, and electrochemical performance to be used in developing electrocoat formulations and applications.
  - Synthesized NMC 532 active particles with a size of about 5 µm at ANL by TVR
  - Characterized changes in ANL-prepared and commercially available NMC materials that result from water soaking
    - Lithium and transition metal leaching
    - Energy storage performance
    - pH and zeta potential

- Identified polymeric resins that are suitable for formulating cathode binders for use in electrocoat application process. Synthesized polymeric resin candidates and evaluated their potential for use as:
  - Binders that can be used in cathode coatings in a lithium-ion battery
  - Binders that will provide acceptable film build when applied by electrocoat.

- Developed a bench-scale electrocoat process for applying cathode coatings with identified binders.

- Produced cathodes with water-based formulation applied on aluminum foil substrate by electrocoat process.
  - Cathodes produced with LFP active materials and identified binders

- Evaluated electrochemical performance in lithium-ion batteries
- Initiated development of electrocoat formulation and application for NCM active materials

Future Achievements

- Optimization of formulation and application to obtain cathode coatings with acceptable electrochemical performance comprising NMC active materials by electrocoat process

- Design, build, and optimize a bench-scale prototype continuous electrocoat process for producing cathode coated aluminum foil.

- Investigate electrocoat process and performance parameters such as edge-to-edge uniformity, coating homogeneity, and bath depletion effects.

- Evaluate EV cell level performance of electrocoat films.
  - Fabricate 1Ah cells and evaluate cell level performance using cathodes produced with the continuous coater.

Technical Discussion

Background

The cost of lithium-ion battery manufacturing must be lowered significantly to battery powered vehicles affordable. At the same time, battery performance must also continue to improve for widespread adoption of electric vehicles. Fundamentally, lithium-ion batteries are a stack of coatings – active materials for both anodes and cathodes are adhered to their respective current collector foils with binders and additives and divided by separators. These coatings make up 28% of the cost of the battery pack and are a critical factor determining life, power stability, and cost. By applying the same proficiency that has made PPG the world leader in electrocoat technologies, we envision bringing to market a lower cost manufacturing process that enhances battery performance and supports battery manufacturing.

Unlike electroplating[8] or electro-polymerization[9] approaches, the electrophoretic deposition process, or "e-coat," uses electrophoresis to drive charged, pre-formed micelles containing binder and active materials to coalesce on the surface of the current collector foil. PPG filled the first ever electrocoat tank with anodic electrocoat for automobile bodies in 1963 and has been credited with almost every major innovation in electrodeposition coatings for nearly half a century. Electrocoat technologies can bring cost and performance benefits to the electrode manufacturing process that cannot be obtained through conventional coatings application processes. Through eliminating hazardous solvents, robustly building a highly-uniform film with tailored characteristics, and introducing manufacturing efficiencies, we envision that electrocoat will simultaneously reduce cost and improve electrode performance.

Introduction

The state of the art for the manufacture of lithium ion cathodes is slot-die coating of a high-viscosity slurry of active battery materials, conductive additives, and a polymeric binder that is dissolved in N-methyl-2-pyrrolidone (NMP). NMP is an expensive consumable in electrode manufacturing with serious health concerns. It is on the candidate list of Substances of Very High Concern for authorization in the European Union. In the United States, NMP is on the EPA's Toxics Release Inventory and the California Department of Occupational Safety and Health has proposed a Threshold Limit Value of 1 ppm in air, similar to occupational exposure limit values established in Japan (1 ppm) and Germany (20 ppm). Alternative organic solvents have been insufficient to meet the needs of incumbent binder systems and present their own cost and exposure difficulties.

The current cost of high-energy lithium-ion batteries (LIBs) is approximately $500-$800/kWh, while the goal is $125/kWh. Main cost drivers are the high cost of raw materials and materials processing, the cost of cell and

---

[8] Mosby, J.M.; Prieto, A.L. *Journal of the American Chemical Society* **2008** *130* (32), 10656.

[9] Trinh, N.D., Saulnier, M., Lepage, D., Schougaard, S.B. *Journal of Power Sources* **2013** *221*, 284.

module packaging, and manufacturing costs. Our proposed project addresses materials processing and manufacturing costs. To estimate the cost savings achievable by converting to an aqueous, electrocoat-based cathode coating system, PPG consulted with Argonne National Lab. Using BatPac, an estimated 17.1% savings on a per-cell basis was determined. Eliminating NMP from the process reduces cost by 8.9%. Further cost savings can be realized by eliminating the need to calender electrodes, and by an expected reduction in binder costs, for an estimated 17.1% savings over state of the art.

Solvent-based electrodeposition of pre-formed cathode active powders for producing electrodes for secondary lithium-ion batteries has been evaluated by several groups.[10,11,12,13,14,15,16,17] A variety of active materials have been electrodeposited onto various current collectors in solvents such as acetone and ethanol. Cathode active particle sizes used for these studies ranged from an average of 300 nm to 10.3µm. Cathodes produced by solvent-based electrodeposition showed promising battery performance for metrics that include discharge capacity/rate capability, coulombic efficiency, and cycle life retention.

However, the use of volatile organic solvents for manufacturing electrode coatings by electrodeposition has a number of serious drawbacks including VOC emissions, explosion risk, health risks from worker exposure, and cost. Using waterborne coatings significantly mitigates most of the concerns associated with organic solvent-based coating formulations. Benefits include lower voltage/current, better process temperature control, and faster deposition rates due to a higher dielectric constant. Binder design, proprietary additives, and electrochemical processing methods are used to ensure quality during manufacturing, to disperse pigment particles and stabilize the aqueous formulation bath against agglomeration and settling. Since charge-bearing functionality typically is hydrophilic, these functional groups are converted by crosslinking during the coating curing process to render the final film less hydrophilic.

Approach

 Electrocoat offers several manufacturing advantages over conventional slot-die or roll-coater application processes. It allows for greater coating density. Because electrophoretic deposition moves solid components to the substrate and dewaters a coating as it deposits, high density coatings with 90% by weight solids content are produced routinely from dilute formulation baths that have low viscosity. As an example, an aqueous wet film with 90% by weight solid content comprised of active, carbon, and binder will produce a dry cathode coating with less than 30 percent porosity. High density in electrodeposited coatings is achieved by controlling packing through particle size distribution where small particles embed in larger particle matrices through electrophoretic impregnation. Deposition of a dense wet film lowers stress in the dried film, a benefit for adhesion and cohesion. The self-insulating nature of the film build leads to high thickness uniformity. Unlike electroplating, electrocoat formulation are comprised of preformed and prequalified materials such as cathode-active powders, conductive carbon additives and binders that are deposited together to form the cathode coating.

The project will develop a viable electrodeposition process and will design and synthesize electrodepositable binders with flexibility and ionic mobility. The project will tailor and fabricate high-energy density active materials for compatibility and formulate stable water-based cathode coating systems. The project will establish electrodeposition process parameters and validate the performance and economics of the technology at a 1Ah scale to ensure a path to commercialization.

---

[10] Kanamura, K; Goto, A.; Hamagami, J.; and Umegaki, T. *Electrochemical and Solid-State Letters* **2000**, *3 (6)*, 259.

[11] Kanamra, K and Hamagami, J. *Solid State Ionics* **2004**, *172*, 303.

[12] Ui, K; Funo, S.; Nagase, H.; Idemoto, Y.; and Koura, N. *Electrochemistry* **2006**, *6*, 474.

[13] Caballero, A.; Hernán, L.; Melero, M.; Morales, J. Moreno, R.; and Ferrari, B. *Journal of Power Sources* **2006**, *158*, 583.

[14] Ferrari, B.; Moreno, R.; Hernán, L.; Melero, M.; Morales, J.; and Caballero, A. *Journal of European Ceramic Society* **2007**, *27*, 3823.

[15] Matsuda, A; Higashi, Y.; Tadanaga, K.; Minami, T.; and Tatsumisago, M. *Key Engineering Materials* **2006**, *314*, 107.

[16] Mazor, A.; Golodnitsky, D.; Burstein, L.; Gladkich, A.; and Peled, E. *Journal of Power Sources* **2012**, *198*, 264.

[17] Prasanna, K.; Subburaj, T.; Jo, Y.N.; and Lee, C.W. Electrochimica Acta **2013** *95*, 295.

Budget Period 1 includes development of the materials necessary for a successful e-coated electrode. Work will be split between concurrent active materials modification and e-coat system development. At the end of BP 1, targeted materials will be selected based on their performance characteristics.

Budget Period 2 will refine the coatings system to improve baseline performance. Cell validation scale will begin to increase, enabling refined quantification of the achievable cost reductions. The design and build of a bench scale coater for representative evaluation will support scale up in BP 3.

Budget Period 3 will be optimize the coating system components to the point that large format cells will be built and evaluated. The budget period includes obtaining optimized, representative electrodes that will be tested for performance properties both independently and within cells

Results

A suitable cathode active material was identified

An active material demonstrating compatibility with the electrocoat bath formulation has been identified. Acceptable electrochemical energy storage performance was demonstrated after soaking a commercially available small-particle NMC 532 powder in a water bath for an extended period to simulate exposure to an electrocoat bath.

Water durability of lithiated cathode pigments is the main concern for developing an aqueous electrocoat process for manufacturing electrodes. An electrocoat process deposits solid coating components from a formulated bath onto a current collector foil and requires that sufficient ionic mobility, electronic conductivity, and mechanical stability be maintained in the assembled film. For this reason, smaller particle size of the active material may become an important product design parameter to ensure that excessive bath viscosity is not required to avoid settling and separation issues as high viscosity can retard ion mobility. Electrochemical performance of lithiated NMC-532 cathode powders in the particle size range of approximately 5 µm to 11µm was evaluated both before and after water soaking these powders and the electrochemical durability of these NMC powders was found to vary considerably depending on the supplier source. The results from this study are presented below in Figure IV-378.
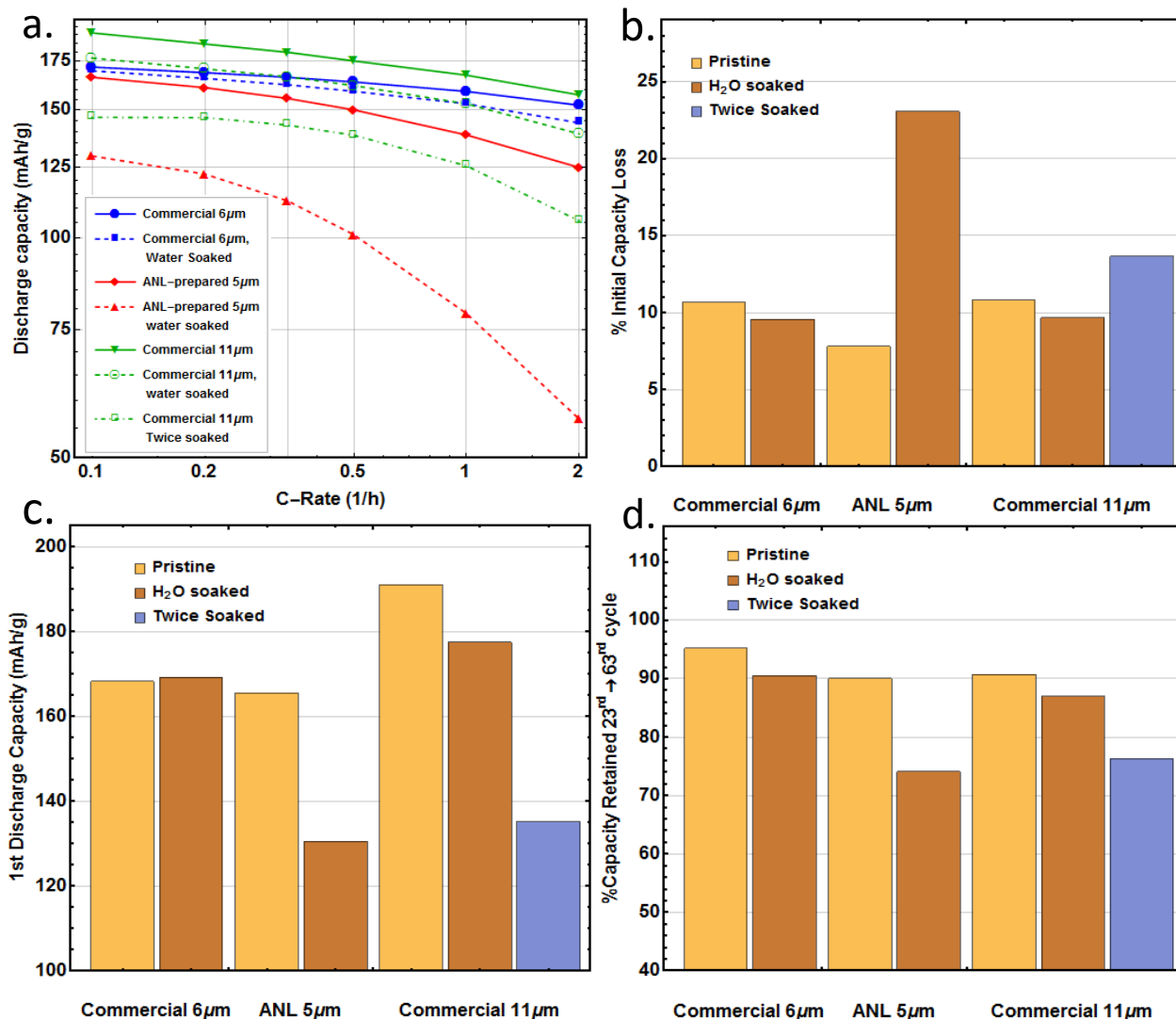
Figure IV-378: Electrochemical characterization of the cathode performance for each active material with and without water exposure. Rate capability (a), initial capacity loss (b), initial discharge capacity (c), and capacity retention (d) highlights the stability of the commercial 6µm material after water processing compared to similar active materials

The active material named "Commercial 6µm" demonstrated acceptable electrochemical performance after exposure to water. After water soaking this Commercial 6µm active material showed minimal initial capacity loss (ICL) and minimal loss in 1st cycle discharge capacity. The rate capability and cycle life were also minimally affected by water soaking with this commercial material.

Commercial 6 µm NCM powder compares favorably relative to the materials synthesized, thus far, by ANL using their TVR method or Commercial 11µm material. Despite having slightly lower initial capacity than Commercial 11µm NCM, the water-soaked Commercial 6µm material exhibited a capacity retention after 63cycles that is superior to both the water-soaked ANL 5µm and Commercial 11µm material.

This superior electrochemical stability in the presence of water in conjunction with the small particle size confirmed that the Commercial 6µm active material is suitable criteria to be effective in an electrocoat formula, and this material was selected for further study in e-coat formulations (see Table IV-52).

Table IV-52: Identification of a Suitable Binder Resin

Binder ID PPG-	Functionality									pH	Zeta (mV)	Mw (relative)	Particle Size (nm)
	1	2	3	4	5	6	7	8	9				
188						40			1	2.51	-34.5	0.091	143
199							1			2.75	-65.8	1.00	153
200		0.45			0.3			1		5.94	-57.7	0.084	85
220							1			2.7	-68.7	0.403	90
221							1			2.7	-64	0.156	157
222							1			2.49	-62.3	0.480	173
237	1									1.77	-51.2	bimodal	147
036	1									2.68	--	0.42	63.3
042	1	0.13								3.02	-62.8	0.17	119
059						1				3.18	-64.8	0.20	137
060						1				2.96	-68.2	0.23	129
182						1				4.7	--	0.86	--
184						1				8.8	--	1.00	--
063	1									2.88	-71.3	0.25	125
072						1				4.42	-63.1	0.24	111
088			1							8.76	-42.9	0.28	201
093			1							8.57	-48.2	0.34	275
101			1							9.04	-26.4	0.23	182
025	1									2.88	-70	0.23	142
107	1			0.45						8.4	-45.9	0.03	N/A
114			1	0.5						5.71	70.2	0.02	N/A
115				0.28		1				6.59	39.4	N/A	N/A
148	0.36						1			5.93	-60.5	--	142

Several new polymeric resins were synthesized with different functional groups to prepare a library of structures for investigating resin performance as electrocoat binders. Structures were varied to probe resin properties such as flexibility, hydrophilicity/hydrophobicity, glass transition (Tg), adhesion, cohesion, and electrochemical stability, among others. Each resin was characterized to determine their zeta potential, particle size, pH, and normalized functionalities; and screened for electrocoat performance. Resins with functionality 7 and functionality 8 as specifically beneficial for the electrodeposition and were down-selected for further study in electrocoat bath formulations.

An electrocoat formulation and application process was developed

The suitability of the identified active material towards an electrocoat process for this formulation is demonstrated through a characterization of the deposition kinetics using two electrocoat resins identified as PPG-200 and PPG-105. In a typical electrocoat bench scale process, the bath containing binder, active material, and carbon is diluted to 5% total solids with deionized water. A strip of battery-grade aluminum foil is immersed in the bath, along with a counter electrode and a thermocouple. The aluminum strip is connected to the anode, and the counter electrode to the cathode, and a constant or ramped voltage is applied.

The kinetics of deposition were characterized as a function of the deposition time. The results are presented below in Figure IV-379 in addition to optical photographs of the film after 20s of deposition. Using this process, films with a theoretical areal capacity exceeding that of a conventional energy cell were assembled onto an aluminum current collector with an areal capacity dependent on deposition time.
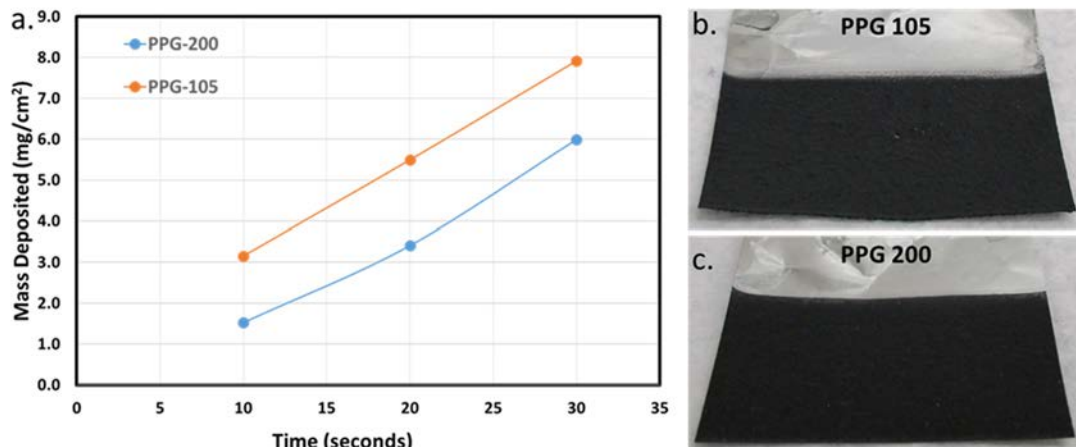

Figure IV-379: (a.) Mass deposited over time for the e-coat formulations using the PPG active material and e-coat binders emphasizing the improved deposition kinetics of the PPG binder system. Photographs of (b) and (c) characterize the film quality and uniformity of the e-coat materials after 20 s of deposition on Al foil

Cathode coatings were applied by electrocoat and energy storage performance was evaluated

In order to characterize the electrochemical stability of the chosen resins, the desired resin was combined with carbon-coated lithium iron phosphate (LFP), super C65, and either PPG-200 or PPG-105. These materials were then cast onto a carbon-coated aluminum current collector using a doctor-blade coating process. The initial charge-discharge curves of these materials are highlighted below in Figure IV-380. These figures illustrate the ability of these resins to form functioning electrochemical energy storage electrodes.

A developmental electrocoat process for electrodes has been established using the electrocoat resins and LFP active materials. Under identical bath conditions, the electrocoat process introduced severe electrode polarization compared with doctor-bladed films that and this polarization inhibited the initial capacity and energy efficiency of the fully assembled electrochemical device. In order to overcome the polarization within the assembled electrode film, a re-formulation of the electrocoat bath was performed to promote electronic conductivity. By introducing a high amount of carbon material to the bath (exceeding 10% by weight), comparable electrochemical performance between the e-coat and drawdown films was obtained. The cathode system including the PPG binder delivers an initial capacity that approaches 150 mAh/g when discharged at a rate of 0.1 C. Future achievements in optimizing the bath formulation, e-coat parameters, and resin chemistry to realize the intrinsic capacity of the previously identified NMC materials will be the focus of the remainder of this project.
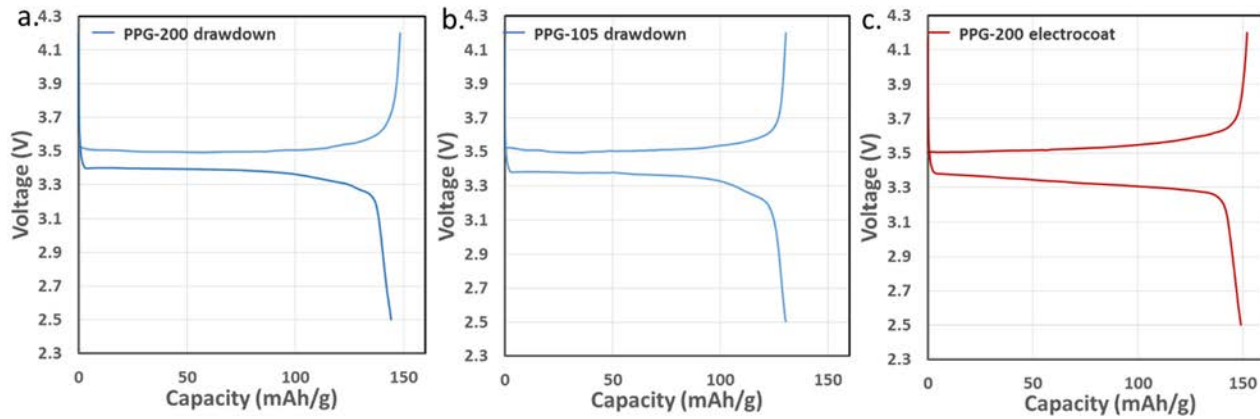
Figure IV-380: Electrochemical performance of doctor-blade assembled LFP electrodes using the e-coat resins (a) PPG-200 and (b) PPG-105. The initial cycle performance demonstrates ideal voltage profiles but moderately reduced capacity expected for LFP active materials. (c) Electrochemical performance of electrocoat assembled LFP electrodes using the e-coat resin PPG-200 and 15% by weight carbon material. This electrocoat film exhibits improved capacity but slightly diminished energy efficiency compared to identical doctor-blade materials

Conclusions

Active materials stable to an electrocoat formulation have been identified. In addition, the mechanisms contributing to active material deactivation in a water bath have been investigated and efforts are underway to produce stable, active materials of smaller particle size for aqueous processing of NMC materials. Novel binder systems capable of electrocoating the NMC active materials have been synthesized. An analysis of the deposition kinetics of these systems has illustrated that the areal capacity of the assembled film is tunable through the deposition time. An optimization of the electrocoat parameters for LFP materials has been accomplished with the intention to translate these deposition systems to NMC materials during the remaining portion of this project. Once established, the optimized bath composition and deposition parameters will be applied to a bench scale continuous system in order to optimize the coating parameters for large scale manufacture. Upon successful completion of the aforementioned tasks, cell-level battery packs will be produced from electrocoated films to gauge the suitability of this assembly process for commercial battery production.

Products

Presentations/Publications/Patents

1. VTO annual merit review, 2016.

IV.F.12. Development of UV Curable Binder Technology to Reduce Manufacturing Cost and Improve Performance of Lithium Ion Battery Electrodes (Miltec UV International)

Gary E. Voelker, Project Director
Dr. John Arnold, Principal Investigator
Miltec UV International
146 Log Canoe Circle
Stevensville, MD 21666
Phone: 410-604-2900
Fax: 410-604-2906
E-mail: gvoelker@miltec.com, jarnold@miltec.com

Colleen Butcher, DOE Program Manager
National Energy Technology Laboratory
626 Cochrans Mill Road
P.O. Box 10940
Pittsburgh, PA 15236-0940
Phone: 412-386-4984; Fax: 412-386-4604
E-mail: Colleen.Butcher@netl.doe.gov

Subcontractors:
Argonne National Laboratory, Argonne, IL
Oak Ridge National Laboratory, Oak Ridge, TN

Start Date: December 1, 2015
End Date: November 30, 2017

Abstract

Objectives

- Provide performance data sufficient for Lithium ion battery manufacturers to commit to the first steps of making HEV, PHEV and/or EV Lithium ion batteries with a UV process.

- Demonstrate high speed (200-300 fpm) coating and UV curing techniques with consistent thickness and edge control and the ability to make cathodes with UV curable binder with performance equal or better than PVDF cathodes.

- Conduct supplemental research on applying a UV cathode layer on top of an existing UV cathode layer to produce a thicker high energy cathode with sufficient porosity.

- In all cases, this revolutionary approach can result in dramatic increases in process speeds as well as significantly reduced capital cost, operating cost, reduced energy consumption and reduced environmental concerns and costs due to the elimination of volatile organic solvents.

Accomplishments

- Hand drawn cathode samples made with 3% by weight UV curable binder were cured at high speeds (200-300 fpm) with reactive impedance, capacity, and long term cycle life equal to PVDF cathodes.

- Completed the installation and began operation of a high speed (200-300 fpm) UV curing system which operates with either a slot die or letterpress coater. The unit accommodates 10" current collector foil with an 8" coating width.

Future Achievements

- Development and optimization efforts will continue to reduce the UV curable binder content to less than 2% by weight for both high power HEV and high energy PHEV and EV applications.

- Single side and double sided coating and UV curing will be demonstrated using slot die and letterpress coating techniques to establish the coating speed limits.

- Demonstrate double and triple layered coatings leading to potentially thick coatings for high energy applications.

Technical Discussion

Background

Previously identified UV curable binders and associated curing technology have been shown to reduce the time required to cure electrode coatings from tens of minutes to less than one second. This revolutionary approach can result in dramatic increases in process speeds and significantly reduced capital costs (a factor of 10 to 20) and operating costs, reduced energy requirements and reduced environmental concerns and costs due to the virtual elimination of volatile organic solvents and associated solvent dryers and recovery systems.

The accumulated advantages of higher speed, lower capital cost, lower operating cost, reduced footprint, lack of VOC recovery, and reduced energy cost is a reduction of 50% in the manufacturing cost of electrodes. When commercialized, the resulting cost reduction in Lithium ion batteries will allow storage device manufacturers to expand their sales in the market and thereby accrue the energy savings of broader utilization of HEVs, PHEVs and EVs in the U.S., and a broad export market is also envisioned. In addition to equipment required to make and UV cure hand drawn cathode samples on high speed web conveyors with UV lamps; Miltec UV has a continuous coating and UV curing system (three very high intensity UV lamps) to demonstrate the primary objectives of the project.

Introduction

The primary objective of the project is to provide performance data sufficient for Lithium ion battery manufacturers to commit to the first steps of making their own HEV, PHEV and/or EV Lithium ion batteries with a UV process. This project involves an iterative R&D effort: making coin cells and pouch cells, followed by testing and analyses, then by adjustments in chemistry, mixing, coating, and UV curing to produce layered pouch cells at high processing speeds (200-300 fpm) with performance equal or greater than that of a conventional PVDF cell. This effort will focus on cathodes made with UV curable binders.

As a supplemental effort, Miltec and its team will investigate high speed coating techniques to demonstrate consistent thickness and edge control and will also conduct supplemental research on applying a UV cathode layer on top of an existing UV cathode layer to produce a thicker high energy cathode with sufficient porosity.

In all cases, this revolutionary approach can result in dramatic increases in process speeds as well as significantly reduced capital cost, operating cost, reduced energy consumption and reduced environmental concerns and costs due to the elimination of volatile organic solvents.

Approach

A major innovation of the use of UV curable binders in LIB electrode manufacturing is the potential for much higher processing speeds. Miltec UV and its partners have shown that once a condition for complete UV curing is determined (speed, thickness, number of lamps, etc.) then there is a linear correlation between process speed and number of UV lamps. For example, it has been shown that if UV curable coating completely cures at a cathode coating thickness of 20 µm with 1 lamp (600 W/in lamp) at a speed of 100 fpm, then that same 20 µm coating will completely cure at a speed of 300 fpm with 3 lamps.

Based on the difficulty of coating UV curable binder with slot die at higher speeds (>150 fpm), it is believed that coating technology other than slot die will most likely be required to achieve the very high process speeds made possible by UV curable binders (100 meters/minute). Miltec will evaluate and adapt the best from two coating processes from the printing industry, flexography and letterpress printing.

Another potentially important innovation made possible with UV curable binders is the ability to make cathodes with multiple layers of coating. This is made possible by the fact that, unlike a solvent based system, the second or subsequent layers can be applied without the solvent in the second layer dissolving material in the layer below and the time between application and cure is so short that the second layer of liquid coating does not have time to flow into the pores of the first layer. Miltec has demonstrated aspects of this innovative capability in both hand drawn and flexo coated samples, but it will really take a moving web to do this correctly. Multilayered coating introduces the ability to make thicker, higher active material loading cathodes for EV applications. It also introduces the ability to change porosities and other characteristics such as material composition (active material and carbon) between layers. Miltec and ORNL will investigate and evaluate multilayered coatings and the potential advantages in this project.

The expected outcome of the project is to generate performance data from multilayer pouch cells (0.5–1.0 Ah) fabricated using UV curable binder cathodes to demonstrate capacity, long term cycling, rate capacity, impedance, and repeatability equal to or better than a pouch cell with cathodes made using PVDF as a binder. Miltec is in contact with battery manufacturers and it is our belief that they will take the next steps once we demonstrate equivalent pouch cell performance. The most likely next step after the completion of this project would be the addition of a UV curing system to an existing cathode manufacturing line as a demonstration project; or possibly a stand-alone demonstration unit because of the relatively low capital and operating cost of a UV curing system.

Results

One of the early primary objectives of this effort was to confirm that the reactive impedance and longer term cycle life of UV curable binder cathodes could be equivalent or better than reference PVDF cathodes in pouch cells. Figure IV-381 shows a comparison of the reactive impedance of a 90/7/3 (NMC 111/carbon/UV curable binder) UV cathode to a 90/5/5 and a 90/8/2 reference PVDF cathode at lower temperatures. The results at ambient temperatures and elevated temperatures were essentially the same. The improvements in reactive impedance, cycle life, adhesion and overall performance were the result of iterative identification and testing of modified UV chemistries, mixing techniques, and application techniques.
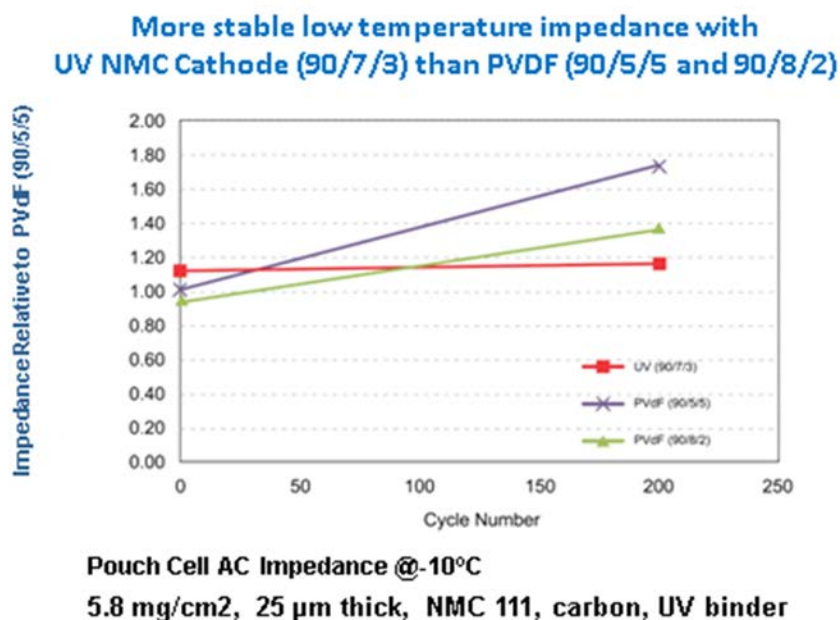

Figure IV-381: Pouch cell cycling of 90/7/3 (NMC-C45-UV binder) shows UV coating has stable AC impedance better than reference PVDF

The importance of improved reactive impedance achieved with UV curable binder was confirmed with pouch cell cycling tests comparing UV curable binder cathodes to reference PVDF cathodes. Figure IV-382 and Figure IV-383 show that 90/5/5 and 90/7/3 UV cathodes have performance equivalent to PVDF reference pouch cells. These tests were conducted at 60°C and 2C cycle rates.
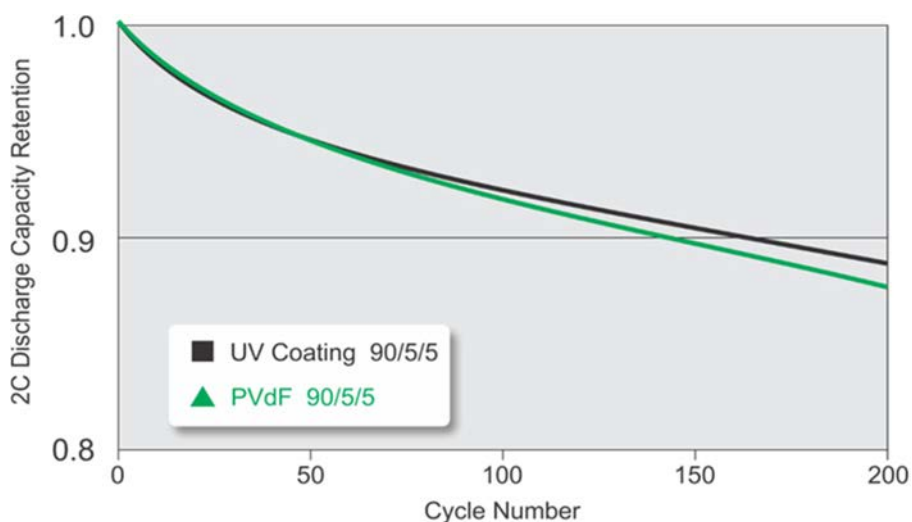

Figure IV-382: UV Cathodes (90/5/5) have equivalent accelerated 60 °C cycling performance as PVDF cathodes with similar loading in single layer pouch cells
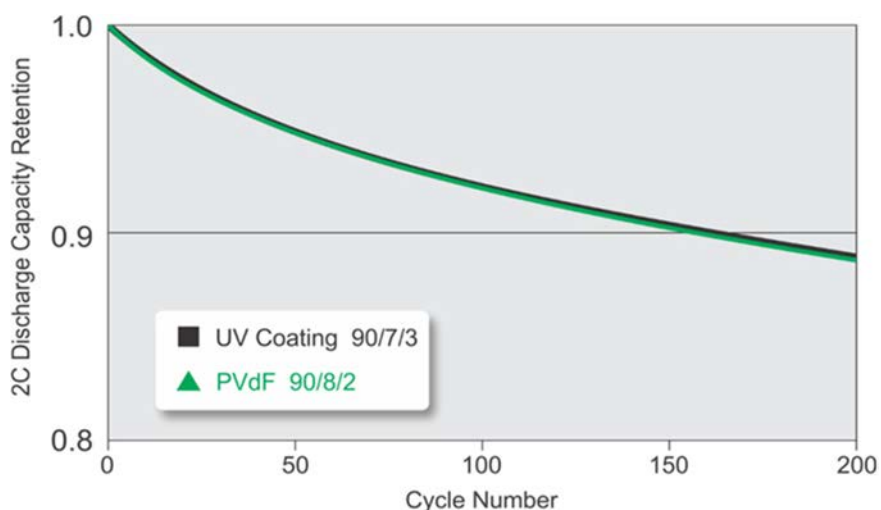

Figure IV-383: UV Cathodes (90/7/3) have equivalent accelerated 60 °C cycling performance as PVDF cathodes with similar loading in single layer pouch cells

Now that we have established that the UV chemistry is stable and equal in performance to PVDF in the environment of an operating NMC battery, we are pursuing a parallel approach to demonstrate the ability to coat and cure at high speeds and to reduce the binder content even further with the goal of matching commercial batteries. So far we have produced electrodes with 3% UV binder with equivalent performance. We have produced coatings with 1 and 2% UV binder with good adhesion and stability but this required increased NMC and reduced carbon content and resulted in unacceptable conductivity.

The slot die/letterpress coating and 3 lamp UV curing system is operational and the focus of an effort to demonstrate the significant cost advantages of UV curing.

A slot die coater with a single UV lamp curing system at Oak Ridge National Laboratory is also operational. This unit is to be used to demonstrate multi-layered cathode coatings using UV curable binder. The project milestone to demonstrate layered coating is March 2017.

Conclusions

Miltec UV International and its subcontractors, Argonne National Laboratory and Oak Ridge National Laboratory have made significant progress toward meeting the goals of this project. A three lamp UV curing system with slot die coater and an interchangeable flexo/letterpress coater with a reel to reel control system capable of coating and curing at 400 feet per minute is operational. Cathode coatings of 3% UV binder have been prepared; made into pouch cells and cycled with performance equal to PVDF reference cells. Cathode coatings of 1 and 2% UV binder have shown significant promise and will be pursued further. This coating and UV curing system will allow Miltec UV to complete the optimization and demonstrate the full potential of this technology. Miltec UV intends to vigorously pursue full development and commercialization of UV systems as applied to Lithium ion battery electrodes.

Products

Presentations/Publications/Patents

1. Arnold, Dr. John, DOE Annual Merit Review Presentation (June 2016, Washington, D.C.)

IV.F.13. Low Cost, Structurally Advanced Novel Electrode and Cell Manufacturing (24M Technologies)

William Woodford, Principal Investigator
24M Technologies, Inc.
130 Brookline Street
Cambridge, MA 02139

Tien Q. Duong, DOE Program manager
U.S. Department of Energy
Advanced Battery Materials Research (BMR)
Vehicle Technologies Office
1000 Independence Avenue, SW
Washington, DC 20585
Phone: (202) 586-7836
E-mail: Tien.Duong@ee.doe.gov

Start Date: October 2014
End Date: September 2016

Abstract

Objectives

24M will demonstrate that its novel electrode and cell design and manufacturing approach can be scaled to mass production of lithium-ion systems for automotive applications. Activities in Phase 1 included increasing the energy density of 24M's electrodes and demonstrating production quality processes. Phase 2 focused on increasing the total size and energy of the system and demonstrating high volume manufacturing methods.

Accomplishments

- 4 large-format (> 100 Ah) can cell prototypes were delivered to Argonne National Laboratory for testing in September 2016; 4 cells were kept at 24M for parallel testing. These cells achieved 100% yield based on capacity tolerance of ± 5% and impedance tolerance of ± 10%.

- Large-format (> 250 cm^2) cathode and anode electrodes successfully formed with yields greater than 95% based on a weight tolerance of ± 5%.

- Large-format (> 250 cm^2) cathode and anode electrodes successfully formed with high-volume manufacturing methods with thickness and weight control of ± 5% each.

- Both cathode and anode volume loadings have been demonstrated in full cells with 10 higher volume % active materials from the program starting point.

Future Achievements

All program milestones and deliverables have been successfully met.

Technical Discussion

Background

24M Technologies, Inc. has developed novel electrode and cell manufacturing technologies that utilize proven and emerging lithium-ion (or other) chemistries which can be leveraged to produce automotive-capable batteries with a smaller ratio of inactive to active material than any previous lithium-ion battery.

Introduction

This program is focused on addressing several of the identified technical barriers to widespread electrification of vehicle technologies in the US. Specifically, the program is structured to increase the energy density of semisolid suspensions while maintaining processability for manufacturing, demonstrate high volume manufacturing capability with a novel electrode and cell manufacturing technology, and to maintain manufacturing quality and tolerance through process scale-up to large-format electrode designs.

Approach

24M's approach to lithium-ion manufacturing utilizes a novel electrode and cell design that requires fewer unit operations to dramatically reduce cell costs. The technology dramatically reduces the capital investment required for lithium-ion manufacturing and requires approximately one-fifth the time of conventional lithium-ion cell fabrication approaches. The manufacturing approach achieves low cost without giant factories (1/5th of conventional lithium-ion manufacturing space), in which production can be scaled with "copy exact" modular plants. This creates the opportunity for locating production near customers for lower cost. The semisolid electrodes developed by 24M require no drying and no organic solvents. Figure IV-384 below highlights the dramatic simplification of the electrode creation processes in 24M's cell manufacturing approach.
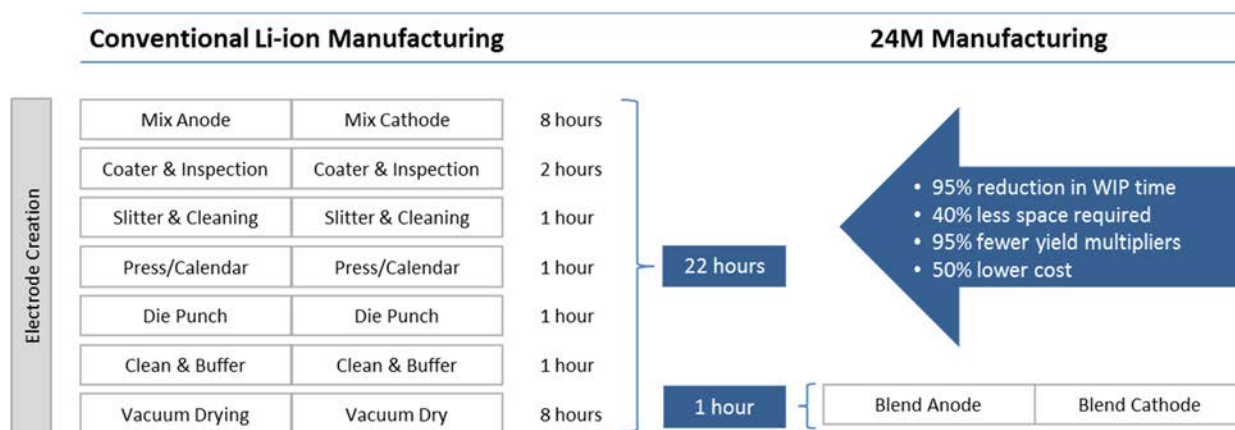

Figure IV-384: Comparison of 24M's novel manufacturing processes to conventional lithium-ion manufacturing approach, highlighting the dramatic reduction of complexity in the electrode creation steps

Results

We have achieved the following progress:

Cathode and anode semisolid loadings increased by 10 volume %

Semisolid cells have been built and demonstrated with cathode and anode semisolid suspensions 10 volume % greater than the program starting point. The cells have been cycled through more than 100 cycles. New formulations and mixing procedures are continuously evaluated to further improve the performance of high-energy semisolid cell designs.

Delivery of 4 large-format (> 100 Ah) prototype cells to Argonne National Laboratory for testing

Four (4) prototype can cells with capacities >100 Ah have been delivered to Argonne National Laboratory for testing. A duplicate set of 4 cells is testing at 24M. The cells are undergoing testing to characterize their capacity, power capability, and cycle life across a range of operating temperatures.

Large-format (> 250 cm^2) cathode and anode electrodes have been successfully formed with yields greater than 95% based on a weight tolerance of $\pm$ 5%.

In Phase 1 of the program, electrode quality metrics were established using the R&D scale prototype cells which have an electrode footprint of 80 cm^2. In Phase 2, equivalent electrode quality and yields > 95% were demonstrated in the scaled-up product-intent electrodes with a footprint of > 250 cm^2. Figure IV-385 below shows electrode weight data for large-format anode and cathode electrodes produced on the Gen2 prototype line at 24M's facility in Cambridge, MA. These data show a >95% yield for anodes and 100% yield for cathodes based on the established program criteria of ± 5%.
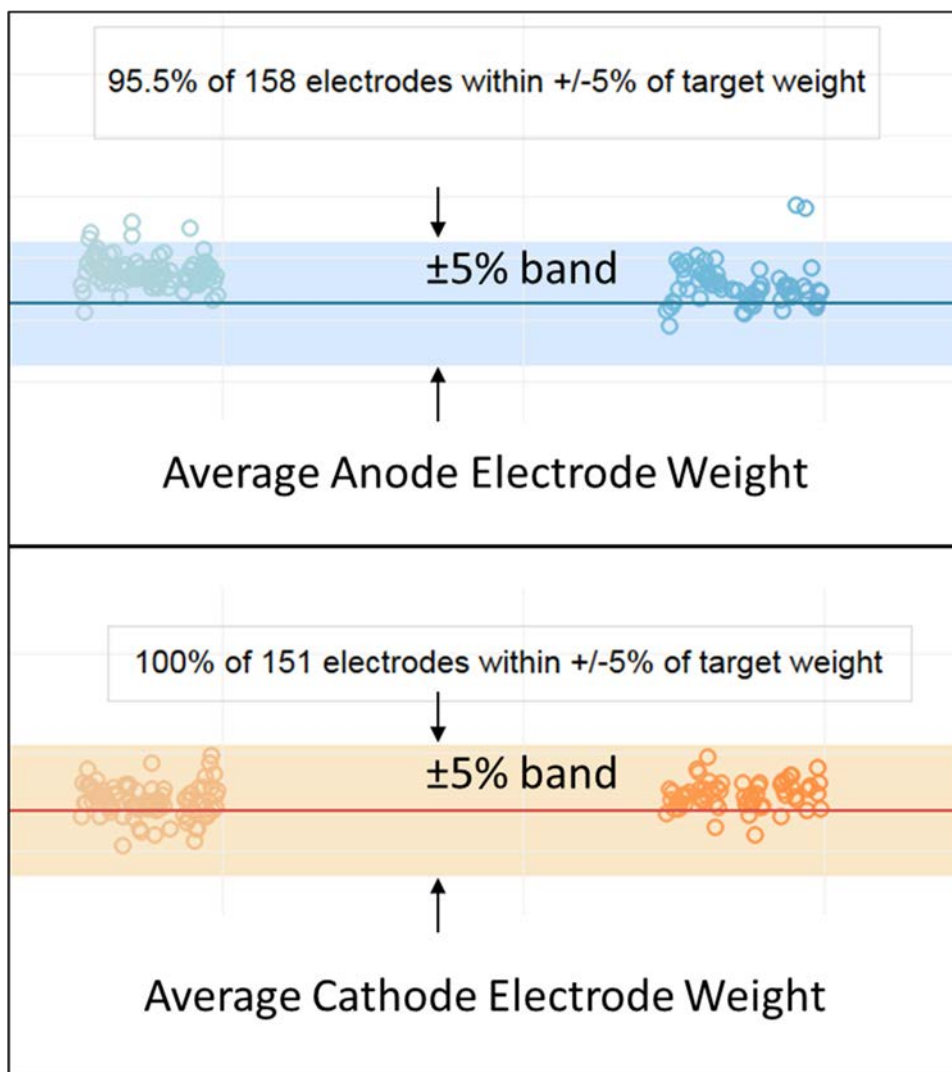

Figure IV-385: Plot of average anode and cathode electrode weights for large-format (> 250 cm²) semisolid electrodes produced on 24M's Gen2 prototype line

Conclusions

All program milestones and deliverables have been successfully completed. 24M is now focused on scaling up the manufacturing of its semisolid cell technology to commercialize its first product, building off the momentum generated in this program. 24M has successfully achieved the Phase 2 Go/No-Go milestone of delivering 4 large-format prototype can cells (> 100 Ah capacity) to Argonne National Laboratory for evaluation. Scale up from the 80 cm^2 footprint R&D cell to the product-intent > 250 cm^2 footprint has been demonstrated with equivalent quality and yield demonstrated in the large format electrodes. The large format electrodes have been successfully integrated into the large-format prototype can cells delivered to Argonne National Laboratory.

Products

1. "Low Cost, Structurally Advanced Novel Electrode and Cell Manufacturing," es245_woodford_2016_o, US DOE Vehicle Technologies Annual Merit Review, 2016.